

WestminsterResearch

<http://www.westminster.ac.uk/westminsterresearch>

**Design, analysis and evaluation of bandpass sigma-delta
modulators**

Al-Janabi, M.

This is an electronic version of a PhD thesis awarded by the University of Westminster.
© Dr Mohammed Al-Janabi, 2000.

The WestminsterResearch online digital archive at the University of Westminster aims to make the research output of the University available to a wider audience. Copyright and Moral Rights remain with the authors and/or copyright owners.

Whilst further distribution of specific materials from within this archive is forbidden, you may freely distribute the URL of WestminsterResearch: (<http://westminsterresearch.wmin.ac.uk/>).

In case of abuse or copyright appearing without permission e-mail repository@westminster.ac.uk

Design, Analysis and Evaluation of Bandpass Sigma-Delta Modulators

Mohammed Al-Janabi

**A thesis submitted in partial fulfilment of the requirements of the
University of Westminster for the degree of Doctor of Philosophy**

**Department of Electronic Systems
School of Computer Science
University of Westminster**

November 2000

Abstract

The inherent analogue nature of the signals encountered in the real world in conjunction with the abundant merits provided by digital techniques together with the increasing use of mixed-signal based systems have created considerable demand for high performance A/D and D/A Σ - Δ converters. Furthermore, the increasing need to perform high-precision data conversion for narrow-band high-frequency signals in communications and broadcasting systems as well as special-purpose instrumentation provide ample justification for development and innovation in the very important field of bandpass Σ - Δ modulation.

The overall aim of this research programme is to investigate, establish, develop and confirm through a combination of theoretical analysis and behavioural level simulations suitable techniques for the design of accurate and simple-to-implement bandpass Σ - Δ modulators.

First of all, the low-to-bandpass frequency transformation technique is further developed to enable the simultaneous specification of the signal bandwidth and noise-shaped band-location for any arbitrary centre frequency. The second technique involves the coincidental placement of the noise transfer function zeros at the centre of the signal region to achieve variable-band noise-shaping. The third approach, which is absolutely novel, employs a first-order sum-filter in combination with fractional-delayers to spectrally shift the noise-shaped band to the desired signal region. Fourthly; a practical step-by-step method is presented for the design of variable-band Butterworth or Chebyshev 2 bandpass Σ - Δ modulators. These techniques are extended to design different as well as combinations of single-loop, multi-stage and multi-bit real and complex coefficient bandpass Σ - Δ modulators.

This thesis, in addition, presents the design analysis and evaluation of a novel class of Σ - Δ modulators that are capable of providing concurrent multiple-band noise-shaping for multi-tone narrow-band input signals. Noise transfer functions which utilise comb filters, slink filters, fractional delay filters, FIR multi-notch and IIR multi-notch bandstop filters are applied for the design of these multi-band Σ - Δ modulators.

Detailed models of these modulators incorporating the quantiser non-linearities and the effect of non-ideal loop-filters are evaluated at the behavioural level. Evaluation tools in Matlab to verify the design by simulation are created, explained and supported with examples to demonstrate that these theoretical techniques work in practice.

The stability of bandpass Σ - Δ modulators is evaluated at the behavioural level using a mixture of Root Locus techniques and the Jury Criterion to determine the stable range of the quantiser gain values. A comprehensive coverage of the main factors that affect stability in high-order Σ - Δ modulators is presented and supported with simulation results.

Detailed guidelines for the choice of modulator topologies as well as coefficient complexity are obtained and presented in tabular form. Graphs and charts are provided which depict modulator performance including in-band signal-to-noise ratios, dynamic ranges as well as regions of stability

This Thesis is Dedicated to:

My mother Leila Shawkat and two sisters Shuhub Al-Janabi and Zainab Al-Janabi for their overwhelming support, encouragement and unwavering patience throughout the course of my studies.

Acknowledgements

There are many individuals who made this work possible. First and foremost, special thanks go to my Director of Studies Dr Izzet Kale for introducing me to the amazing world of Σ - Δ modulation and for his valuable ideas and suggestions, boundless enthusiasm, extreme patience and continued encouragement throughout the course of this study. I extend my thanks to my second supervisor Dr Dik Morling for his insightful comments and intuitive approach in problem solving. I would like to thank Dr Doug Neale, my third supervisor, for his invaluable advice and persistent encouragement.

I would like to offer my gratitude to Dr Andrzej Tarczynski and Mr David Thompson for their extremely valuable discussions on technical matters related to non-linear control theory. I extend my thanks to Professor Gerry Cain and Dr Anush Yardim for introducing me to the fascinating world of digital signal processing.

I would also like to thank Me Steve Lawson for his encouragement, valuable advice, constant attention and willingness to always help out at very short notice.

My gratitude is extended to my colleagues Mr Martin Giles and Mr Mucahit Kozak for their extremely useful discussions, constructive criticism and insight on the subject of Σ - Δ modulation. Special thanks go to my colleague Mr Bobby Mughal for his brilliant technical assistance on intricate matters relating to Matlab and Simulink.

I am greatly indebted to all research colleagues in CMSA for their support and fruitful discussions that helped me in producing this thesis. These include Dr Artur Krukowski, Mr Lorenzo Pasquato, Mr Jeremi Gryka, Dr Hanu Sun, Mr Ediz Cetin, Miss Dragana Barjamovic and Mr Mohammed Rezki.

I also would like to thank all my colleagues at the Department of Electronic Systems for their expert knowledge, invaluable advice and continued words of encouragement.

List of Contents

Abstract.....	<i>I</i>
Dedication.....	<i>II</i>
Acknowledgments.....	<i>III</i>
List of Contents.....	<i>IV</i>
List of Publications.....	<i>VIII</i>
List of Symbols and Abbreviations.....	<i>X</i>
Chapter 1 Introduction.....	1
1.1 Introduction to Sigma-Delta Modulation.....	1
1.2 Contributions by the Author.....	3
1.2.1 Original Contributions.....	3
1.2.2 Development/Extended Contributions.....	4
1.3 Organisation of Thesis.....	5
1.4 Conventional Nyquist Rate A/D Converters.....	7
1.5 Oversampling A/D Converters.....	9
1.6 Sigma-Delta Modulation.....	10
1.7 Digital-to-Analog Σ - Δ Modulators.....	12
1.8 The Classical Linear White Noise Model.....	13
1.9 First-Order Σ - Δ Modulator.....	14
1.10 Higher-Order Distributed Feedback Σ - Δ Modulators.....	19
1.11 Multi-Bit Σ - Δ Modulators.....	21
1.12 Simulation Approach.....	23
1.13 Performance and Accuracy Criteria.....	24
1.13.1 Oversampling Ratios and Bandwidth.....	24
1.13.2 In-Band Signal-to-Noise Ratios (SNR).....	25
1.13.3 Maximum Stable Input Amplitude.....	28
1.13.4 Dynamic Range (DR).....	28
1.13.5 Tones.....	29
1.13.6 Other Performance Measures.....	30
1.14 Concluding Remarks to Chapter 1.....	30
Chapter 2 Bandpass Σ-Δ Modulation.....	32
2.1 An Overview on Bandpass Σ - Δ Modulation.....	32
2.2 Survey of Publications to the Field of Bandpass Σ - Δ Modulation.....	35
2.3 Survey of the Implementations of Bandpass Σ - Δ Modulators.....	39
2.4 Applications of Bandpass Σ - Δ Modulators.....	40
2.5 The Lowpass-to-Bandpass Transformation Method - Mid-Band Resonance.....	40

2.6 Higher-Order Narrowband Mid-Band Resonator-Based Bandpass Σ - Δ Modulators.....	45
2.7 The Lowpass-to-Bandpass Transformation Method - Non-Mid-Band Resonance.....	51
2.8 Extension of the Transformation Approach to Specifying Bandwidths.....	54
2.9 Criteria for the Design of Variable-Band Bandpass Σ - Δ Modulators.....	59
2.10 The FIR Notch-Filter (FNF) Approach.....	62
2.11 The IIR Notch-Filter (INF) Approach.....	72
2.12 The Complex FIR Notch-Filter (CFNF) Approach.....	75
2.13 The Complex IIR Notch-Filter (CINF) Approach.....	81
2.14 Overview on the Fractional Delay Filter (FDF) Approach.....	83
2.15 FIR Fractional Delay Case.....	86
2.16 Allpass IIR Fractional Delay Case.....	87
2.17 Evaluation of the FDF Technique.....	88
2.18 A Methodology for the Design of Bandpass Σ - Δ Modulators.....	91
2.19 Chain of Resonators with Weighted Feedforward Summation.....	96
2.20 Chain of Accumulators with Feedforward Summation & Local Resonator Feedbacks.....	98
2.21 Chain of Resonators with Distributed Feedback.....	102
2.22 The Sodini Interpolative Σ - Δ modulator Topology.....	104
2.23 Non-Idealities in Resonator-Based Bandpass Σ - Δ Modulators.....	109
2.24 Concluding Remarks of Chapter 2.....	110
Chapter 3 Multi-Stage MASH Bandpass Σ-Δ Modulators.....	115
3.1 Overview on Bandpass MASH Σ - Δ Modulators.....	115
3.2 Review of published MASH Σ - Δ Modulators.....	117
3.3 Design Methodology for MASH Bandpass Σ - Δ Modulators.....	119
3.4 Fourth-Order 2-2 MASH Bandpass Σ - Δ Modulators.....	127
3.5 Sixth-Order MASH Bandpass Σ - Δ Modulators.....	130
3.5.1 Triple-Stage 2-2-2 MASH Bandpass Σ - Δ Modulators.....	130
3.5.2 Double-Stage 4-2 MASH Bandpass Σ - Δ Modulators.....	133
3.5.3 Double-Stage 2-4 MASH Bandpass Σ - Δ Modulators.....	136
3.6 Eighth-Order MASH Bandpass Σ - Δ Modulators.....	139
3.6.1 Quadruple-Stage 2-2-2-2 MASH Bandpass Σ - Δ Modulators.....	139
3.6.2 Triple-Stage 4-2-2 MASH Bandpass Σ - Δ Modulators.....	142
3.6.3 Triple-Stage 2-4-2 MASH Bandpass Σ - Δ Modulators.....	144
3.6.4 Triple-Stage 2-2-4 MASH Bandpass Σ - Δ Modulators.....	147
3.6.5 Double-Stage 4-4 MASH Bandpass Σ - Δ Modulators.....	149
3.7 Complex Second-Order MASH Bandpass Σ - Δ Modulators.....	151
3.8 Complex Third-Order Bandpass MASH Σ - Δ Modulators.....	153
3.8.1 Complex Triple-Stage 1-1-1 MASH Bandpass Σ - Δ Modulators.....	153

3.8.2 Complex Double-Stage 2-1 MASH Bandpass Σ - Δ Modulators.....	155
3.9 Complex Fourth-Order Bandpass MASH Σ - Δ Modulators.....	156
3.9.1 Complex Triple-Stage 2-1-1 MASH Bandpass Σ - Δ Modulators.....	157
3.9.2 Complex Double-Stage 2-2 MASH Bandpass Σ - Δ Modulators.....	158
3.10 FIR Fractional-Delay Double-Stage Bandpass MASH Σ - Δ Modulators.....	158
3.11 FIR Fractional-Delay Triple-Stage Bandpass MASH Σ - Δ Modulators.....	160
3.12 FIR Fractional-Delay Quadruple-Stage Bandpass MASH Σ - Δ Modulators.....	161
3.13 Double-Stage Non-Resonator-Based MASH Bandpass Σ - Δ Modulators.....	162
3.13.1 Identical Loop-Filter Stages in Double-Stage Bandpass MASH Σ - Δ Modulators..	163
3.13.2 Dissimilar Loop-Filter Stages in Double-Stage Bandpass Σ - Δ Modulators.....	164
3.14 Double-Stage Resonator/Non-Resonator Based Bandpass Σ - Δ Modulators.....	165
3.15 Double-Stage Inverse Comb-Bandpass Filter Based Bandpass Σ - Δ Modulators.....	167
3.15.1 Single-Loop Case.....	167
3.15.2 Double-Loop Case.....	168
3.16 Concluding Remarks for Chapter 3.....	170
Chapter 4 Multi-Band Bandpass Σ-Δ Modulators.....	175
4.1 Introduction to Multi-Band Σ - Δ Modulators.....	175
4.2 Applications for Multi-Band Σ - Δ Modulators.....	176
4.3 Comb Filter Approach.....	177
4.4 Complex Comb Filter Approach (CCFA).....	181
4.5 Slink Filter Approach.....	184
4.6 Complex Slink Filter Approach (CSFA).....	187
4.7 Comb Filter Fractional-Delay Approach.....	189
4.8 FIR Fractional-Delay Multi-Band Σ - Δ Modulators.....	190
4.9 Allpass IIR Fractional-Delay Multi-Band Σ - Δ Modulators.....	192
4.10 Multi-Notch Filter Approach.....	195
4.11 Complex Multi-Notch Approach (CMNFA).....	198
4.12 IIR Multi-Notch Filter Approach (IMNFA).....	200
4.13 Concluding Remarks to Chapter 4.....	203
Chapter 5 Stability in Bandpass Σ-Δ Modulators.....	206
5.1 An Overview on Stability.....	206
5.2 Chronological Survey of Contributions to the Field of Stability in Σ - Δ Modulation..	207
5.3 Different Definitions and Interpretations of Stability.....	208
5.4 Review of Existing Rules-of-Thumb.....	209
5.5 Stability using the Root Locus Techniques.....	210
5.5.1 Root Locus Analysis of Fourth-Order Bandpass Σ - Δ Modulators.....	211

5.5.2 Ideal Fourth-Order Mid-Band Resonator Σ - Δ Modulator.....	211
5.5.3 Variable-Band Resonator-Based Bandpass Σ - Δ Modulators.....	212
5.5.4 Non-Ideal Variable-Band Frequency Bandpass Σ - Δ Modulator.....	213
5.6 Detailed Behavioural-Level Simulations to Assess Stability.....	215
5.7 Factors that Affect Modulator Stability.....	216
5.7.1 Amplitude and Type of Input Signal.....	216
5.7.2 Modulator Order.....	217
5.7.3 Feedback Coefficients.....	222
5.7.4 Feedforward Loop-Filter Gains.....	228
5.7.5 Number of Delayers.....	232
5.7.6 Effect of Dither on Stability.....	236
5.7.7 Dependence of Modulator Stability on the Number of Quantisation Levels.....	237
5.7.8 Dependence of Modulator Stability on Multi-Sinusoidal Inputs.....	238
Chapter 6 Evaluation of Current Findings	
6.1 Concluding Remarks.....	242
6.4 Recommendations for Future Work.....	248
References.....	249
Appendix A.....	264

List of Publications

[MAJ95] Al-Janabi, M., I. Kale and R.C.S. Morling, "MASH structures for bandpass sigma-delta modulators", *IEE Colloquium on Oversampling and Sigma-Delta Strategies for Digital Signal Processing*, pp. 3/1-3/6, London, November 1995.

[MAJ96] Al-Janabi, M., I. Kale and R.C.S. Morling, "Measurement and characterisation of MASH bandpass sigma-delta modulators for direct IF analog-to-digital conversion", *International Workshop on ADC Modelling*, pp. 147-152, Smolience Castle, Slovak Republic, May 1996.

[MAJ97a] Al-Janabi, M., I. Kale and R.C.S. Morling, "Effective-fourth-order resonator-based MASH bandpass sigma-delta modulator", *International Conference on Acoustics, Speech and Signal Processing*, vol.3, pp. 2493-2496, Munich, Germany, April 1997.

[MAJ97b] Al-Janabi, M., I. Kale and R.C.S. Morling, "Variable centre frequency resonator based bandpass Σ - Δ modulator", *Electronics Letters*, vol. 33, no. 24, pp. 2008-2009, November 1997.

[MAJ98a] Al-Janabi, M., I. Kale and R.C.S. Morling, "An analysis of non-ideal variable centre frequency narrow-band bandpass Σ - Δ modulators", *International Symposium on Communication Systems & Digital Signal Processing*, vol. 1, pp. 289-292, Sheffield Hallam University, UK, April 1998.

[MAJ98b] Al-Janabi, M., I. Kale and R.C.S. Morling, "Stability evaluation of tunable resonator-based bandpass Σ - Δ modulators via root locus analysis", *International Symposium on Communication Systems & Digital Signal Processing*, vol. 1, pp. 441-444, Sheffield Hallam University, UK, April 1998.

[MAJ98c] Al-Janabi, M., I. Kale and R.C.S. Morling, "Tunable centre frequency resonator-based bandpass Σ - Δ modulators", *IEEE Instrumentation and Measurement Technology Conference*, vol. 2, pp. 1248-1252, St. Paul, Minnesota, USA, May 1998.

[MAJ99a] Al-Janabi, M., I. Kale and R. C. S. Morling, "Increasing the variability of centre frequency locations in multiple-band sigma-delta modulators via the use of fractional delay filters", *Third International Conference on A/D and D/A Conversion Techniques and their Applications*, pp. 30-33, University of Strathclyde, Glasgow, UK, July 1999.

[MAJ99b] Al-Janabi, M., I. Kale and R. C. S. Morling, "A comparative study of complex multiple-band noise-shaping sigma-delta modulators for multi-tone input signals", *Midwest Symposium on Circuits and Systems*, Las Cruces, New Mexico, August 1999.

[MAJ99c] Al-Janabi, M., I. Kale and R. C. S. Morling, "Application of fractional delay filters to tune the centre frequency location of single-band sigma-delta modulators", *Midwest Symposium on Circuits and Systems*, Las Cruces, New Mexico, August 1999.

[MAJ99d] Al-Janabi, M., I. Kale and R. C. S. Morling, "Concurrent noise-shaping for multiple narrow-band single-loop and multi-stage sigma-delta modulators", *Fourth International Workshop on ADC Modelling and Testing*, pp. 27-32, Bordeaux, France, September 1999.

[MAJ99e] Al-Janabi, M., I. Kale and R. C. S. Morling, "Narrow-band variable centre frequency single-loop and multi-stage sigma-delta modulators for bandpass signals", *IEEE Transactions for Instrumentations and Measurement*, vol. 48, no. 5, pp. 873-877, October 1999.

[MAJ00] Al-Janabi, M., I. Kale and R. C. S. Morling, "Methods for the transfer function design of multiple narrow-band bandpass sigma-delta modulators", accepted for publication in *Computer Standards & Interfaces Journal*.

List of Symbols and Abbreviations

<i>AA</i>	Anti-Aliasing
f_B	Signal Bandwidth
f_C	Variable centre frequency
f_N	Nyquist frequency
f_S	Sampling frequency
T_S	Sampling Period
Q	Number of quantisation output levels or codes
$\Sigma - \Delta$	Sigma-Delta
Δ	Quantisation step-size
N	Number of resolution bits
σ_n^2	Quantisation noise variance or power
σ_{bn}^2	In-band quantisation noise power
ν	Normalised frequency
ν_C	Normalised centre frequency
ν_B	Normalised bandwidth
ν_L	Normalised lower frequency
ν_H	Normalised higher frequency
<i>NTF</i>	Noise Transfer Function
<i>STF</i>	Signal Transfer Function
<i>PSD</i>	Power Spectral Density
$x(k)$	Discrete-time input signal to modulator
$y(k)$	Discrete-time output signal from modulator
$d(k)$	Discrete-time dither signal
$e(k)$	Discrete-time error signal
$q(k)$	Discrete-time quantisation error
$u(k)$	Discrete-time input to the quantiser
$x_{AA}(t)$	Band-limited continuous-time analogue input signal
$x_{AA}(kT)$	Band-limited discrete-time analogue input signal
$x_{AAQ}(kT)$	Band-limited discrete-time discrete-amplitude input signal
ρ	Pole radius
z^{-1}	Unit delay operator
dB	Decibel
dc	Zero frequency signal
CMOS	Complementary Metal Oxide Semiconductor

FD	Fractional Delay
FFT	Fast Fourier Transform
FIR	Finite Impulse Response
IIR	Infinite Impulse Response
PZP	Pole-Zero Pattern
rms	Root mean square
SNR	Signal-to-Noise Ratio
OSR	OverSampling Ratio
DR	Dynamic Range
SFDR	Spurious Free Dynamic Range
SNDR	Signal-to-Noise plus Distortion Ratio
NPR	Noise Power Ratio
MSIA	Maximum Stable Input Amplitude (to the modulator)
VLSI	Very Large Scale Integration
A/D	Analog-to-Digital
D/A	Digital-to-Analog
SC	Switch Capacitor
SI	Switch Current
CT	Continuous-Time
I/Q	In-Phase/Quadrature

Chapter 1

Introduction to the Concepts of Sigma-Delta Modulation

1.1 Introduction to Sigma-Delta Modulation

Sigma-delta (Σ - Δ) modulation utilises oversampling, noise-shaping as well as simple-to-implement and relatively high tolerance analogue components to accomplish high precision Analogue-to-Digital A/D and Digital-to-Analogue D/A conversion for low to medium signal bandwidth applications. Several comprehensive publications, which explain the basic underlying principles and detail the operation of these highly useful modulators can be found in [Azi96]-[Can92]-[Hau91]-[Nor97]-[Ste98]-[Tom94] and [Ben99]. A summary of some of the major milestones in the history of Σ - Δ modulators since their inception in the mid 1950s is presented below in Table 1.1

Authors	Description	Year	Ref
Cutler	Earliest reported description employing the concept of feedback to enhance the resolution of a coarse quantiser.	1960	[Cut60]
Spang and Schultheiss	Development of Cutler's system by proposing to include a FIR loop-filter in the feedback path.	1962	[Spa62]
Inose and Yasuda	The creation of the Σ - Δ modulator in its current form, where the loop-filter was transferred inside the loop.	1963	[Ino63]
Candy	The complete design, analysis and fabrication of a 1 st -order lowpass Σ - Δ modulator operating at $f_s = 40$ MHz having 8-bit resolution.	1974	[Can74]
Candy	The design, building and testing of a lowpass Σ - Δ modulator with 13-bit resolution operating at $f_s = 8$ MHz.	1976	[Can76]
Ritchie	The creation of a high-order Σ - Δ modulator in the form of a chain of integrators with distributed feedback to avert instability.	1977	[Rit77]
Candy	Detailed analysis and characterisation of the double-loop single-stage lowpass Σ - Δ modulator.	1985	[Can85]
Hayashi	The invention of the multi-stage (MASH) Σ - Δ modulator as an alternative for the design of stable higher-order Σ - Δ modulators.	1986	[Hay86]
Lee and Sodini	Presentation of a technique for the design of stable high-order Σ - Δ modulators.	1987	[Lee87]
Adams	Proposition of a simple design approach and several easy-to-implement topologies for higher-order Σ - Δ modulators.	1991	[Ada91]

Table 1.1 Milestones in the History of Σ - Δ modulation.

Despite the significant and popular use of Σ - Δ modulators, there is not, to-date, a universal closed form solution that fully describes the dynamic properties of these modulators. The existing models for the analysis of Σ - Δ modulators can be broadly categorised into approximate linear models, accurate statistical models and non-linear dynamic models. The linear model approach used in [Agr83]-[Can85]-[Cha90]-[Ada91] is relatively accurate at predicting the overall shape of the noise transfer function. However, it fails to predict stability and tonality behaviour, because it does not take into consideration the constant output power criterion of single-bit Σ - Δ modulators. Developments of the linear model so as to comply with the constant power criterion were attempted, but these were partially successful [Qiu93]. More accurate linear methods that employed Describing Function techniques to model the non-linear quantiser are documented in [Ard87]-[Ris94]. These methods did not completely characterise the stability and tonality of Σ - Δ modulators, because they assumed a particular mathematical function for the quantisation noise. Root Locus Techniques were applied in [Bai94]-[Sti88], where the quantiser was modelled as a variable gain block. The motivation there was to plot the modulator poles with respect to the quantiser gain in order to establish a more realistic stability range for the modulator.

Accurate models based on ergodic theory, which fully describe the output spectra of first-order and multi-stage Σ - Δ modulators are documented in [Gra90]. Non-linear dynamics techniques to estimate the bounds of the internal states of these modulators are fully analysed in [Fee96]. These techniques are more rigorous compared with their linear counterparts, but are very much modulator-specific.

The lack of a theoretical model that can precisely predict the stability range and tonal properties of Σ - Δ modulators, when in overload mode, provides ample justification for resorting to behavioural level simulations. These are shown by many designers and practitioners to be the most appropriate means of evaluating the performance of Σ - Δ modulators, because they take into account the actual non-linearity of the quantiser.

Lowpass Σ - Δ modulators have appeared in many commercial products for A/D and D/A conversion applications as well as mixed-signal DSP devices with on-chip coding [Ste98]. A summary of some of these products with their web-site addresses is given below in Table 1.2.

Product	Company	Web-site address
AD1859	Analog Devices	http://www.analog.com
AD1879	Analog Devices	http://www.analog.com
ADS1212	Burr-Brown	http://www.burr-brown.com
DAC1719	Burr-Brown	http://www.burr-brown.com
CS4390	Crystal Semiconductor	http://www.crystal.com
CS5334	Crystal Semiconductor	http://www.crystal.com
MC145073	Motorola	http://www.mot-sps.com
ADC16071	National Semiconductor	http://www.national.com
ADC16471	National Semiconductor	http://www.national.com
SAA7350	Philips	http://www.semiconductors.philips.com
SAA7360	Philips	http://www.semiconductors.philips.com
TLC320AD58C	Texas Instruments	http://www.ti.com

Table 1.2 A Selection of Commercial Products that Σ - Δ Modulators.

A major literature survey, which was carried out at the outset of this research programme showed that there was a large gap in the area of bandpass Σ - Δ modulation. Indeed Table 1.2 confirms that to the best knowledge of the author and [Ste98] that there is not a commercial product to-date that employs bandpass Σ - Δ modulators. This coupled with the increasing demand for high-resolution and relatively simple-to-implement A/D converters represented the prime motivation behind this work.

1.2 Contributions by the Author

The contributions by the author in this thesis can be broken down into two categories: First, original contributions covering novel propositions, techniques and topologies specifically-related to the field of bandpass Σ - Δ modulation. Second, extensions or developments of the work of other Σ - Δ experts, which was judged by the author to be worthy of research.

1.2.1 Original Contributions

- A novel technique is proposed for the design of narrow-band variable-band Σ - Δ modulators, whose noise transfer functions utilise a first-order sum-filter in conjunction with fractional delayers to accommodate different passband centre to

sampling frequency ratios. These FIR and allpass IIR fractional delay filters result in the spectral shifting of the zeros of the noise transfer function to the signal band of interest for any specified centre frequency input waveform.

- The design, analysis and evaluation of complex variable-band and fractional-delay filter based bandpass MASH Σ - Δ modulators.
- The design, analysis and evaluation of the double-stage variable-band resonator-bandpass Σ - Δ modulator.
- The design, analysis and evaluation of the double-stage single-loop inverse-comb/bandpass Σ - Δ modulator.
- The design, analysis and evaluation of the double-stage double-loop inverse-comb/bandpass Σ - Δ modulator.
- The complete design analysis and evaluation of double and triple band Σ - Δ modulators. These are based on the noise transfer functions of comb, slink, fractional delay comb, FIR and IIR multi-notch filters. These analyses are extended to complex comb, complex slink, complex multi-notch FIR and complex multi-notch IIR NTF based Σ - Δ modulators.
- The derivation of analytical expressions, which employ the Jury Criterion in conjunction with Root Locus Techniques, in order to determine the stable range of quantiser gain values of variable-band bandpass Σ - Δ modulators.

1.2.2 Development/Extended Contributions

- The development of the lowpass-to-bandpass transformation technique where the signal bandwidth as well as the centre of the variable noise-shaping band can be defined for any high-level narrow-band specification.
- The development of a technique that is well suited for the design of variable-band bandpass Σ - Δ modulators based on the noise transfer functions of FIR notch-filters, IIR notch-filters, complex FIR notch-filters and complex IIR notch-filters.
- A practical step-by-step methodology for the design of bandpass Σ - Δ modulators.
- The design, analysis and evaluation of different combinations of variable-band bandpass MASH Σ - Δ modulators, whose constituent stages contain single- and multi-bit lower-order Σ - Δ modulators.

- The design analysis and evaluation of MASH Σ - Δ modulators, which utilise non-resonator based loop-filters in their individual stages and IIR bandstop filters in their cancellation circuitry.
- The development of simple-to-use routines in Matlab, which can compute the loop-filter, feedback and feedforward coefficients for a variety of single-stage, multi-stage and multi-band Σ - Δ modulator topologies.
- The creation of a library in Simulink/Matlab, which contains over fifty single-stage, multi-stage and multi-band Σ - Δ modulators.
- The development of Matlab routines that can quantitatively evaluate the resolution and stability of any variable-band bandpass Σ - Δ modulator.
- A detailed treatment of the factors that affect stability in Σ - Δ modulators including modulator order, feedback coefficients, feedforward loop-filter gains, number of delays, initial conditions, noise-shaping band location, dither, number of quantisation levels as well as the amplitude and type of the input signal.

1.3 Organisation of the Thesis

In chapter 1, the fundamentals of Nyquist rate and oversampling rate A/D converters are reviewed, focusing in particular on the theory and advantages of oversampled Σ - Δ converters. A brief comparison is then made between A/D and D/A Σ - Δ modulators. This is followed by a discussion of the merits and limitations of the linear white noise model in the context of Σ - Δ modulator analysis. The operation of a first-order Σ - Δ modulator is explained and is supported with time-domain and frequency-domain analysis. The chapter continues by providing an overview of high-order distributed feedback, multi-stage and multi-bit Σ - Δ modulators. The chapter culminates by explaining the simulation approach and defining specifically the performance criteria that are employed for the evaluation of Σ - Δ modulators throughout this thesis.

Chapter 2 presents an overview on bandpass Σ - Δ modulators including an up-to-date review of hardware implementations and potential applications. Mid-band resonator based Σ - Δ modulators are analysed and evaluated. The prime objective of this chapter is to develop and present novel single-stage single-bit Σ - Δ modulators that can accommodate different passband to sampling frequency ratios overcoming the popular $f_s / 4$ restriction. Four techniques are presented for the design of variable-band bandpass Σ - Δ modulators. The first involves the development of the lowpass-to-bandpass transformation technique

where the signal bandwidth as well as the noise-shaping band centre frequency can be defined for any high-level narrow-band specification. The second referred to as the Coincidental-Zero-Placement (CZP) technique involves placing the zeros of the noise transfer function at the centre of the desired noise-shaping band. The third method, which is novel, utilises a first-order sum-filter in conjunction with fractional delayers to spectrally transfer the noise-shaping band to the desired signal region. The fourth technique details a practical step-by-step methodology for the design of variable-band Butterworth or Chebyshev 2 based bandpass Σ - Δ modulators. Simulation results demonstrating the applicability of these techniques to complex variable-band and multi-bit bandpass Σ - Δ modulators are also shown. Several commonly used Σ - Δ modulators are analysed and where appropriate structural modifications are made so as to allow variable-band noise-shaping. The chapter also provides linearised analysis supported with detailed simulations on the effect of non-idealities of the performance of these modulators.

Chapter 3 provides the design procedure and analysis of variable-band resonator-based multi-stage (MASH) bandpass Σ - Δ modulators. The four techniques considered are based on the noise transfer functions of real-coefficient FIR notch filters, complex FIR notch filters, fractional delayers in conjunction with first-order sum-filters and Butterworth/Chebyshev 2 bandstop filters. The design analysis and use of several new bandpass MASH Σ - Δ modulators are presented including the double-stage resonator/non-resonator and double-stage inverse comb/bandpass Σ - Δ modulators. A comparative study is given based on a mixture of linear modelling, behavioural level simulations and maximal achievable performance such as in-band Signal-to-Noise Ratio (SNR), Dynamic Ranges (DR) and tonality.

Chapter 4 presents the design analysis and evaluation of a novel class of programmable narrow-band bandpass Σ - Δ modulators, that can achieve concurrent multiple noise-shaping bands for multi-tone input signals. Five different techniques based on the noise transfer functions of comb filters, slink filters, fractional-delay comb filters, FIR multi-notch and IIR multi-bandstop filters, are applied for the design of these multi-band Σ - Δ modulators. It is also demonstrated through analysis and simulations that these techniques can be easily extended to design complex multi-band noise-shaping Σ - Δ modulators.

In chapter 5, the stability of bandpass Σ - Δ modulators is evaluated by using a variable gain model for the quantiser. Root locus techniques in combination with the Jury Criterion are employed to determine the stable range of the quantiser gain values. The

chapter continues to discuss in detail and evaluate the main factors that affect the stability of Σ - Δ modulators such as input amplitude, modulator order, feedback coefficients, feedforward loop-filter gains, number of delayers, initial conditions, noise-shaping band-location and composition of the input signal. The ultimate, but yet the most important objective of this chapter is to provide more accurate guidelines for the design of single- and multi-bit bandpass Σ - Δ modulators.

1.4 Conventional Nyquist Rate A/D Converters

Analogue-to-digital conversion is the process of converting a continuous time analogue signal to an equivalent discrete sequence of numbers having finite precision. Typical examples include flash converters, serial-parallel (subranging/ripple) converters, pipelined converters, multiplexing converters and successive approximation converters [Mit93].

Conventional Nyquist converters can be described in terms of three separate processes namely, Anti-Aliasing (AA) filtering, uniform time-domain sampling and amplitude quantisation [Is94]-[Mit93]. A block diagram of a general Nyquist rate converter is shown in Figure 1.1.

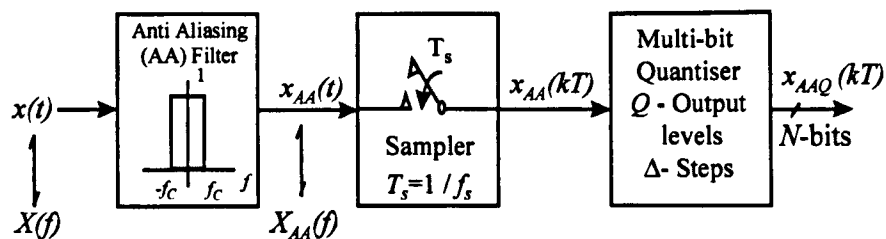


Figure 1.1 Block Diagram of a Conventional Nyquist Rate A/D Converter.

The purpose of the AA filter is to limit the bandwidth of the incoming signal $x(t)$ to a maximum of half the sampling frequency f_s , in order to avoid the overlapping of signals (i.e. aliasing). The sampler converts the band-limited continuous-time analogue input signal $x_{AA}(t)$ to a signal that is discrete in time and continuous in amplitude $x_{AA}(kT_s)$. This signal is sampled at uniformly spaced intervals of time T_s , where T_s is the inverse of the sampling frequency f_s . In the frequency domain, the sampling process generates periodic replicas of the signal spectrum at multiple frequency intervals of f_s . Therefore, it is essential to comply with the Nyquist criterion, which stipulates that f_s has to be at least

twice the highest frequency component of the input signal. This criterion may also be expressed in terms of $f_S \geq 2f_B$, where f_B is the input signal bandwidth. If the highest frequency harmonic is more than half f_S , then interference between the repeated versions of the signal spectrum will take place resulting in distorted outputs [Ism94]-[Mit93]-[Pro92].

Conventional rate converters sample the analogue signal at the Nyquist frequency $f_N = 2f_B$. Sampling at the Nyquist rate necessitates the use of an AA filter with a very sharp transition band in order to ensure adequate aliasing protection. This stringent specification increases the complexity of the analogue AA filter considerably [Pro92]-[Mit93].

The quantisation process involves the discretisation of the amplitude of the signal. The signal $x_{AA}(kT_S)$ that enters the quantiser is converted to a signal that is discrete in both time and amplitude $x_{AAQ}(kT_S)$. A quantiser with Q output quantisation codes may be represented by $Q = 2^N$, where N is the number of resolution bits. Another important parameter is the quantisation step-size Δ , which is defined by $\Delta = 2V / (Q - 1)$, where V represents voltage. One of the main disadvantages of Nyquist rate A/D converters is the requirement for extremely small quantisation step sizes for modest resolutions. For example, a converter that has 16 bits of resolution will have $Q = 2^{16} = 65536$ quantisation levels resulting in a quantisation step-size of $\Delta = 2V / (Q - 1) = 30.5 \mu V$ for an input range of $\pm 1 V$. This simple calculation shows that such accuracies are virtually unattainable with the majority of analogue integrated circuit components [Azi96]-[Orf96]. Various calibration and laser trimming techniques exist, but these have their limitations [Tom94].

One of the main problems encountered in any A/D device is that it is a non-linear system due to the presence of the quantiser. The simplest approach to represent the non-linear quantiser is to adopt the additive white noise model with its associated assumptions and statistical properties in order to enable the application of linear theory [Azi94]-[Orf96]-[Opp99]-[Pro92]. The quantisation noise power σ_n^2 or variance for a $Q = 2^N$ output quantisation levels and $\Delta = 2V / (Q - 1) = 2V / (2^N - 1)$ is given by

$$\sigma_n^2 = \left(\frac{\Delta^2}{12} \right) = \frac{1}{12} \left(\frac{2V}{2^N - 1} \right)^2 \quad (1.1)$$

High resolution Nyquist converters are difficult to implement in existing VLSI technologies due to the need for high precision analogue components, greater vulnerability to noise and interference as well as the very steep roll-off demanded of the analogue AA filter. These practical limitations have contributed towards the resurgence of oversampling converters [Tom94].

1.5 Oversampling A/D Converters

Oversampling converters achieve high resolution by using simple and relatively high tolerance analogue components at the expense of the requirement for faster and more complicated digital circuitry. These converters reduce the necessity for precise sample and hold circuitry, overcome the need for trimming or calibration and impose less restrictions on the performance requirements of the analogue AA filters that precede the sampling operation. However, these advantages are gained at the price of greater digital complexity for the decimation filter [Azi96]-[Ism94]-[Pro92]-[Tom94].

These converters perform sampling and quantisation at significantly higher rates compared with the Nyquist frequency $f_S \gg f_N$. This implies that more samples are taken from the analogue input waveform over a given time interval. The much larger ratio of the sampling rate to that of the signal bandwidth means that this excess sampling speed can in general be traded for improved amplitude resolution. The resultant magnitudes of the quantisation errors are considerably lower in oversampling converters, because more samples are taken over the same time interval. From the frequency-domain point of view, the effect of oversampling is to uniformly distribute this constant quantisation noise power over a much wider frequency range, thereby substantially reducing the amount of quantisation noise in the in-band region. [Azi96]-[Pro92]. A block diagram of an oversampled A/D converter is shown in Figure 1.2.

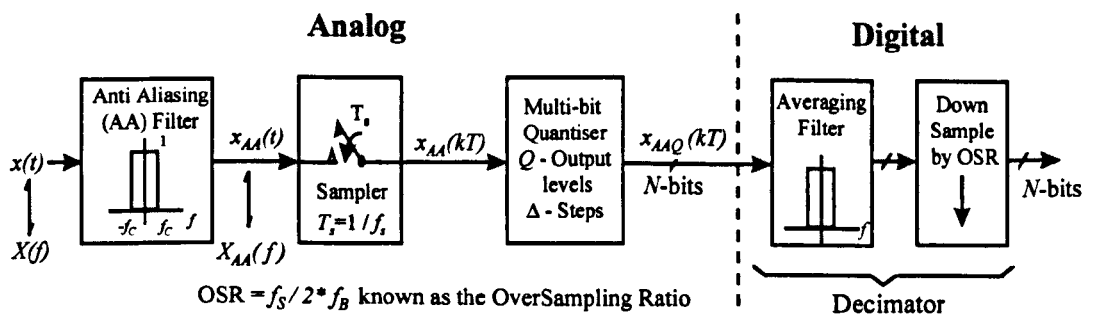


Figure 1.2 Block Diagram of an Oversampling A/D Converter.

This in-band noise power is given by

$$\sigma_{bn}^2 = \int_{-f_B}^{f_B} \frac{\sigma_n^2}{f_S} df = \sigma_n^2 \left(\frac{2f_B}{f_S} \right) \quad (1.2)$$

The design specifications of the analogue AA filter are substantially reduced because oversampling results in a much wider transition band between the cut-off and Nyquist frequencies, (i.e. AA filter passband is much narrower compared with its transition band). However, a price is paid in the digital domain, which requires the subsequent digital filter to attenuate as much out-of-band quantisation noise power as possible [Azi96]. A less obvious advantage that is served by the use of this digital filter is that any other noise that may have remained in the transition band after the AA filter will be furthermore attenuated [Azi96].

Practical difficulties still exist with standard oversampling converters in spite of their numerous advantages. Extremely high resolutions are virtually unattainable because gigantic sampling frequencies are needed which to-date are beyond the scope of existing CMOS techniques [Azi96]-[Ste98].

1.6 Sigma-Delta Modulation

Sigma-delta (Σ - Δ) modulation is a popular technique that may be employed in A/D conversion for low to medium signal bandwidth applications. Typical areas of application include high-fidelity audio, speech processing, metering applications, data-acquisition and voiceband data telecommunications [Azi96]-[Can92]-[Hau91].

Σ - Δ modulation utilises oversampling and noise-shaping in order to achieve a high level of resolution. It is well known that oversampling leads to the reduction of quantisation noise power in the signal band of interest by distributing this fixed amount of noise over a much wider frequency range. This in-band quantisation noise can be further suppressed by a process known as noise-shaping. This technique does not reduce the magnitude of the quantisation noise, but instead causes most of this shaped noise to be shifted outside the signal band of interest, where it can be subsequently removed by using an appropriate digital filter [Azi96]-[Can92]-[Ste98].

A comparison based on the amount of quantisation noise power for Nyquist, oversampling and Σ - Δ A/D converters is shown in Figure 1.3. It is seen that all the

quantisation noise power occurs across the signal bandwidth for the Nyquist case. In oversampling converters, the in-band quantisation noise power is significantly reduced, because this fixed noise is distributed over a much greater frequency area. Noise-shaping Σ - Δ modulation achieves more quantisation noise attenuation in the signal region by pushing away significant amounts of this unwanted noise outside the signal band. Since the signal power is the same in all three cases, this implies that the best in-band SNR is accomplished by using Σ - Δ modulators [Kal96]-[Mor96c].

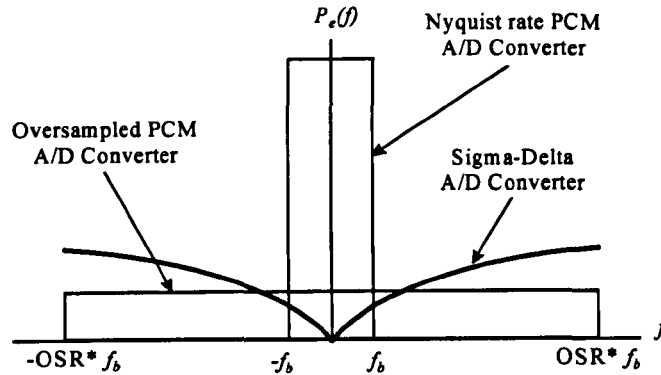


Figure 1.3 Comparison of Quantisation Noise PSD for three A/D Converter Techniques.

The benefits of Σ - Δ A/D converters include inherent linearity due to the 1-bit quantiser, reduced AA filter complexity, greater tolerance to device and component non-idealities and a straight-forward trade-off between bandwidth and resolution. The general block diagram of a Σ - Δ A/D converter is shown in Figure 1.4. This system contains a continuous-time AA filter, a uniform sampler, a discrete-time analogue filter embedded in feedback loop and a digital decimator.

The analogue section may be implemented using Switched Capacitor (SC) [Baz98]-[Chu98]-[Jan93]-[Lon93]-[Sin95] or Switched Current (SI) [Pat94]-[Ros95]-[Ros99] technology. Continuous-time Σ - Δ modulators have been designed and implemented for numerous communication systems applications [Che99]-[Eng99b]. They are different from discrete-time implementations in that they can be implemented by using LC filters [Gao98]-[Sho94]. Continuous-time modulators can operate at very high sampling rates, because they do not require input sample and hold circuits. In addition, the use of continuous-time filters allows very low noise figures compared with discrete-time filters. However, good linearities of the loop-filter and D/A converter are quite difficult to attain for continuous-time modulators [Che99]-[Sho94].

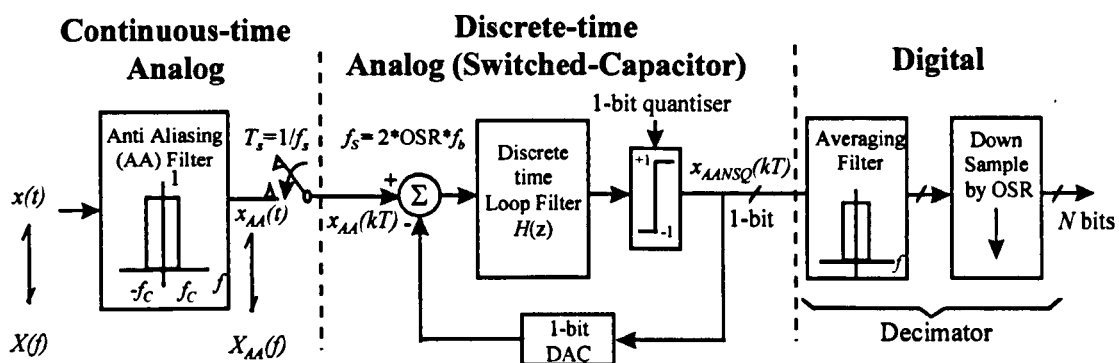


Figure 1.4 Block Diagram of an Oversampled Noise-Shaping Σ - Δ A/D Converter.

1.7 Digital-to-Analogue Σ - Δ Modulators

Oversampled Σ - Δ modulators can be equally used to improve the accuracy of D/A conversion, where digital complexity and speed can be traded for relatively high-tolerance analogue circuitry [Can92]-[Nor97, pp. 309]-[Tom94, pp. 224], Figure 1.5 contrasts the block diagrams of A/D and D/A Σ - Δ modulators.

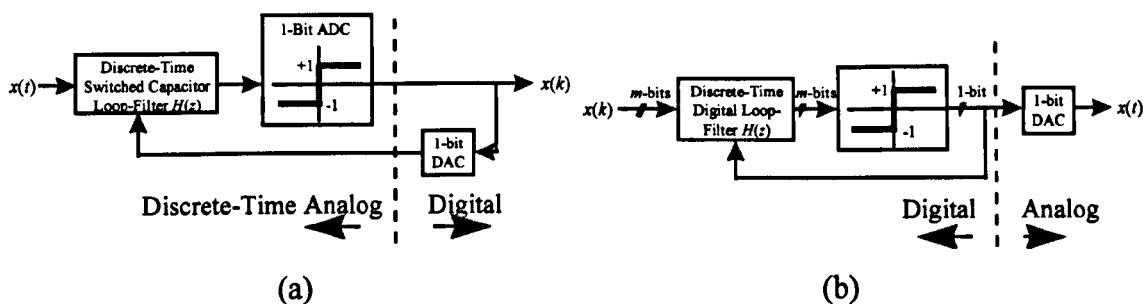


Figure 1.5 Σ - Δ Modulator Configuration (a) as A/D converter (b) as D/A converter.

The input $x(k)$ to the D/A structure is a multi-bit digital signal. This signal then feeds into the loop-filter, which with the aid of the feedback pushes the quantisation noise components outside the signal region. The multi-bit digital signal leaving the loop-filter is truncated to a single-bit before entering the 1-bit D/A converter. Note also that the circuitry in D/A Σ - Δ modulators is predominantly digital as opposed to A/D Σ - Δ modulators where it is mainly analogue. Detailed design analysis for high resolution multiplier-free Σ - Δ modulators for D/A applications are reported in [Hau95].

1.8 The Classical Linear White Noise Model

Quantisation is an inherently non-linear operation making the exact analysis of Σ - Δ modulators a very complicated process, thus necessitating the use of approximate linear methods. The simplest model can be represented by a summer having two inputs as shown in Figure 1.6.

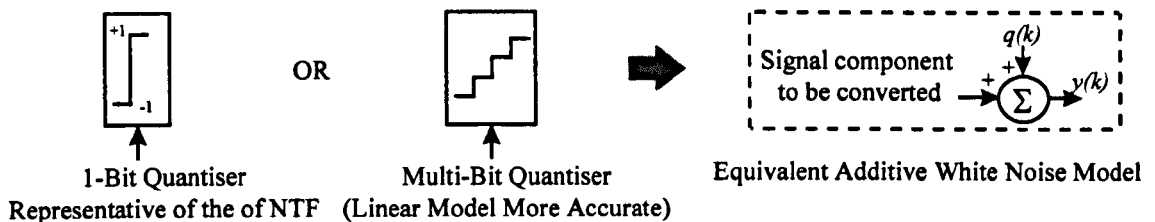


Figure 1.6 The Equivalent Linearised White Noise Model.

The first represents the signal components and the second input depicts the quantisation noise. The latter is modelled by a unity-gain white noise source and is assumed to be uncorrelated with the input signal.

This model has several limitations, which have to be considered when investigating the behaviour and performance of the overall modulator [Ada91]-[Gra90b]. First; it assumes that the quantisation noise has unity gain neglecting the fact that the quantiser gain depends on the properties of the modulator input signal. Second; this model cannot predict the effect of the input signal and loop-filter initial conditions on the stability of the modulator. Third; the tonal behaviour including the location and strength of the limit cycle oscillations cannot be established from such a model. Fourth; the inclusion of a scaling factor prior to the quantiser in the modulator will not affect the decision of the quantiser as the sign of a number does not change by multiplication. However, this gain factor will affect the transfer function of the modulator in a significant way. Fifth; this model does not obey the constant output power criterion, which is an inherent feature of single-bit Σ - Δ modulators. In other words, making the linear model stable does not guarantee that the real non-linear modulator is stable [Ada91]-[Gra90b]-[Nor97, pp. 44].

Despite these constraints, the additive white noise model is straightforward to apply and is widely used by many practitioners in the field for preliminary design analysis. It provides a reasonably accurate representation of the overall spectral shape of the noise transfer function for single-bit Σ - Δ modulators. More accurate analysis and performance

evaluation can be achieved subsequently by detailed simulations that take into account the actual non-linearity of the quantiser [Can92].

This model depicts the quantisation spectra of high-order single-bit modulators, dithered modulators or multi-bit modulators more accurately as the quantisation noise in all these cases becomes more randomised [Azi96]-[Nor97, pp. 44].

1.9 First-Order Σ - Δ Modulator

The first-order Σ - Δ modulator shown in Figure 1.7 consists of a loop-filter and a 1-bit quantiser (A/D converter) in the feedforward path as well as a 1-bit D/A converter in the feedback path. The modulator input goes to the quantiser via the loop-filter. The quantiser output signal is feedback and subtracted from the input at the summing junction. The positive and negative errors between the input and output signals are all accumulated in the loop-filter. These errors, which essentially depend on the amplitude and complexity of the input signal, cancel each other out after a number of clock cycles. It is seen from Figure 1.7 that the digital output is converted by means of a 1-bit D/A converter and then subtracted from the analogue input. The resultant error is transmitted through the loop-filter and the 1-bit quantiser respectively [Azi96]-[Can92]-[Tom94].

The loop-filter is designed so as to provide a large gain in the in-band region. The modulator output at these frequencies is dependent on the feedback implying that the modulator performance is quite insensitive to the tolerance of the constituent analogue circuitry of the loop-filter. The tolerance for imprecise analogue components is a key advantage and is directly responsible for the robustness of Σ - Δ modulators. The feedback must contain a delay equal to at least one sample period to make the modulator realisable. This delay could also be embedded in the loop-filter as shown in Figure 1.7 [Can92]-[Tom94].

For non-single-bit modulators, the linearity of the modulator output depends to a large extent on the linearity of the D/A. This means that a non-linear D/A will result in harmonic distortion, thus increasing the quantisation noise in the in-band region [Azi96]-[Nor97, pp. 244].

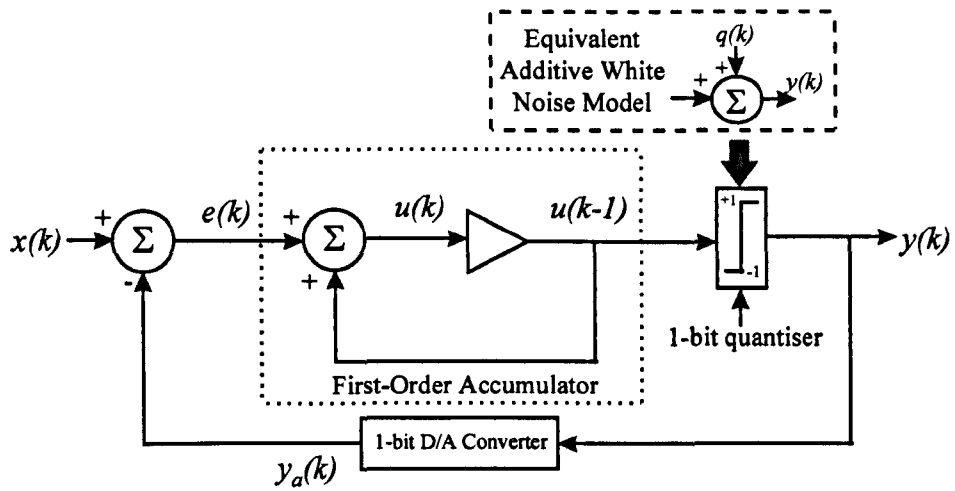


Figure 1.7 Conventional First-Order Lowpass Σ - Δ Modulator.

An example of the exact operation of a first-order is illustrated in Figure 1.8 for a dc input signal of 0.6, assuming that the output initial condition of the loop filter $u(k-1) = 0$, where T_{LC} is the period of the Limit Cycle.

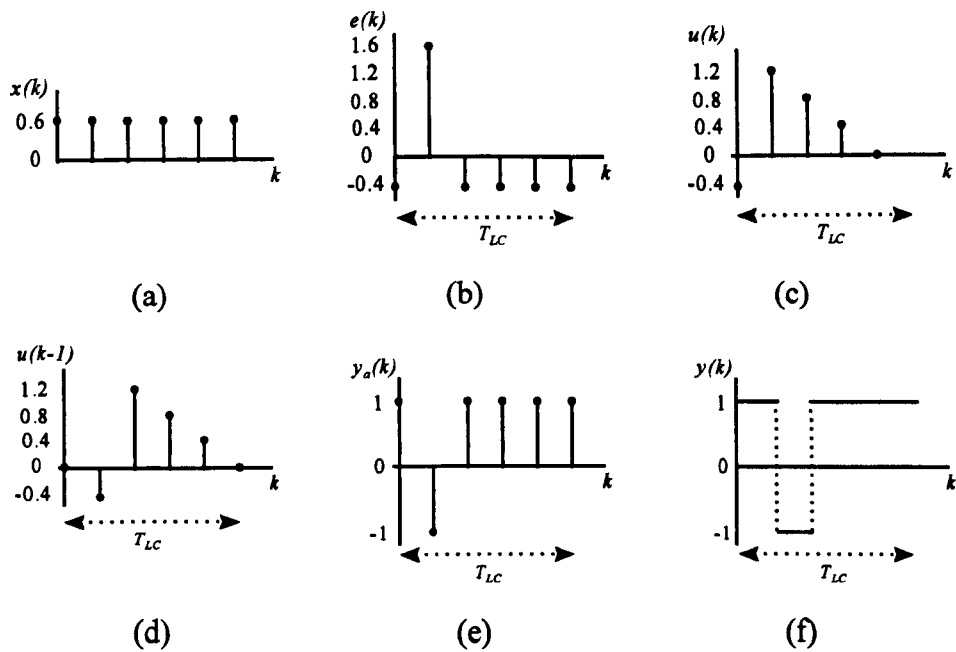


Figure 1.8 Time-Domain Response of a First-Order Lowpass Σ - Δ Modulator: (a) dc input $x(k)$, (b) error signal $e(k)$, (c) output signal at summation node of accumulator $u(k)$, (d) accumulator output signal $u(k-1)$, (e) converted analogue signal $y_a(k)$, (f) quantised output signal $y(k)$.

Table 1.3 shows the signal values at each node of the Σ - Δ modulator, where it can be seen that a maximum of 5 clock cycles containing four 1's and a single -1 are needed to

represent an input amplitude of 0.6, (i.e. $(4(1) + 1(-1))/5 = 0.6$). This analysis demonstrates that the average stream of 1's and -1's of the modulator output over the duration of a cycle is equivalent to the input signal. A Σ - Δ modulator generates outputs composed of ± 1 for any other types of input signal, where its amplitude is determined by the relative density of 1's and -1's.

k	$x(k)$	$e(k)$	$u(k)$	$u(k-1)$	$y_a(k)$	$y(k)$
0	0.6	-0.4	-0.4	0	1	1
1	0.6	1.6	1.2	-0.4	-1	-1
2	0.6	-0.4	0.8	1.2	1	1
3	0.6	-0.4	0.4	0.8	1	1
4	0.6	-0.4	0	0.4	1	1
5	0.6	-0.4	-0.4	0	1	1
6	0.6	1.6	1.2	-0.4	-1	-1

Table 1.3 Discrete-Time Analysis of the First-Order Σ - Δ Modulator.

The stability of a Σ - Δ modulator depends on the input signal, the loop-filter coefficients, initial conditions as well as the modulator order. The first-order ideal accumulator-based Σ - Δ modulator in Figure 1.7 can be shown to be permanently stable for comparator output levels of ± 1 if the input to the system never exceeds unity. Given that $e(k) = x(k) - y_a(k)$ and that $v(k) = x(k) - y_a(k) + u(k-1)$, the analysis provided in Table 1.4 shows that all the internal signals within the modulator never exceed ± 2 for the worst case input signal amplitude fluctuation from +1 to -1 and vice-versa. This implies that $-2 \leq u(k-1) \leq +2$, which means that the quantiser can not become overloaded.

k	$x(k)$	$e(k)$	$u(k)$	$u(k-1)$	$y_a(k)$	$y(k)$
0	1	0	0	0	1	1
1	-1	-2	-2	0	1	1
2	-1	0	-2	-2	-1	-1
3	1	2	0	-2	-1	-1
4	1	0	0	0	1	1

Table 1.4 Worst-Case Discrete-Time Analysis Demonstrating the Inherent Stability of a First-Order Σ - Δ modulator.

A modulator becomes unstable when the quantiser input amplitude significantly exceeds the magnitude of the signal in the feedback path. The input signals in the feedforward path continue growing indefinitely causing the quantiser to enter into chaotic and unrecoverable oscillations.

The modulator stability can be more accurately evaluated by examining the amplitude and nature of the quantiser input signal. Several comparable rules of thumb have been proposed, which are used to estimate the point at which the quantiser input signal diverges, thus leading to modulator instability.

The operation of a first-order Σ - Δ modulator may be further understood by the use of mathematical analysis in the frequency-domain where the linear model discussed in Section 1.9 is applied. This linear modeling process enables the overall modulator to be characterised by a Signal Transfer Function (STF) $H_S(z)$ and a Noise Transfer Function (NTF) $H_N(z)$:

$$H_S(z) = \frac{L(z)}{1 + L(z)} \quad \text{and} \quad H_N(z) = \frac{1}{1 + L(z)} \quad (1.3)$$

where $L(z)$ is the formed loop-filter. Mathematical manipulation shows that both $H_S(z)$ and $H_N(z)$ are inter-related as demonstrated by the expression below:

$$H_N(z) = 1 - H_S(z) \quad (1.4)$$

The z-domain transfer function of $H(z)$ in this case is given by

$$L(z) = \frac{z^{-1}}{1 - z^{-1}} \quad (1.5)$$

which implies that the overall output expression in the z-domain is

$$Y_1(z) = z^{-1}X(z) + (1 - z^{-1})Q(z) \quad (1.6)$$

where $H_S(z) = z^{-1}$ and $H_N(z) = (1 - z^{-1})$.

It can be observed from both of the above expressions that the input signal has been merely delayed by one sample resulting in no distortion. However, the quantisation noise has been shaped by a first-order differencer, which is effectively equivalent to a crude highpass filter. Thus, the quantisation noise has been shifted to higher frequencies leaving the input signal completely intact. Closer inspection of the NTF reveals that virtually infinite attenuation is achieved at dc (i.e. $z = 1$).

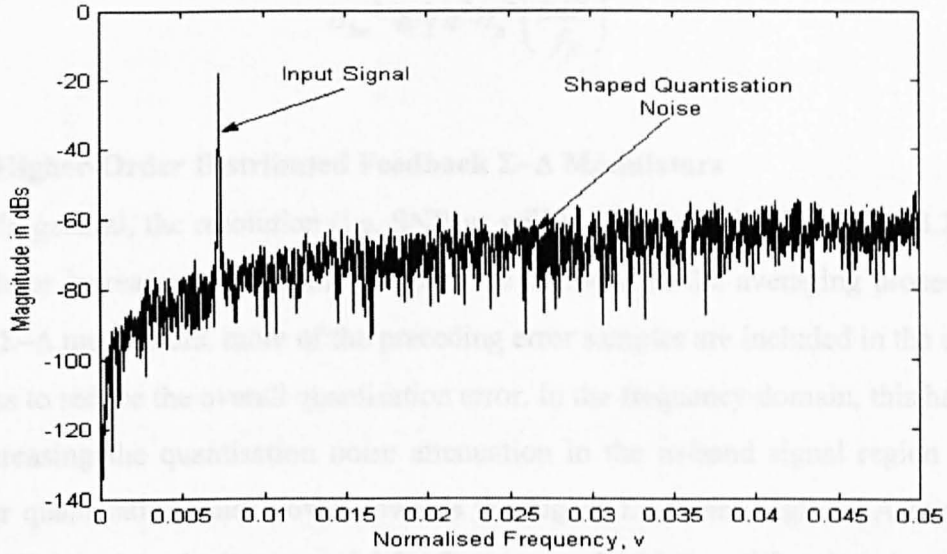


Figure 1.9 Magnitude Spectrum of an accumulator-based lowpass Σ - Δ modulator.

Figure 1.9 shows the simulation results of a first-order Σ - Δ modulator in the frequency-domain employing a simple 1-bit non-linear quantiser. An input sinusoid having a frequency f_C of 0.025. These simulation results confirm theoretical expectations in that the input appears undistorted in the baseband region. The signal has been Fourier-transformed to a delta function in the frequency-domain and the quantisation noise has been shaped away to higher frequencies. Dither is added prior to the quantiser input to substantially alleviate the level of tones in the frequency spectrum.

Theoretical expectations coupled with simulation results confirm that with sufficiently large f_S , Σ - Δ modulators can achieve very respectable SNRs using only 1-bit quantisers. The performance of Σ - Δ modulators is primarily dependent on the NTF which has a magnitude frequency response of

$$H_N(f) = 2 \left| \frac{\sin \pi f}{f_S} \right| \quad (1.7)$$

The in-band quantisation noise power is given by

$$\sigma_{bn}^2 = \int \frac{\sigma_n^2}{f_S} |H_N(f)|^2 df \quad (1.8)$$

where σ_n^2/f_S is the power spectral density of the quantisation noise. This ultimately yields in-band quantisation noise power provided that $f_S \gg f_B$ and where σ_{bn}^2 can be expressed to a good approximation as

$$\sigma_{bn}^2 \cong \frac{1}{3} \pi^2 \sigma_n^2 \left(\frac{2f_B}{f_S} \right)^3 \quad (1.9)$$

1.10 Higher-Order Distributed Feedback Σ - Δ Modulators

In general, the resolution (i.e. SNR as will be discussed in Section 1.13.2) of a Σ - Δ modulator increases, when more samples are included in the averaging process. In high-order Σ - Δ modulators, more of the preceding error samples are included in the cancellation process to reduce the overall quantisation error. In the frequency-domain, this has the effect of increasing the quantisation noise attenuation in the in-band signal region by shifting greater quantisation noise power towards the higher frequency regions. A comparison of the NTFs based on the linear model for first-, second-, third- and fourth-order conventional lowpass Σ - Δ modulators is shown in Figure 1.10.

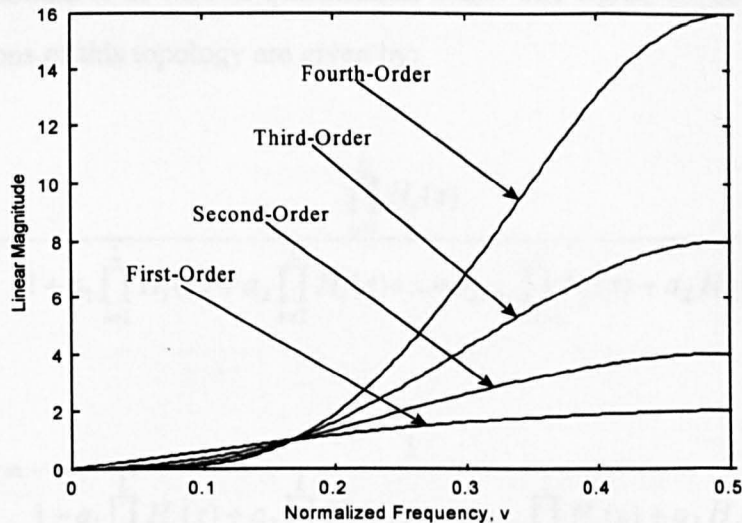


Figure 1.10 Comparison of the NTF Magnitude Spectra for First-, Second-, Third- and Fourth-Order Σ - Δ modulators.

The order of a Σ - Δ modulator may be simply increased by employing the distributed feedback topology, where the modulator output signal feeds back in a distributive manner at the input summing nodes of each loop-filter as shown in Figure 1.11 [Ada91]-[Rit77].

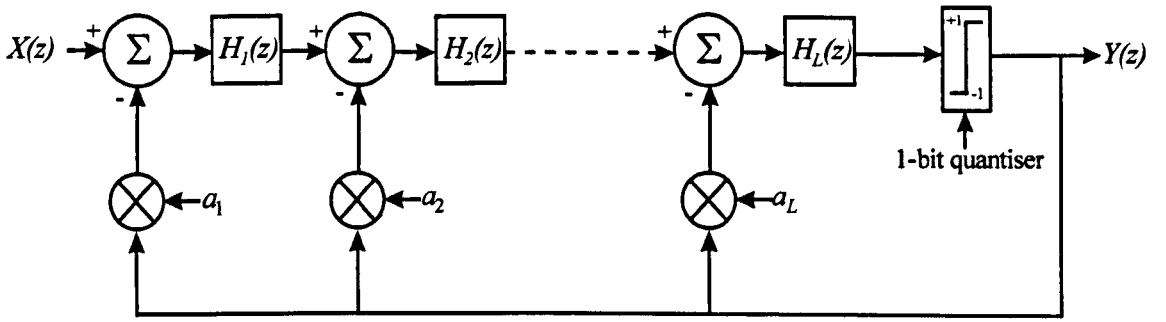


Figure 1.11 Chain of Accumulators with Distributed Feedback.

The signal feeding into the loop-filter is the summation of two inputs. The first input path is the output of the previous loop-filter and the second is the 1-bit output signal scaled by a feedback coefficient. Thus, each loop-filter output contains a combination of the input signal to the modulator as well as quantisation noise. The signal $H_S(z)$ and noise $H_N(z)$ transfer functions of this topology are given by:

$$H_S(z) = \frac{\prod_{i=1}^L H_i(z)}{1 + a_1 \prod_{i=1}^L H_i(z) + a_2 \prod_{i=2}^L H_i(z) + \dots + a_{L-1} \prod_{i=L-1}^L H_i(z) + a_L H_L(z)} \quad (1.10)$$

$$H_N(z) = \frac{1}{1 + a_1 \prod_{i=1}^L H_i(z) + a_2 \prod_{i=2}^L H_i(z) + \dots + a_{L-1} \prod_{i=L-1}^L H_i(z) + a_L H_L(z)} \quad (1.11)$$

Higher-order single-bit Σ - Δ modulators are more prone to instability compared with first-order Σ - Δ modulators. Their stability depends on the feedback coefficients, gain factors in the loop-filter, the modulator input amplitude, the type of input signal and its harmonic content as well as the total delay in the feedback loop [Bai93]. Note that the Σ - Δ modulator coefficients may be adjusted to ensure or improve stability as long as the desired specifications of the noise-shaping function are maintained [Bai94]-[Nor97, pp. 141].

Higher-order single-bit structures are capable of producing respectable SNRs for modest OSRs, are less tonal and have low sensitivity to component mismatches [Ada91]. However, the resultant sharp rise of the quantisation noise in the out-of-band region

imposes more stringent specifications on the decimation filter [Tom94]. The desirability for high resolution coupled with the outlined design challenges have resulted in the existence of many alternative types and combinations of higher-order Σ - Δ modulator topologies as reported in [Ada91].

1.11 Multi-bit Σ - Δ modulators

An alternative means of improving the resolution of Σ - Δ modulators is to replace the single-bit quantiser with a multi-bit quantiser as shown below in Figure 1.12. Multi-bit noise-shaping Σ - Δ modulators generate less quantisation noise by as much as 6 dB per additional bit, compared with conventional 1-bit modulators [Nor97, pp.244]-[Tom, pp. 224].

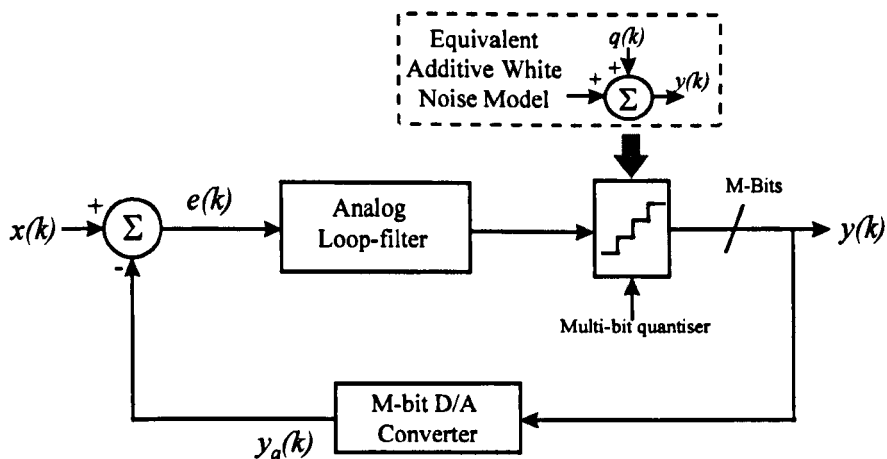
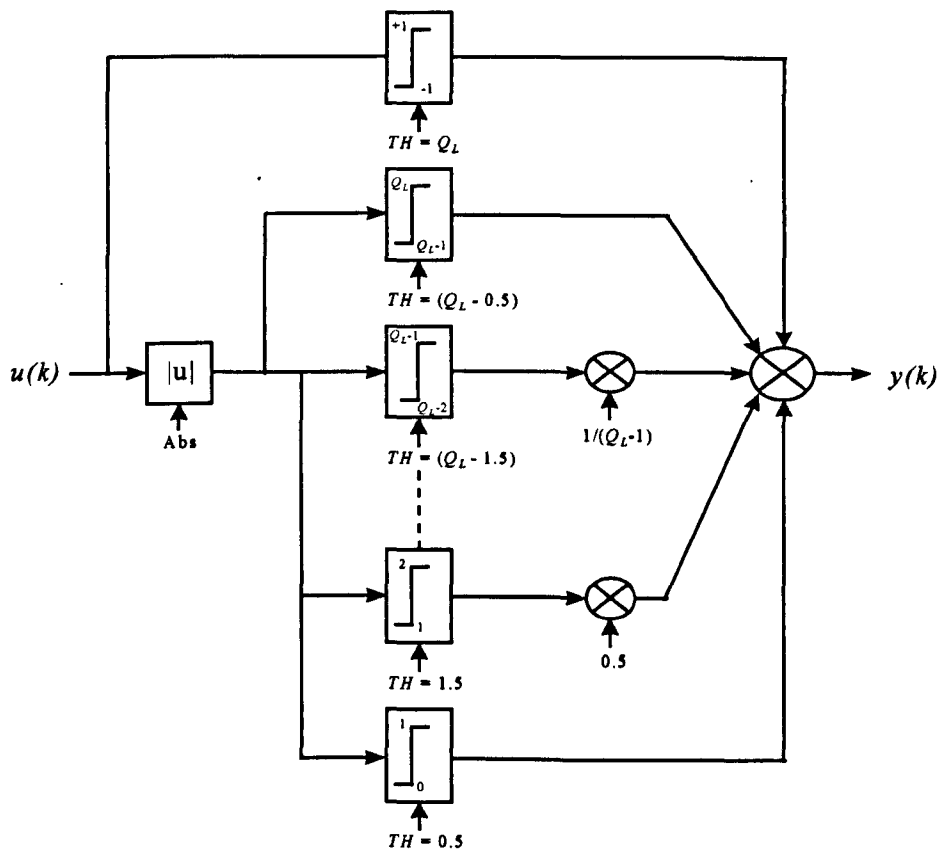
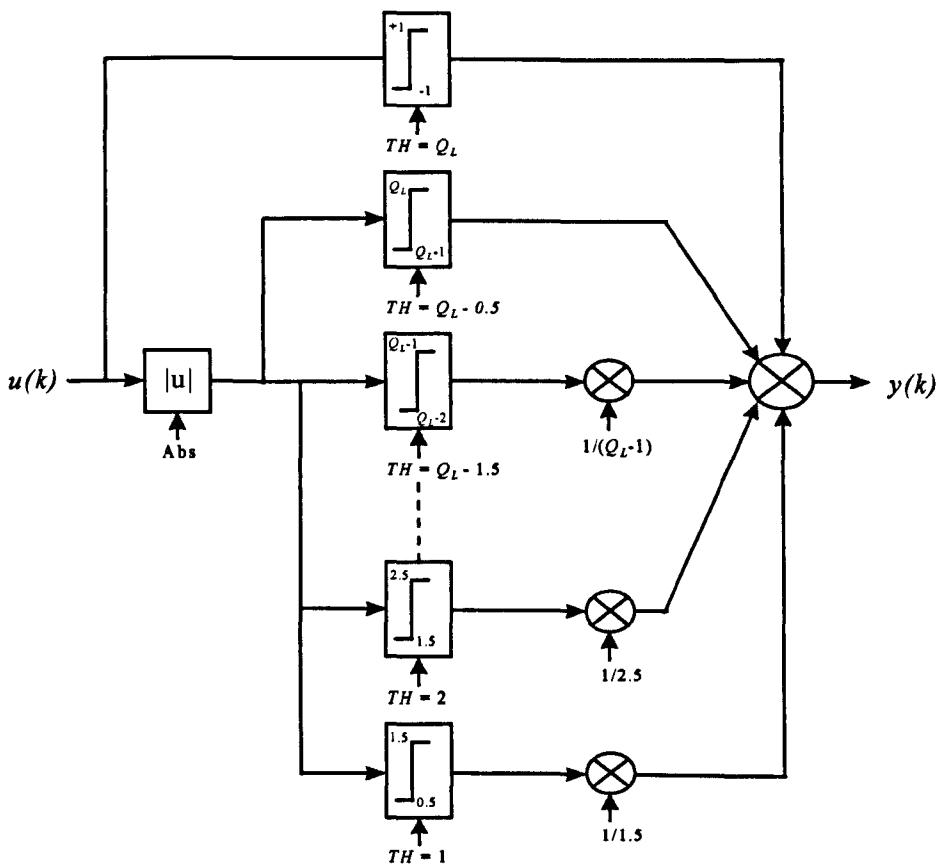


Figure 1.12 General Block Diagram of a Multi-Bit Σ - Δ Modulator.

Multi-bit quantisers containing an odd and an even number of levels were designed by the author in Simulink. A block diagram representation of both models shows that these consist of two-level comparators as shown in Figure 1.13, where TH represents the threshold value for each comparator and Q_L is the quantisation level.



(a)



(b)

Figure 1.13 Multi-Level Quantiser Model (a) Odd Number (b) Even Number.

Multi-bit Σ - Δ modulators are capable of generating high SNRs for reasonably low OSRs. They are much easier to stabilise, thus facilitating the design of higher-order systems. The presence of more levels causes the quantisation noise to be more randomised, thus reducing the occurrence of spurious tones across the frequency spectrum. The reduction in quantisation noise alleviates the constraints on the post output filter that must remove the out-of-band quantisation noise. The use of multi-bit quantisers makes the modulator more linear, thus making the adoption of the additive white noise model for analysis more realistic. Also, the gain of a multi-level quantiser tends towards unity as the number of levels is increased [Sti88]-[Nor97, pp. 244].

The inherent linearity offered by single-bit A/D Σ - Δ converters is not preserved with multi-bit A/D converters, because the latter require multi-bit D/A in the feedback path, whose linearity directly affects that of the output signal. The errors resulting from the D/A converter benefit from oversampling, but not noise-shaping [Sim89]-[Tom94, pp. 224].

1.12 Simulation Approach

The non-existence to-date of a theoretical model [Gra89a] that can precisely predict the stability range and tonal properties of Σ - Δ modulators, when in overload mode, provides ample justification for resorting to behavioural level simulations. These are shown by many designers and practitioners to be the most appropriate means of evaluating the performance of Σ - Δ modulators. The time taken for behavioural methods to deliver the results of the simulated topologies is much shorter compared with device and circuit-based macro-models. Furthermore, Σ - Δ modulators can be constructed and re-configured quite easily. Needless to say, behavioural level simulations must be performed before the circuit is designed as these help to validate the modulator performance with relative ease. The main objective is to adequately simulate all the characteristics. Both a large number of time steps and input values must be used to examine long term behaviour and identify any irregularities [Ben99]-[Nor97, pp. 447].

All the Σ - Δ modulators in this thesis utilise a simulation environment, Simulink in Matlab, to model and simulate the behaviour of Σ - Δ modulators in discrete-time using floating-point arithmetic for the analogue parts and the actual single-bit quantiser.

These simulations are conducted by injecting a single-tone or multiple tone sinusoids to all Σ - Δ modulators for an input block length of 282144 samples. The first 20000 output samples from the modulator are excluded as transient points. The remaining 262144 (2^{18}) output samples are transformed using a Hanning-windowed Fast Fourier Transform (FFT)

on the output of the modulator. Note that the FFT length is always chosen to be a multiple of 2 to enhance simulation speed in Matlab. The input amplitude is progressively increased in steps of 0.01 from 0 to 1 for $k \in [0 \dots 282144]$. Each modulator is evaluated with zero initial conditions at first. This procedure is then repeated for a random choice of initial conditions, ranging from -0.1 to +0.1. Figure 1.14 shows a plot comparing the simulation time versus the number of simulated points for a second-order single-stage Σ - Δ modulator.

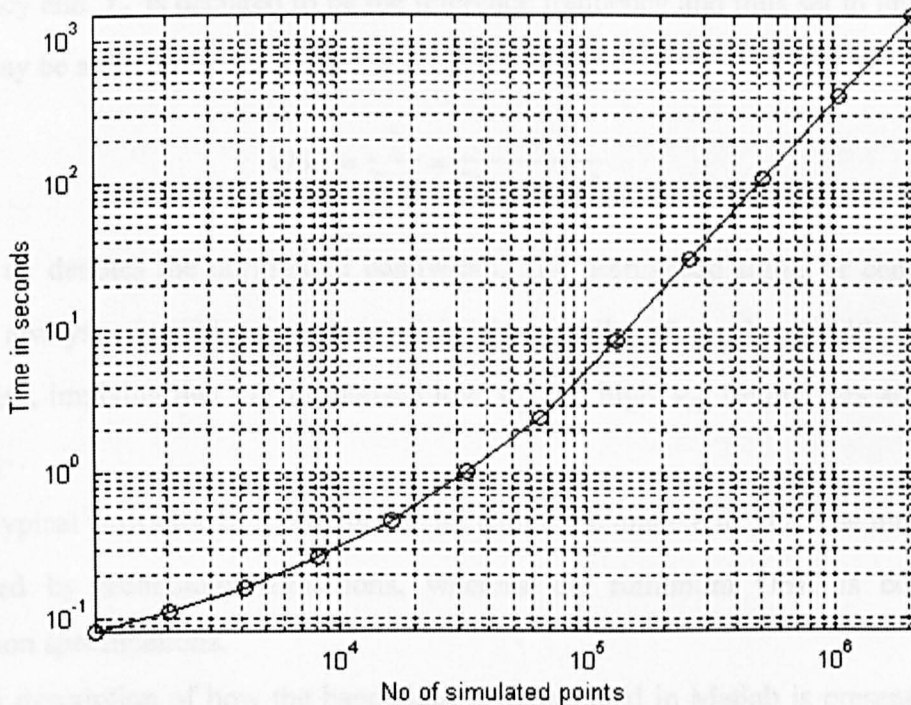


Figure 1.14 A Comparison of Simulation Time versus Number of Simulated Samples

1.13 Performance and Accuracy Criteria

This section presents the most commonly used evaluation criteria by practitioners to verify the operation and assess the quality of Σ - Δ modulator topologies. A description of how these performance measures are developed into automated routines in Matlab to facilitate and improve simulation speed is provided. The ability to build Σ - Δ modulator structures in Simulink with relative ease coupled with these automated Matlab based tools provide both rapid and reliable means for novice and experienced engineers to accurately model and evaluate any Σ - Δ modulator topology.

1.13.1 Oversampling Ratios and Bandwidth

The OverSampling Ratio (OSR) is defined as the ratio of the sampling frequency f_S to that of twice the signal bandwidth f_B . This is mathematically given by:

$$OSR = f_s / 2f_B \quad (1.12)$$

The signal bandwidth refers to the range of frequencies, where the power of the signal components is concentrated. Given that this thesis primarily deals with the design of Σ - Δ modulators at the behavioural level, it is more convenient to express all frequencies in terms of their normalised equivalents ν 's (i.e. $\nu = f / f_s$), where f is the input signal frequency and f_s is declared to be the reference frequency and thus set to unity. Thus, the OSR may be alternatively expressed as:

$$OSR = \frac{1}{2\nu_B} = \frac{1}{2(\nu_H - \nu_L)} \quad (1.13)$$

where ν_B denotes the normalised bandwidth. The normalised signal or centre frequency ν_C is always assumed to be located in the middle of the bandwidth, unless stated otherwise, implying that the normalised low ν_L and high ν_H frequencies are equi-distant from ν_C .

Typical OSRs for Σ - Δ modulators lie within the range 8 to 512. The maximum f_s is restricted by technology limitations, whereas the minimum OSR is constrained by resolution specifications.

A description of how the bandwidth is determined in Matlab is presented next. It is well known that any discrete-time signal in Matlab is represented by samples or bins, whose number N_{SAM} is decided by the user. For a given OSR, the bin positions of ν_L and ν_H and consequently ν_B are given by:

$$N\nu_L = \left(\nu_C - \frac{1}{4 OSR} \right) \quad \text{and} \quad N\nu_H = \left(\nu_C + \frac{1}{4 OSR} \right) \quad (1.14)$$

The difference between $N\nu_H$ and $N\nu_L$ is the number of bins representing ν_B , which simplifies to $(N_{SAM} / 2 OSR)$.

1.13.2 In-Band Signal-to-Noise Ratio (SNR)

The in-band Signal-to-Noise Ratio (SNR) is a fundamental performance measure that is used to assess the degree of resolution of any Σ - Δ modulator. It is defined as the ratio of the signal power to that of the in-band quantisation noise power [Azi96]-[Can92]-[Pro92] and is usually expressed in dBs as shown below:

$$SNR = 10 \log_{10} \left(\frac{\text{Signal Power}}{\text{Inband Noise Power}} \right) \quad (1.15)$$

The theoretical expression using the additive linear white noise model for the SNR of an L^{th} -order lowpass Σ - Δ modulator is given by

$$SNR = 10 \log_{10}(\sigma_x^2) - 10 \log_{10}(\sigma_{bn}^2) - 10 \log_{10} \left(\frac{\pi^{2L}}{2L+1} \right) + (20L+10) \log OSR \quad (1.16)$$

This analytically derived expression demonstrates that the SNR improves by approximately 9 dBs or 1.5 bits of resolution for every doubling of the OSR for a given modulator order. A further enhancement of 6 dBs can be achieved for every corresponding increase in modulator order. This expression only provides a rough estimate. More accurate readings can be obtained by performing long simulation runs based on Σ - Δ modulator models in Simulink. The retrieved data is more reliable, because the Σ - Δ model uses the actual non-linear component, i.e. the 1-bit quantiser, therefore circumventing the need to make any assumption about the properties of the quantisation noise. The simulated SNR figures are calculated by dividing the signal power by the sum of the powers of all the bins of the in-band quantisation noise. The corresponding mathematical expressions are:

$$SNR_L = \frac{\sum_{-0.5}^{0.5} |X(\nu)|^2}{\sum_{-\nu_B/2}^{\nu_B/2} |H_N(\nu)|^2} \quad (1.17)$$

$$SNR_B = \frac{\sum_0^{0.5} |X(\nu)|^2}{\sum_{\nu_L}^{\nu_H} |H_N(\nu)|^2} \quad (1.18)$$

where the SNR for a lowpass signal, the SNR for a bandpass signal, the input signal spectrum and the magnitude spectrum of the NTF are represented by SNR_L , SNR_B , $X(\nu)$ and $H_N(\nu)$ respectively.

There are two simulation methods for computing the in-band quantisation noise power. The simplest involves subtracting the input signal from the modulator output so as to only acquire all the bins that depict the NTF. The in-band quantisation noise region can be then computed for a given bandwidth. This method is restricted to working for input tones that reside in the middle of the notch of the NTF. Any slight misalignment in the signal location creates a phase-shift, which prevents the complete cancellation of the input

signal. For the majority of such cases, the estimation of this phase-shift and the subsequent re-adjustment of the signal notch becomes rather complicated.

The complication arising from the above method has led to the creation of the following empirically-derived general-purpose approach. Here, the in-band quantisation noise is computed by identifying both the location and the number of bins that represent the input signal and then removing them from the output spectrum. This yields a good estimation of the actual NTF, which can be used to calculate the in-band SNR. It should be noted that the signal width in terms of bin numbers largely depends on the number of sample points.

This method was verified with the first approach for a variety of frequencies and their corresponding NTFs, where total input signal cancellation was accomplished. The discrepancy between the two methods for a range of input amplitude levels was less than 0.5 dB.

The amplitude of all signals following the FFT command need to be normalised to unity by dividing by the FFT length, before subsequent calculations are carried out. This measure is particularly crucial for sinusoidal signals as these transform to impulses in the frequency-domain.

It should be stated that both the signal and in-band quantisation noise powers were scaled down by $3/8$ due to the amplitude of the Hanning window. A derivation from first principles by the author proving this value is included in Appendix A for completion. There is no need for any correction factor as far as the in-band SNR is concerned as both entities are reduced equally. However, if the input or in-band quantisation noise powers are individually required, then their corresponding simulated values need to be scaled-up by $8/3$ so as to normalise the amplitude back to unity.

Each SNR curve is generated from 100 input amplitudes ranging from full-scale down to the input amplitude level, whose power equals the total in-band quantisation noise power (i.e. until the SNR value is 0 dB). Each point is calculated using a 262144 point Hanning windowed FFT.

Note that the in-band SNR deteriorates for very large input amplitudes due to quantiser overloading. In addition, in-band SNR degradation also occurs for small input levels as a result of little signal power.

1.13.3 Maximum Stable Input Amplitude

The non-existence to date of a theoretical model [Gra90] that can precisely predict the stability range of a Σ - Δ modulator when in overload mode provides a powerful argument for resorting to behavioural level simulations. In this thesis, the stability of a Σ - Δ modulator is evaluated by increasing the input amplitude from 0 to 1 in steps 0.01 for $k \in [0 \dots 282144]$ with a random choice of initial conditions ranging from 0 to 0.1. The stability of any Σ - Δ modulator can be reliably predicted by monitoring the quantiser input amplitude $q_{IN}(k)$ as described in [Sch93]. Knee plots are used to establish the input amplitude that results in $q_{IN}(k)$ exploding towards infinity. A knee value for $q_{IN}(k)$ as given below is declared to be a suitable upper-limit to indicate instability.

$$|q_{IN}(k)| \leq 10 \quad (1.19)$$

The first quantiser input amplitude that reaches 10 is declared to be the threshold quantiser input, $q_{INMAX}(k)$. Its corresponding input signal amplitude is therefore determined and declared to be the Maximum modulator Stable Input Amplitude (MSIA). This process is repeated 10 times with a different set of initial conditions where the worst-case MSIA value is retained.

It may be argued that the input quantiser constraint is rather conservative. It is plausible that $q_{IN}(k)$ may quite harmlessly exceed 10 momentarily, before subsiding back to much lower values. This may especially occur in the case of higher-order single-bit Σ - Δ modulators. However, in the opinion of the author, it is better to underestimate as real world signals can rarely be completely band-limited. This practicality coupled with non-idealities in implementation support the argument for being prudent. A recommendation in [Sch91b] goes further by stating that MSIA should never exceed 85-90% of the peak input amplitude as a safety margin. This precaution becomes more significant in the case of aggressive NTFs, e.g. Chebyshev as opposed to Butterworth bandstop filters.

1.13.4 Dynamic Range (DR)

Another useful type of performance measure is the Dynamic Range (DR), which is defined as the range of input amplitudes for which the Σ - Δ modulator produces a positive SNR. A theoretically derived DR based on the linearised additive white noise model for an L^{th} - order lowpass Σ - Δ modulator is given by:

$$DR = \frac{3}{2} \left(\frac{2L+1}{\pi^{2L}} \right) (2^N - 1)^2 OSR^{2L+1} \quad (1.20)$$

which shows that DR depends on the OSR, the loop-filter order L and the quantiser resolution N [Nor97, pp. 220]-[Pro92].

As far as simulations are concerned, the DR is computed by finding the difference between the maximum x_{MAX} and minimum x_{MIN} input amplitudes. x_{MAX} refers to the maximum input amplitude level for which the modulator remains stable. On the other hand, x_{MIN} is defined as the input amplitude level, where the input signal power equals the in-band quantisation noise power. The DR is quite often expressed in dBs as shown below:

$$DR = 20 \log_{10}[x_{MAX} - x_{MIN}] \quad (1.21)$$

1.13.5 Tones

Numerous publications involving precise theoretical analyses [Gra89a]-[Gra89b], simulations studies such as [Dun96a]-[Nor97, pp. 75-140] as well as behavioural-level simulations carried out by the author have shown that the quantisation noise spectra of Σ - Δ modulators exhibit discrete tones. Tones are spectral peaks, whose presence in the signal region degrade the resolution of a Σ - Δ modulator. The emergence of these tones is attributed to the following factors:

First; the majority of quantisers employed in Σ - Δ modulators only have two output levels, thus increasing the possibility of similar patterns appearing in the output signal. Furthermore, single-bit quantisers can not handle extremely small input amplitudes, such as 0, by periodically oscillating between +1 and -1 in the time-domain. This oscillatory pattern is translated into a single-tone at $f_S/2$ in the frequency domain [Azi96]-[Ris94]. Second; the quantiser input samples become heavily correlated due to oversampling. Third; the lower order modulators, particularly those that employ simple-coefficient loop-filters such as accumulators and resonators tend to generate fewer, but higher-amplitude tones due to the more finite number of internal signal amplitude levels [Hei91]. These tones become especially undesirable, if they appear in the signal region as this leads to distorted signal outputs and inferior resolution. The amplitude of the tones, the number of times at which they occur as well as their locations in the frequency spectrum depend on the amplitude and type of input signal [Sim89].

There are essentially three techniques that can be used to suppress these tones. The first involves deliberately injecting a white noise signal (i.e. dither) prior to the quantiser input, which randomises the quantisation noise spectrum for a given modulator. The inclusion of dither just before the quantiser takes advantage of noise-shaping, which has the effect of limiting the amount of quantisation noise in the signal region [Nor97, pp. 75]. The second approach involves de-stabilising the limit cycle oscillations responsible for these tones by making the loop-filter chaotic. A small shift in the pole positions of the loop-filter provides a successful means of breaking-up the limit cycle oscillations responsible for the appearance of these objectionable tones [Ris94]-[Sch94]. Third; the use of random initial conditions in the loop-filter sections provides an alternative means of disturbing the periodicity of these limit cycles. Care has to be taken to ensure that the upper limit of these random initial conditions is constrained to appropriate levels, especially for high-order single-bit Σ - Δ modulators [Koz00].

1.13.6 Other Performance Measures

It is worth noting that there are three other types of performance measures found in the open literature. The first is the Signal-to-Noise Distortion Ratio (SNDR) which is defined as the ratio of the power of the input signal to the power of the in-band quantisation noise including harmonic distortion. The second is Spurious Free Dynamic Range (SFDR), which is defined as the power of the input signal to the power of the largest spurious tone for a given Σ - Δ modulator output signal in the frequency domain [Wep95]. The third is the Noise Power Ratio (NPR) which is defined as the ratio of the power spectral density of the noise outside the frequency band to the power spectral density of the noise inside the frequency band [Wep95].

1.14 Concluding Remarks to Chapter 1

In this chapter, the fundamental concepts of Σ - Δ modulators were discussed and compared with conventional Nyquist rate and oversampling A/D converters. The author's contributions to this research programme were stated, where a clear distinction was made between original contributions and extended/development contributions. The latter referred to the work of other Σ - Δ experts, which was judged to be worthy of further research. A summary of the major milestones in the history of Σ - Δ modulators, since their birth in the 1950's was presented. This was followed by a detailed explanation of first- and higher-order lowpass Σ - Δ modulators, including the popular distributed feedback topology. A

description of multi-bit $\Sigma\text{-}\Delta$ modulators was presented, demonstrating the models of the used multi-level quantisers. The simulation approach that has been used to evaluate these $\Sigma\text{-}\Delta$ modulators was described. The chapter concluded by describing the performance criteria that are commonly used to evaluate and assess the accuracy of these modulators such as signal-to-noise ratios and dynamic ranges. A discussion of the reasons for the occurrence of tones in the outputs of these modulators followed by methods to reduce the impact on the resolution of $\Sigma\text{-}\Delta$ modulators was also provided.

Chapter 2

Bandpass Σ - Δ Modulation

2.1 An Overview of Bandpass Σ - Δ Modulation

The concepts of conventional lowpass Σ - Δ modulation are applied to bandpass signal frequency ranges, whose frequency content lie in a narrowband [Pea87]-[Gai89]-[Sch89]-[Hor91]. The resulting system is referred to as a bandpass Σ - Δ modulator [Bry94]-[Jan91b]-[Jan93]-[Thu95]-[Tro93]. In a similar manner to the lowpass case, bandpass Σ - Δ modulators combine oversampling and quantisation noise-shaping to trade-off operation speed for improved amplitude resolution [Pat94]. Many of the advantages are also retained such as reduced anti-alias filter complexity, inherent linearity for single-bit quantiser modulators and robust analogue implementation [Fra95]-[Jan93]-[Nor97, pp. 282].

This implies that Σ - Δ modulation can now be employed to perform A/D conversion directly for high frequency narrow-band signals overcoming the necessity of modulating down to dc first [Fra95]. A diagram showing the constituent building-blocks of a typical bandpass Σ - Δ A/D converter is given in Figure 2.1.

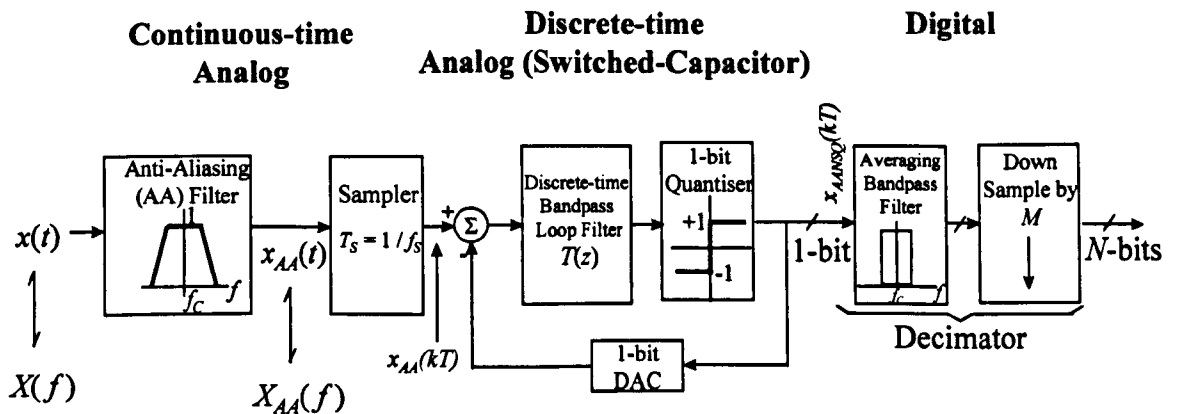


Figure 2.1 Block Diagram of a Bandpass Noise-Shaping Σ - Δ A/D Converter.

Compared with a lowpass Σ - Δ A/D converter, the lowpass AA filter, loop-filter and decimator are replaced with equivalent bandpass filters, whose centre frequencies may reside at any spectral location away from dc. A single-bit bandpass Σ - Δ modulator produces an output signal normally consisting of a string of +1's and -1's, whose average is equivalent to the input analogue signal to the modulator. From a frequency-domain

perspective, bandpass Σ - Δ modulators are designed such that the bulk of the quantisation noise is spectrally shifted to either side away from the signal band [Sch91c] as illustrated in Figure 2.2. Note that f_C and f_B refer to the centre frequency and bandwidth respectively.

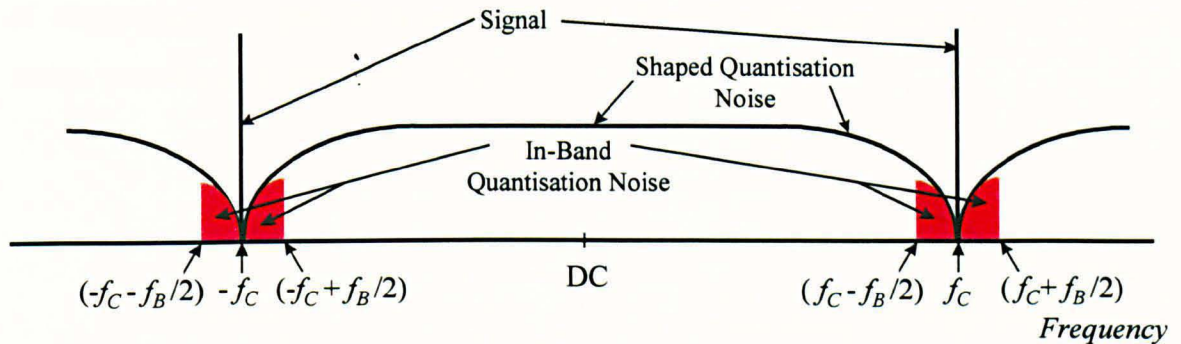


Figure 2.2 Quantisation Noise-Shaping in Bandpass $\Sigma - \Delta$ Modulation.

The original signal, as a result, is left virtually unaffected with substantially less in-band quantisation noise. The shifted quantisation noise as well as any out-of-band signal harmonics and spurious tones are then attenuated by employing an appropriate bandpass filter [Dre91]-[Sch90]. Subsequently; a down-sampler is used to reduce the sampling frequency of the bandpass filtered signal to the Nyquist rate [Dre91]-[Sch90]-[Jan91a].

Bandpass Σ - Δ modulators can be also employed to perform high-resolution D/A conversion [Leo97a]-[Leo97b]. However, it should be made clear from the outset that this thesis primarily deals with the design and evaluation of bandpass Σ - Δ modulators for A/D applications.

The sampling theorem for bandpass signals states that the sampling frequency is only required to be twice the bandwidth of the input signal implying that much higher OSRs can be attained for relatively modest sampling frequencies [Dre91]-[Pro92]. This means that bandpass Σ - Δ modulators can achieve high SNRs at these significantly lower sampling frequencies in contrast with the lowpass case, where f_s is required to be many times greater than the highest frequency component. For example, the conversion of a signal centred at 2 MHz with 20 kHz bandwidth. With a 20 MHz sampling frequency, a lowpass converter would provide five times oversampling, whereas a bandpass Σ - Δ converter would achieve 500 times oversampling [Bry94]-[Dre91]-[Jan91b]-[Jan93].

This chapter starts by providing a chronological survey of reported publications, an up-to-date review of hardware implementations and a summary of potential applications of bandpass Σ - Δ modulators. The existing lowpass-to-bandpass frequency transformation

techniques for mid-band and variable-band resonator-based bandpass Σ - Δ modulators are explained and analysed in greater depth to demonstrate their limitations.

This background information sets the scene for the core objective of the chapter, which is to present, develop and propose different approaches for the system-level design of single-stage bandpass Σ - Δ modulators. A flow-line diagram summarising all these design procedures is illustrated in Figure 2.3.

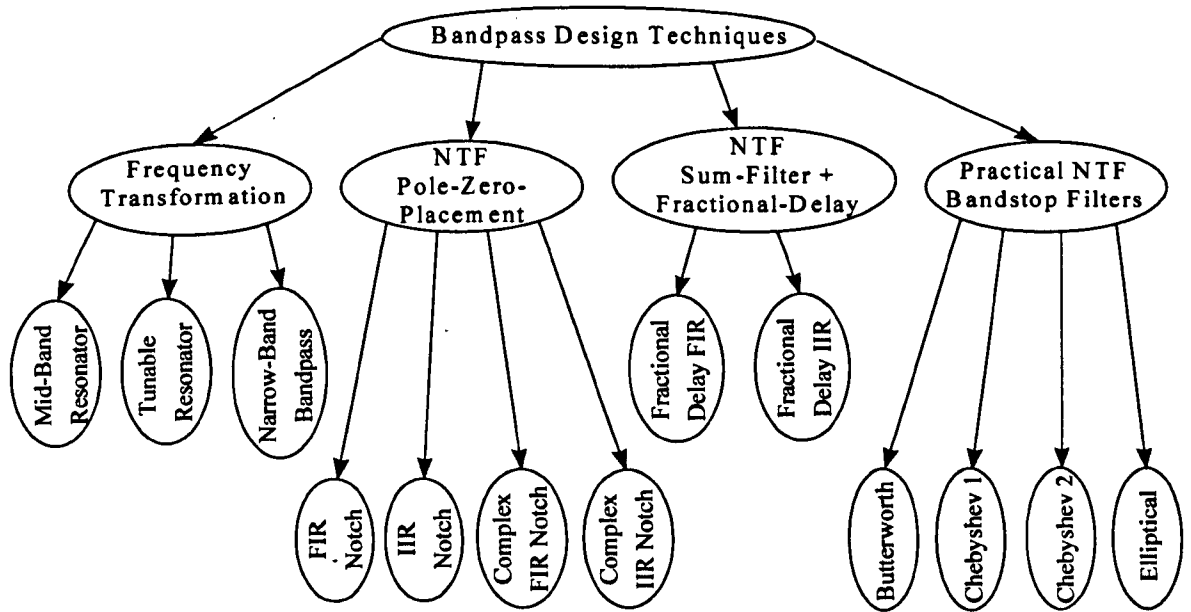


Figure 2.3 Different Techniques for the Design of Bandpass Σ - Δ Modulators.

The following summarises the author's contributions to this chapter: First, the development of the lowpass-to-bandpass transformation technique, where the signal bandwidth as well as the centre of the variable noise-shaping band can be defined for any behavioural-level narrow-band specification. Second, the development of a technique that is well suited for the design of variable-band bandpass Σ - Δ modulators based on the noise transfer functions of FIR notch-filters, IIR notch-filters, complex FIR notch-filters and complex IIR notch-filters. Third, an alternative novel technique for the design of variable-band bandpass Σ - Δ modulators is proposed, which utilises a first-order sum-filter in conjunction with fractional-delayers to spectrally transfer the noise-shaping band to the desired signal location. Fourth, a practical step-by-step methodology for the design of bandpass Σ - Δ modulators based on well-known filter family types is presented and supported with extensive simulation results. Fifth, several commonly used Σ - Δ modulator topologies are analysed and where appropriate structural modifications are made in order to allow variable-band noise-shaping. Simple-to-use routines, which can compute the required

coefficients for any system-level set of specifications as well as a library containing the corresponding Σ - Δ modulator topologies have all been created in Matlab and Simulink respectively. Sixth, detailed simulations of the effect of non-unity gain and leaky resonators on the overall noise-shaping response, in-band SNRs and tonality of a fourth-order bandpass Σ - Δ modulator are also provided.

2.2 Survey of Publications to the Field of Bandpass Σ - Δ Modulation

This section presents a chronological survey of reported publications made by various pioneers, engineers, practitioners and theoreticians to the field of bandpass Σ - Δ modulation as given in Table 2.1. These publications cover rigorous theoretical analyses, detailed behavioural investigations of new techniques and topologies as well as actual experimental results obtained from hardware implementations.

A Resume of Publications on Bandpass Σ - Δ Modulation	Ref
A method and detailed schematic diagram of a bandpass Σ - Δ A/D converter for mobile radio applications.	[Gai89]
Design analysis & simulation of the first reported 4 th -order bandpass Σ - Δ modulator: $f_S = 8$ MHz, $f_C = 1$ MHz, $f_B = 8$ kHz, 16-bit resolution for narrow-band communication applications.	[Sch89]
A practical method for the design of a digital bandpass decimator for A/D bandpass Σ - Δ converters: $f_S = 8$ MHz, $f_C = 1$ MHz, $f_B = 8$ kHz, OSR = 512, SNR = 107.4 dB.	[Sch90]
The design, analysis & simulation of an interpolative bandpass A/D converter.	[Dre91]
A 2 nd -order Σ - Δ modulator, which provides noise-shaping at any centre frequency location.	[Hor91]
Design methodology of a 4 th -order bandpass Σ - Δ A/D converter for a digital AM receiver application: $2.16 \text{ MHz} < f_S < 6.40$ for $f_B = 10$ kHz, $\nu_C = \frac{1}{4}$.	[Jan91a]
SC design & simulation of a 6 th -order bandpass Σ - Δ modulator: $f_S = 3$ MHz, $f_C = 455$ kHz, $f_B = 20$ kHz, SNR = 94 dB for half-scale input.	[Jan91b]
Design & SC realisation of 2-stage double-input bandpass Σ - Δ modulator using single- and multi-bit quantisers: $f_S = 66$ kHz, $15.5 \text{ kHz} < f_C < 16.5$ kHz, in-band noise < -70 dB.	[Pin91]
Design of a 4 th -order bandpass Σ - Δ A/D converter of IF signals to baseband I/Q format: $f_S = 10$ MHz, $f_C = 2.5$ MHz, $f_B = 100$ kHz, SFDR = 95 dB.	[Thu91]
The design, description & comparative evaluation of 3-types of bandpass Σ - Δ converters for IF applications.	[Thu92]
A technique for achieving centre frequency tunability in bandpass Σ - Δ modulation by employing a lowpass-to-bandpass frequency transformation.	[Har93a]
First reported fully monolithic implementation of a 4 th -order bandpass Σ - Δ A/D converter: $f_S = 1.82$ MHz, $f_C = 455$ kHz, $f_B = 10$ kHz, SNR = 63 dB for half-scale input.	[Jan93]

SC design & 1 μ CMOS implementation of a 4 th -order bandpass Σ - Δ modulator: $f_s = 7.2$ MHz, $f_c = 1.8$ MHz, $f_B = 30$ kHz, 15-bit resolution.	[Lon93]
Design of 4 th -order bandpass Σ - Δ A/D converter for direct IF conversion: $f_s = 1.82$ MHz, $f_c = 455$ kHz, $f_B = 10$ kHz, OSR = 91, SNDR = 65 dB.	[Bry94]
Design and 2 μ CMOS fabrication of a 4-channel parallel A/D converter for wide-band signals: $f_s = 4.3$ MHz, noise null adjustment $v_B = 0.2$ to 0.3 steps = 0.005, SNDR = 36.4 dB.	[Cor94]
A novel 8 th -order bandpass Σ - Δ modulator architecture suitable for the A/D conversion of an IF signal at 10.7 MHz, resolution = 13 bits.	[Gou94]
A new architecture for a digital radio receiver containing a novel complex bandpass Σ - Δ modulator is presented that allows the A/D conversion on the I/Q outputs of quadrature mixer	[Jan94a]
SI circuit design & 1.2 μ CMOS implementation of an 8 th -order bandpass Σ - Δ modulator: $f_s = 40$ MHz, $f_c = 10$ MHz, $f_B = 150$ kHz, SNR = 90 dB.	[Pat94]
Design and implementation of a CT 4 th -order bandpass Σ - Δ modulator based on the pulse-invariant transformation: $f_s = 80$ MHz, $f_c = 20$ MHz, $f_B = 1$ MHz, SNR = 56.3 dB.	[Sho94]
Describing the use of phase corrective techniques to improve the performance of CT, 1 st , 2 nd and 3 rd order bandpass Σ - Δ A/D converters.	[Thu94a]
A method of stabilising high-order bandpass Σ - Δ modulators is presented, where a limiter is employed to prevent quantiser overloading.	[Thu94b]
Design, analysis & simulation of a tunable narrow-band 2 nd -order bandpass A/D converter for a mobile communication receiver.	[Yan94]
Design of a 2 nd -order complex bandpass Σ - Δ modulator that outperforms 4 th -order real-coefficient bandpass Σ - Δ modulator by an SNR of 7.5 dB for $v_C = 1/4$.	[Azi95]
Design of SC circuit of a 4 th -order bandpass Σ - Δ modulator. Eldo simulations show that for $f_s = 102.4$ MHz, $f_c = 25.5$ MHz, $f_B = 5$ MHz, SNDR = 28.5 dB.	[Baz95]
A method for the design of high-order bandpass Σ - Δ modulators that uses inverse notch-filter sections and optimisation of the pole & zero positions to improve resolution & stability.	[Bel95]
A novel 4 th -order bandpass Σ - Δ modulator SC architecture that uses fewer components is proposed. SC simulated $f_s = 10$ MHz, $f_c = 2.5$ MHz, $f_B = 200$ kHz, OSR = 25, SNR = 52 dB.	[Fra95]
SI design & 0.8 μ CMOS implementation of a 4 th -order bandpass Σ - Δ modulator: $f_s = 10$ MHz, $f_c = 2.5$ MHz, $f_B = 30$ kHz, SNR = 60 dB for -8.2 dB sine-input.	[Ros95]
New method for designing CT LC bandpass Σ - Δ modulators based on DAC pulse shaping: 4 th -order results are $f_s = 200$ MHz, $f_c = 50$ MHz, $f_B = 2$ MHz, SNR = 64.3 dB.	[Sho95]
SC design & 0.8 μ BiCMOS implementation of 2 nd -order bandpass Σ - Δ modulators: $f_s = 42.8$ MHz, $f_c = 10.7$ MHz, $f_B = 200$ kHz, SNR = 57 dB comparing active & passive sensitivities.	[Sin95]
A ratio-independent SC design technique & 2 μ CMOS implementation of a 4 th -order bandpass Σ - Δ modulator: $f_s = 8$ MHz, $f_c = 2$ MHz, $f_B = 30$ kHz, SNR = 56 dB.	[Son95]
Overview, design & implementation of bandpass Σ - Δ modulation for A/D conversion of IF signals in narrow-band communication applications.	[Thu95]

SC design in 0.5 μ CMOS of a 6 th -order multi-bit (9-level) bandpass Σ - Δ modulator DAC, $f_S = 24.576$ MHz, $f_C = 6.144$ MHz, $f_B = 1.536$ MHz, SNR = 60 dB.	[And96]
Analytical derivation of the initial states that result in oscillations of zero-input 2 nd -order resonator-based bandpass Σ - Δ modulators.	[Dav96]
System-level design, behavioural-level and SC simulations of complex-signal Σ - Δ modulators for quadrature bandpass A/D conversion.	[Dia96]
Application of the theory of non-linear dynamics to the analysis of second-order bandpass Σ - Δ modulators for more accurate prediction of stability and resolution.	[Fee96]
The use of an 8 th -order bandpass Σ - Δ modulator in a phase-locked-loop application is described: $f_S = 24$ MHz, $f_C = 6$ MHz, OSR = 64, SNR = 93 dB.	[Her96]
A technique based on placing a notch in the image band of the NTF reduces the effect of mismatches between the real & imaginary channels of complex bandpass Σ - Δ modulators.	[Jan96a]
Design & simulation of a 6 th -order bandpass Σ - Δ modulator with multi-stage polyphase decimator: $f_S = 3$ MHz, $f_C = 455$ kHz, $f_B = 22$ kHz, SNR = 124.3 dB for composite sine inputs	[Kru96]
SC design & 0.8 μ BiCMOS implementation of a 4 th -order bandpass Σ - Δ modulator for ultrasound imaging: $f_S = 160$ MHz, $f_C = 5$ MHz, $f_B = 2.5$ kHz, DR = 84 dB.	[Nor96b]
This paper gives the history and describes the theory of bandpass Σ - Δ modulation and summarises some of the results reported in the literature.	[Sch96]
A digital method of stabilising CT 3 rd -order bandpass Σ - Δ modulator is presented, where oscillations are detected & internal variables are reset to initial values.	[Tla96]
SC design & implementation (0.8 μ BiCMOS) of 8 th -order bandpass Σ - Δ modulator, DR = 130 dB.	[Abc97]
SC design & implementation (0.5 μ double-poly CMOS) of 4 th -order bandpass Σ - Δ modulator, $f_S = 160$ MHz, $f_C = 40$ MHz, $f_B = 2$ MHz, SNDR = 45 dB.	[Baz97]
Comparison of cascade-of-integrators & cascade-of-resonators bandpass Σ - Δ modulators based on SNRs for SC implementation. A 4 th -order modulator exploiting best practical features of both is proposed.	[Bot97]
SC design & implementation (2 μ CMOS) of a 6 th -order cascade-of-resonators bandpass Σ - Δ modulator: 80 dB, $\nu_B = 0.004$ and $\nu_C = 0.25$.	[Chu97]
Implementation of 4 th -order bandpass Σ - Δ modulator with digital programmable passband $\nu_C = 0.2$ to 0.3; SNRs are 47 dB and 59 dB for f_S of 2.36 MHz & 1.25 MHz for $\nu_B = 0.005$.	[Cor97]
Analytical conditions for the state-variables of zero-input oscillation bounds are derived for a 2 nd -order resonator based bandpass Σ - Δ modulator are derived.	[Dav97]
Design & implementation of a 4 th -order quadrature bandpass Σ - Δ modulator converting 3.75 MHz I & Q inputs at $f_S = 10$ MHz attaining 67 dB DR for GSM $f_B = 200$ kHz, SNDR = 62 dB	[Jan97]
Design & fabrication of a 4 th -order bandpass Σ - Δ modulator: $f_S = 3.2$ GHz, $f_C = 800$ MHz, $f_B = 30$ kHz, 66 dB & 41 dB SNRs for f_B 's of 100 kHz & 25 MHz	[Jay97]
Design & simulation of a high-speed multiplier-free higher-order digital bandpass Σ - Δ modulator: $f_S = 42.8$ MHz, $f_C = 10.7$ MHz, $f_B = 200$ kHz, DR = 72 dB.	[Leo97a]

Implementation of a high-speed multiplier-free 6 th - & 8 th - order digital bandpass Σ - Δ modulators using Xilinx FPGA: $f_s = 42.8$ MHz, $f_c = 10.7$ MHz, $f_B = 200$ kHz, DR = 72 dB.	[Leo97b]
SC design & 2 μ CMOS implementation of a 4 th -order bandpass Σ - Δ modulator with five digitally programmable passband locations: $f_s = 827$ kHz $\nu_C = 1/4$, $\nu_B = 0.0025$.	[Liu97]
SC design & 0.6 μ CMOS implementation of a 2-path interleaved 4 th -order bandpass Σ - Δ modulator for digital IF extraction: $f_s = 40$ MHz, $f_c = 20$ MHz, $f_B = 200$ kHz, DR = 75 dB.	[Ong97]
Design & implementation of a tunable 40 MHz-70 MHz CT 4 th -order bandpass Σ - Δ modulator: $f_s = 200$ MHz, $f_c = 50$ MHz, $f_B = 200$ kHz, SNR = 46 dB for $k_1 = k_2 = -10$ dB.	[Sho97]
Design, simulation & breadboard prototype of a robust 4 th -order bandpass Σ - Δ modulator for direct conversion to baseband with I/Q paths: $f_s = 100$ kHz, $f_c = 25$ kHz.	[Tao97a]
SC design & implementation (0.5 μ double-poly CMOS) of a 4 th -order bandpass Σ - Δ modulator, $f_s = 160$ MHz, $f_c = 40$ MHz, $f_B = 1.25$ MHz, SNDR = 45 dB.	[Baz98]
SC design & implementation (2 μ CMOS) of a 4 th - and a 6 th -order bandpass Σ - Δ modulators. SNRs are 73 dB & 80 dB for $\nu_B = 0.0025$ & 0.002 respectively for $\nu_C = 1/4$.	[Chu98]
Design and 0.5 μ bipolar implementation of an integrated LC CT 2 nd -order bandpass Σ - Δ modulator: $f_s = 3.8$ GHz, $f_c = 950$ MHz, $f_B = 200$ kHz, SNR = 59 dB.	[Gao98]
Design of a multi-bit 4 th -order bandpass Σ - Δ modulator for an RF-to-digital receiver providing 16-bit resolution over $f_B = 100$ MHz for 10 MHz $< f_c < 900$ MHz.	[Pel98]
SC design & investigation of a novel 6 th -order bandpass Σ - Δ modulator, $f_s = 15$ MHz, $f_c = 400$ kHz, $f_B = 100$ kHz, SNR = 96.4 dB.	[Bot99]
Exact theoretical analysis of 2 nd -order bandpass Σ - Δ modulators for sinusoidal inputs.	[Cha99]
Methods for reducing SNR, DR and MSIA losses caused by excess loop delay in CT higher-order and multi-bit lowpass & bandpass Σ - Δ modulators.	[Che99c]
Stability analysis incorporating the concept of phase uncertainty and a methodology for the design of high-order CT bandpass Σ - Δ modulators.	[Eng99a]
The effects of bandpass Σ - Δ modulation on orthogonal frequency division multiplexing is analysed and investigated at the behavioural level.	[Gar99]
SC design & 0.8 μ BiCMOS implementation of an 8 th -order bandpass Σ - Δ modulator: $f_s = 42.8$ MHz, $f_c = 10.7$ MHz, $f_B = 200$ kHz, DR = 67 dB.	[Lou99]
Analysis of the limit-cycle behaviour of a double-loop 4 th -order bandpass Σ - Δ modulator at $\nu_C = 1/4$. Scaling is applied to stabilise modulator.	[Man99]
Systematic analysis of SI non-idealities on bandpass Σ - Δ modulator performance. Practical guidelines validated by detailed time-domain simulations are provided.	[Ros99]
A reduced sample-rate bandpass Σ - Δ modulator architecture is designed & simulated: $f_s = 124$ MHz, $f_c = 512$ MHz, $f_B = 1$ MHz, SNR = 68 dB.	[Ste99]
Analysis of timing jitter on the DR of discrete- & continuous-time bandpass Σ - Δ modulators.	[Tao99]

Table 2.1 Chronological Survey of Contributions for Bandpass Σ - Δ Modulation.

2.3 Survey of the Implementations of Bandpass Σ - Δ Modulators

Bandpass Σ - Δ modulators can be realised by using continuous-time circuits [Che99]-[Eng99b] with off-chip LC resonators [Gao98]-[Sho94], monolithic discrete-time SC circuits [Chu98]-[Jan93]-[Lon93]-[Sin95] or SI circuits [Pat94]-[Ros95]-[Ros99]. SC is the most preferable analogue technique for the implementation of Σ - Δ modulators, because of its high circuit accuracy [Baz97]. An up-to-date summary encompassing all the hardware implementations of bandpass Σ - Δ modulators is given below in Table 2.2.

<i>Order</i>	f_s MHz	f_c MHz	f_B kHz	<i>OSR</i>	SNR_p dBs	<i>Ref</i>
4	10	2.5	80	62.6	60	[Dre90]
4	10	2.5	100	50	67	[Thu91]
4	1.82	0.455	10	91	63	[Jan93]
4	7.2	1.8	30	120	75	[Lon93]
4	26	6.5	200	65	55	[Tro93]
8	40	10	150	133.33	90	[Pat94]
4	80	20	1000	40	56.3	[Sho94]
4	10	2.5	30	166.67	60	[Ros95]
2	42.8	10.7	200	107	57	[Sin95]
4	8	2	30	133.33	56	[Son95]
6	24.576	6.144	1536	8	60	[And96]
4	160	5	2.5	32	65	[Nor96b]
8	42.8	10.7	200	107	---	[Abc97]
4	160	40	2000	40	45	[Baz97]
6	0.5	0.127	0.0005	500	85	[Chu97]
4	1.25	0.25-0.375	6.25	100	59	[Cor97]
4	2.358	0.472-0.707	11.79	100	47	[Cor97]
4	10	3.75	200	25	62	[Jan97]
4	3200	800	25000	64	41	[Jay97]
8	42.8	10.7	200	107	---	[Leo97b]
4	0.827	0.20675	2.067	200	67	[Liu97]
4	40	20	200	100	72	[Ong97]
4	200	50	200	500	46	[Sho97]
2	3800	950	200	9500	59	[Gao98]
8	42.8	10.7	200	107	52	[Lou99]

Table 2.2 Survey of Bandpass Σ - Δ Modulator Implementations.

2.4 Applications of Bandpass Σ - Δ Modulators

Bandpass Σ - Δ modulators are well suited in communication systems, special-purpose instrumentation and spectrum analysers for narrow-bandwidth input sources [Thu92]-[Lon93]-[Sch96]-[Nor97]. A typical practical application for bandpass A/D conversion is in digital radio systems, where the IF signal of a superhetrodyne radio receiver can be directly digitised, allowing subsequent signal processing operations such as IF filtering and demodulation functions to be performed with greater accuracy [Bry94]-[Jay97]. This technique avoids dc offset and low frequency noise problems (i.e. compared with mixing and down conversion to baseband) [Pat94]. It also overcomes I/Q mismatches in quadrature demodulation, since this stage is performed digitally [Abc97]-[Gao98]-[Har93]-[Jan93]-[Lou99]-[Sin95]-[Son95]-[Thu92]. In addition, these modulators enable the digitisation of weak IF signals with relatively low cost and high precision [Gar99].

In AM digital radio receivers, the placement of the A/D interface closer to the antenna eliminates the need for the mixers and IF amplifiers, resulting in a reduced component count, robustness and greater accuracy. The use of digital filters improves the phase linearity and facilitates programmability and testability [Jan91a]-[Lon93]-[Sch89]-[Eng99b].

Other viable applications that require high-resolution A/D conversion include receivers for digital mobile cellular telephony [Gou94], high-speed modems [Baz95], satellite communication services [Chu97] and voice-band telecommunications. These bandpass converters are also suitable for portable receiver applications with channel allocation bandwidths under 20 MHz, RF carrier frequencies below 1 GHz [Gao98], for example, pagers, cordless telephones, wireless electronic mail and personal communication devices [Jan94]-[Jan97]-[Ong97]-[Tao99].

A further promising application is in phased-array ultrasound imaging using 1-bit bandpass Σ - Δ A/D converters [Nor96], where the overall analogue hardware can be simplified in exchange for increased digital signal processing complexity. A more recent applicable development is in on-chip signal generators for built-in-self-test [Vei96]. A phase locked-loop frequency synthesiser using a bandpass Σ - Δ digital oscillator as the frequency reference was also reported in [Her96] as another potential application.

2.5 The Lowpass-to-Bandpass Transformation Method - Mid-Band Resonance

The simplest method for designing narrow-band bandpass Σ - Δ modulators involves starting with a suitable lowpass accumulator-based Σ - Δ modulator and then applying the

discrete lowpass-to-bandpass frequency transformation, $z^{-1} \rightarrow -z^{-2}$ [Sch92]-[Lon93]-[Baz95]. A physical interpretation of this is that each delay element is replaced by a double delayer and a inversion. This has the effect of moving the zeros of the NTF from DC to the half-Nyquist frequencies as shown by the PZPs in Figure 2.4.

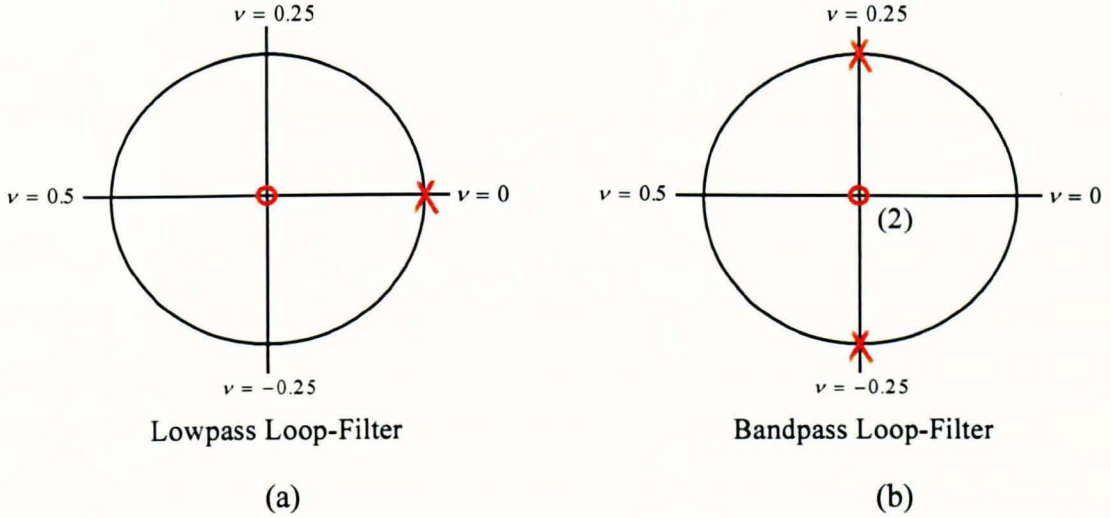


Figure 2.4 Pole-Zero Patterns of (a) 1st-Order Accumulator, (b) 2nd-Order Resonator.

Thus, the relationship between the sampling and centre frequencies for this popular special case is given by $f_C = \frac{1}{4} f_S$. The loop-filter becomes a second-order resonator $R(z)$ given by:

$$R(\nu) = \frac{1}{(1 - e^{-j2\pi(0.25)})(1 - e^{-j2\pi(-0.25)})} \rightarrow R(z) = \frac{1}{1 + z^{-2}} \quad (2.1)$$

where both zeros are stationed at the origin and the two complex conjugate poles are placed on the unit-circle at the half-Nyquist frequencies ($z = \pm j$), thus achieving resonance at $\nu_C = \frac{1}{4}$. At the resonant frequency, the mid-band resonator loop-filter has no phase-shift, whereas the double-delayer in the feedback path at this particular frequency introduces a 180° phase-shift.

$$\text{i.e. } z^{-2} = e^{-j4\pi f_C/f_S} = e^{-j\pi} = -1 \quad (2.2)$$

For this reason, the modulator output signal is added to, rather than subtracted from the input signal at the summing node.

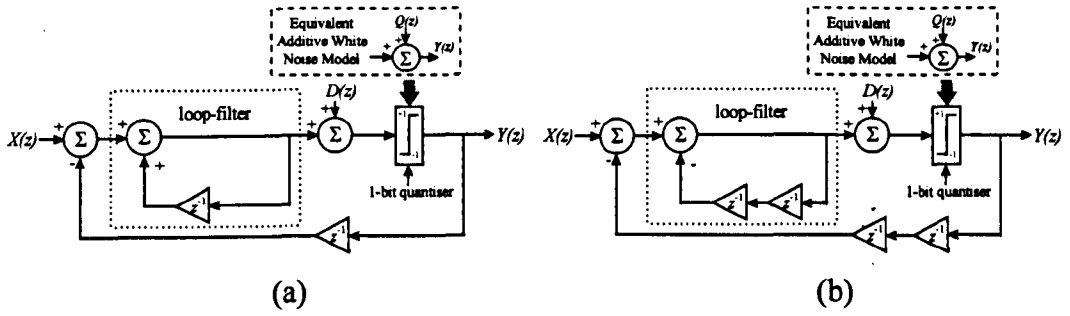


Figure 2.5 Block Diagrams of (a) 1st-Order Accumulator-Based Lowpass, (b) 2nd-Order Resonator-Based Bandpass Σ - Δ Modulators.

Figure 2.5 presents the block diagrams of a conventional lowpass first-order Σ - Δ modulator and the newly derived second-order mid-band resonator-based Σ - Δ modulator. Although, the loop-filter is actually second-order containing poles at each of the one-quarter and three-quarter sampling frequencies, it results in what is known as an effective-first-order bandpass Σ - Δ modulator, because the other pole is really contributing to noise-shaping at the corresponding negative centre frequency.

An output expression for this second-order Σ - Δ modulator in the z -domain can be obtained by representing the 1-bit quantiser by an additive white noise model and then applying linear analysis. This resultant output $Y(z)$ becomes:

$$Y(z) = X(z) + (1 - jz^{-1})(1 + jz^{-1})Q(z) = X(z) + (1 + z^{-2})Q(z) \quad (2.3)$$

where $X(z)$ and $Q(z)$ are the input and quantisation noise signals respectively. This approximate mathematical expression demonstrates that the quantisation noise is nulled at the half-Nyquist frequency by a second-order notch-filter, leaving the original signal undistorted. For implementation purposes, the loop and feedback filters are often combined into a single transfer function, resulting in the slightly modified output signal shown below:

$$Y(z) = z^{-2}X(z) + (1 + z^{-2})Q(z) \quad (2.4)$$

In order to enable the second-order mid-band resonator-based Σ - Δ modulator to produce the correct noise-shaping in a simulation environment, it needs to be excited by an additive scaled dither signal at the quantiser input. In the absence of dither, the magnitude spectrum of this modulator consists of a string of strong-tones, whose location, mode of repetition and amplitude directly depend on the signal amplitude of the input sinusoid. For example, the magnitude spectrum for unity-amplitude input sinusoids contains purely three distinct tones positioned at the dc, half-Nyquist and Nyquist frequencies with no noise-

shaping. The corresponding tone strengths are -12.04 dB, -12.04 dB and -18.06 dB respectively. For half-scale sinusoids, five tones whose amplitudes are -8.52 dB, -18.06 dB, -18.06 dB, -18.06 dB and -24.08 dB are generated at the normalised centre frequencies of 0, 0.125, 0.25, 0.375 and 0.5 respectively.

The amplitude of the majority of these tones is reduced as their number increases across the spectrum. This observation verifies the constant output power criterion. A very small amplitude dither signal in the order of μV 's is required to stimulate the modulator to achieve proper noise-shaping. In practice, however, larger amplitude dither signals (i.e. 0.1 \rightarrow 0.5 of full-scale) are deemed necessary to accomplish more significant quantisation noise randomisation, in order to reduce strong-amplitude tones to noise floor levels. Tone reduction can be achieved at the expense of degraded in-band SNR.

Simulations have also revealed that this modulator can be made to deliver spectral noise-shaping without a dither signal by exciting it with an irrational-amplitude sinusoid. The immediate benefit is that the absence of dither does not compromise the modulator resolution. However, this type of excitation mechanism is deemed unreliable, because it is only restricted to making the modulator operational for non-finite-amplitude input signals. Furthermore, all the examined noise-shaping spectra corresponding to a hundred random input amplitude combinations exhibited strong spectral content.

Simulations have demonstrated that changing the initial conditions of the loop- and feedback filters from zero to random numbers and vice-versa, unfortunately does not trigger this modulator into proper operation. The location and number of these tones were seen to be totally independent of the initial condition values for this particular second-order Σ - Δ modulator. The amplitudes of these tones, however, were observed to vary slightly for different combinations of random initial conditions.

It was observed through detailed simulations that the injection to the modulator input of a sinusoid positioned at the exact band centre location produced a noise-shaping response that exhibited a multitude of dominant tones. The shifting of the input frequency slightly from the band-centre (i.e. by 0.01%) causes a randomisation effect to many of these limit cycle oscillations resulting in a significantly improved noise-shaping spectrum with fewer tones. The application of this frequency offset not only eradicated many of these spurious tones, but it also acted as a third alternative to excite this modulator into accomplishing spectral noise-shaping. This frequency-offset mechanism has been employed in numerous topologies [Baz95]-[Rib94], but to the best knowledge of the author, no explanation has been reported to-date.

A fourth alternative means that can trigger this modulator into noise-shaping operation in the absence of dither is to make this modulator chaotic by shifting the two conjugate poles of the loop-filters slightly outside the unit-circle [Sch94]. The movement of these poles substantially reduces the periodicity of these limit cycle oscillations, resulting in weaker and fewer tones appearing in the magnitude spectrum. This method should be applied with great care as minor shifts in the position of the poles due to non-idealities in implementation can render the modulator unstable. Simulations have furthermore confirmed that this method, unlike dither, can not suppress all the tones across the spectrum. This complies with the observations made in [Dun96a].

This second-order Σ - Δ modulator was evaluated for an input sinusoid at $\nu_C = 0.25$ for a wide range of amplitude levels. The simulations demonstrated that its magnitude spectrum contained tones, whose locations and amplitudes varied with respect to the magnitude of the input signal. For example, the spectrum for a half-scale input amplitude contained two tones at $1/8$ and $3/8$ as shown in Figure 2.6(a).

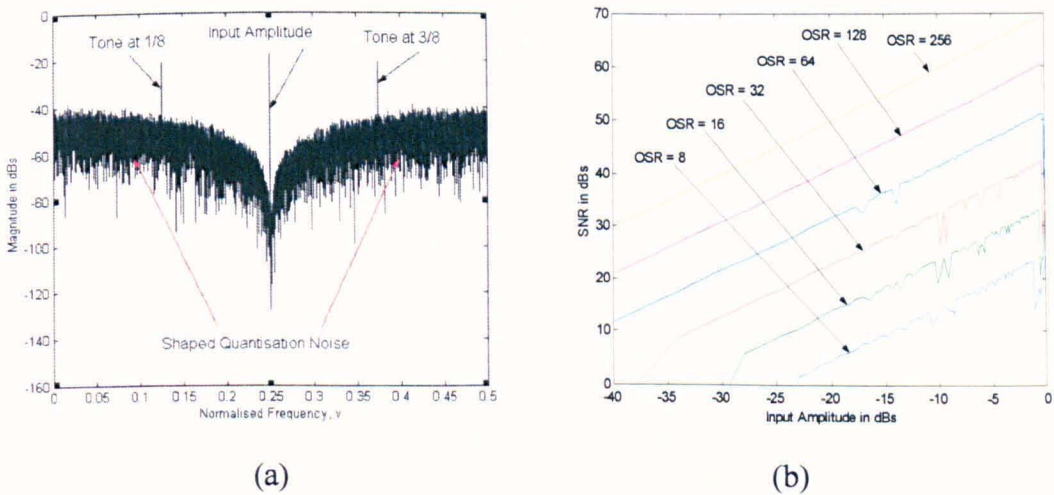


Figure 2.6 Second-Order Mid-Band Resonator-Based Bandpass Σ - Δ Modulator
(a) Magnitude Spectrum, (b) SNR Curves for OSRs.

Peak SNR values of 24.9 dB, 33.9 dB, 42.8 dB, 51.7 dB, 60.8 dB and 69.7 dB are attainable for OSRs of 8, 16, 32, 64, 128 and 256 respectively. In addition, the average increase in the SNR is found to be 9.2 dB for each doubling in the OSR. Furthermore, the fluctuations in the SNR curves in Figure 2.6(b) for large input amplitudes for OSRs of 8, 16 and 32 are primarily attributed to the presence of relatively strong in-band tones. Small OSRs imply larger bandwidths and these in turn are likely to encompass more tones. The location, strength and frequency of these tones, as already discussed in Section 1.13.5, depends on the amplitude and frequency of the input waveform. For very small input

amplitude signals, the SNR curves become very non-linear, because of the presence of many closely adjacent tones within the signal region. Moreover, the out-of-band tones especially at dc and Nyquist become more dominant as the input signal diminishes in amplitude. It was observed that the dc tone for a whole range of input amplitudes is always larger than its Nyquist counterpart by as much as 5 dB.

2.6 Higher-Order Mid-Band Resonator-Based Bandpass Σ - Δ Modulators

This transformation can be quite easily applied for the design of higher-order mid-band resonator-based bandpass Σ - Δ modulators. A generalised PZP for an L^{th} -order mid-band resonator-based bandpass Σ - Δ modulator is shown in Figure 2.7 (a).

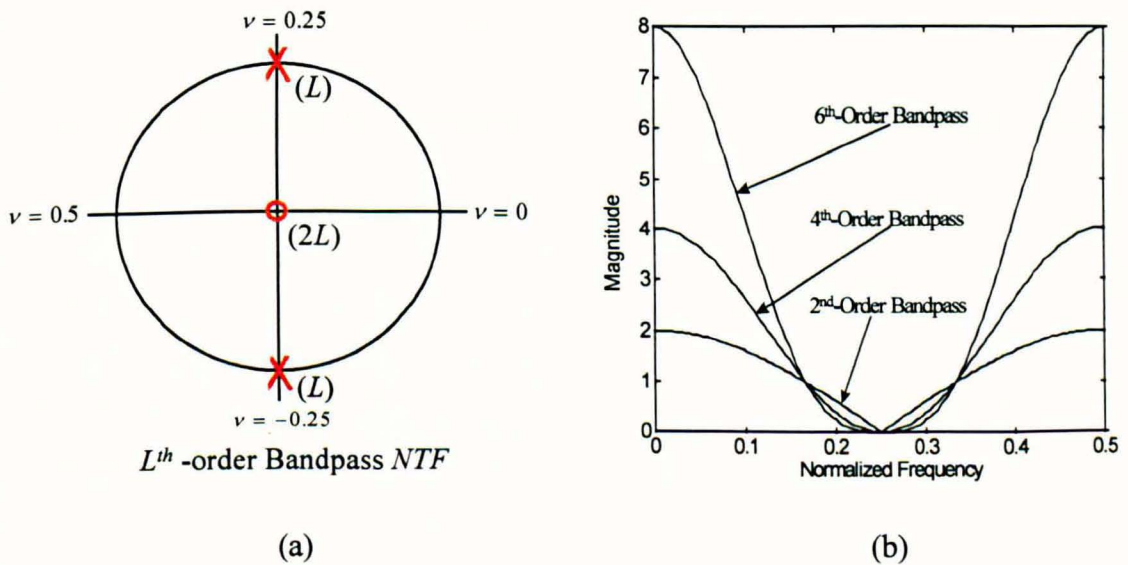


Figure 2.7 (a) Pole-Zero-Pattern of the NTF of an L^{th} -Order Resonator-Based Bandpass Σ - Δ Modulator, (b) NTF Magnitude Spectra of 2nd-, 4th- and 6th- Order Bandpass Σ - Δ Modulators.

A further advantage, as with the lowpass case, is that smaller sampling frequencies can be used to yield the same resolution to meet a given specification compared with lower-order Σ - Δ modulators. Figure 2.8 presents an L^{th} -order chain of mid-band resonators with distributed feedback topology.

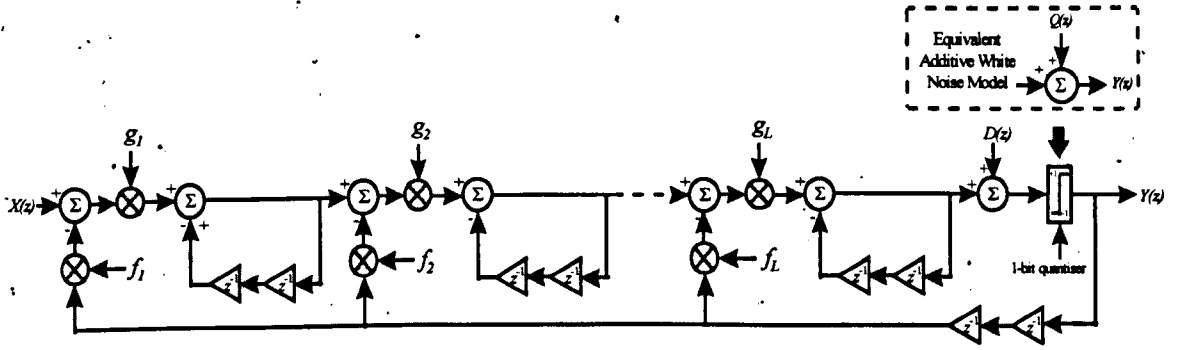


Figure 2.8 An L^{th} -order chain of mid-band resonators with distributed feedback.

Using linearised analysis and assuming the feedback as well as the feedforward coefficients to be all unity results in an output given by:

$$Y(z) = X(z) + (1 + z^{-2})^L Q(z) \quad (2.5)$$

A theoretical expression corresponding to the NTF of (2.5) for the shaped quantisation noise is given by

$$\sigma_{shn}^2 = \frac{\sigma_n^2}{f_S} \left[\left| H_N(z) \right|_{z=e^{j2\pi fT}}^2 \right] = \frac{\sigma_n^2}{f_S} \left[\left| (1 + z^{-2})^L \right|_{z=e^{j2\pi fT}}^2 \right] = \frac{\sigma_n^2}{f_S} (2 \cos 2\pi fT)^{2L} \quad (2.6)$$

Integrating over the signal bandwidth $f_B = f_S/2 \text{ OSR}$, gives the in-band noise power σ_{bn}^2 of the modulator.

$$\sigma_{bn}^2 = 2 \int_{f_C - f_B/2}^{f_C + f_B/2} \sigma_{shn}^2(f) df \quad (2.7)$$

$$\sigma_{bn}^2 \equiv \frac{\sigma_n^2}{2^{2L} \pi f_S T} \left\{ \left(\frac{2L}{L} \right) 2\pi f_B T + \sum_{k=0}^{L-1} \left(\frac{2L}{k} \right) \frac{\sin \left[4\pi \left(f_C + \frac{f_B}{2} \right) (L-k) T \right] - \left[4\pi \left(f_C + \frac{f_B}{2} \right) (L-k) T \right]}{L-k} \right\} \quad (2.8)$$

The in-band quantisation noise is reduced by $(3L + 3) \text{ dB}$ for each octave increase in the OSR, where L denotes the order of the notch-filter [Sch89]-[Jan91b]. The theoretical results depicting the decrease in the in-band quantisation noise with respect to the OSR for different modulator orders are presented in Figure 2.9.

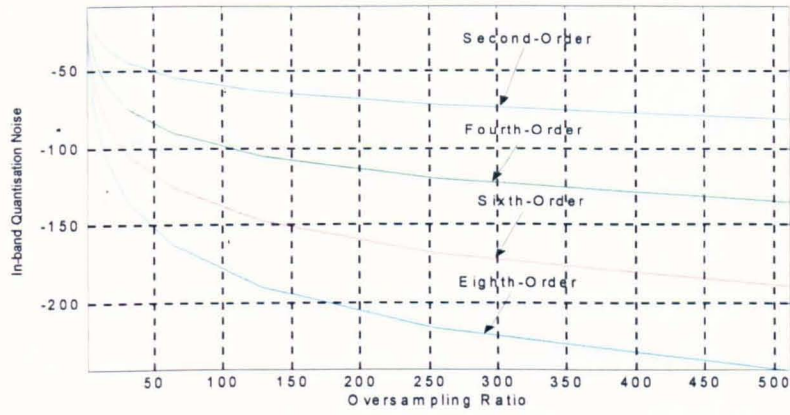


Figure 2.9 Theoretical In-band Quantisation Noise (in dBs) Curves versus OSR for Second-, Fourth-, Sixth- and Eighth-Order Bandpass Σ - Δ Modulators.

The magnitude spectrum of a fourth-order resonator-based bandpass Σ - Δ modulator for a half-scale single-tone sinusoid exactly centred at $\nu_C = 0.25$ is shown in Figure 2.10 (a).

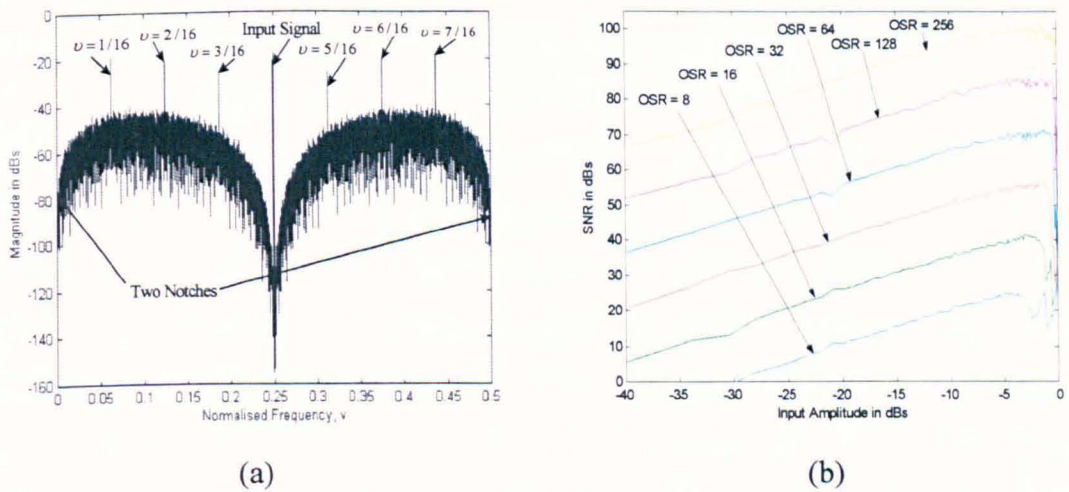


Figure 2.10 Fourth-Order Mid-Band Resonator-Based Bandpass Σ - Δ Modulator
(a) Magnitude Spectrum, (b) SNR Curves.

This spectrum is seen to contain six distinct tones positioned at $1/16$, $2/16$, $3/16$, $5/16$, $6/16$ and $7/16$ as well as two notches at DC and the Nyquist frequency. Detailed simulations have shown that the magnitude spectrum of Σ - Δ modulators that contain a few strong-power tones or many low-power tones due to very low input amplitudes often exhibit notches at the same time. Since the output power of a single-bit Σ - Δ modulator is always unity irrespective of the input amplitude, these notches unavoidably occur to compensate for the presence of these tones. This modulator was evaluated for different input amplitude

levels and zero initial conditions, where the number of tones and their locations were seen to depend primarily on the amplitude of the input signal. The two notches remained at $\nu = 0$ and $\nu = 0.5$ for all input amplitudes.

Simulations indicate that the locations, strength and density of the tones in the spectrum for this fourth-order Σ - Δ modulator for an input signal amplitude of 0.5 and a dither signal of 0.01 amplitude is very sensitive to the initial conditions of the resonators of the loop-filter. Peak SNR values of 34.4 dB, 48.8 dB, 64.2 dB, 79.3 dB, 94.8 dB and 110.3 dB are attainable for OSRs of 8, 16, 32, 64, 128 and 256 respectively. In addition, the average increase in the SNR is found to be 15.2 dB for each doubling in the OSR. The simulations also reveal that the SNR curves in Figure 2.10(b) begin to decrease, when the quantisation noise power due to overloading exceeds the power of the input signal. For small input levels, the SNR reduction is attributed to the concurrent decrease of the input signal power and the increased occurrence of in-band tones. Modulators containing quantisers that have few and/or an even number of levels exhibit more tones in their spectral content, due to the absence of the zero threshold as this increases the occurrence of oscillations for small amplitude signals.

Higher-order single-bit resonator-based bandpass Σ - Δ modulators are prone to instability for large-amplitude input signals, because the signal levels in the modulator feedforward path increase more rapidly compared with those in the feedback. The feedback path is made ineffective and as a result, the 1-bit quantiser becomes constantly overloaded.

One simple heuristic solution is to choose suitable values for the feedback coefficients to make the magnitude of the feedback signals comparable to those circulating in the feedforward path. Intuitively, these coefficient values should be increased in powers comparable in value with the peak amplitude increase of the modulator order NTF. These feedback coefficients are numbered f_2 , f_1 and f_0 from the resonator nearest the quantiser. Simulations have confirmed that this increase is proportional to $(L-1)$ for feedback coefficients closest to the quantiser decreasing in successive powers for consecutive feedback coefficients away from the quantiser. Integer coefficient combinations are easier to use, e.g. 1, 3, 9 or 1, 4, 16 or 1, 5, 25 for f_0 , f_1 and f_2 respectively. Alternatively; small gains for the resonators can be used to reduce the magnitude of the signals in the feedforward path [Bos88]-[Baz95].

The envelope of the NTF for the 6th-order resonator-based Σ - Δ modulator, when all the coefficients are set to unity, rises very steeply for the out-of-band magnitude reaching a peak value of 18.1 dB at $\nu = 0$ and $\nu = 0.5$ - well above the threshold tolerated by the 1-

bit quantiser. The NTF magnitude can be reduced by including feedback coefficients to the modulator, whose values have to sufficiently exceed unity so as to provide adequate signal strength to counter-balance the large amplitude levels in the feedforward path. Figure 2.11 shows that the NTF magnitude for different combinations of feedback coefficients. It is seen that the NTF magnitude decreases as the feedback coefficients increase - this naturally has the desirable effect of enhancing modulator stability.

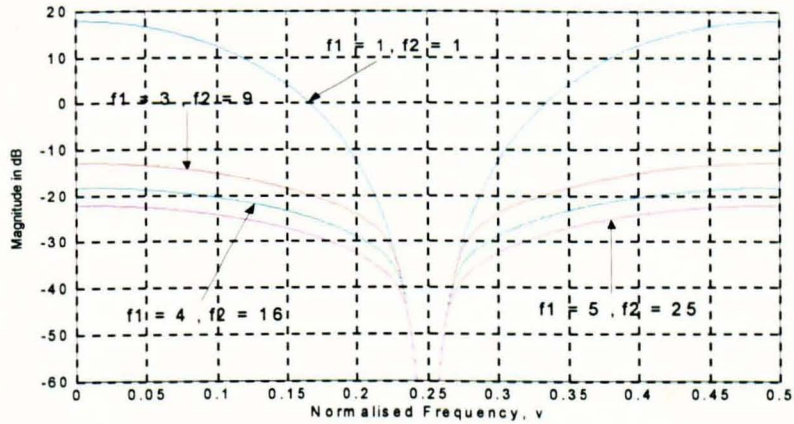


Figure 2.11 NTF Magnitude Comparison for Different Feedback Coefficients for a Sixth-Order Bandpass Σ - Δ Modulator.

The magnitude spectrum of a sixth-order bandpass Σ - Δ modulator for an input amplitude of 0.5 and dither signal of 0.01 contained distinct tones located at equi-spaced multiples of $\nu = 1/64$ as well as four notches positioned at $\nu = 0, 0.125, 0.375$ and 0.5 . More unexpected notches appear in the spectrum in order to compensate for the presence of strong-power tones, especially for large-input amplitudes. The periodicity and strength of these tones were seen to be a function of the input amplitude. However, the location of the extra notches was shown to be independent of the signal amplitude. Furthermore, the use of different sets of feedback coefficients was demonstrated to be independent of the tones and the extra notches.

Furthermore, increasing the amount of dither at the quantiser input helps to reduce these tones considerably, but at the expense of increased quantisation noise in the signal region. This also causes the notches to almost disappear confirming the earlier intuitive explanation that the presence of strong-power tones is related to the existence of notches as a means of power compensation.

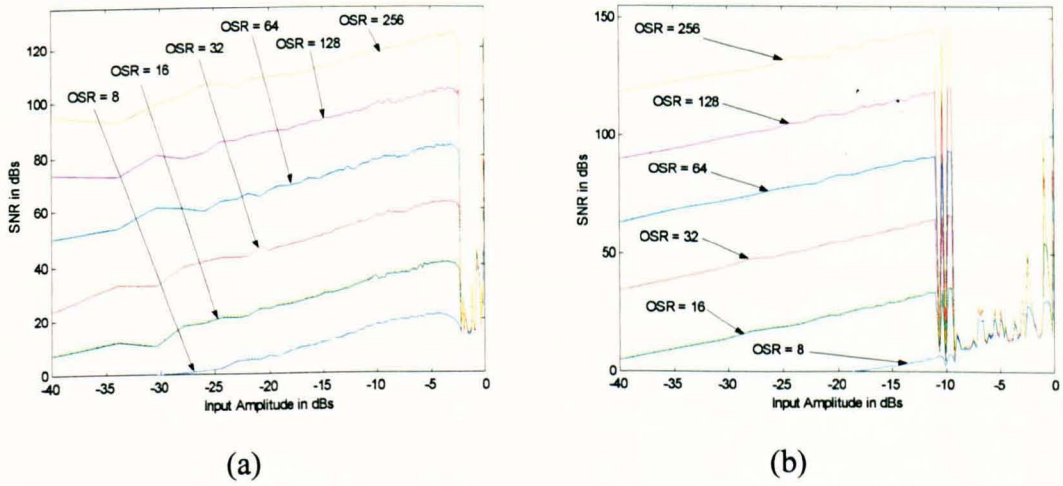


Figure 2.12 SNR Curves of Mid-Band Resonator-Based Bandpass Σ - Δ Modulators for different OSRs , (a) Sixth-Order, (b) Eighth-Order.

The SNR curves for a 6th-order and an 8th-order Σ - Δ modulators given in Figure 2.12 demonstrate that significant improvements in the in-band SNRs and DRs are accomplished for higher modulator orders and OSRs. For the sixth-order Σ - Δ modulator, peak SNR values of 47.9 dB, 64.5 dB, 79.7 dB, 95.3 dB, 113.8 dB and 134.2 dB are attainable for OSRs of 8, 16, 32, 64, 128 and 256 respectively. In addition, the average increase in the SNR is found to be 15.6 dB for each doubling in the OSR.

The maximum achievable SNR values for the eighth-order modulator are 31.4 dB, 55.8 dB, 85.3 dB, 112.1 dB, 138.8 dB and 157.7 dB for the same corresponding OSRs. In addition, the average increase in the SNR is found to be 26.4 dB for each doubling in the OSR. Furthermore, Figure 2.12 shows that the SNRs for the 6th and 8th order modulators are substantially reduced as a result of modulator instability for all input amplitudes beyond -2.2 dB and -10.5 dB respectively.

Mid-band resonator-based bandpass Σ - Δ modulators are relatively easy to design and invariably exhibit symmetrical noise-shaping magnitude spectra. This symmetry helps to maintain stability and reduce the specification requirement of the decimation filter. However, two major limitations exist with the $z^{-1} \rightarrow -z^{-2}$ transformation technique. Firstly; it only works for one centre frequency, i.e. $\nu_C = 1/4$. Secondly, it always requires a stable lowpass Σ - Δ modulator prototype. Fortunately; these constraints can be overcome by employing variable-band noise-shaping modulators as will be explained in the following sections.

2.7 The Lowpass-to-Bandpass Transformation Method - Non-Mid-Band Resonance

This section describes a technique that was proposed in [Har93] and [Sch96] that can achieve noise-shaping tunability for very narrow-band bandpass $\Sigma\text{-}\Delta$ modulators. This method basically involves the insertion of a tuneable allpass filter in cascade with each delayer of a stable lowpass $\Sigma\text{-}\Delta$ modulator prototype, causing the loop-filter poles to be shifted around the unit-circle to the designated centre frequency of interest. This discrete-time lowpass-to-bandpass transformation is given by

$$z^{-1} \rightarrow -z^{-1} \left[\frac{\beta + z^{-1}}{1 + \beta z^{-1}} \right] \quad (2.9)$$

where $\beta = \cos(2\pi f_c / f_s)$. Positive and negative β values deliver noise-shaped passbands for the normalised centre frequency ranges $0.25 < \nu_c < 0.5$ and $0 < \nu_c < 0.25$ respectively, whereas the case $\beta = 0$ degenerates to the mid-band resonance case (i.e. $z^{-1} \rightarrow -z^{-2}$) that was discussed Sections 2.5 and 2.6.

The application of this spectral transformation to a first-order accumulator-based lowpass $\Sigma\text{-}\Delta$ modulator results in the following loop- and feedback transfer functions. These are given by:

$$H(z) = \frac{1}{1 - 2\beta z^{-1} + z^{-2}} \quad \text{and} \quad F(z) = -(\beta z^{-1} + z^{-2}) \quad (2.10)$$

A suitable topology of a second-order bandpass $\Sigma\text{-}\Delta$ modulator incorporating these modifications is shown in Figure 2.13, where $D(z)$ represents the dither gain.

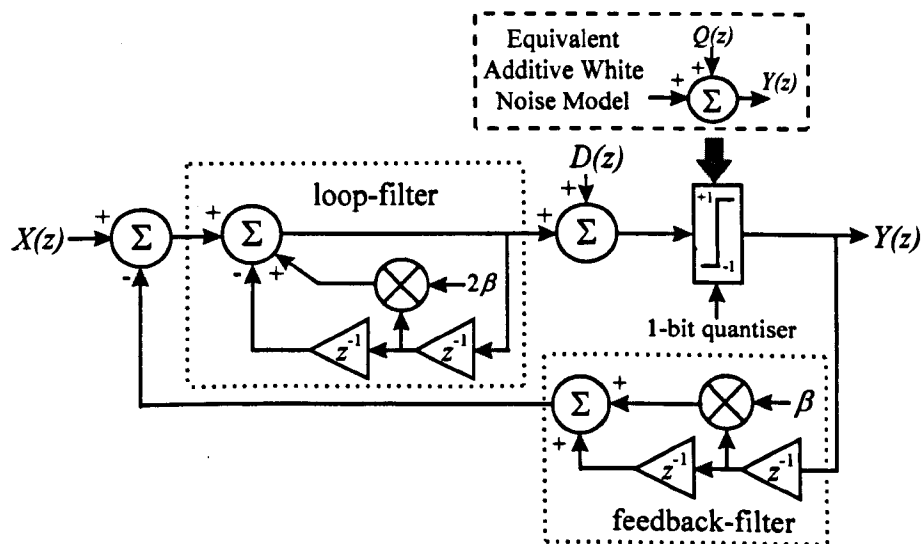


Figure 2.13 Second-Order Bandpass $\Sigma\text{-}\Delta$ Modulator using Frequency Transformation.

The magnitude spectrum for a 2nd-order Σ - Δ modulator tuning at $\nu_C = 5/64$ for input and dither signal amplitudes of 0.5 and 0.01 is shown in Figure 2.14(a). Magnitude spectra corresponding to a whole range of small and medium strength input levels exhibited relatively fewer tones in comparison with their mid-band resonator counterparts. This is due to the more complicated composition of the loop-filter, which imparts more state values and thus weaker spectral tones. Figure 2.14 (b) shows that, unlike the mid-band resonator case, the SNR curves become noticeably non-linear for input signal amplitudes exceeding -5 dB. This non-linearity is caused by the asymmetrical noise-shaping response for non-mid-band resonator frequencies, which is responsible for the amplification of the internal signal levels in the modulator feedforward path. Careful behavioural-level simulations showed that the quantiser was never overloaded for the mid-band resonator case. However, for $\nu_C = 5/64$, the quantiser input amplitude invariably exceeded the quantiser dynamic range by as much as 2 or 3 times, giving rise to spurious tones. Some of these manifest themselves in the in-band region, therefore accounting for the apparent SNR dip for high-input signal amplitudes. Simulations also confirm that unlike the $z^{-1} \rightarrow -z^{-2}$ spectral transformation, the modulator dynamics including stability are not preserved.

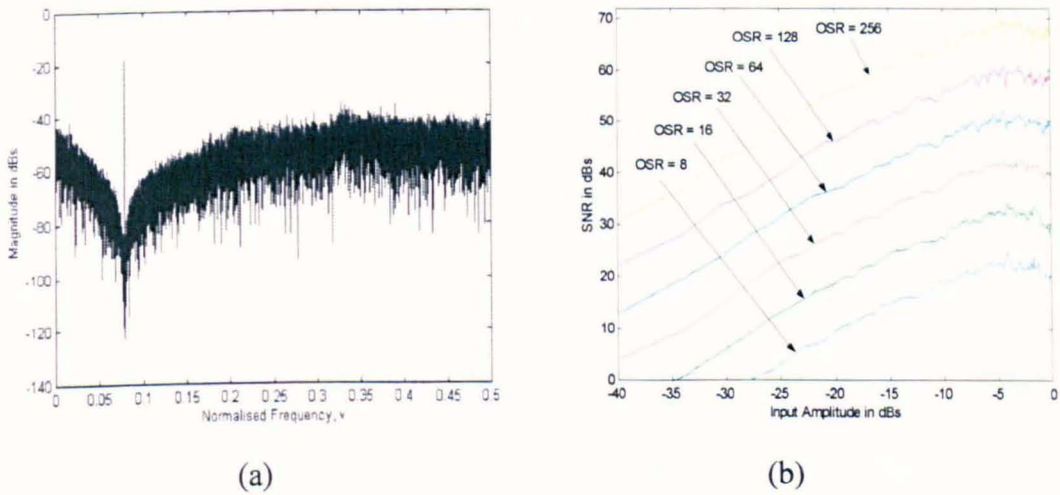


Figure 2.14 Second-Order Variable-Band Resonator-Based Bandpass Σ - Δ Modulator at $\nu_C = 5/64$ (a) Magnitude Spectrum, (b) SNR Curves for different OSRs.

Peak SNR values of 22.3 dB, 31.4 dB, 39.7 dB, 49.4 dB, 58.3 dB and 67.3 dB are attainable for OSRs of 8, 16, 32, 64, 128 and 256 respectively.

This transformation is then extended to a second-order lowpass Σ - Δ modulator. The loop-filters $H_1(z)$ and $H_2(z)$ as well as the feedback filter $F(z)$ are identical to the transfer functions in (2.9). However, this newly derived 4th-order bandpass Σ - Δ modulator

may be simplified by embedding the feedback term into the second loop-filter making $H_2(z)$ a delayed resonator. The new transfer functions for this modulator become:

$$H_2(z) = -(\beta z^{-1} + z^{-2}) / (1 - \beta z^{-1} + z^{-2}) \quad \text{and} \quad F(z) = 1 \quad (2.11)$$

while $H_1(z)$ remains unchanged.

Simulations show that this 4th-order modulator remains unstable when all its coefficients are set to unity. In order to stabilise this modulator, the gain of the first-resonator had to be reduced. A value of 0.125 was empirically found to suffice, thus enabling this modulator to perform noise-shaping at $\nu_C = 5/64$ as can be shown in Figure 2.15(a).

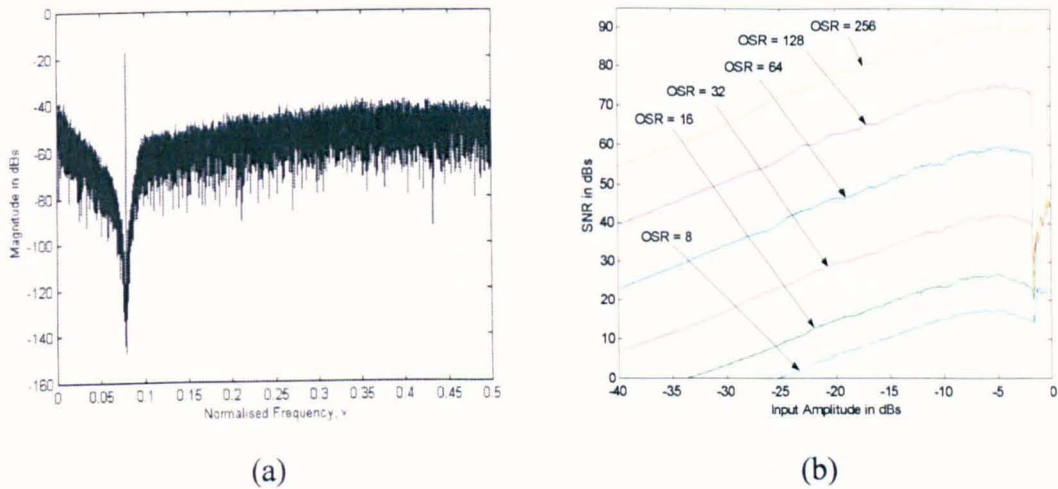


Figure 2.15 Fourth-Order Variable-Band Resonator-Based Bandpass Σ - Δ Modulator at $\nu_C = 5/64$ (a) Magnitude Spectrum, (b) SNR Curves for Different OSRs.

A family of SNR curves for various OSRs is illustrated in Figure 2.15(b), where this modulator is shown to become unstable for a sinusoidal input amplitude exceeding -2.1 dB. This is in contrast to the 4th-order mid-band resonator case, which does not destabilise until its input amplitude exceeds -1 dB. Peak SNR values of 22.8 dB, 43.8 dB, 44.2 dB, 56.5 dB, 72.4 dB and 88.7 dB are attainable for OSRs of 8, 16, 32, 64, 128 and 256 respectively.

Simulations confirm that further reductions in this gain value are deemed necessary if this modulator is required to perform noise-shaping for centre frequencies that are smaller than $5/64$. This potential to instability is attributed to the uneven shoulder gains of the non-mid-band resonator loop-filters $H_1(z)$ and $H_2(z)$. This 4th-order modulator was evaluated for different-amplitude sinusoids ranging from $0 \rightarrow 1$ for the full-range of normalised frequencies to determine the lower and upper frequency thresholds before the onset of

instability. When all the gain coefficients are set to unity, Figure 2.16 demonstrates that this modulator remains only stable for the range $0.22 < \nu_C < 0.28$.

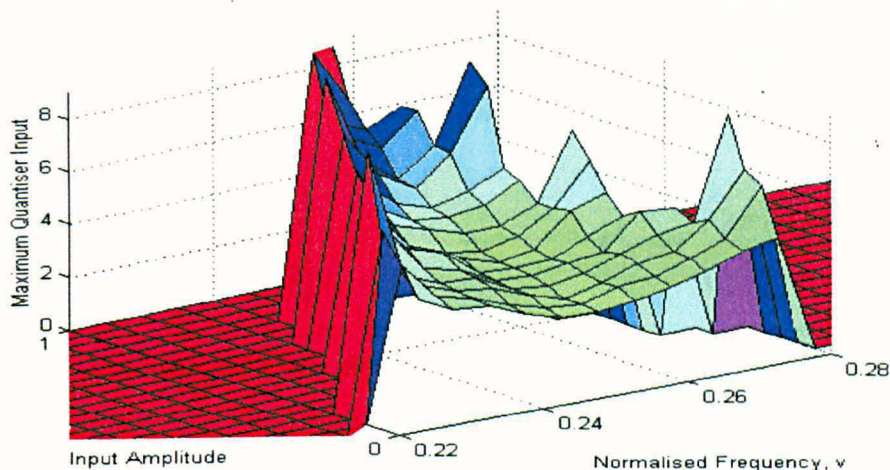


Figure 2.16 3-D Plot illustrating the Stable Range of Normalised Centre Frequencies for a Fourth-order Variable-Band Resonator-Based Bandpass Σ - Δ Modulator.

This transformation technique is simple to apply and provides flexibility in that noise-shaping can be provided for any centre frequency across the spectrum. However, it has several drawbacks. First; a working lowpass Σ - Δ modulator is always required, whose noise-shaping properties and stability are not maintained after the transformation. Second; the uneven shoulder gains attributed to the non-mid-band resonator transfer function jeopardise modulator stability and impose tighter specifications on the post bandpass decimator. Third; good resolution can only be achieved for extremely narrow bandwidths, normally a single frequency. Fourth; the designer is only limited to specifying the centre frequency location and OSR, having no freedom over specifying the parameters that control the stable and tonal properties of the modulator.

It is quite evident that this lowpass-to-bandpass transformation has numerous constraints. This necessitated the development of existing techniques to circumvent some of these limitations and explore alternative novel approaches that can deliver enhanced noise-shaping spectra and better resolution.

2.8 Extension of the Transformation Approach to Specifying Bandwidths

The lowpass-to-bandpass transformation technique proposed in [Har93] and [Sch96] and discussed in Section 2.7 restricts the designer to only specifying the centre frequency of the noise-shaping band. In this section, this transformation is developed so as to allow

the designer to specify the bandwidth as well as the centre frequency location for a given NTF. This is given by:

$$z^{-1} \rightarrow -\frac{z^{-2} + \left(\frac{2\alpha k}{k+1}\right)z^{-1} + \left(\frac{k-1}{k+1}\right)}{\left(\frac{k-1}{k+1}\right)z^{-2} + \left(\frac{2\alpha k}{k+1}\right)z^{-1} + 1} \quad (2.12)$$

where

$$\alpha = \frac{\cos \left[\frac{2\pi(\nu_H + \nu_L)}{2} \right]}{\cos \left[\frac{2\pi(\nu_H - \nu_L)}{2} \right]} \quad \text{and} \quad k = \cot \left(\frac{2\pi(\nu_H - \nu_L)}{2} \right) \quad (2.13)$$

Before delving into the detailed analysis, it is useful at first to discuss the main characteristics that are associated with this technique. First; it allows the designer to define the signal bandwidth making it more suitable for applications, whose inputs are composed of a multitude of harmonics. This is in contrast to the procedure in Section 2.7, which only permits the specification of the centre frequency, totally disregarding the width of the modulator input signal. Second; the shoulder gain levels of the NTF and subsequently the loop-filter are equal for any arbitrary band-location across the spectrum. This serves to enhance stability, particularly, for higher-order modulators circumventing the need for the incorporation of stability scaling factors. Third; the design process using this transformation is straightforward to apply to any conventional lowpass Σ - Δ modulator prototype. This simply requires the substitution of each delay element of the lowpass prototype with the more elaborate expression given in (2.12). Fourth; the magnitude spectra of all the examined modulators using this transformation for $\nu_C = 17/64$ and $\nu_B = 1/32$ exhibited noticeably fewer tones in their spectra. This is attributed to the more complicated coefficients of the loop-filter, which imparted a wider range of state values. Needless to say, a larger variety of internal signal amplitudes helps to reduce the recurrence of similar patterns, thus leading to fewer strong spectral tones. Simulations also confirm that the quantiser input levels are almost always within the threshold boundaries of the quantiser. This substantially reduces the formation of tones, especially for large input amplitudes. Fifth; the poles and zeros of the NTF are coincidentally positioned on the unit-circle. This may simplify the complexity of the loop-filter coefficients, but certainly does not yield optimum in-band SNRs.

In order to facilitate the design of bandpass Σ - Δ modulators using this transformation, a programme has been written in Matlab, which can evaluate the loop-filter coefficients

based on the specification of ν_C , ν_B , modulator order and dither gain. An annotated outline of this programme's algorithm is given below:

STEP 1: Specify the normalised centre frequency ν_C as well as the bandwidth ν_B of the intended design. For a symmetrical signal-band, ν_B is defined in terms of the normalised lower ν_L and upper ν_H frequencies as illustrated below in (2.14)

$$\nu_L = \nu_C - \Delta\nu_B/2 \quad \text{and} \quad \nu_H = \nu_C + \Delta\nu_B/2 \quad (2.14)$$

STEP 2: Determine the coefficients α and k using (2.13) and substitute them into the transformation given in 2.12.

STEP 3: Select the NTF for a stable lowpass Σ - Δ modulator.

STEP 4: Apply this transformation to each delayer term of the prototype NTF. Note that higher-order delayers need to be replaced with a cascade combination of this transformation, whose number equals the order of each delayer component.

STEP 5: Scale down the NTF so that its first coefficient becomes 1 in order to satisfy the causality criterion. Note that this transformation, unlike the previous two in Sections 2.5 and 2.7, can not be directly applied to the loop-filter, because it contains constant terms in both numerator and denominator, inevitably violating the causality criterion.

STEP 6: Verify the peak amplitude of the NTF spectrum to ensure that it complies with Lee's stability criterion.

STEP 7: The loop-filter $L(z)$ can be analytically obtained by re-arranging the NTF expression such that

$$L(z) = (1 - NTF)/NTF \quad (2.15)$$

STEP 8: Enter the coefficients of $L(z)$ into the modulator and simulate it at the behavioural-level to confirm the correctness of its operation.

A generalised loop-filter expression, which is used by this programme is given below:

$$L_L(z) = \frac{\beta_1 z^{-1} + \beta_2 z^{-2} + \dots + \beta_{L-1} z^{-(L+1)} + \beta_L z^{-L}}{\alpha_0 + \alpha_1 z^{-1} + \alpha_2 z^{-2} + \dots + \alpha_{L-1} z^{-(L+1)} + \alpha_L z^{-L}} \quad (2.16)$$

The corresponding algebraic loop-filter coefficients for the first-order differencer-based NTF are $\beta_1 = a_1(1 - a_2)$, $\beta_2 = (a_2^2 - 1)$, $\alpha_0 = (1 + a_2)$, $\alpha_1 = -2a_1$ and $\alpha_2 = (1 + a_2)$.

The loop-filter coefficients for a second-order differencer-based NTF are:

$$\beta_1 = 2a_1(1 - a_2^2), \beta_2 = -2 - 2a_2(1 - a_2 - a_2^2) + a_1^2(2a_2 - 3 + a_2^2),$$

$$\beta_3 = 2a_1(2 + a_2 - 2a_2^2 - a_2^3), \beta_4 = (2a_2^3 + a_2^4 - 1 - 2a_2), \alpha_0 = (1 + a_2)^2, \alpha_1 = -4a_1(1 + a_2)$$

$$\alpha_2 = 2(1 + 2a_2^2 + 2a_1^2 + a_2^2), \alpha_3 = -4a_1(1 + a_2), \alpha_4 = (1 + a_2)^2.$$

The numerical coefficient values for the first-, second- and third-order based NTFs and loop-filters for the $\Delta v = 1/32$ case are given in Table 2.3.

Noise Transfer Function				Loop-Filter			
First-Order Differencer Case							
n_1	0.1970	d_1	0.1793	β_1	-0.0177	α_1	0.1970
n_2	1	d_2	0.8207	β_2	-0.1793	α_2	1
Second-Order Differencer Case							
n_1	0.3940	d_1	0.3586	β_1	-0.0353	α_1	0.3940
n_2	2.0388	d_2	1.6735	β_2	-0.3653	α_2	2.0388
n_3	0.3940	d_3	0.2943	β_3	-0.0996	α_3	0.3940
n_4	1	d_4	0.6735	β_4	-0.3265	α_4	1
Third-Order Differencer Case							
n_1	0.5909	d_1	0.5380	β_1	-0.0530	α_1	0.5909
n_2	3.1164	d_2	2.5585	β_2	-0.5579	α_2	3.1164
n_3	1.1895	d_3	0.8888	β_3	-0.3008	α_3	1.1895
n_4	3.1164	d_4	2.0997	β_4	-1.0167	α_4	3.1164
n_5	0.5909	d_5	0.3623	β_5	-0.2286	α_5	0.5909
n_6	1	d_6	0.5527	β_6	-0.4473	α_6	1

Table 2.3 NTF and Loop-Filter Coefficients for Extended Transformation Technique

The magnitude spectra for a second- and third-order differencer-based NTF for a sinusoidal input amplitude of 0.4, $\nu_C = 17/64$, $\Delta\nu = 1/32$ and dither signal = 0.05 are shown in Figure 2.17.

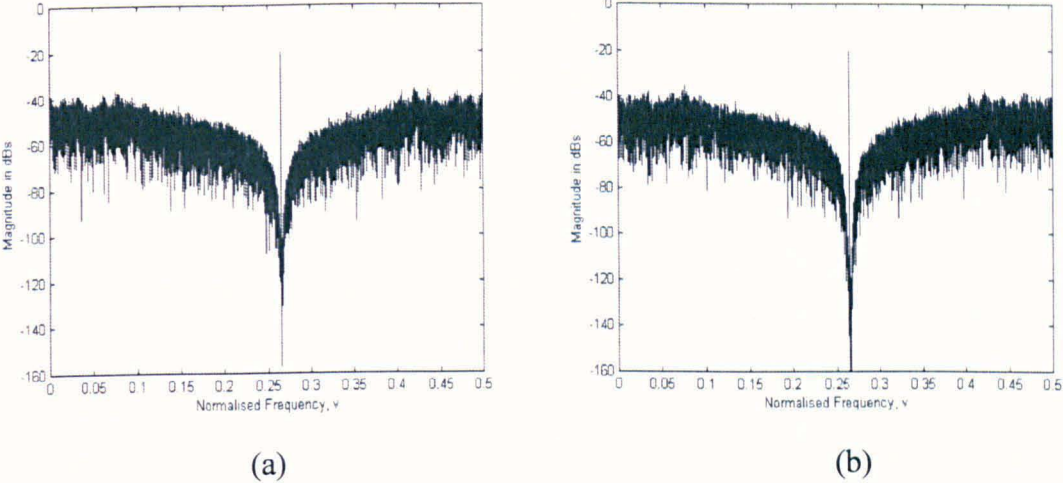


Figure 2.17 Magnitude Spectra using Extended Transformation Approach of a Σ - Δ Modulator at $\nu_C = 17/64$ based on NTFs (a) 2nd-Order Differencer, (b) 3rd-Order Differencer.

The plots in Figure 2.18 show a family of SNR curves for different OSRs for the 1st, 2nd and 3rd order differencer-based NTFs at $\nu_C = 17/64$. Peak SNRs values of 24.9 dB, 34.6 dB, 44.2 dB, 52.8 dB, 61.5 dB and 71.1 are achievable for OSRs of 8, 16, 32, 64, 128 and 256 respectively for the 1st-order case.

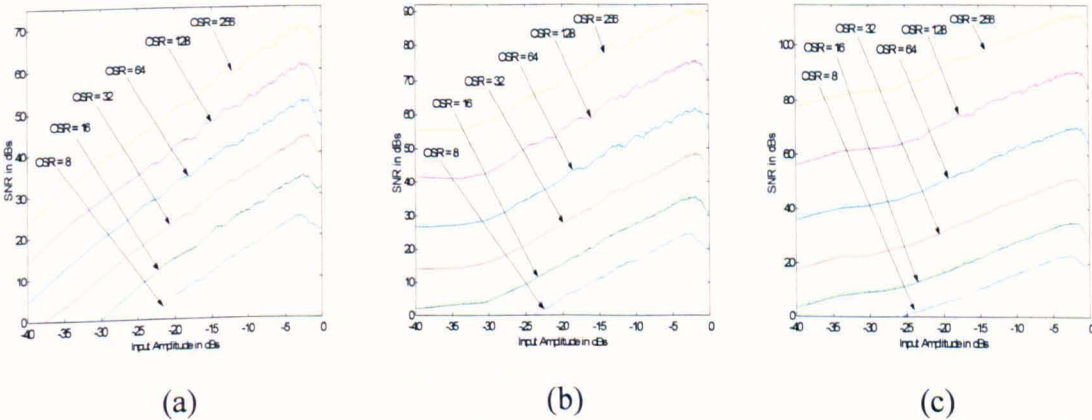


Figure 2.18 SNR Curves using the Extended Transformation Approach of a Σ - Δ Modulator at $\nu_C = 17/64$ based on the NTF of: (a) 1st-Order Differencer, (b) 2nd-Order Differencer and (c) 3rd-Order Differencer.

Similarly; the corresponding set of maximum SNRs for the 2nd-differencer case are 24.6 dB, 35.5 dB, 48.4 dB, 61.8 dB, 75.8 dB and 90.6 dB and the for 3rd-order case, these are 23.2 dB, 34.1 dB, 47.2 dB, 59.3 dB, 68.7 dB and 76.1 dB respectively. In addition, the average increase as a result of doubling the OSR for the 1st, 2nd and 3rd order differencer-based modulators are given by 8.9 dB, 13.1 dB and 17.5 dB respectively. Simulations have also shown that this method does not deliver good SNRs for extremely narrow-bandwidths. This is explained by the fact that the very close clustering of the NTF zeros to the poles do not allow the zeros to accomplish sufficient attenuation in the signal region.

2.9 Criteria for the Design of Variable-Band Bandpass Σ - Δ Modulators

Most of the published work on resonator-based bandpass Σ - Δ modulators has involved utilising a convenient centre frequency that is one quarter of the sampling frequency as confirmed by the literature surveys in Sections 2.2 and 2.3. This section presents several methods for the design of narrow-band bandpass Σ - Δ modulators that can accommodate different passband to sampling frequency ratios, overcoming the popular $f_s/4$ restriction.

All the considered methods will assume that the 1-bit quantiser is modelled by an equivalent additive noise source in order to enable the application of linear theory. As already discussed, this linear model has many limitations, but it provides an adequate general approximation of noise-shaping properties of dithered Σ - Δ modulators. It enables the designer to manually derive reasonably accurate models for the loop- and feedback filters for any noise transfer function specification. The effect of parameter variation on the overall modular characteristics as well as useful intuitive understanding of modulator operation can also be gained from this linear model.

The final theoretical performance of a Σ - Δ modulator has to be verified through detailed behavioural simulations, which incorporate the actual non-linear quantiser. The ultimate design stage may include adjusting the modulator feedforward and/or feedback coefficient(s) to achieve more effective noise-shaping and better resolution. It may also involve varying the amount of dither at the quantiser input or modifying the loop-filter initial conditions to suppress in-band tones.

A block diagram of a single-stage Σ - Δ modulator is shown in Figure 2.19, where $L(z)$ and $F(z)$ depict the loop- and feedback transfer functions and $X(z)$, $Y(z)$, $Q(z)$ and $D(z)$ represent the input, output, quantisation noise and dither signals respectively.

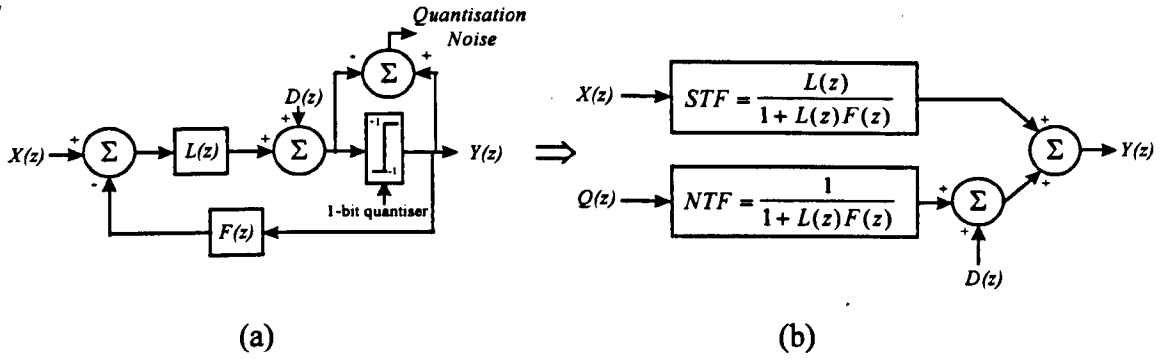


Figure 2.19 Block Diagram of (a) Single-Stage Σ - Δ Modulator, (b) Equivalent Linear Model.

This linearised approach enables the modulator to be characterised by a Signal Transfer Function (STF) $H_S(z)$ and a Noise Transfer Function (NTF) $H_N(z)$ as shown in Figure 2.19 (b). The expressions for the $H_S(z)$ and $H_N(z)$ are given by:

$$H_S(z) = \frac{L(z)}{1 + L(z)F(z)} \quad \text{and} \quad H_N(z) = \frac{1}{1 + L(z)F(z)} \quad (2.17)$$

The loop- and feedback filters can be analytically derived by re-arranging the expression for the $H_N(z)$ as shown below:

$$F(z)L(z) = (1 - H_N(z))/H_N(z) \quad (2.18)$$

The individual transfer functions for $F(z)$ and $L(z)$ can be simply obtained by separating the numerator and denominator expressions such that $F(z) = (1 - H_N(z))$ and $L(z) = 1/H_N(z)$.

It is useful at this stage to define a set of criteria that will ensure the design of stable high-resolution variable-band bandpass Σ - Δ modulators.

The causality criterion requires the loop around the quantiser to contain at least one delay. This condition must be met to ensure that the preceding quantisation error values are used to form the current input to the quantiser. If this criterion is not satisfied then the modulator can not be implemented. This causality rule is usually applied to the NTF and is mathematically depicted by

$$\lim_{z \rightarrow \infty} H_N(z) = 1 \quad (2.19)$$

which implies that the NTF numerator and denominator polynomials must be of the same order with both leading coefficients set to unity. This can be accomplished by incorporating the delayer component either in the loop-filter $L(z)$ or feedback filter $F(z)$. Note that the

simultaneous insertion of delayers in both $L(z)$ and $F(z)$ causes unnecessarily large phase shifts in the modulator spectral responses, as confirmed by simulations, leading to instability.

The modulator NTF must satisfy the stability criterion according to [Lee87b]. Making the approximately derived linear model stable does not guarantee the stability of the modulator due to the presence of the non-linear quantiser. A non-linear system may become unstable, if the out-of-band noise gain gets too high. Extensive empirical investigation by Lee, taking into account component and manufacturing tolerances requires the NTF to satisfy (2.20):

$$|H_N(z)| \leq 1.6 \quad (2.20)$$

The stability of higher-order single-bit bandpass Σ - Δ modulators can be further enhanced by designing NTFs that do not exhibit gain peaks in the magnitude spectra in order to control the signal amplitude levels within the modulator, thereby avoiding quantiser overloading.

The deployment of the NTF zeros and consequently loop-filter poles exactly on the unit-circle at the desired centre frequency accomplishes maximum in-band quantisation noise attenuation resulting in a very deep 'V-shaped' notch. This can be mathematically verified by ensuring that the squared and constant term coefficients of the resonator denominator are both equal to unity [Sig95]. If the loop-filter poles are positioned at the wrong frequency (i.e. wrong angle in the z -plane), then the noise notch will be improperly centred. More seriously, the movement of the resonator poles inside the unit-circle reduces the resonator gain (i.e. Q -factor) at the centre frequency of interest. The in-band notch becomes shallower resulting in a poor noise-shaping response and a lower in-band SNR. If the radii of the resonator poles are reduced by more than 5% from unity, then the noise-shaped magnitude spectrum begins to exhibit more tones.

From a time-domain point-of-view, the leakage factor in the resonator is responsible for the creation of a permanent error between the modulator input and output signals, thus accounting for the lower SNR performance.

It can be reasonably argued that the internal signal levels within the modulator will have smaller amplitudes, which implies that the limit cycle oscillations will be disturbed less often resulting in the occurrence of more identical sample patterns in the time-domain.

The slight movement of some or all the resonator poles outside the unit-circle increase the vulnerability of the modulator towards instability. This, however, causes the

break-up of some of the limit cycle oscillations resulting in fewer tones appearing across the spectrum.

The noise-shaping characteristics of the modulator are related to the loop-filter characteristics including the accuracy and locations of its poles and zeros, the initial conditions of the loop-filter, the number of levels in the quantiser as well as the type and amplitude of the input signal. The use of coincidental zeros, integers or multiple of 2 coefficients in the NTFs and loop-filter simplify the hardware complexity of Σ - Δ modulators [Nor97, pp. 282].

The NTF method circumvents the need to obtain or design a lowpass Σ - Δ modulator prototype by starting the design process directly for the bandpass Σ - Δ modulator. This is particularly useful for the design of higher-order modulators, where the maximum magnitude gain of the noise-shaping spectrum can be exactly determined and reduced if necessary to ensure modulator stability.

2.10 The FIR Notch-Filter (FNF) Approach

This method is based on positioning the zeros of the real-coefficient NTF in conjugate pairs on the unit-circle at the selected centre frequency location to provide maximum signal-band attenuation. The zeros of the NTF are located at $e^{\pm j2\pi\nu_c}$, where ν_c is the normalised centre frequency of interest. The poles of the NTF, however, are permanently stationed at the origin of the unit-circle. The NTF is given by:

$$H_N(z) = 1 - 2 \cos \alpha z^{-1} + z^{-2} \quad (2.21)$$

The expressions for the loop $L(z)$ and feedback $F(z)$ filters can be analytically obtained by substituting the $H_N(z)$ into (2.21) resulting in

$$L(z) = 1 / 1 - 2 \cos \alpha z^{-1} + z^{-2} \quad \text{and} \quad F(z) = 2 \cos \alpha z^{-1} - z^{-2} \quad (2.22)$$

The corresponding Pole-Zero-Patterns (PZPs) for $H_N(z)$, $L(z)$ and $F(z)$ are given below:

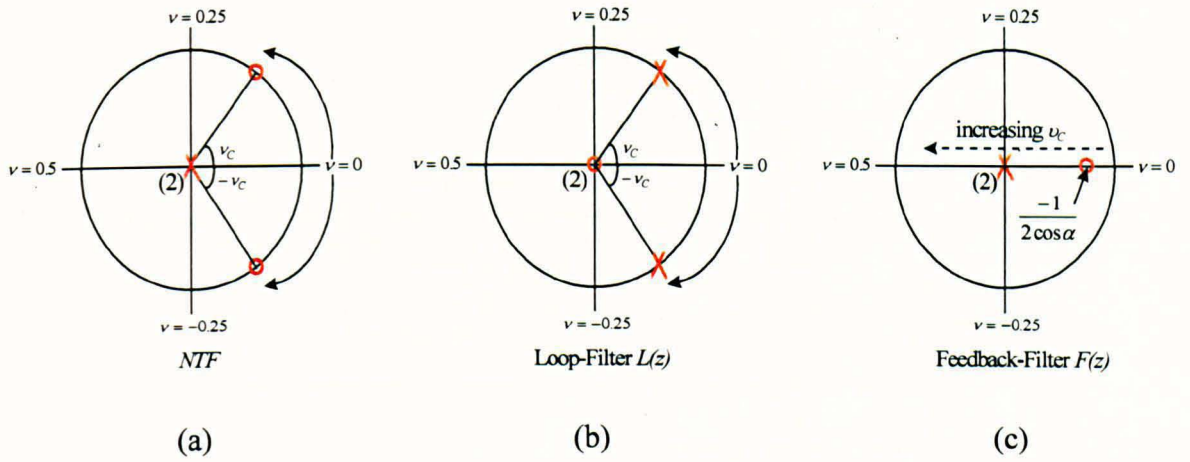


Figure 2.20 Pole-Zero-Patterns of (a) FIR Notch-Filter NTF, (b) Loop-Filter, (c) Feedback Filter.

This linear analysis reveals that a double delayer on its own in the feedback path, unlike the mid-band resonator case, is insufficient to completely cancel the denominator components of STF and NTF in (2.17) to unity. Simulations confirm that improper denominator cancellation lowers the in-band quantisation noise attenuation. The inclusion of a weighted single-delayer (i.e. $2 \cos 2\pi v_C z^{-1}$) in summation with the double delayer in the feedback path, depicted by $F(z)$, achieves the necessary cancellation and thus provides more effective noise-shaping. Note that $F(z)$ degenerates to a double-delayer only when $v_C = 1/4$. Simulations confirm that smoother magnitude spectra and better in-band SNRs are accomplished with the inclusion of the $(2 \cos 2\pi v_C z^{-1})$ term in the modulator feedback path.

The second-order Σ - Δ modulator shown in Figure 2.5(b) is up-graded so as to enable it to achieve noise-shaping for any normalised centre frequency in the range $0 < v_C < 0.5$. The variation of the noise-shaping band location is achieved by changing the value of β where $\beta = 2 \cos 2\pi v_C$. This corresponds to the movement of the poles of $L(z)$ along the unit-circle to the specified centre frequency location. The modified resonator-based Σ - Δ modulator structure is illustrated in Figure 2.21. Note that $\beta = \beta_1 = \beta_2 = 1$ in this case.

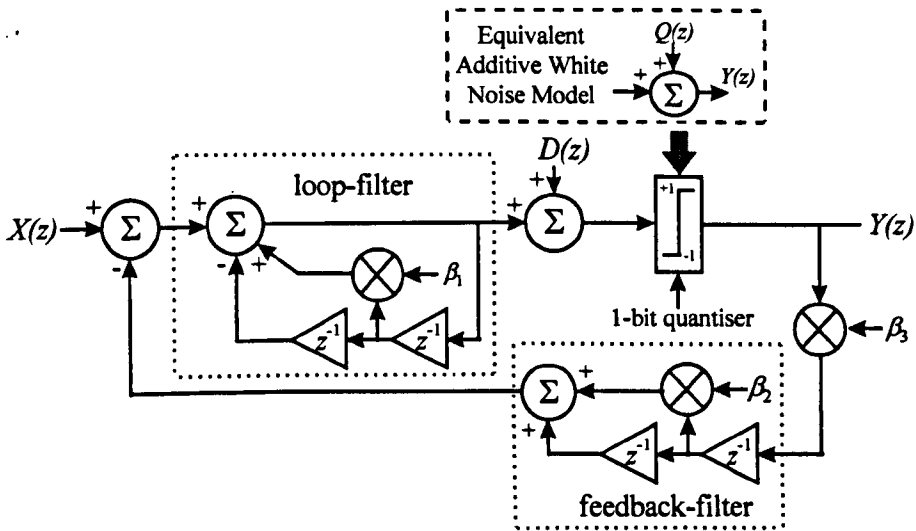


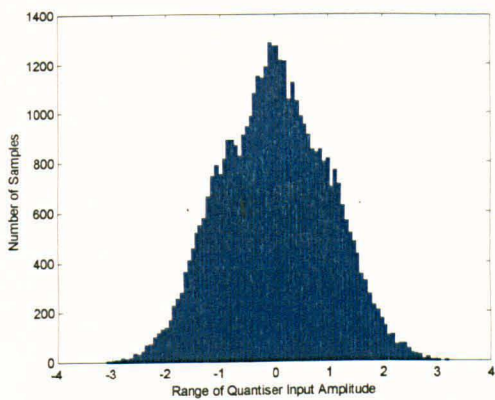
Figure 2.21 Variable-Band Second-Order Bandpass Σ - Δ Modulator.

The linearised output expression for structure shown in Figure 2.21 is

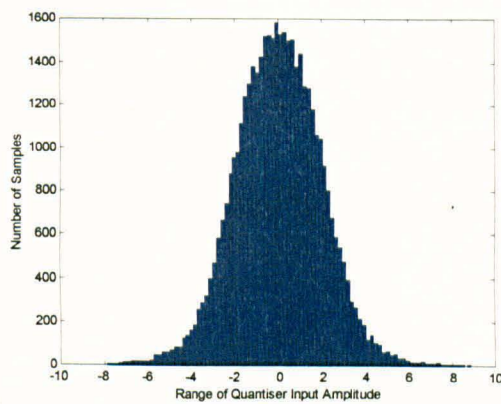
$$Y(z) = X(z) + (1 - \beta z^{-1} + z^{-2})Q(z) \quad (2.23)$$

where $H_S(z)$ is equal to unity and $H_N(z) = (1 - \beta z^{-1} + z^{-2})$.

The NTF for non-mid-band centre frequencies exhibit asymmetrical magnitude responses. This imbalance in shoulder gain levels reaches peak values of $(2 - \beta)$ for $0 \leq \nu_C \leq 0.25$ and $(2 + \beta)$ for $0.25 \leq \nu_C \leq 0.5$. This unevenness is transferred into the loop-filter characteristics as a result of the NTF of (2.23) resulting in asymmetrical magnitude spectra. This asymmetry causes the amplification of some of the internal signal levels in the modulator, especially at the quantiser input. Figure 2.22(a) and 2.22(b) contrast the histograms of the quantiser input for a second-order modulator for a 0.7 input amplitude sinusoid for $\nu_C = 1/4$, and $\nu_C = 1/64$, where larger input quantiser amplitudes are clearly observed with the latter case.



(a)

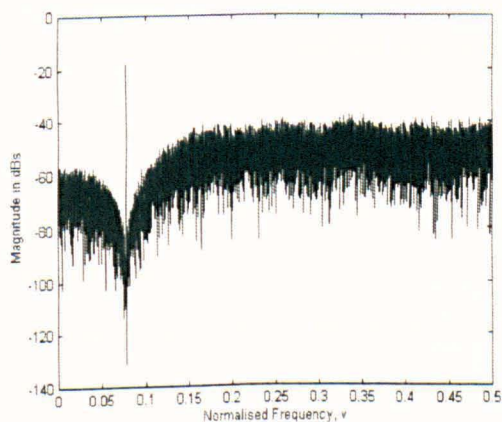


(b)

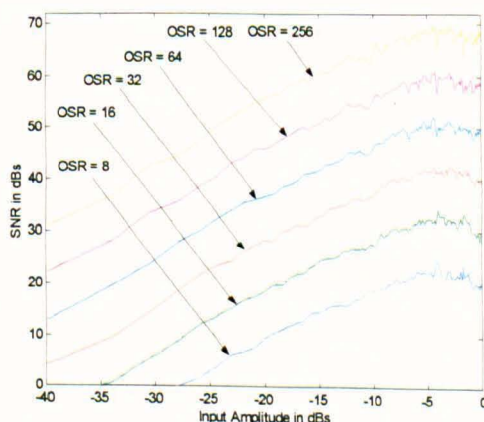
Figure 2.22 Histograms of the Range of Quantiser Input Amplitude for a Variable-Band Second-Order Σ - Δ Modulator at (a) $v_C = 1/4$, (b) $v_C = 1/64$.

Simulations confirm that this second-order Σ - Δ modulator remains stable up to full scale input amplitudes for all values of v_C , despite the large internal signal levels. The family of SNR curves in Figure 2.23 exhibit non-linearities for large input amplitudes due to quantiser overloading.

The degree of non-linearity becomes more noticeable for noise-shaping bands that are positioned close to dc or Nyquist due to the disparity of the shoulder gain levels of the NTF. Figure 2.23 also shows that this modulator exhibits better in-band SNR curves (by as much as 3 dB) for $v_C = 5/64$, $v_C = 17/64$ and $v_C = 29/64$ compared with those obtained for the modulator in Figure 2.13. This improvement is attributed to the β coefficient in the feedback path, which is doubled in value compared with the Harris lowpass-to-bandpass transformation technique. Thus, it is concluded that this bandpass Σ - Δ modulator provides more effective noise-shaping by as much as an extra half-bit of resolution compared with its sister topology in Figure 2.13.



(a)



(b)

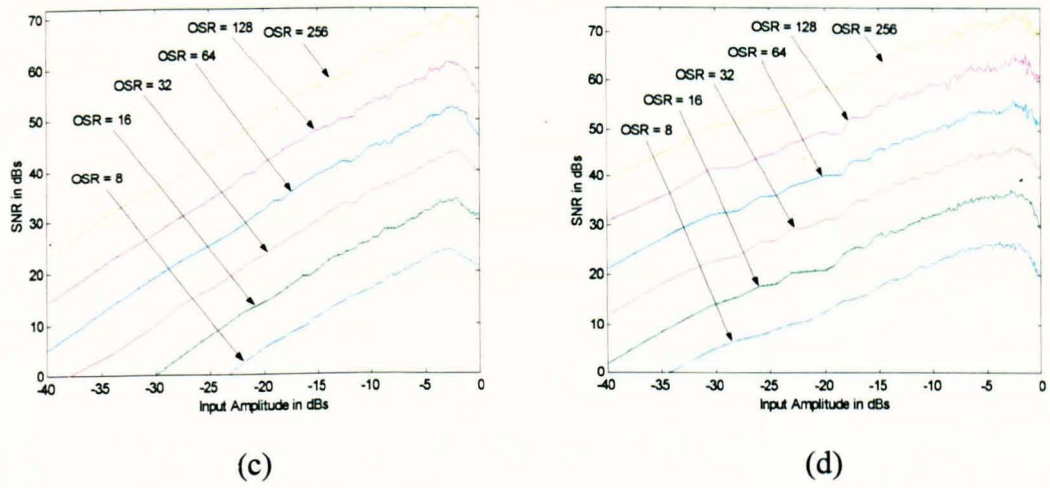


Figure 2.23 (a) Magnitude Spectrum of a Second-Order $\Sigma\text{-}\Delta$ Modulator at $\nu_C = 5/64$, SNR Curves versus Input Amplitudes for Variable-Band Bandpass $\Sigma\text{-}\Delta$ Modulators for Different OSRs at (b) $\nu_C = 5/64$, (c) $\nu_C = 17/64$ and (d) $\nu_C = 29/64$.

For non-mid-band second-order $\Sigma\text{-}\Delta$ modulators, the additional middle-term coefficient, (i.e. β) leads to the creation of more state values, resulting in more tones having smaller amplitudes. However, the magnitude spectrum corresponding to noise-shaping bands at $\nu_C = 1/6$ and $\nu_C = 1/3$ exhibits more distinct tones compared with other centre frequencies. The strength of these tones is attributed to the simple integer coefficients of the loop-filter, which yield fewer and more frequent state values. These integer coefficients create finite-amplitude internal signals, which occur at exact bin locations. This explains why the magnitude spectra for $\nu_C = 1/6$, $\nu_C = 1/4$ and $\nu_C = 1/3$ are more tonal compared with other values of ν_C .

A more hardware-efficient second-order bandpass $\Sigma\text{-}\Delta$ modulator combining $L(z)$ and $F(z)$ into a single filter that is more suitable for implementation purposes as given by (2.24). The modified linearised output expression has been altered as depicted by:

$$Y(z) = (\beta z^{-1} - z^{-2})X(z) + (1 - \beta z^{-1} + z^{-2})Q(z) \quad (2.24)$$

It should be noted that in spite of this STF change, the variation in the magnitude and phase characteristics in the in-band signal region between (2.23) and (2.24) are negligible.

This technique can be extended to higher-order $\Sigma\text{-}\Delta$ modulators, where improved in-band SNRs and DRs can be accomplished for any variable centre frequency. Higher-order NTFs can be simply designed by coincidentally positioning multiple conjugate pairs of

quadrupled in amplitude compared with the mid-band case. This explains why non-mid-band fourth-order Σ - Δ modulators are less stable in comparison with their mid-band counterparts.

The 3-D plot in Figure 2.25(b) demonstrates that this fourth-order bandpass Σ - Δ modulator is stable up to an input amplitude of unity, with 1% dither and under random initial conditions for the mid frequency range $0.218 \leq \nu_C \leq 0.282$. The modulator instability, outside this range, is attributed to the rising shoulder gain levels of the resonator at low and high frequencies for $0 < \nu_C < 0.218$ and $0.282 < \nu_C < 0.5$ respectively.

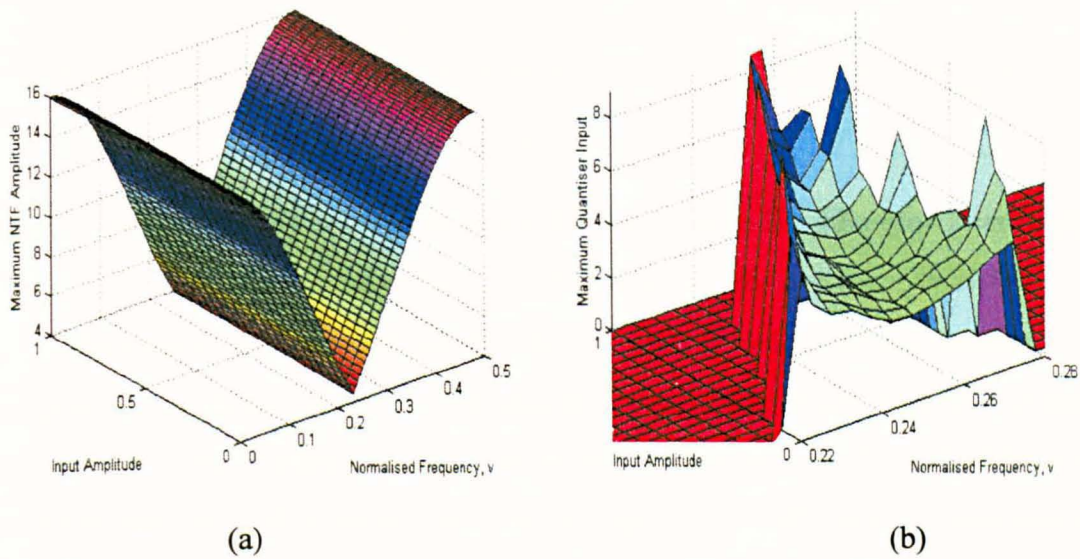


Figure 2.25 (a) Maximum NTF Amplitude, versus Input Signal Amplitude versus Normalised Frequency, (b) 3-D Plot illustrating the Stable Range of Normalised Centre Frequencies for a Fourth-order Variable-Band Resonator-Based Bandpass Σ - Δ Modulator.

The effect of this asymmetry becomes even more significant for higher-order variable-resonator based modulators, because the signals in the feedforward path in the modulator are effectively amplified by the gain of L resonators in cascade, thus overloading the 1-bit quantiser.

The modulator in Figure 2.24 can be made stable for all centre frequencies by reducing the gains α_1 and α_2 in the feedforward path. A conservative empirical rule-of-thumb, which was found to work for a whole range of centre frequencies involved using the inverse of the peak NTF magnitude for the g_1 coefficient. The gain of the first loop-filter is the most critical as this has global control over all the internal signal levels of the modulator. The stability of this variable-band fourth-order Σ - Δ modulator was evaluated

for a whole range of centre frequencies. A family of SNR curves for three different centre frequencies are shown below in Figure 2.26. The premature instability experienced by this modulator at frequencies very close to DC or Nyquist is caused by the disproportionate shoulder gain levels of the loop-filter.

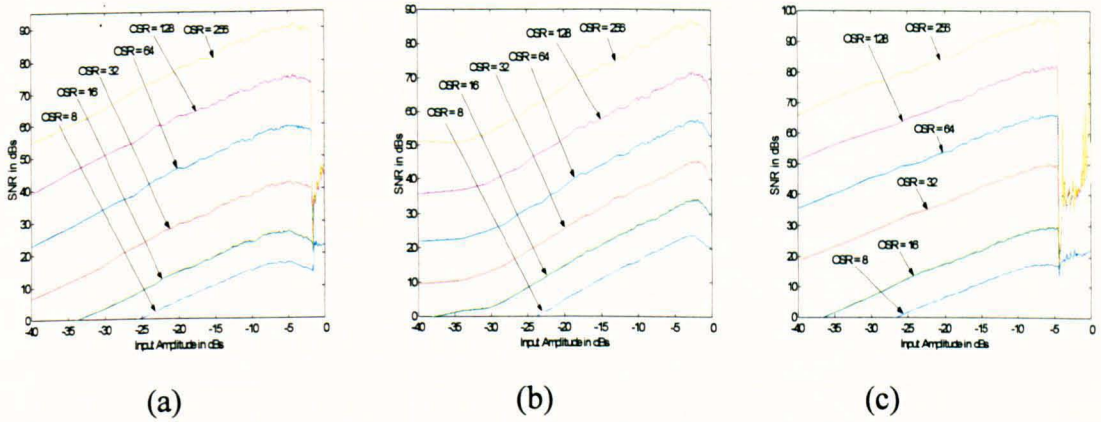


Figure 2.26 Family of SNR Curves versus for the Variable-Band Fourth-Order Bandpass Σ - Δ Modulators at (a) $\nu_C = 5/64$, (b) $\nu_C = 17/64$ and (c) $\nu_C = 29/64$.

Behavioural level simulations for the 2nd and 4th-order variable resonator based bandpass Σ - Δ modulator show that the peak SNRs and DRs remain relatively constant for any arbitrary centre frequency as can be deduced from the results in Table 2.4. Simulations also show that the SNR is improved by an average of 15.6 dB for every doubling of the OSR for all examined frequencies in Table 2.4.

ν_C	Second-Order Peak SNR/dBs	Fourth-Order Peak SNR/dBs	Second-Order DR/dBs	Fourth-Order DR/dBs
1:8	55.8	94.7	59.8	101.7
1:7	55.1	93.6	59.0	99.8
1:6	55.0	93.4	58.1	98.6
3:16	54.9	92.6	58.8	97.6
1:5	56.8	93.3	57.8	96.8
3:8	56.3	94.8	59.7	100.4
2:5	56.7	94.7	60.5	99.4

Table 2.4 Peak SNRs and DRs for 2nd and 4th Order Bandpass Σ - Δ Modulators

This modulator can be also stabilised by replacing the single-bit quantiser with a multi-bit quantiser. The use of a multi-level quantiser generates small quantisation error

signals, which help to control the amplitude levels of the internal signals in the modulator. Compared with the single-bit quantiser case, these relatively small signal levels do not overload the quantiser as often, resulting in more stable modulators.

a	8-levels	a	9-levels	a	10-levels
0.8	$0.142 < v_C < 0.353$	0.8	$0.124 < v_C < 0.371$	0.8	$0.108 < v_C < 0.393$
0.5	$0.129 < v_C < 0.371$	0.5	$0.115 < v_C < 0.384$	0.5	$0.107 < v_C < 0.393$
0.1	$0.129 < v_C < 0.371$	0.1	$0.102 < v_C < 0.399$	0.1	$0.098 < v_C < 0.402$
0.01	$0.116 < v_C < 0.384$	0.01	$0.103 < v_C < 0.402$	0.01	$0.098 < v_C < 0.397$
a	11-levels	a	12-levels	a	13-levels
0.8	$0.093 < v_C < 0.402$	0.8	$0.088 < v_C < 0.424$	0.8	$0.057 < v_C < 0.442$
0.5	$0.080 < v_C < 0.420$	0.5	$0.068 < v_C < 0.429$	0.5	$0.045 < v_C < 0.469$
0.1	$0.067 < v_C < 0.433$	0.1	$0.063 < v_C < 0.442$	0.1	$0 < v_C < 0.5$
0.01	$0.054 < v_C < 0.446$	0.01	$0.050 < v_C < 0.450$	0.01	$0 < v_C < 0.5$
a	14-levels	a	15-levels	a	16-levels
0.8	$0 < v_C < 0.46$	0.8	$0 < v_C < 0.5$	0.8	$0 < v_C < 0.5$
0.5	$0 < v_C < 0.5$	0.5	$0 < v_C < 0.5$	0.5	$0 < v_C < 0.5$
0.1	$0 < v_C < 0.5$	0.1	$0 < v_C < 0.5$	0.1	$0 < v_C < 0.5$
0.01	$0 < v_C < 0.5$	0.01	$0 < v_C < 0.5$	0.01	$0 < v_C < 0.5$

Table 2.5 Stable Range of v_C versus the Number of Quantiser Levels for a 4th-Order Variable-Resonator Based Bandpass Σ - Δ Modulator.

Detailed simulation results were carried out for the 4th-order variable-resonator based bandpass Σ - Δ modulator to establish the relationship between the stable range of normalised frequencies with respect to the number of quantiser levels. Table 2.5 summarises these results, where it can be clearly seen that the stable range of normalised frequencies increases with more quantisation levels. Note that a refers to the amplitude of the input signal to the modulator. This modulator for an amplitude dither signal of 0.01 requires at least 15 levels to remain stable up to an input signal amplitude of 0.8 and needs 16 levels (i.e. 4-bits) for it to remain stable up to full-scale input amplitude. A further observation is that the stable range of normalised frequencies increases as the input amplitude signal decreases in value. This confirms that the stable range of normalised

frequencies is a function of both the input signal amplitude as well as the location of the noise-shaping band.

A family of SNR curves for the 4th-order variable-band bandpass Σ - Δ modulator for different quantiser levels is shown in Figure 2.27, where the linearity of the SNR plots is seen to improve as the number of quantiser levels increases.

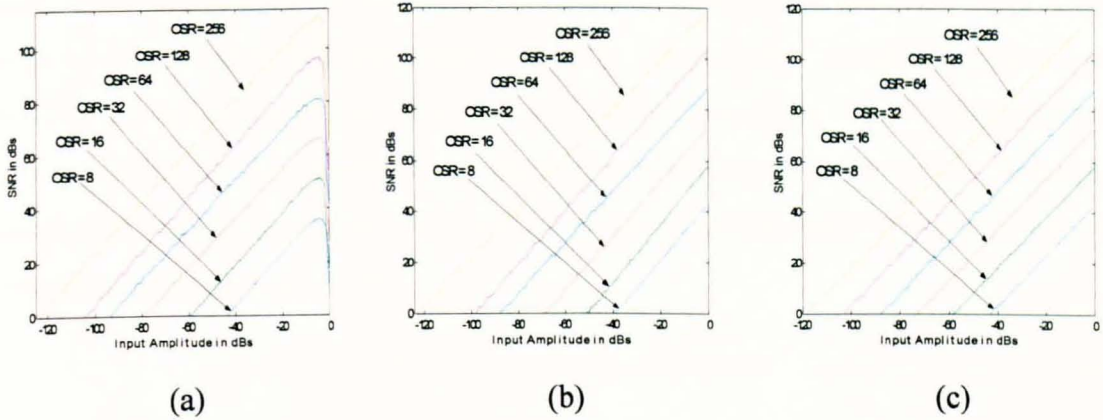


Figure 2.27 Family of SNR Curves for the Fourth-Order Bandpass Σ - Δ Modulator at $\nu_C = 17/64$: (a) 3-levels, (b) 5-levels and (c) 15-levels.

The maximum achievable SNR for this 4th-order bandpass Σ - Δ modulator for different combinations of multi-level quantisers and OSRs are shown in Table 2.6. As expected, the peak SNR figures increase in proportion to the number of levels in the quantiser. However, a point is reached, where this SNR improvement ceases, making it unnecessary to utilise quantisers with additional levels. For this modulator, the critical number of levels appears to be between 5 and 6 based on the results presented in Table 2.6.

OSR	Peak SNRs in dBs					
	2-levels	3-levels	4-levels	5-levels	6-levels	15-levels
8	26.5	36.3	42.2	43.2	43.3	43
16	41.9	51.4	57.1	58.1	58.3	58.5
32	57.1	66.4	72.2	72.9	73.4	73.2
64	72	81.3	87	88.5	88.4	88.5
128	87.2	96.9	102.6	102.7	103.8	103.1
256	102	111.7	117.2	117.8	119.4	118.6

Table 2.6 Peak SNR values versus the Number of Quantiser Levels for a 4th-Order Variable-Resonator Based Bandpass Σ - Δ Modulator at $\nu_C = 17/64$.

A third alternative of obtaining stability is to utilise IIR notch filters for the NTF as will be explained in the next section.

2.11 The IIR Notch-Filter (INF) Approach

The uneven shoulder gain levels of the magnitude spectrum for most frequencies is a major drawback of the FNF technique. Another limitation is that the notch has a relatively large bandwidth implying that other frequency components, including unwanted tones, close to the desired nulls may be included in the in-band signal region. This constraint is also unsuitable for very narrow-band applications. These two problems can be solved by placing the conjugate pole pairs of the NTF at the same frequency of the null, but with a reduced magnitude as given by:

$$H_N(z) = (1 - 2 \cos \alpha z^{-1} + z^{-2}) / (1 - 2\rho \cos \alpha z^{-1} + \rho^2 z^{-2}) \quad (2.30)$$

where ρ is the magnitude of the NTF poles. The deployment of the poles close to the zeros at the same frequency creates resonance in the null region, which simultaneously reduces the notch bandwidth and increases its attenuation at the selected centre frequency.

Theoretical analysis backed-up with simulations indicate that more effective notches are attainable when $\rho > 0.9$. The placement of the poles close to the band edges helps to alleviate the out-of-band gain in order to achieve stability of higher-order bandpass Σ - Δ modulators.

The two spectral magnitudes of FIR and IIR notch filter for $\nu_C = 5/64$, are shown in Figure 2.28, where almost a threefold gain reduction is attained by making $\rho > 0.9$.

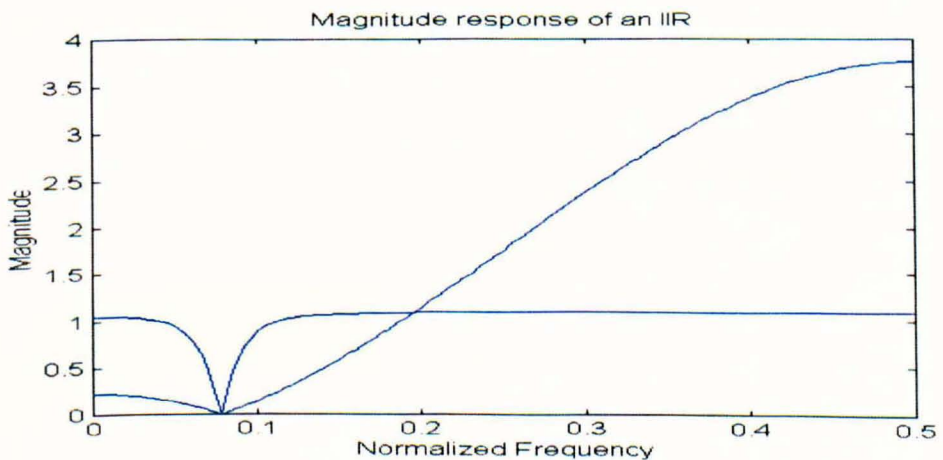


Figure 2.28 A NTF Magnitude Comparison of FIR and IIR Notch-Filter Based Variable-Band Second-Order Σ - Δ Modulator at $\nu_C = 5/64$.

The PZPs of $H_N(z)$, $L(z)$ and $F(z)$ belonging to this technique are shown in Figure 2.29.

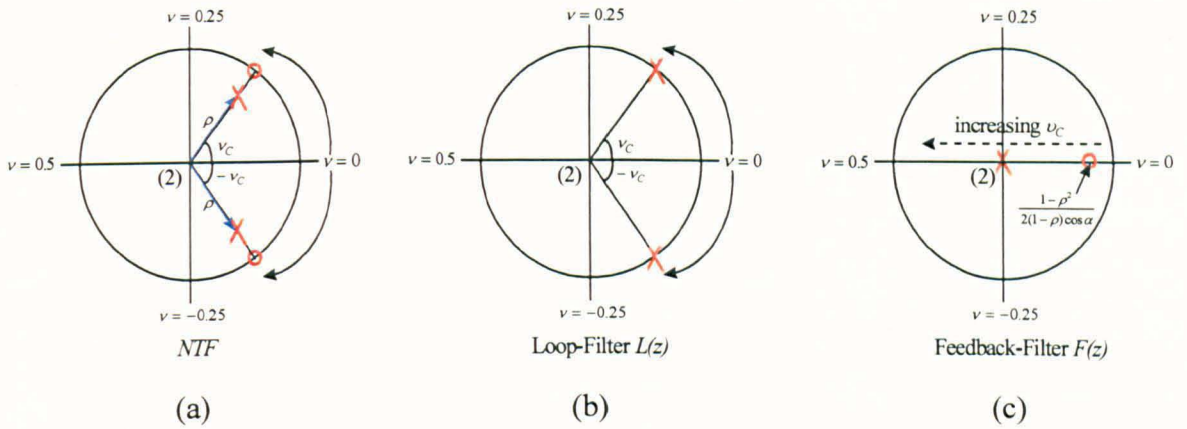


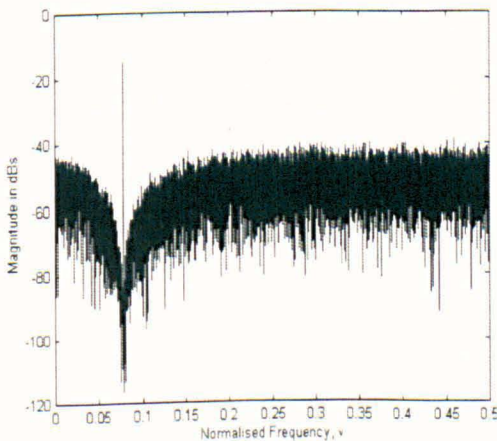
Figure 2.29 PZPs of (a) IIR Notch-Filter NTF, (b) Loop-Filter, (c) Feedback Filter.

The corresponding loop- and feedback transfer functions are given by:

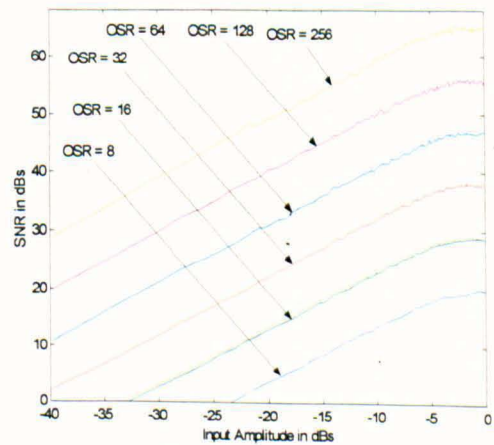
$$L(z) = 1 / (1 - 2 \cos \alpha z^{-1} + z^{-2}) \quad \text{and} \quad F(z) = 2 \cos \alpha (1 - \rho) z^{-1} + (\rho^2 - 1) z^{-2} \quad (2.31)$$

Figure 2.30(a) confirms the correct operation of the INF approach by showing this modulator achieving noise-shaping at $v_c = 5/64$ for an input level of 0.5 and dither amplitude of 0.05.

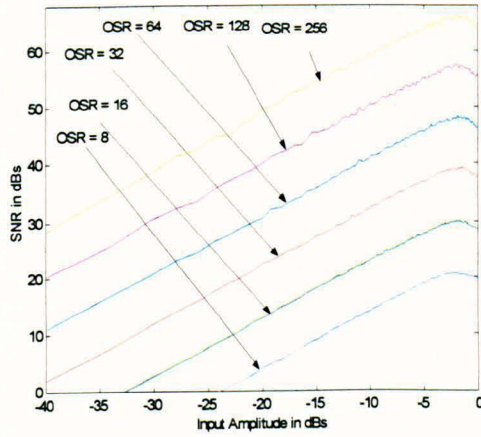
The family of SNR curves in Figure 2.30(b) are shown to exhibit greater linearity compared with those obtained using the FNF approach. These linear characteristics are attributed to less frequent quantiser overloading, which leads to the generation of fewer tones for high input amplitudes.



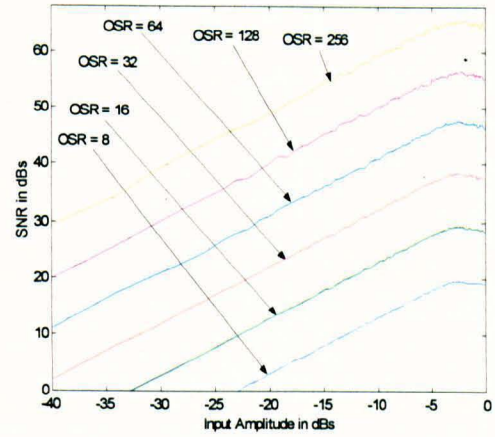
(a)



(b)



(c)



(d)

Figure 2.30 Variable-Band Second-Order Bandpass Σ - Δ Modulator (a) Noise-Shaping Magnitude Spectrum at $\nu_C = 5/64$, SNR Curves versus Input Amplitudes (b) $\nu_C = 5/64$, (c) $\nu_C = 17/64$ and (d) $\nu_C = 29/64$.

The design analysis of this technique can be quite easily extended to fourth-order modulators, where better resolution is achievable for a broader range of centre frequencies without having to incorporate further scaling factors. This NTF is given by:

$$H_N(z) = (1 - 2 \cos \alpha z^{-1} + z^{-2})^2 / (1 - 2\rho \cos \alpha z^{-1} + \rho^2 z^{-2})^2 \quad (2.32)$$

The careful placement of the poles in relation to the zeros for an IIR NTF significantly reduces the out-of-band gains to moderate levels and therefore enhances modulator stability. The corresponding loop and feedback filters are:

$$L(z) = 1 / (1 - 2\beta z^{-1} + (2 + \beta^2)z^{-2} - 2\beta z^{-3} + z^{-4}) \quad (2.33)$$

$$F(z) = 2\beta(1 - \rho)z^{-1} + (2\rho^2 + \rho^2\beta^2 - 2 - \beta^2)z^{-2} + 2\beta(1 - \rho^3)z^{-3} + (1 - \rho^4)z^{-4} \quad (2.34)$$

The SNR curves for the 4th- and 6th-order bandpass Σ - Δ modulators for three different ν_C values are presented in Figure 2.31 and 2.32.

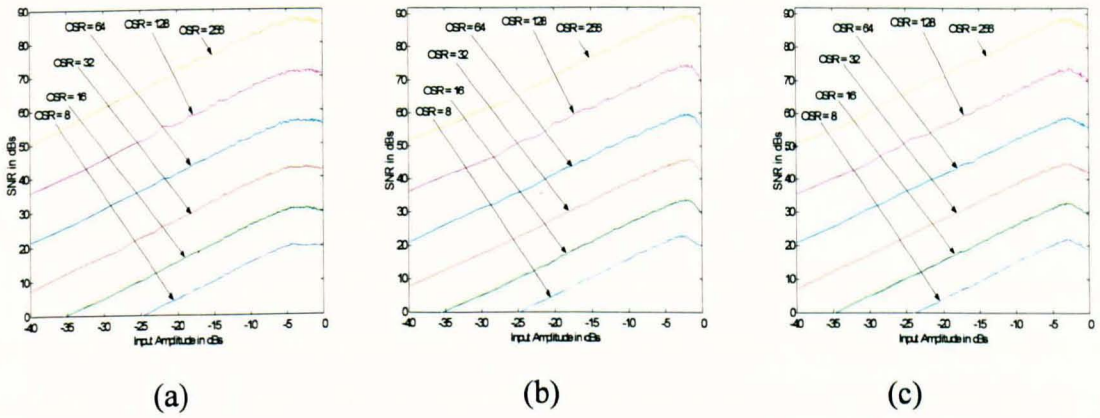


Figure 2.31 SNR Curves versus Input Amplitudes for the IIR NTF Based Fourth-Order Bandpass Σ - Δ Modulators at (a) $\nu_C = 5/64$, (b) $\nu_C = 17/64$ and (c) $\nu_C = 29/64$.

These curves show that the INF approach gives better DRs especially for very small and large centre frequencies. The use of IIR NTFs allows the poles to move closer to the zero locations, so as to even out the shoulder gain levels of NTF for any notch location in the spectrum. However, it should be made clear that this improved resolution is obtained at the expense of having more complicated loop-filters in the modulator.

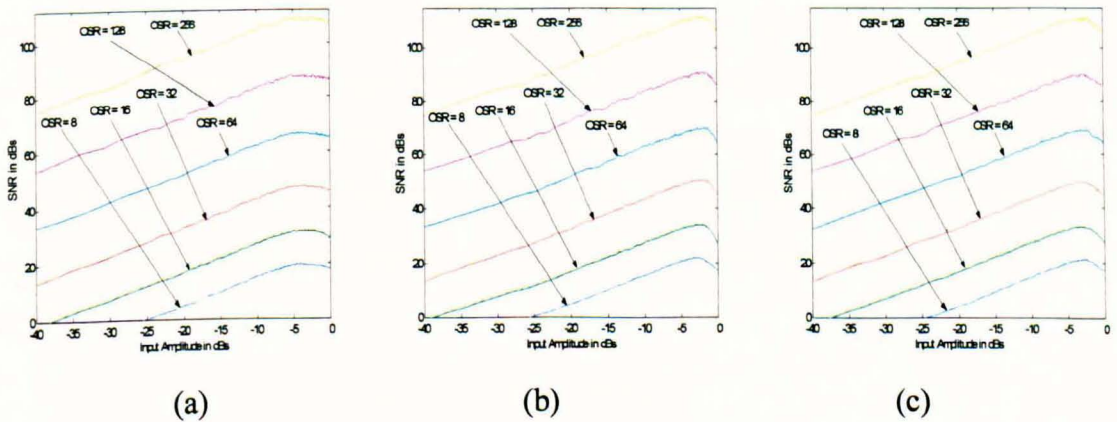


Figure 2.32 SNR Curves versus Input Amplitudes for the IIR NTF Based Sixth-Order Bandpass Σ - Δ Modulators at (a) $\nu_C = 5/64$, (b) $\nu_C = 17/64$ and (c) $\nu_C = 29/64$.

2.12 The Complex FIR Notch-Filter (CFNF) Approach

The majority of the publications on bandpass Σ - Δ modulators have employed real-coefficient NTFs [Sch92]-[Jan93]-[Lon93]-[Tro94] with a few exceptions such as [Jan94a]. These have utilised complicated band-stop filters for their NTFs, which have resulted in less hardware-efficient Σ - Δ modulators, containing many multipliers. The

motivation behind this section is to present the design analysis of complex FIR notch filter based Σ - Δ modulators, whose building blocks constitute fewer multipliers.

A complex bandpass Σ - Δ modulator can take a pair of in-phase and quadrature phase analogue input signals and perform accurate A/D conversion directly generating a pair of high-speed bit-streams [Jan94].

The main advantage of complex Σ - Δ modulators is that the poles and zeros are not restricted to having conjugate pairs, implying that better in-band quantisation noise attenuation can be attainable, compared with a real-coefficient modulator of the same order. Complex Σ - Δ modulators offer greater resolution and design flexibility at the expense of an additional quantiser and signal paths for the imaginary components of the signals in the modulator [Jan94].

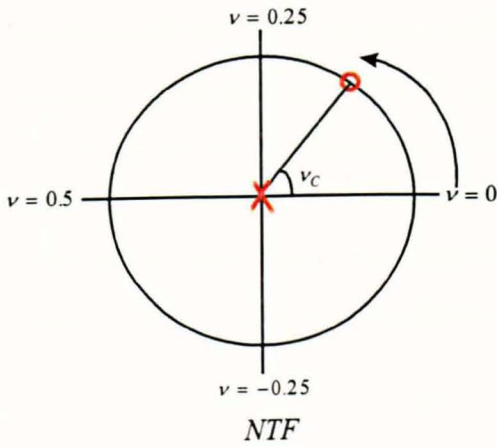
A complex bandpass Σ - Δ modulator is not restricted to having a symmetrical magnitude response around dc, thus making it a viable candidate for the generation of single side-band noise-shaping [Jan96]. The noise-shaping can be observed for the combined complex signal, but not for either the real or imaginary part independently, because the NTF is complex [Azi95].

Complex bandpass Σ - Δ are suitable for the quadrature A/D conversion of signals in monolithic radio receivers [Dia96]-[Li99]. They are also well-suited for the A/D conversion of signals for single-IF receivers and Image-Reject (IR) receivers [Swa97].

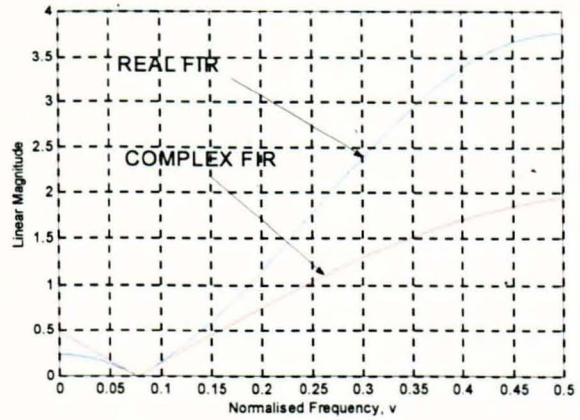
The complex FIR notch filter technique is based on positioning the zeros of the Complex Noise Transfer Function (CNTF) $H_{CN}(z)$ on the unit-circle at the specified positive centre frequency to achieve maximum in-band quantisation noise attenuation. This CNTF is given by:

$$H_{CN}(z) = (1 - e^{j2\pi\nu_C} z^{-1}) \quad (2.35)$$

Figure 2.33(a) shows the PZP for CNTF for an arbitrary ν_C . Figure 2.33(b) contrasts the real- and complex- coefficient NTFs for $\nu_C = 5/64$, where it is seen that the peak magnitude gain of the latter is almost halved. This significant reduction in the CNTF magnitude for all ν_C values provides a stability advantage, whose effects become more apparent for higher-order Σ - Δ modulators.



(a)



(b)

Figure 2.33 (a) CNTF PZP of First-Order Notch Filter (b) NTF Magnitude of Real and Complex First-Order Σ - Δ Modulator at $\nu_c = 5/64$.

The corresponding complex loop $CL(z)$ and feedback $CF(z)$ transfer functions are given by:

$$CL(z) = 1 / 1 - e^{j2\pi\nu_c} z^{-1} \quad \text{and} \quad CF(z) = e^{j2\pi\nu_c} z^{-1} \quad (2.36)$$

The combination of $CL(z)$ and $CF(z)$ simplifies the overall transfer function, thus yielding the complex first-order resonator-based Σ - Δ modulator shown in Figure 2.34.

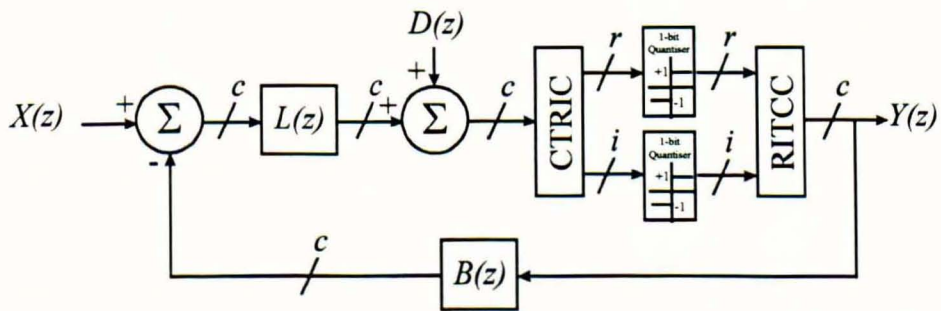


Figure 2.34 Single-Stage Dithered Complex Resonator-Based Bandpass Σ - Δ Modulator

This structure consists of a complex programmable resonator, a Complex-To-Real-Imaginary Converter (CTRIC), two physical quantisers (for the real and imaginary channels respectively) and a Real-Imaginary-To-Complex Converter (RITCC) in the feedforward path. The labels r , i and c denote real, imaginary and complex signal paths. The noise-shaped location in the frequency spectrum is determined by the pole location of this

variable-band resonator. A small amount (5%) of dither $D(z)$ is added at the output of the resonator to alleviate the amplitude and occurrence of spurious tones.

Each of the two quantisers can be modelled as a summer having two inputs, one representing the desired component of the signal (real or imaginary) and the other representing white noise. This linear modelling process enables the overall modulator to be characterised by an equivalent output expression given by:

$$Y(z) = e^{j2\pi v_C} z^{-1} X(z) + (1 - e^{j2\pi v_C}) Q(z) \quad (2.37)$$

This analysis indicates that the poles and zeros of this complex modulator are simply those of a rotated accumulator-based lowpass Σ - Δ modulator [Jan94]. The magnitude spectrum tuning at $v_C = 0.125$ is given below in Figure 2.35.

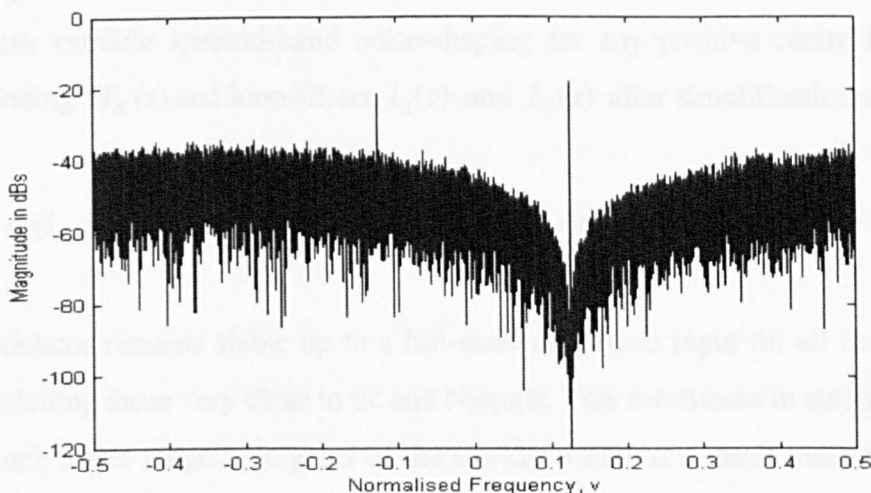


Figure 2.35 Magnitude Spectrum of First-Order Complex Modulator at $v_C = 0.125$.

The complex variable-band NTF reaches a maximum gain of 2 for both dc and Nyquist. This implies that the 1st-order complex variable-band Σ - Δ modulator never overloads the quantiser provided its input does not exceed unity. This is in contrast to its real-coefficient counterpart, which reaches a peak magnitude gain of 4. This ‘non-overloading’ situation explains why the family of SNR curves shown in Figure 2.36 exhibit fewer non-linearities compared with those illustrated in Figure 2.23 for the real NTF case.

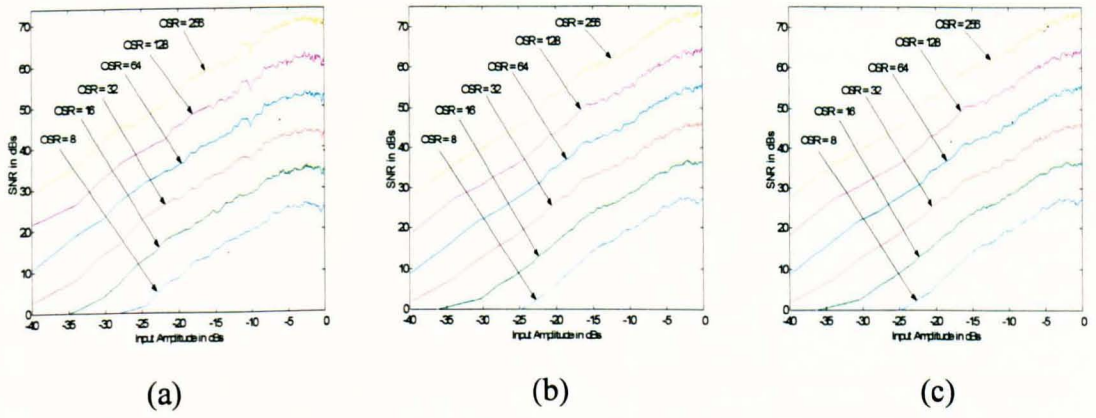


Figure 2.36 SNR Curves for the Complex FIR NTF Based First-Order Bandpass $\Sigma\text{-}\Delta$ Modulators at (a) $\nu_C = 5/64$, (b) $\nu_C = 17/64$ and (c) $\nu_C = 29/64$.

This analysis is extended to a complex second-order bandpass $\Sigma\text{-}\Delta$ modulator, which can accomplish variable spectral-band noise-shaping for any positive centre frequency. The corresponding $H_N(z)$ and loop-filters $L_1(z)$ and $L_2(z)$ after simplification are given by:

$$H_N(z) = (1 - e^{j2\pi\nu_C})^2, \quad L_1(z) = 1/(1 - e^{j2\pi\nu_C}), \quad L_2(z) = e^{j2\pi\nu_C}/(1 - e^{j2\pi\nu_C} z^{-1}) \quad (2.38)$$

This modulator remains stable up to a full-scale amplitude input for all the noise-shaping bands including those very close to dc and Nyquist. This robustness in stability is attributed to the much lower magnitude gains of the CNTF, which as a result maintain significantly smaller internal signal levels in the modulator. The presence of two instead of three summation terms in the CNTF could quantitatively account for the improved stability performance as the maximum possible CNTF peak is 4 instead of 16.

Complex third-order noise-shaping can be achieved, but on this occasion, additional feedback coefficients are deemed necessary to maintain modulator stability as was discussed in Section 2.6. The magnitude spectra for complex IIR notch-filter based second and third order $\Sigma\text{-}\Delta$ modulators for a single-tone sinusoid of 0.5 and dither signal of 0.05 are shown in Figure 2.37.

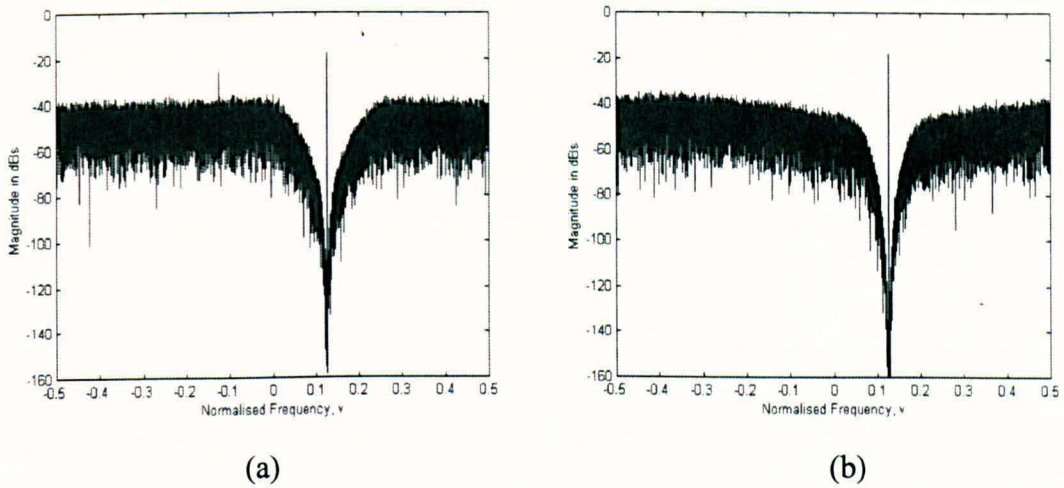


Figure 2.37 Magnitude Spectrum for Complex IIR notch-filter Based (a) Second, (b) Third Order Σ - Δ modulators at $\nu_C = 0.125$.

The family of SNR curves in Figure 2.38 show that larger DRs can be achieved with the complex 2^{nd} -order Σ - Δ modulator as opposed to its real-coefficient counterpart. However, the SNR curves for $\nu_C = 29/64$ display inferior resolution for very high amplitude inputs as depicted in Figure 2.38. The very close proximity of this particular noise-shaping band to Nyquist in contrast with the other two frequencies means that the NTF gains are relatively larger. The bigger gains amplify the input signal to the quantiser causing it to overload more prematurely. This produces limit cycle oscillations in the spectrum including the in-band region, thus accounting for the poor resolution.

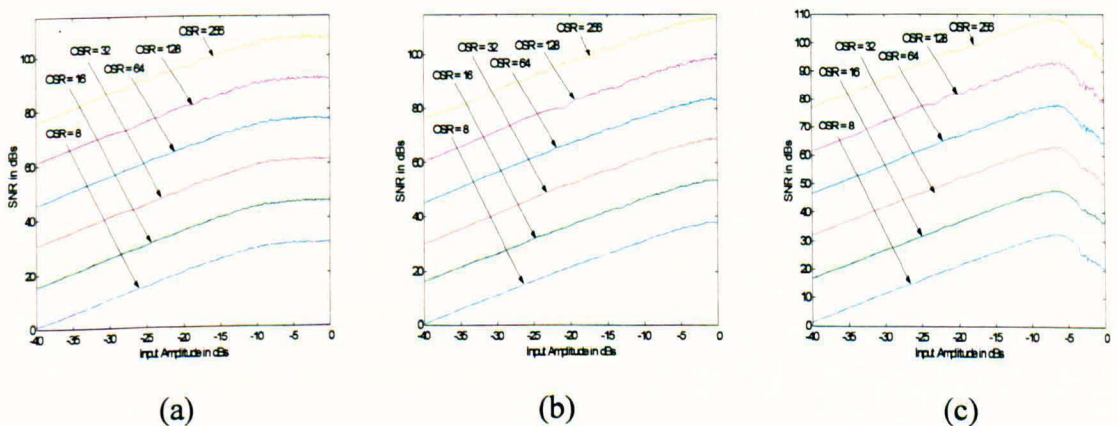


Figure 2.38 SNR Curves for the Complex FIR NTF Based Second-Order Bandpass Σ - Δ Modulators at (a) $\nu_C = 5/64$, (b) $\nu_C = 17/64$ and (c) $\nu_C = 29/64$.

2.13 The Complex IIR Notch-Filter (CINF) Approach

Complex IIR notch filters can be employed to provide narrow-band bandpass Σ - Δ modulators that can deliver better noise-shaping responses and enhanced resolution. This technique is based on positioning the zeros of CINF on the unit-circle at the positive centre frequency of interest to achieve maximum quantisation noise attenuation. The CINF is given by:

$$H_{CN}(z) = (1 - e^{j2\pi\nu_C} z^{-1}) / (1 - \rho e^{j2\pi\nu_C} z^{-1}) \quad (2.39)$$

The corresponding loop and feedback filters are:

$$L(z) = 1 / (1 - e^{j2\pi\nu_C} z^{-1}) \quad \text{and} \quad F(z) = (1 - \rho) e^{j2\pi\nu_C} z^{-1} \quad (2.40)$$

The NTF PZP for a typical variable-band complex IIR first-order is shown in Figure 2.39 (a). The magnitude spectrum for a complex IIR based first-order Σ - Δ modulator at $\nu_C = 0.125$ is presented in Figure 2.39(b).

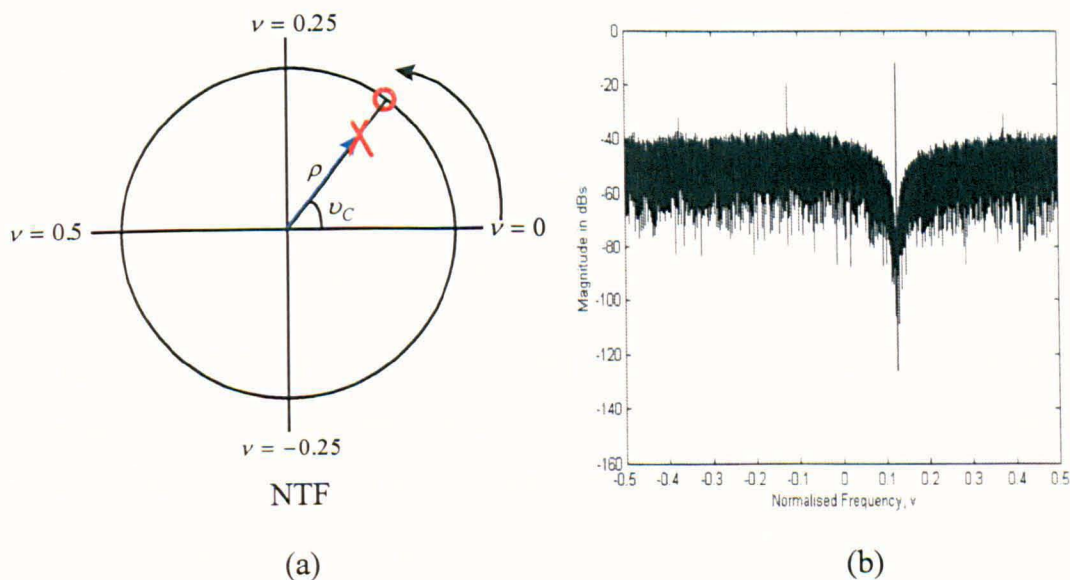


Figure 2.39 (a) CINF PZP of First-Order Notch Filter (b) Magnitude Spectrum of Complex First-Order Σ - Δ Modulator at $\nu_C = 0.125$ of b) First-Order bandpass Σ - Δ Modulators.

The SNR curves for $\nu_C = 5/64$ and $\nu_C = 29/64$ are relatively linear as illustrated in Figure 2.40. This linearity is attributed to the combined effect of non-quantiser overloading and the use of IIR NTFs, which reduce the disparity of the shoulder-gain levels of the loop-filter. However, the fluctuations of the curves for $\nu_C = 17/64$ for OSRs of 128 and 256 is caused by the presence of tones in the in-band region.

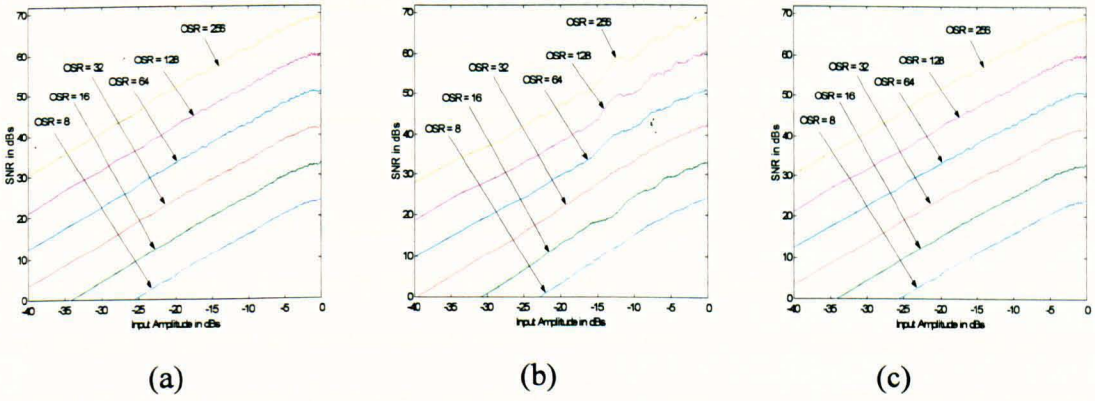


Figure 2.40 SNR Curves versus Input Amplitudes for the Complex IIR NTF Based First-Order Bandpass Σ - Δ Modulators at (a) $\nu_C = 5/64$, (b) $\nu_C = 17/64$ and (c) $\nu_C = 29/64$.

In a similar manner, a second-order complex IIR notch filter can be designed to accomplish improved in-band SNRs and DRs. Its CNTF is given by:

$$H_{CN}(z) = (1 - 2e^{j2\pi\nu_C}z^{-1} + e^{j4\pi\nu_C}z^{-2}) / (1 - 2\rho e^{j2\pi\nu_C}z^{-1} + \rho^2 e^{j4\pi\nu_C}z^{-2}) \quad (2.41)$$

The corresponding complex loop $CL(z)$ and feedback $CF(z)$ filters are given by:

$$CL(z) = 1 / (1 - 2e^{j2\pi\nu_C}z^{-1} + e^{j4\pi\nu_C}z^{-2}) \quad (2.42)$$

$$CF(z) = (1 - 2e^{j2\pi\nu_C}(1 - \rho)z^{-1} + e^{j4\pi\nu_C}(\rho^2 - 1)z^{-2}) \quad (2.43)$$

The family of SNR curves of this complex 2nd-order bandpass Σ - Δ modulator for three different centre frequencies are shown in Figure 2.41. These linear-like SNR characteristics are attributed to the IIR NTFs and the more complex loop-filters.

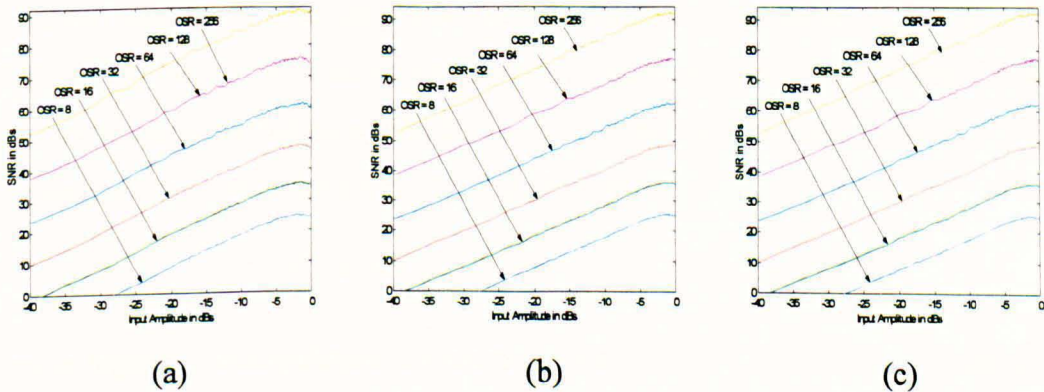


Figure 2.41 SNR Curves versus Input Amplitudes for the Complex IIR NTF Based Second-Order Bandpass Σ - Δ Modulators at (a) $\nu_C = 5/64$, (b) $\nu_C = 17/64$ and (c) $\nu_C = 29/64$.

2.14 Overview on the Fractional Delay Filter (FDF) Approach

This section presents a novel technique for the design of narrow-band Σ - Δ modulators with an embedded tuneable centre frequency mechanism. The method under consideration demonstrates that the use of a sum-filter combined with a fractional-delayer provide the flexibility of adjusting the noise-shaping band location to cater for any narrow-band variable centre frequency input signal. It is initially demonstrated that the inclusion of pure integer delays in combination with sum-filters in these modulators restricts noise-shaping to a few centre frequency locations. This limitation is overcome by designing a NTF, which is formed by a first-order sum-filter depicted by $(1+z^{-1})$ [Cun92] in conjunction with fractional-delayers [Laa96], to accommodate different passband centre to sampling frequency ratios. These FIR and IIR allpass fractional-delayers result in the spectral shifting of the zeros of the NTF to the signal band of interest.

The combination of a first-order sum-filter and an FIR or IIR allpass Fractional-Delay (FD) filter [Laa96] form the NTF, whose zeros are distributed close to the unit-circle at the selected centre frequency. The order of the NTF depends on the order of the FD filter approximation and is represented by a generalised non-integer value D . The parameter D can be expressed as the summation of two variables, (i.e. $D = f + r$), where f is the delay of the FD filter itself (including the fractional component) and r is the additional unit-delay, whose inclusion is compulsory to satisfy the causality criterion. This implies that the NTF design should take into account the extra phase shift imparted by this unit-delay.

It was originally thought that the numerator of the NTF could be scaled to unity to comply with the causality criterion without having to introduce the additional delay term z^{-r} . However, the required scaling of the NTF was found to be very excessive (of the order of 50-60) leading to automatic modulator instability. Regrettably; it was concluded that NTF scaling did not provide an appropriate solution for both the FIR and IIR allpass FD filter techniques, leaving no option but to incorporate the additional delayer.

The general expression for the FD NTF is given by:

$$H_N(z) = 1 + z^{-D} \Rightarrow H_N(v) = 1 + e^{-j2\pi v_c D} \quad (2.44)$$

Simple algebraic manipulation demonstrate that $e^{-j2\pi v_c D} = -1 = 1 \angle \pi$, yielding a simple, but important relationship between v and D as shown below:

$$v = \frac{1}{2D} = \frac{1}{2(f+r)} \quad (2.45)$$

This means that an arbitrary normalised centre frequency can be attained by determining the necessary total delay D that must be incorporated in the NTF, so that the null of the 1st-order sum-filter is spectrally transferred to the corresponding signal frequency band. It is seen from (2.45) that the use of pure integer values for D can only cater for a very limited choice of centre frequencies. For example, setting $D = 2$ can achieve noise-shaping at $\nu_C = 0.25$, which confirm existing theory.

Figure 2.42 together with (2.45) demonstrate that ν_C is inversely proportional to D , implying that centre frequencies close to dc require larger values of D . More interestingly, the tunability of a centre frequency location between 0.25 and 0.5 using this technique can only be achieved by employing a non-integer value for D . For example, $D = 1.3$ is required for $\nu_C = 0.385$.

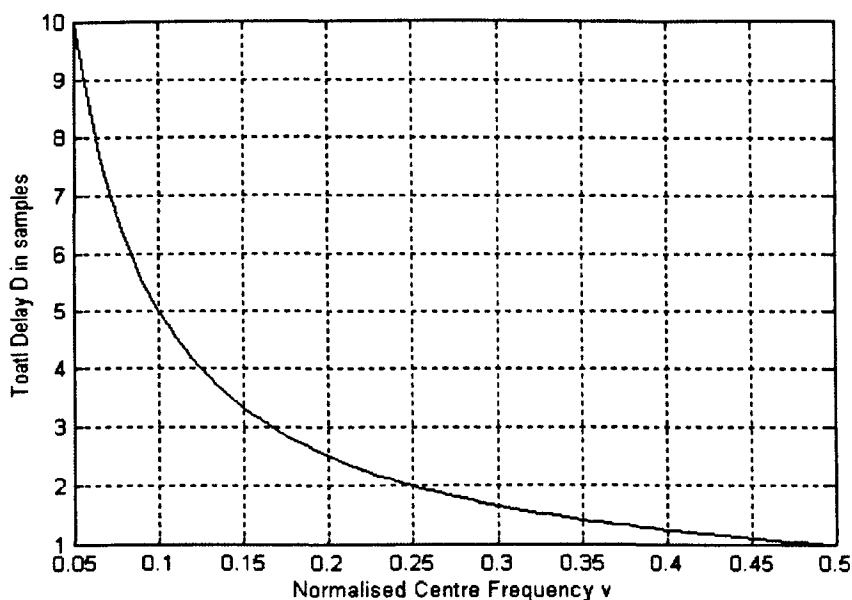


Figure 2.42 Total Delay D in Modulator versus Normalised Centre Frequency ν_C .

It is convenient for explanation purposes to categorise the centre frequency ranges, as far as this method is concerned, according to their required D values as illustrated in Table 2.7.

ν_C Ranges	D
$\nu_C \leq \frac{1}{6}$	$D \geq 3$
$\frac{1}{6} \leq \nu_C \leq \frac{1}{4}$	$3 \geq D \geq 2$
$\frac{1}{4} \leq \nu_C \leq \frac{1}{3}$	$2 \geq D \geq \frac{3}{2}$
$\frac{1}{3} \leq \nu_C \leq \frac{1}{2}$	$\frac{3}{2} \geq D \geq 1$

Table 2.7 Required Total Delay D Values for Different Centre Frequency Ranges.

Delay values in excess of 3 can be attained with accuracy for $\nu_C \leq \frac{1}{6}$. However, making $D \geq 3$ leads to the creation of multiple notches across the spectrum, which increase the amplitude level of the out-of-band quantisation noise to compensate for the redundant notches. This rise in the out-of-band quantisation noise has two disadvantages, the requirement of a more complicated post digital filter that has greater attenuation capability and to a lesser extent, vulnerability to modulator instability. Detailed simulations confirm that accurate centre frequency tunability for $\frac{1}{6} \leq \nu_C \leq \frac{1}{4}$ is achievable by utilising either a fourth-order FIR or second-order IIR allpass FD filter.

A feature of FD filters that becomes more critical, particularly, in the IIR allpass case is the inherent delay of the FD filter itself [Laa96], making small values of D virtually unattainable and, thus restricting noise-shaping to only half the available range, i.e. $0 \leq \nu_C \leq 0.25$. For example, Figure 2.42 shows that a D value of 1.4 is required to achieve tunability at $\nu_C = 0.367$. A second-order IIR allpass filter can produce the necessary fraction of 0.4, but in addition generates its own delay, which happens to be 2 in this case. Moreover, r must be set to a minimum value of unity to satisfy the causality criterion [Jan93]. This means that D becomes 3.4 instead of the desired 1.4. A further shortcoming associated with the FD filters is that their accuracy deteriorates at very high frequencies.

Fortunately; this inherent practical limitation can be circumvented by designing an FD filter that will give a centre frequency equal to $(0.5 - \nu_C)$ and then applying a lowpass to highpass transformation ($z^{-1} \rightarrow -z^{-1}$) to yield the desired centre frequency. An example demonstrating the accuracy of this procedure is shown in Figure 2.48.

An alternative solution is to design IIR filters, which can provide very small group delays. This was achieved with limited success by designing a fourth-order lowpass Chebyshev filter that yielded a group delay of 0.1.

The single-loop dithered Σ - Δ modulator shown in Figure 2.43 is a suitable topology for the application of the FDF approach. This modulator comprises a loop-filter $T(z)$ (with an in-built fractional delay) and a 1-bit quantiser in the feedforward path. In addition, an amplitude of 0.01 of white noise dither $D(z)$ is added prior to the quantiser input to whiten the quantisation noise and substantially reduce tones [Nor92]. This structure also contains a cascade combination of a variable bulk integer delayer z^{-r} and a FD filter $C(z) \cong z^{-f}$ [Laa96] in the feedback path. The noise-shaping properties of dithered Σ - Δ modulators may be analysed by modelling the 1-bit non-linear quantiser by an equivalent noise source in order to make linear analysis possible. Despite the linear approximation, this approach delivers results which are representative [Can92]. The NTF and STF of the modulator shown in Figure 2.43 are:

$$H_N(z) = \frac{1}{1 + z^{-r}C(z)T(z)} \quad \text{and} \quad H_S(z) = \frac{T(z)}{1 + z^{-r}C(z)T(z)} \quad (2.46)$$

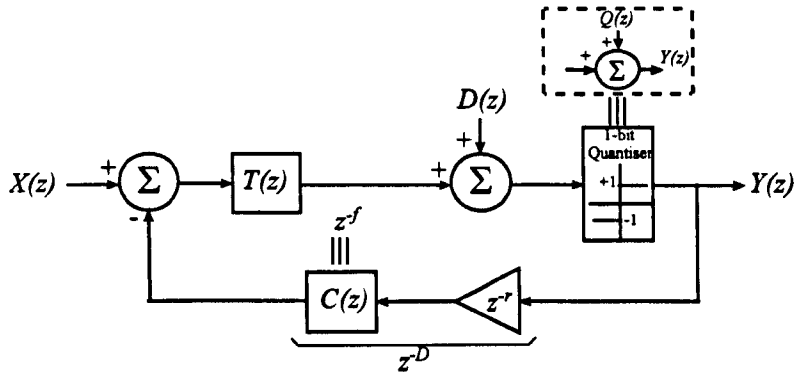


Figure 2.43 Single-Stage Dithered FDF Based Σ - Δ Modulator.

This analysis can be extended to higher-order single-bit Σ - Δ modulators in order to acquire improved noise-shaping responses and more respectable in-band SNRs and DRs. The NTF is given by:

$$H_N(z) = (1 + z^{-D})^L \quad (2.47)$$

where the order of $H_N(z)$ is the product of L and the order of the FD filter approximation.

2.15 FIR Fractional Delay Case

The FIR FD filter $C(z)$ is designed by the use of the maximally flat Lagrange technique [Laa96] whose coefficients $c(k)$ are defined as:

$$c(k) = \prod_{n=0, n \neq k}^N \frac{D-n}{k-n}, \quad k = 0, 1, \dots, N. \quad (2.48)$$

The Lagrange approximation is well suited for use in Σ - Δ modulators, because the peak of its magnitude never exceeds unity [Laa96]. This particular property considerably reduces the occurrence of instability. The new mathematical expression for $H_N(z)$ incorporating the FIR FD filter becomes

$$H_N(z) = 1 + z^{-r}(c_0 + c_1z^{-1} + \dots + c_{(N-1)}z^{-(N-1)} + c_Nz^{-N}) \quad (2.49)$$

The resultant loop $T(z)$ and feedback $C(z)$ filters are:

$$T(z) = \frac{1}{1 + z^{-r}(c_0 + c_1z^{-1} + \dots + c_{(N-1)}z^{-(N-1)} + c_Nz^{-N})} \quad (2.50)$$

$$C(z) = z^{-r}(c_0 + c_1z^{-1} + \dots + c_{(N-1)}z^{-(N-1)} + c_Nz^{-N}) \quad (2.51)$$

The coefficients for some of the FIR FD filter approximations for $N = 4$, are shown in Table 2.8.

v_C	f	r	h_0	h_1	h_2	h_3	h_4
0.238	1.1	1	1	-0.0285	0.9405	0.1045	-0.0165
0.227	1.2	1	1	-0.048	-0.864	0.216	-0.032
0.185	1.7	1	1	-0.0455	0.3315	0.7735	-0.0595
0.179	1.8	1	1	-0.032	0.216	0.864	-0.048

Table 2.8 Loop-Filter and Feedback Filter Coefficients for Some Centre Frequencies using the FIR FDF Approach.

These FD filters have the same numerator and denominator orders which imply that the value for r must be at least equal to 1, so as to comply with the causality criterion [Jan93]. It should be noted that the FIR FD filter does not have a linear phase (except when FD = 0.5) due to the asymmetry of the coefficient of $H_N(z)$ [Laa96].

2.16 Allpass IIR Fractional Delay Case

An alternative means of representing FD filters is by using the FD allpass maximally flat group-delay approximation [Laa96]. The advantage is that an IIR digital filter can provide the same or even better FD filter characteristics with fewer coefficients compared with FIR filters. These allpass filters have unity magnitude and much improved group

delay responses for the entire frequency range. The filter coefficients of an N^{th} -order FD filter are:

$$\alpha_k = (-1)^k C_k^N \prod_{n=0}^N \frac{D-N+n}{D-N+k+n} \quad \text{for } k = 0, 1, 2, \dots, N \quad (2.52)$$

The resultant loop and feedback filters become:

$$T(z) = \frac{1 + b_1 z^{-1} + \dots + b_{(N-2)} z^{-(N-2)} + b_{(N-1)} z^{-(N-1)}}{1 + a_1 z^{-1} + \dots + a_{(N-1)} z^{-(N-1)} + z^{-N}} \quad (2.53)$$

$$C(z) = -c z^{-r} \frac{\alpha_N + \alpha_{N-1} z^{-1} + \dots + \alpha_1 z^{-(N-1)} + z^{-N}}{1 + \alpha_1 z^{-1} + \dots + \alpha_{(N-1)} z^{-(N-1)} + \alpha_N z^{-N}} \quad (2.54)$$

The coefficients for some of the allpass IIR FD filter approximations for $N = 3$, are shown in Table 2.9.

ν_C	α_1	α_2	b_1	b_2	b_3	a_1	a_2	a_3
0.1	-0.8	0.2	-0.8	0.2	0	-0.6	-0.6	1
0.185	0.2222	-0.021	0.222	-0.021	0	0.201	0.201	1
0.208	0.5	-0.0294	0.5	-0.0294	0	0.4706	0.4706	1
0.448	1.4	0.5091	-1.4	-0.0591	0	0.8919	-0.8919	-1

Table 2.9 Loop-Filter and Feedback Filter Coefficients for Some Centre Frequencies using the IIR Allpass FDF Approach.

2.17 Evaluation of the FDF Technique

Discrete-time behavioural level simulations were carried out for the single-stage single-bit and single-stage multi-bit Σ - Δ modulators to demonstrate the correct operation of the proposed approach. Figure 2.44 shows the magnitude spectra of FIR FD filter based Σ - Δ modulators tuning at $\nu = 0.185$, where it can be observed that improved noise-shaping performance is accomplished with the double stage eighth-order Σ - Δ modulator. Figure 2.45 shows the magnitude spectrum of a single-stage allpass IIR FD filter based Σ - Δ modulator, where it can be seen that a lower amount of in-band quantisation noise is retained in the signal region compared with the FIR case. Simulations reveal that this improvement becomes even more significant at high frequencies due to the unity magnitudes and enhanced phase responses of the IIR allpass FD filter.

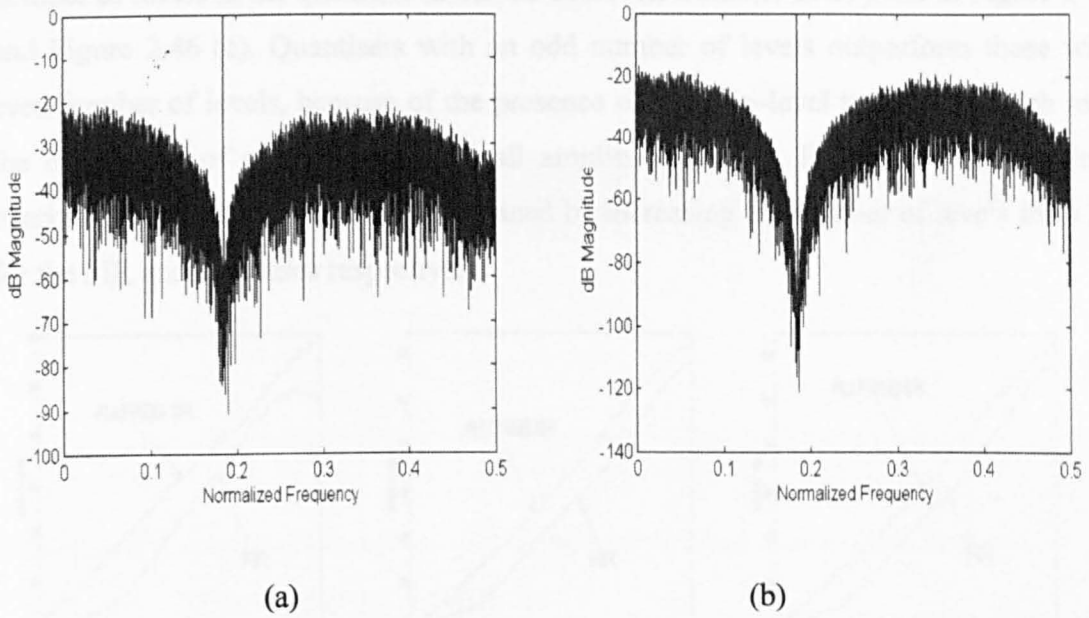


Figure 2.44 Magnitude Spectra at $\nu_C = 0.185$ using the FDF Approach for (a) Single-Stage Fourth-Order Σ - Δ modulator (b) Double-Stage Eighth-Order Σ - Δ Modulator.

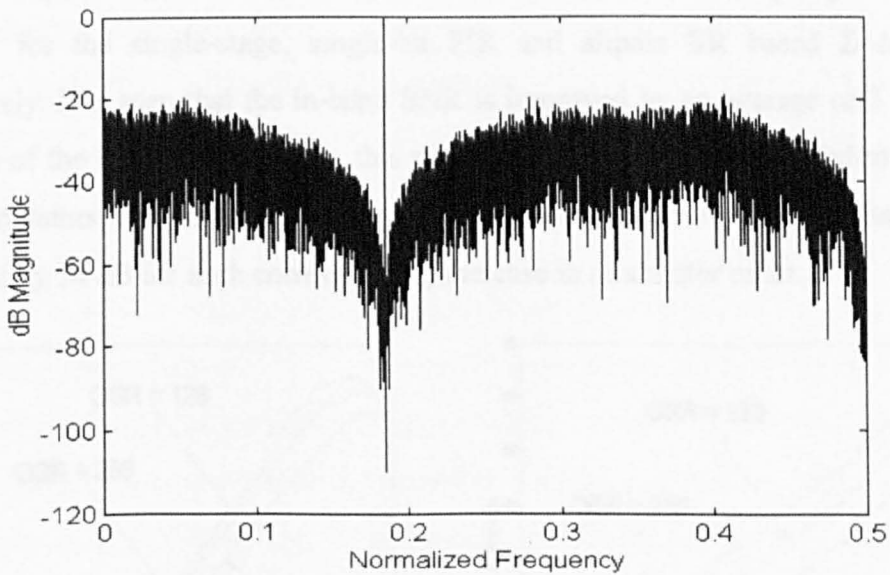


Figure 2.45 Magnitude Spectrum of a Single-Stage Third-Order IIR Allpass Σ - Δ Modulator at $\nu_C = 0.185$.

Figure 2.46(a) quantitatively verifies that the in-band SNR for the allpass IIR case improves by an average of 7.3 dB compared with the FIR FD case for a single-stage Σ - Δ modulator. Better in-band SNRs can be alternatively accomplished by increasing the

number of levels in the quantiser as can be observed from the SNR plots in Figure 2.46 (b) and Figure 2.46 (c). Quantisers with an odd number of levels outperform those with an even number of levels, because of the presence of the zero-level threshold, which reduces the occurrence of oscillations for small amplitude signals. For peak input amplitudes, nearly 1.5 and 1-bit in resolution are gained by increasing the number of levels from 2 to 5 for the FIR and IIR cases respectively.

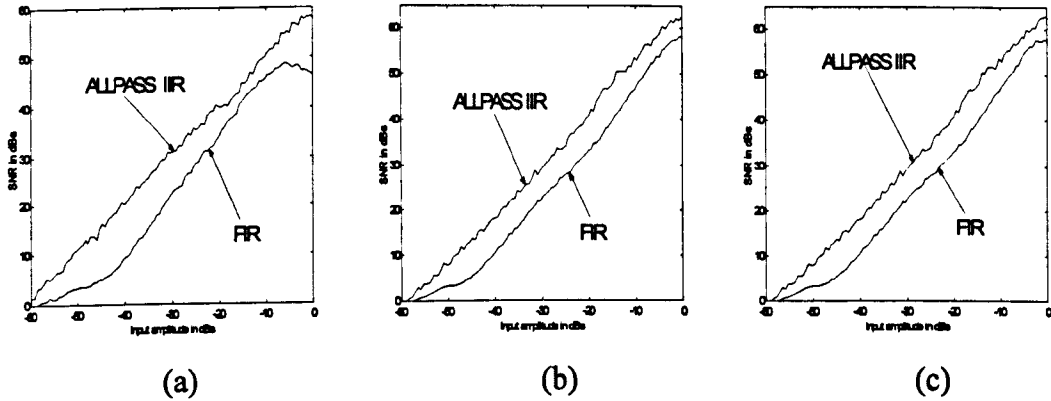


Figure 2.46 SNR Curves of FIR & Allpass IIR Single-Stage Σ - Δ Modulators
(a) 2-Level, (b) 3-Level, (c) 5-Level.

Figure 2.47 (a) and (b) illustrate the in-band SNR results for oversampling ratios of 64, 128 and 256 for the single-stage, single-bit FIR and allpass IIR based Σ - Δ modulators respectively. It is seen that the in-band SNR is improved by an average of 3 dB for every doubling of the OSR. Furthermore, this new technique is further extended to higher-order Σ - Δ modulators using FIR FD filters, where it is seen from Figure 2.46 that the SNR is improved by 14 dB for each corresponding increase in modulator order.

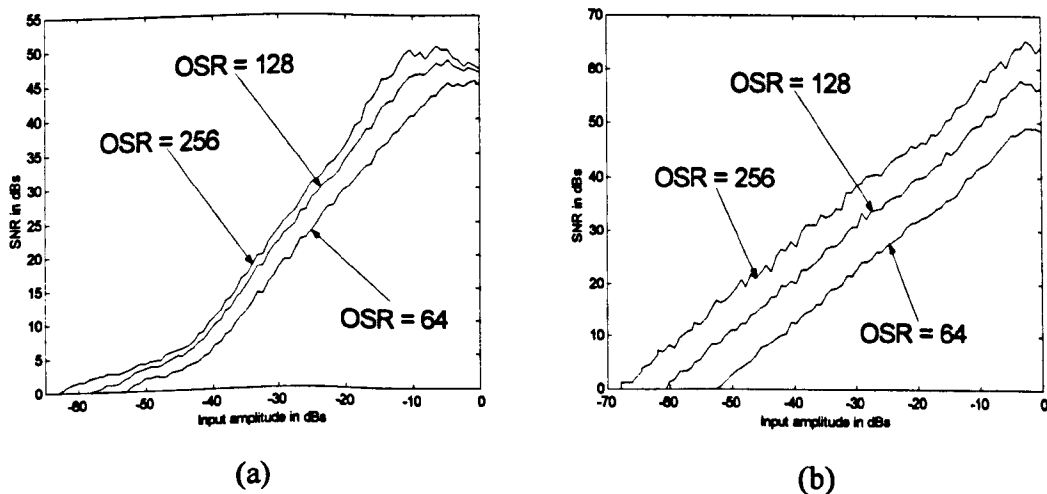


Figure 2.47 SNR Curves of Single-Stage Σ - Δ Modulators for (a) FIR, (b) Allpass IIR.

Figure 2.48 demonstrates noise-shaping using the FDF approach at $\nu_C = 0.448$.

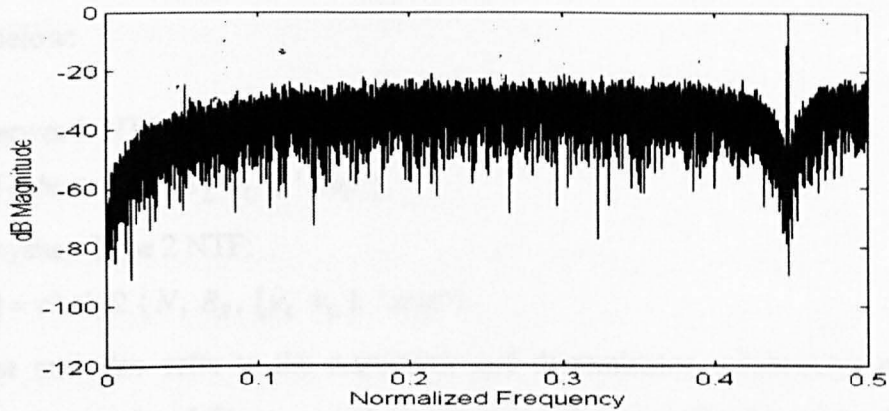


Figure 2.48 Magnitude Spectrum of a Single-Stage Third-Order IIR FDF Σ - Δ Modulator at $\nu_C = 0.448$.

2.18 A Methodology for the Design of Bandpass Σ - Δ Modulators

This section presents a simple practical step-by-step approach for the design of single-stage bandpass Σ - Δ modulators. The NTF design of these modulators is based on the use of Butterworth and Chebyshev 2 bandstop filters. This approach, however, can be extended to other types of filter families. This section also provides a few guidelines that can be applied to further improve the resolution of these custom-made NTFs.

It is important before proceeding with the actual design analysis to understand the interrelationships between the specification parameters that affect the spectral characteristics and resolution of Butterworth and Chebyshev 2 filters.

Butterworth filters exhibit monotonic passbands and stopbands, low pass-band ripples and relatively wide transition bands [Cun92]-[Orf96]-[Pro92]. The peak out-of-band spectral magnitude of 2nd, 4th, 6th and 8th order Butterworth NTFs are 0.78 dB, 1.16 dB, 1.64 dB and 2.14 dB respectively for $\Delta\nu = 0.06$. A higher NTF order results in a wider stop-band with greater attenuation at the cost of a higher overall NTF gain.

Chebyshev 2 filters have a monotonic passband and an equi-ripple stopband. Chebyshev 2 also provides low pass-band distortion and exhibit sharp transition bands, thus requiring a lower-order filter to meet a given specification compared with Butterworth filters. For a given a NTF order, stop-band ripples can be traded for wider stop-bands and increased NTF magnitudes [Cun92]-[Orf96]-[Pro92].

STEP 1: Select a modulator order N , a NTF filter family type, bandwidth $\Delta\nu$, passband ripple (R_p) needed for (Chebyshev 1 and Elliptical filters) and stopband ripple (R_s)

required for (Chebyshev 2 and Elliptical filters). A straightforward procedure for obtaining the NTF for any filter family type involves using the Matlab Signal Processing Toolbox as indicated below:

For a Butterworth NTF:

$$[num, den] = butter(N, [v_L v_U], 'stop')$$

For a Chebyshev Type 2 NTF:

$$[num, den] = cheby2(N, R_S, [v_L v_U], 'stop')$$

where *num* and *den* refer to the numerator and denominator polynomials of the NTF, *stop* refers to a stop-band filter, v_L and v_U represent the normalised lower and upper 3dB frequencies and are given by:

$$v_L = v_C - \Delta v/2 \quad \text{and} \quad v_U = v_C + \Delta v/2 \quad (2.55)$$

STEP 2: Scale the NTF so that the first sample of the impulse response becomes 1, in order to meet the causality criterion. This can be achieved in Matlab by typing $nums = num / num(1)$, where *nums* contains the newly scaled coefficients of the numerator polynomial of the NTF.

STEP 3: Check the peak magnitude of the NTF spectrum to ensure that it does not exceed 2 (or more practically 1.6) to comply with Lee's stability criterion.

STEP 4: The loop- and feedback transfer functions can be analytically obtained by rearranging the expression for the NTF as shown below:

$$F(z)L(z) = (1 - H_N(z))/H_N(z) \quad (2.56)$$

where $F(z)$ and $L(z)$ may be determined by separating the numerator and denominator expressions such that $F(z) = (1 - H_N(z))$ and $L(z) = 1/H_N(z)$.

STEP 5: Enter the coefficients of $F(z)$ and $L(z)$ into the modulator and simulate it at the behavioural level using Simulink in Matlab to confirm the correctness of its operation.

STEP 6: If the in-band SNR value is not sufficiently high then

- a) increase the modulator order provided the peak amplitude of $H_N(z)$ satisfies Lee's Criterion,
- b) increase the OSR provided the bandwidth specification is not violated,
- c) increase the number of levels in the quantiser,
- d) reduce the dither such that the in-band tones do not become too strong.
- e) resort to an optimisation algorithm where the poles and zeros of the $H_N(z)$ are shifted to more optimal positions in the z -plane to achieve better resolution.

The noise $H_N(z)$, loop-filter $H(z)$ and signal $H_S(z)$ transfer functions of an eighth-order Σ - Δ modulator are given by

$$H_N(z) = \frac{1 + b_1z^{-1} + b_2z^{-2} + b_3z^{-3} + b_4z^{-4} + b_5z^{-5} + b_6z^{-6} + b_7z^{-7} + b_8z^{-8}}{1 + a_1z^{-1} + a_2z^{-2} + a_3z^{-3} + a_4z^{-4} + a_5z^{-5} + a_6z^{-6} + a_7z^{-7} + a_8z^{-8}} \quad (2.57)$$

$$H(z) = \frac{c_1z^{-1} + c_2z^{-2} + c_3z^{-3} + c_4z^{-4} + c_5z^{-5} + c_6z^{-6} + c_7z^{-7} + c_8z^{-8}}{1 + b_1z^{-1} + b_2z^{-2} + b_3z^{-3} + b_4z^{-4} + b_5z^{-5} + b_6z^{-6} + b_7z^{-7} + b_8z^{-8}} \quad (2.58)$$

$$H_S(z) = \frac{c_1z^{-1} + c_2z^{-2} + c_3z^{-3} + c_4z^{-4} + c_5z^{-5} + c_6z^{-6} + c_7z^{-7} + c_8z^{-8}}{1 + a_1z^{-1} + a_2z^{-2} + a_3z^{-3} + a_4z^{-4} + a_5z^{-5} + a_6z^{-6} + a_7z^{-7} + a_8z^{-8}} \quad (2.59)$$

where the b 's are the most important parameters since they are responsible for controlling the magnitude of the in-band quantisation, the a 's for reducing the overall spectral magnitude of the NTF to avoid overloading the quantiser and the c 's are simply given by $c_N = a_N - b_N$. The coefficients of $H_N(z)$, $H(z)$ and $H_S(z)$ for these 8th-order modulators as well as those for the 6th-order modulators are all presented in Table 2.10.

Two 8th-order bandpass Σ - Δ modulators that can achieve noise-shaping at $\nu_C = 0.125$ were designed using this technique. The first employed a Butterworth filter for its NTF and its spectral magnitude response is shown in Figure 2.49(a). The second utilised a Chebyshev 2 bandstop filter for its NTF and its magnitude spectrum is shown in Figure 2.49(b).

Coeff	6 th -Order		8 th -Order	
	Butter	Cheby2	Butter	Cheby2
c_1	0.2674	0.5218	0.3496	0.5612
c_2	-1.1020	-2.0898	-1.9228	-3.0245
c_3	2.0014	3.6605	4.933	7.5912
c_4	-2.0426	-3.6128	-7.6396	-11.5149
c_5	1.1568	1.9836	7.6698	11.3379
c_6	-0.3145	-0.5259	-5.0247	-7.2989
c_7	-	-	1.9995	2.8593
c_8	-	-	-0.3895	-0.5501
a_1	-4.2616	-4.2426	-5.6821	-5.6569
a_2	9.0536	8.9999	16.1072	15.9998
a_3	-11.3895	-11.3135	-28.5119	-28.2838
a_4	9.0536	8.9999	34.2863	33.9993
a_5	-4.2616	-4.2426	-28.5119	-28.2838
a_6	1	1	16.1072	15.9998
a_7	-	-	-5.6821	-5.6569
a_8	-	-	1	1

Table 2.10 Loop-Filter Coefficients for 6th and 8th Order Bandpass Σ - Δ Modulators based on the NTFs of Butterworth and Chebyshev 2 Filters.

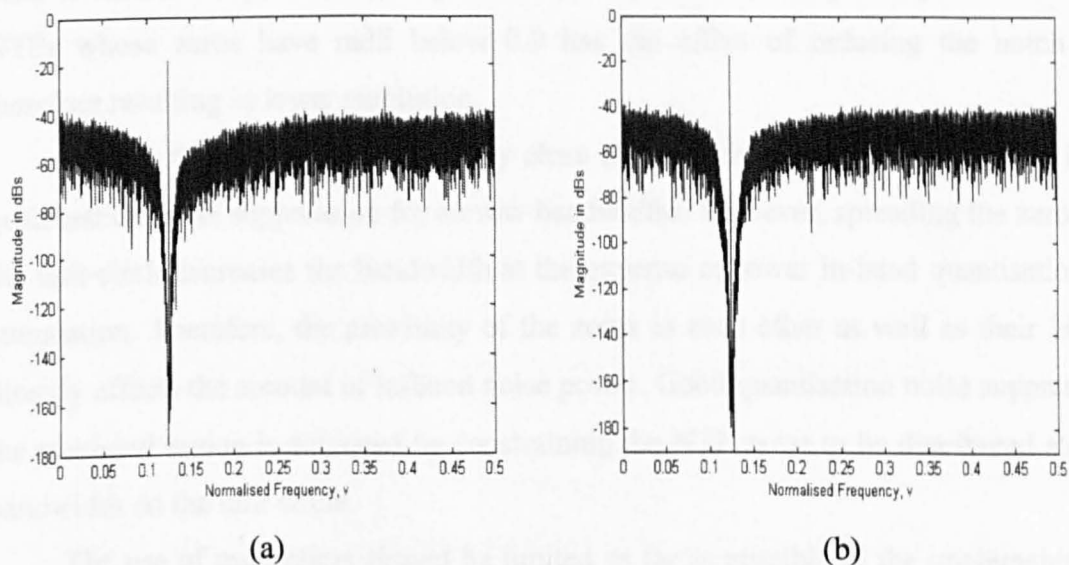


Figure 2.49 Magnitude Spectra of an Eighth-Order Σ - Δ modulator at $\nu_C = 0.125$
(a) Butterworth, (b) Chebyshev 2.

Simulations showed that the in-band SNR that is achieved by a Chebyshev 2 bandpass Σ - Δ modulator outperforms its Butterworth counterpart by as much as 15 dB. This better

resolution is attributed to the distribution of the zeros across the signal region, which accomplished greater attenuation and therefore better SNRs. This is in contrast to the Butterworth based Σ - Δ modulator, whose zeros are placed in a coincidental manner. Furthermore, the spectral responses of the Chebyshev 2 was less tonal. This is explained by the fact that a Chebyshev 2 loop-filter is more complicated, thus resulting in the generation of more state values. This increases the decorrelation of the quantisation noise and therefore results in fewer tones.

The following present some considerations when designing Σ - Δ modulators:

The loop-filter should be designed to ensure that the input signal is transmitted through the modulator with the least amount of distortion in its spectral characteristics. Better quantisation noise attenuation is achieved by distributing the zeros of the NTF across the signal bandwidth as opposed to placing them coincidentally at the same centre frequency. The STF zeros should simultaneously provide a flat magnitude in the signal region and a low out-of-band gain. The constant magnitude helps to preserve the input signal, while the small out-of-band gain enhances the stability of the modulator by alleviating the amplitude of the out-of-band signals.

The zeros of the NTF should be positioned on the unit-circle and inside the signal band to ensure adequate in-band quantisation noise attenuation [Azi95]. The selection of NTFs whose zeros have radii below 0.9 has the effect of reducing the notch depth, therefore resulting in lower resolution.

Placing the zeros of the NTF very close to each other accomplishes greater in-band quantisation noise suppression for narrow bandwidths. However, spreading the zeros along the unit-circle increases the bandwidth at the expense of lower in-band quantisation noise attenuation. Therefore, the proximity of the zeros to each other as well as their locations directly affects the amount of in-band noise power. Good quantisation noise suppression in the passband region is achieved by constraining the NTF zeros to be distributed along the bandwidth on the unit circle.

The use of multipliers should be limited as far as possible in the implementation of D/A higher-order bandpass Σ - Δ modulators. As well as slowing down the operation of the modulator, multipliers occupy large portions of silicon area. When used, they should be in powers of 2 as these can be simply implemented by hardware shifts with minimum speed penalties [Hau95].

The envelope of the quantisation noise rises more sharply as the modulator order is increased. This may increase the modulator vulnerability to instability and at the very least

reduce the overload point resulting in lower DRs. The demands on the decimator become more severe as a result of the steepness of the quantisation noise.

The following sections present several commonly used Σ - Δ modulator topologies, which are well-suited for the implementation of mid-band and variable-band noise-shaping bandpass Σ - Δ modulators [Ada91].

2.19 Chain of Resonators with Weighted Feedforward Summation

The chain of accumulators with weighted feedforward summation in [Tom94, pp. 235] has been modified by replacing the constituent accumulators of the loop-filter with mid-band resonators, thus enabling it to achieve noise-shaping at $\nu_C = 0.25$. The loop-filter consists of a cascade connection of mid-band resonators of the form $z^{-2}/(1+z^{-2})$ in the feedforward path, where the output of each resonator is scaled and summed up prior to the quantiser input as shown in Figure 2.50.

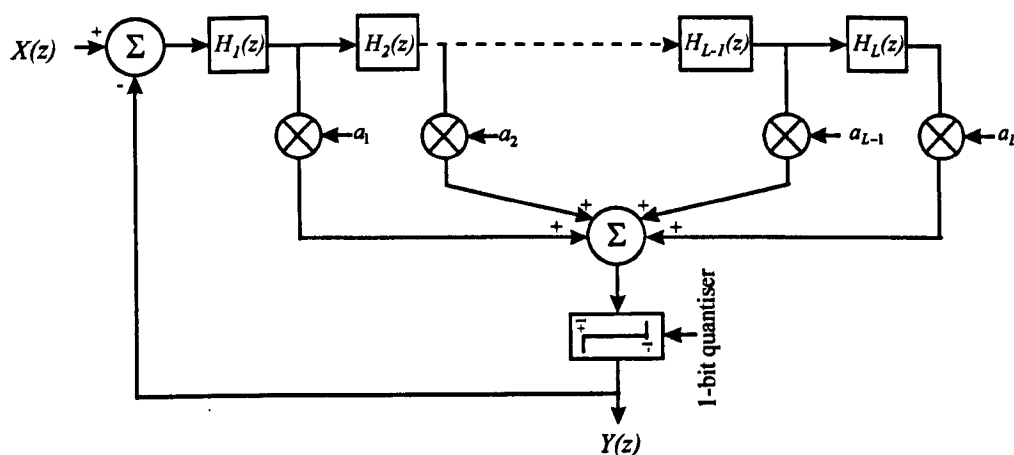


Figure 2.50 Chain of Resonators with Weighted Feedforward Summation.

The generalised analytical NTF expression given in 2.61 verifies that the NTF zeros or loop-filter poles are totally independent of the weighting coefficients, therefore restricting this topology to achieve noise-shaping at mid-band resonance. The feedforward coefficients (i.e. the a 's), however, allow the adjustment of the NTF pole locations so as to obtain a maximally flat out-of-band gain with a reduced magnitude. The reduced NTF gain coupled with the flat NTF magnitude enhances stability significantly, particularly for higher-order Butterworth bandpass Σ - Δ modulators.

$$H_S(z) = \frac{a_1 H_1(z) + a_2 H_1(z)H_2(z) + \dots + a_{L-1} \prod_{i=1}^{L-1} H_i(z) + a_L \prod_{i=1}^L H_i(z)}{1 + a_1 H_1(z) + a_2 H_1(z)H_2(z) + \dots + a_{L-1} \prod_{i=1}^{L-1} H_{L-1}(z) + a_L \prod_{i=1}^L H_L(z)} \quad (2.60)$$

$$H_N(z) = \frac{1}{1 + a_1 H_1(z) + a_2 H_1(z)H_2(z) + \dots + a_{L-1} \prod_{i=1}^{L-1} H_{L-1}(z) + a_L \prod_{i=1}^L H_L(z)} \quad (2.61)$$

The feedforward coefficients are $a_1 = -0.3090$, $a_2 = 0.0417$ for the 4th-order Butterworth Σ - Δ modulator and $a_1 = -0.4390$, $a_2 = 0.0912$, $a_3 = -0.0086$ for the 6th-order Butterworth Σ - Δ modulator. The weighting of these coefficients was seen to decrease progressively in relation to the order of the resonators inside the modulator. In other words, the latter coefficients diminish in value to cope with the accumulative effects of the preceding resonators.

These modulators were simulated for an input sinusoid and dither signal whose amplitudes were 0.5 and 0.05 respectively. The resulting magnitude spectra are shown in Figure 2.51. Both of them contained two distinct tones at $\nu_C = 0.125$ and $\nu_C = 0.375$ verifying that these tones are independent of the modulator order and essentially related to the amplitude level of the modulator input signal. As expected, the 6th-order modulator was capable of accomplishing greater quantisation noise suppression in the signal region, compared with its 4th-order counterpart. This observation is supported with the SNR curves shown in Figure 2.52. The maximum achievable SNR figures for the 4th-order were 25.2 dB, 37 dB, 50.2 dB, 64.6 dB, 79.5 dB and 94 dB for OSRs of 8, 16, 32, 64, 128 and 256 respectively. This is in contrast to the 6th-order modulator peak SNR, which were 25.5 dB, 39 dB, 57.1 dB, 77.8 dB, 99.4 dB and 119.1 dB for the same OSRs. Note that the SNR improvement with respect to the modulator order, becomes significant for the higher OSRs. However, there was virtually no SNR gain between the 4th and 6th order modulators for the lower OSRs of 8 and 16. Figure 2.52 (b) also shows that this modulator became unstable for input amplitudes beyond -1.5 dB. This of course is attributed to the accumulative effect of the resonators in the feedforward path.

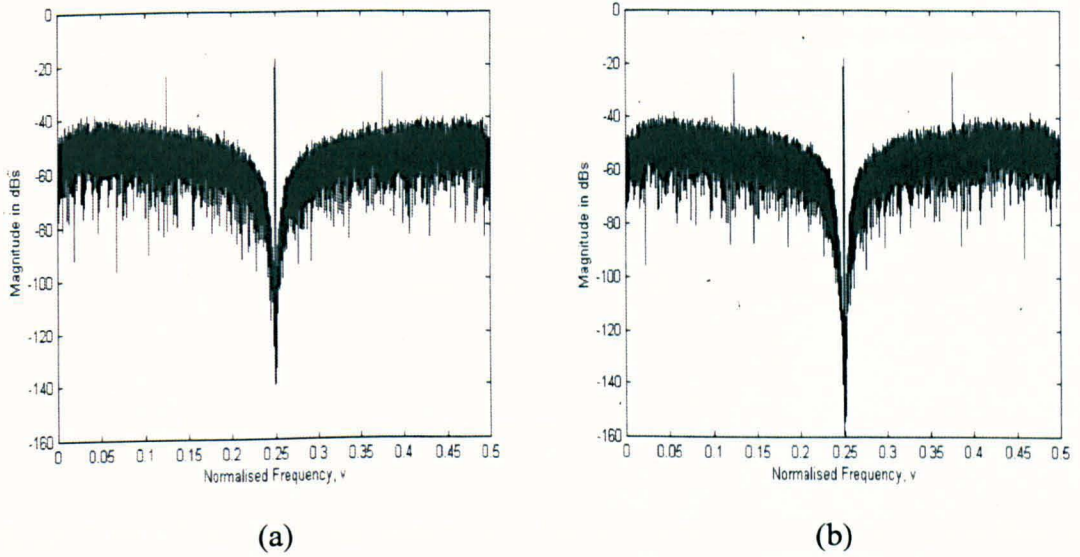


Figure 2.51 Magnitude Spectra of Chain of Resonators with Weighted Feedforward Summation Butterworth Σ - Δ modulator at $\nu_C = 0.25$ (a) 4th-Order, (b) 6th-Order.

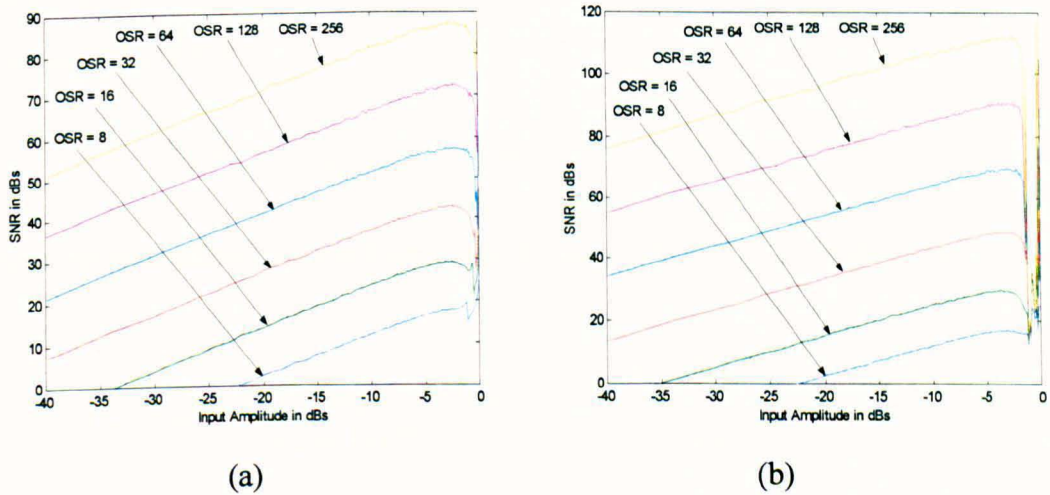


Figure 2.52 SNR Curves at $\nu_C = 0.25$ for (a) 4th-Order, (b) 6th-Order Variable-Band Bandpass Σ - Δ Modulators.

2.20 Chain of Accumulators with Feedforward Summation & Local Resonator Feedbacks

This topology contains a summation of weighted accumulators in the feedforward path as well as an internal negative feedback term around pairs of accumulators [Tom94, pp. 235]. The outputs of all the constituent accumulators are summed and fed to the quantiser input as illustrated in Figure 2.53.

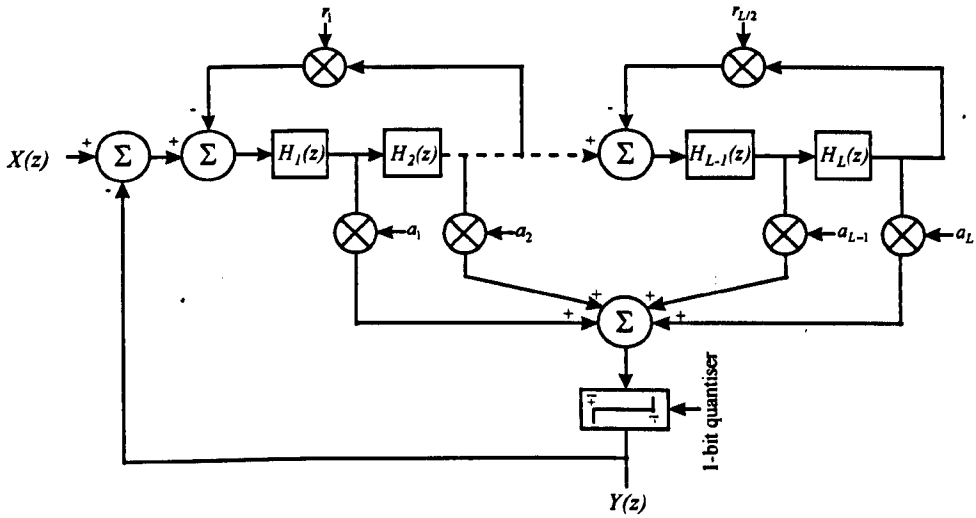


Figure 2.53 Chain of Accumulators with Feedforward Summation and Local Resonator Feedbacks.

The presence of the internal feedback loop as well as the coefficient r provides the flexibility of moving the loop-filter poles away from DC to any normalised centre frequency up to Nyquist. The signal $H_S(z)$ and noise $H_N(z)$ transfer functions of this topology are given by:

$$H_S(z) = \frac{H_{FR}(z)}{1 + H_{FR}(z)} \quad \text{and} \quad H_N(z) = \frac{1}{1 + H_{FR}(z)} \quad (2.62)$$

where the generalised transfer function of the loop-filter $H_{FR}(z)$ is given by:

$$H_{FR}(z) = \frac{a_1 H_1(z) + a_2 H_1(z) H_2(z)}{1 + r_1 H_1(z) H_2(z)} + \dots + \frac{a_{L-1} \prod_{i=1}^{L-1} H_i(z) + a_L \prod_{i=1}^L H_i(z)}{1 + r_2/2 H_{L-1}(z) H_L(z)} \quad (2.63)$$

It is demonstrated analytically that the use of a delayed accumulator followed by a delay-free accumulator satisfy the causality criterion as well as ensuring that the poles of the composite resonator are permanently stationed on the unit-circle to provide maximum gain in the signal region. This is given by:

$$H_{FR}(z) = \frac{(a_1 + a_2)z^{-1} - a_1 z^{-2}}{1 - (2 - r_1)z^{-1} + z^{-2}} \quad (2.64)$$

If both accumulators employ a delay term in the numerator, the composite resonator will be less effective, because the poles will not be on the unit-circle as given by:

$$H_{FR}(z) = \frac{(a_1 + a_2)z^{-1} - a_1z^{-2}}{1 - 2z^{-1} + (1 + r_1)z^{-2}} \quad (2.65)$$

For positive real values of r , the poles move vertically away from the unit-circle resulting in a significant gain reduction at the resonant frequency. For negative real values of r , the poles move horizontally along the real axis in opposite directions leading eventually to modulator instability.

The coefficients based on Butterworth and Chebyshev 2 NTFs were derived for this topology with the aid of a programme written in Matlab. A listing of these coefficients specific to this topology for different modulation orders is presented in Table 2.11.

Butterworth		Chebyshev 2	
Second-Order			
a_1	0.1988	a_1	0.5686
a_2	-0.0573	a_2	-0.1665
r_1	0.5772	r_1	0.5857
Fourth-Order			
a_1	0.2673	a_1	0.3575
a_2	-0.0475	a_2	-0.0483
a_3	$1.44 \cdot 10^{-5}$	a_3	0.0044
a_4	-0.0207	a_4	-0.0404
r_1	0.5772	r_1	0.5984
r_2	0.5772	r_2	0.5732
Sixth-Order			
a_1	0.3564	a_1	0.4289
a_2	-0.0441	a_2	-0.0353
a_3	0.0061	a_3	0.0185
a_4	-0.0425	a_4	-0.0678
a_5	-0.0044	a_5	-0.0084
a_6	0.0012	a_6	0.0025
r_1	0.5722	r_1	0.6012
r_2	0.5772	r_2	0.5705
r_3	0.5772	r_3	0.5857

Table 2.11 Chain of Accumulators with Feedforward Summation and Local Resonator Feedbacks Coefficients for 2nd-Order, 4th-Order and 6th-Order Butterworth and Chebyshev 2 Bandpass Σ - Δ Modulators.

These modulators were designed to provide noise-shaping at $\nu_C = 0.125$, where the magnitude spectra corresponding to the 6th-order Butterworth and Chebyshev 2 cases are shown in Figure 2.54. A tone is observed at $\nu_C = 0.375$ for both spectra, indicating that this was attributed to the amplitude of the input sinusoid and independent of the NTF. The SNR curves in Figure 2.55 and 2.56 demonstrate that the Chebyshev 2 based bandpass Σ - Δ modulator deliver better resolution. This is attributed to the greater flexibility of the distribution of the NTF zeros across the spectrum, thus resulting in greater in-band quantisation noise attenuation. For the Chebyshev 2 based modulators, Figure 2.56 shows that there is very little SNR improvement as the OSR increases from 128 to 256.

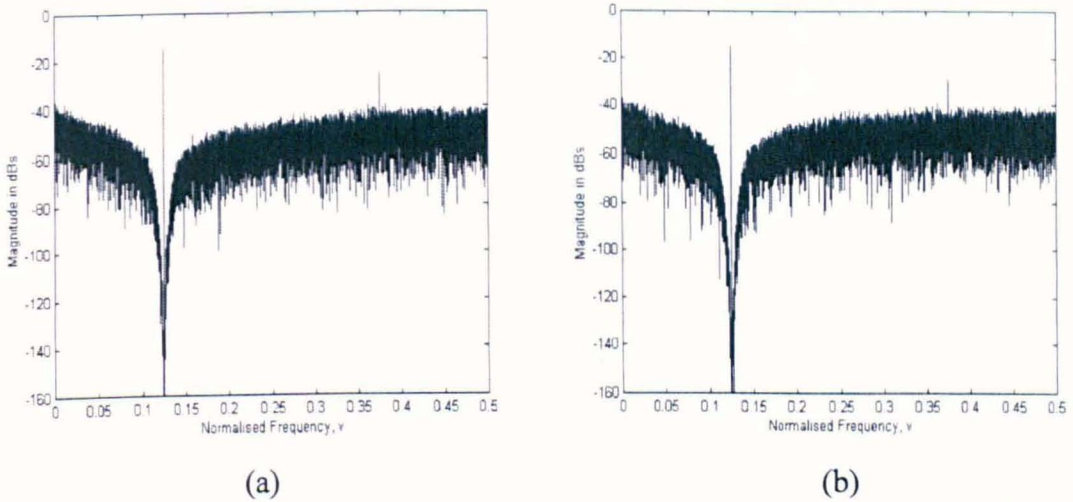


Figure 2.54 Magnitude Spectra of a 6th-Order Chain of Accumulators with Feedforward Summation & Local Resonator Feedbacks Σ - Δ modulator at $\nu_C = 0.125$
 (a) Butterworth, (b) Chebyshev 2.

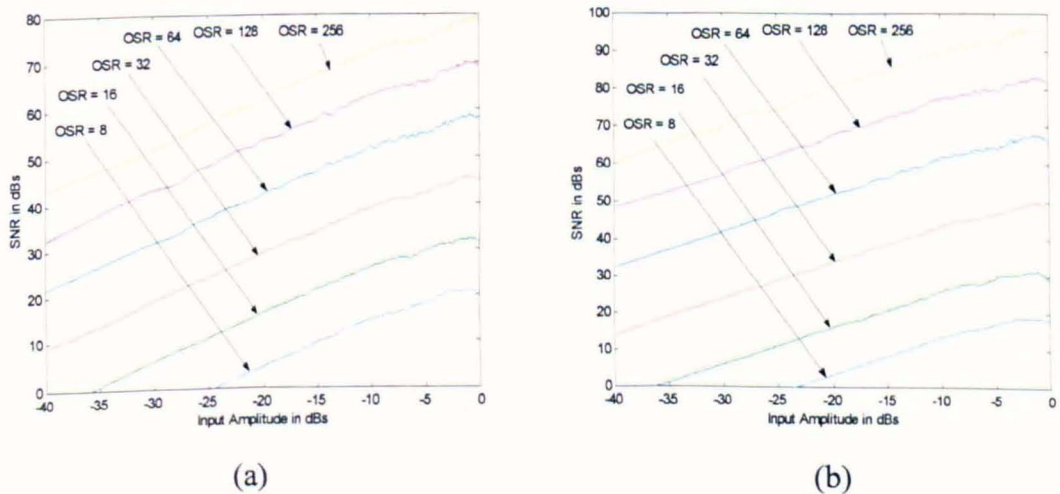


Figure 2.55 SNR Curves at $\nu_C = 0.25$ for (a) 4th-Order, (b) 6th-Order Butterworth Based Variable-Band Bandpass Σ - Δ Modulators.

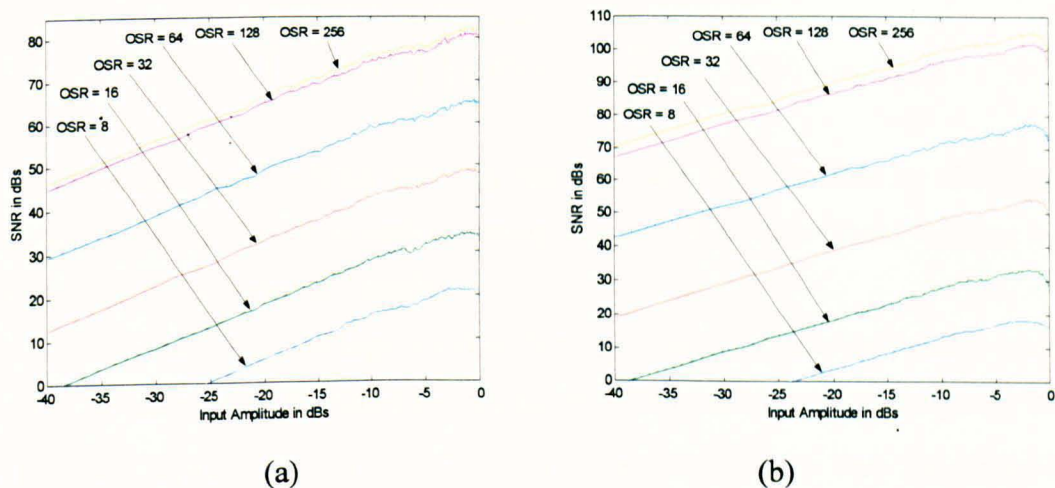


Figure 2.56 SNR Curves at $\nu_C = 0.25$ for (a) 4th-Order, (b) 6th-Order Chebyshev 2 Based Variable-Band Bandpass Σ - Δ Modulators.

2.21 Chain of Resonators with Distributed Feedback

This topology [Tom94, pp. 235] was modified by replacing all its accumulators with delayed resonators of the form $z^{-2}/(1+z^{-2})$ to make it perform bandpass Σ - Δ modulation. This topology consists of mid-band resonators in the feedforward path together with the distributed feedback that is subtracted from the output of the preceding mid-band resonator. The output node of each accumulator is appropriately scaled to control the amplitude level of the signals in the feedforward path to maintain stability as illustrated in Figure 2.57.

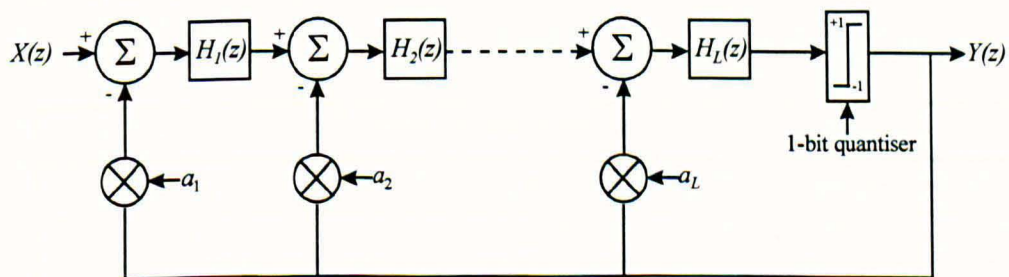


Figure 2.57 Chain of Resonators with Distributed Feedback.

The signal $H_S(z)$ and noise $H_N(z)$ transfer functions of this topology are given by:

$$H_S(z) = \frac{\prod_{i=1}^L H_i(z) + \prod_{i=2}^L H_i(z) + \dots + \prod_{i=L-1}^L H_i(z) + H_L(z)}{1 + \prod_{i=1}^L a_i H_i(z) + \prod_{i=2}^L a_i H_i(z) + \dots + \prod_{i=L-1}^L a_{L-1} H_i(z) + a_L H_L(z)} \quad (2.66)$$

$$H_N(z) = \frac{1}{1 + \prod_{i=1}^L a_i H_i(z) + \prod_{i=2}^L a_i H_i(z) + \dots + \prod_{i=L-1}^L a_{L-1} H_i(z) + a_L H_L(z)} \quad (2.67)$$

The distributed feedback topology can be made more flexible by allowing a path from the input signal node to each summing junction of the constituent building blocks of the loop-filter as reported in [Ada91].

Furthermore, this topology could be further extended to provide variable-band noise-shaping by substituting the mid-band resonators with a variable centre frequency resonator of the form $a(nz^{-1} + z^{-2})/(1 - dz^{-1} + z^{-2})$. The flexibility to vary the signal band is achieved at the expense of greater hardware complexity. Each new resonator requires two multipliers, one in the denominator to ensure that the poles are positioned at the specified centre frequency on the unit-circle and the other in the numerator to provide more effective noise-shaping.

Two modulator designs were carried out for this topology. The first and the simplest was the 6th-order bandpass Σ - Δ modulator, which used mid-band resonators to achieve noise-shaping at $\nu_C = 0.25$. The second was that of a 4th-order modulator that was capable of noise-shaping at $\nu_C = 0.125$. The design process was more elaborate and required 6 coefficients. The n and d coefficients are responsible for shifting the location of the noise-shaping band to the relevant centre frequency. The a coefficients are used to control the amplitude of the internal signal levels in the feedforward path. A listing of the coefficients for both designs is presented in Table 2.12.

6 th -Order Butterworth at $\nu_C = 0.25$					
a_1		a_2		a_3	
-0.0943		-0.2077		-0.4390	
4 th -Order Butterworth at $\nu_C = 0.125$					
a_1	a_2	n_1	d_1	n_2	d_2
-0.1352	-0.3091	-0.7120	-1.4228	-0.7111	-1.4228

Table 2.12 Coefficients of Chain of Resonators with Distributed Feedback Butterworth 4th-Order and 6th-Order Bandpass Σ - Δ Modulators.

The magnitude spectrum in Figure 2.58 demonstrate the correct operation of these modulators. The SNR curves for the variable-band 4th-order bandpass Σ - Δ modulator are

illustrated in Figure 2.59. Peak SNRs of 21.1 dB, 32.5 dB, 45.7 dB, 59 dB, 70.1 dB and 79 dB are achieved for OSRs of 8, 16, 32, 64, 128 and 256 respectively.

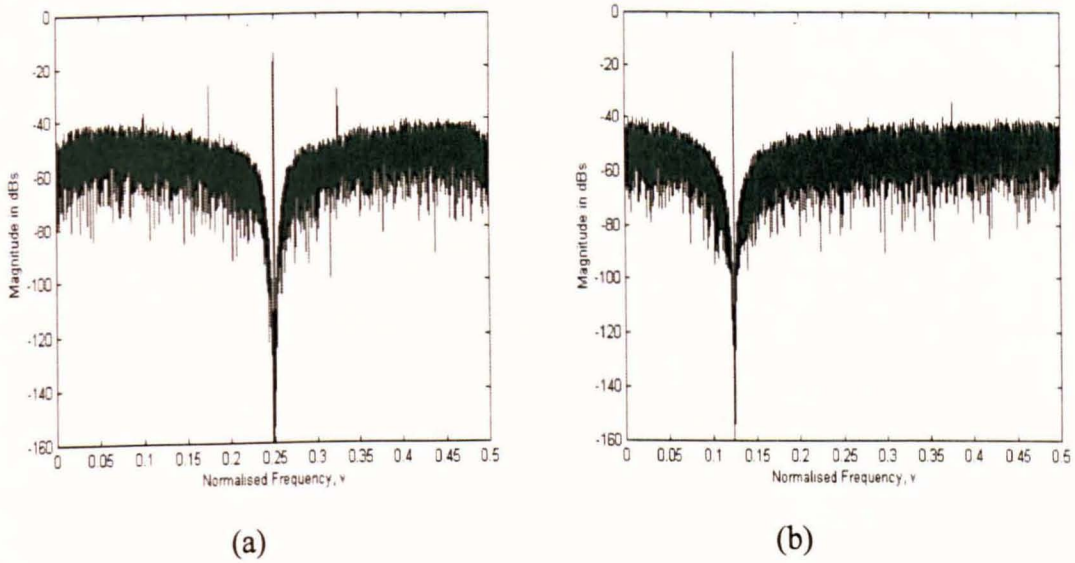


Figure 2.58 Magnitude Spectra of Chain of Resonators with Distributed Feedback Butterworth Σ - Δ Modulator (a) 6th-Order at $\nu_C = 0.25$, (b) 4th-Order at $\nu_C = 0.125$.

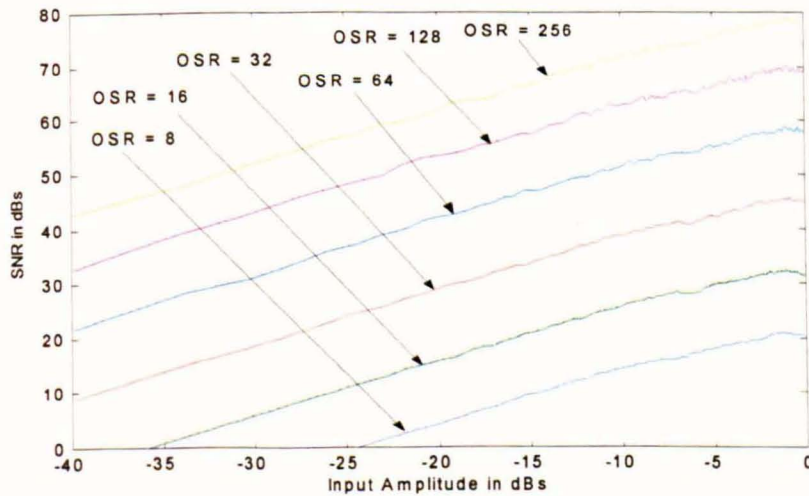


Figure 2.59 SNR Curves for a 4th-Order Chebyshev 2 Based Variable-Band Bandpass Σ - Δ Modulators at $\nu_C = 0.125$.

2.22 The Sodini Interpolative Σ - Δ modulator Topology

Interpolative modulators contain both feedforward and feedback coefficients in the transfer function of the modulator as shown in Figure 2.60. These coefficients are chosen to improve stability as well as ensuring quantisation noise reduction in the signal region. In this topology, the poles of the modulator are spread across the signal region to reduce the

in-band quantisation noise. The zeros are selected to decrease the magnitude of the quantisation noise spectrum at high frequencies.

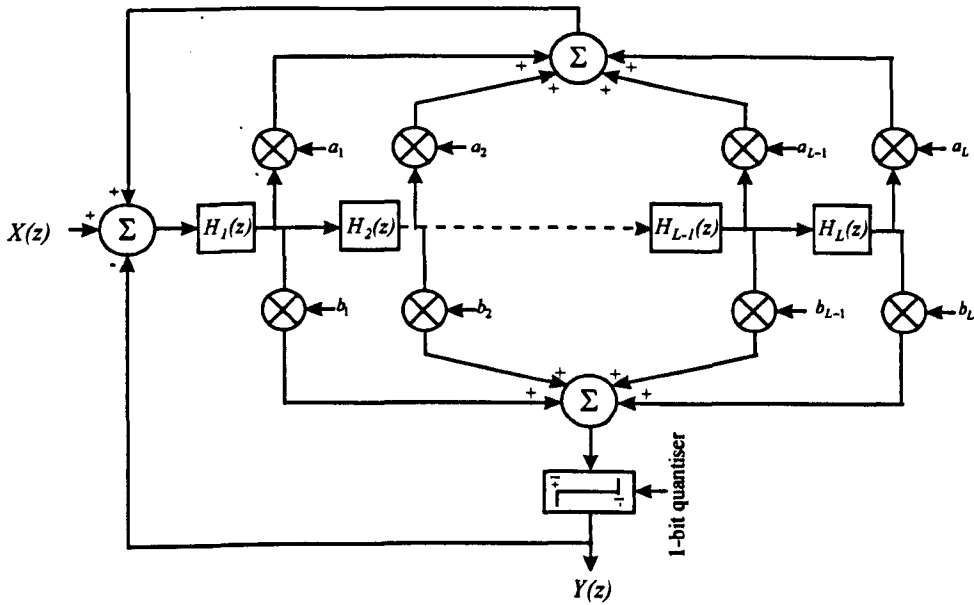


Figure 2.60 The Sodini Interpolative Σ - Δ Modulator Topology.

The signal $H_S(z)$ and noise $H_N(z)$ transfer functions of this topology are given by:

$$H_S(z) = \frac{b_0 + b_1 H_1(z) + b_2 H_1(z) H_2(z) + \dots + b_{L-1} \prod_{i=1}^{L-1} H_i(z) + b_L \prod_{i=1}^L H_i(z)}{1 + b_0 + (b_1 - a_1) H_1(z) + (b_2 - a_2) H_1(z) H_2(z) + \dots + (b_L - a_L) \prod_{i=1}^L H_L(z)} \quad (2.68)$$

$$H_N(z) = \frac{1 - a_1 H_1(z) - a_2 H_1(z) H_2(z) - \dots - a_{L-1} \prod_{i=1}^{L-1} H_i(z) + a_L \prod_{i=1}^L H_i(z)}{1 + b_0 + (b_1 - a_1) H_1(z) + (b_2 - a_2) H_1(z) H_2(z) + \dots + (b_L - a_L) \prod_{i=1}^L H_L(z)} \quad (2.69)$$

The coefficients for the 4th and 6th order bandpass Σ - Δ modulator interpolative topology were derived for a variable noise-shaping band location at $\nu_C = 0.125$ and are given in Table 2.13. The magnitude spectra corresponding to the 6th-order Butterworth and Chebyshev 2 bandpass Σ - Δ modulators are shown in Figure 2.61. These modulators were simulated for an input sinusoid and dither signal, whose amplitudes were 0.5 and 0.05 to compare their spectra with the preceding topologies. A tone at $\nu_C = 0.375$ can be perceived confirming once again that the location and to a lesser extent the strength of these tones are independent of the modulator topology and are primarily a function of the input signal amplitude.

Butterworth		Chebyshev 2	
Fourth-Order			
b_1	0.2198	b_1	0.3092
b_2	0.0587	b_2	0.0929
b_3	0.0581	b_3	0.0731
b_4	-0.0481	b_4	-0.0681
a_1	-1.1544	a_1	-1.1716
a_2	-1.4876	a_2	-1.5146
a_3	-0.6664	a_3	-0.6860
a_4	-0.3332	a_4	-0.3430
Sixth-Order			
b_1	0.3123	b_1	0.3935
b_2	0.2801	b_2	0.3699
b_3	0.3110	b_3	0.3926
b_4	0.0290	b_4	0.0344
b_5	0.0043	b_5	-0.0021
b_6	-0.0379	b_6	-0.0492
a_1	-1.7316	a_1	-1.7574
a_2	-2.7311	a_2	-2.7868
a_3	-2.1913	a_3	-2.2598
a_4	-1.5764	a_4	-1.6324
a_5	-0.5769	a_5	-0.6030
a_6	-0.1923	a_6	-0.2010

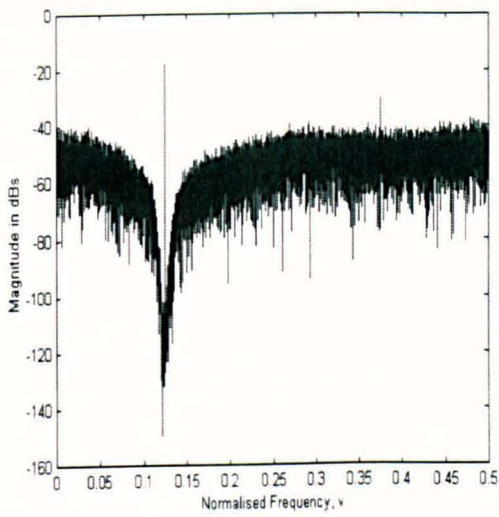
Table 2.13 The Sodini Interpolative Coefficients for 2nd-Order, 4th-Order and 6th-Order Butterworth and Chebyshev 2 Bandpass Σ - Δ Modulators.

Table 2.14 summarises the peak SNRs that are achieved for a variety of Butterworth and Chebyshev 2 based bandpass Σ - Δ modulators for the interpolative and the Chain of Accumulators with Feedforward Summation Local Resonator Feedback (CAFSLRFB) topologies for $\nu_C = 0.125$.

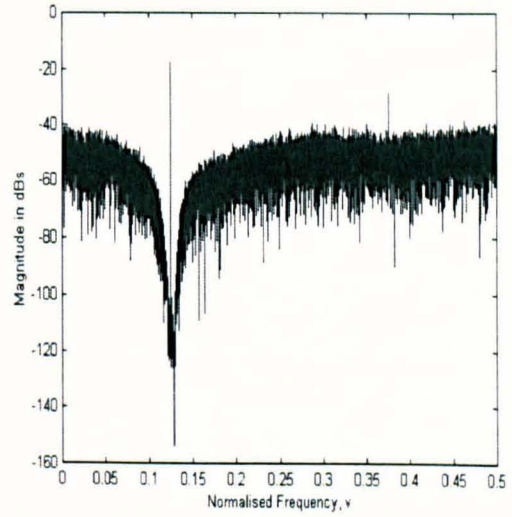
Mod	CAFSLRFB				Interpolative			
	4 th	6 th						
8	21	18.9	21.6	18.5	21	19	21.5	18.4
16	32.4	31.5	34.2	33.5	32.3	31.4	34.3	33.4
32	45.7	50	49	54.5	45.5	49.5	49.2	53.7
64	58.9	67.9	65.7	77.7	58.8	65.8	56.6	69.4
128	70.1	83.6	81.3	102.2	69.1	74.8	81.3	74
256	79.7	96.4	82.6	105.4	77.4	79.7	82.5	77

Table 2.14 A Comparison of the Peak SNR values between the CAFSLRFB and Interpolative Topologies for Different OSRs.

Several conclusions can be drawn based on the results in Table 2.14 as well as from detailed behavioural-level simulations. For the 4th-order Butterworth based modulator, the CAFSLRFB SNRs were marginally better for OSRs of 128 and 256 compared with the interpolative case as illustrated in Figure 2.62. For the 6th-order Butterworth based modulator, whose magnitude spectrum is shown in Figure 2.61 (a), the CAFSLRFB outperformed its interpolative counterpart by as much as 8.8 dB and 16.7 dB for OSR of 128 and 256 respectively as shown in Figure 2.63. However, for the other OSRs, the SNR characteristics were very comparable. For the 4th-order Chebyshev 2 based bandpass Σ - Δ modulator, the SNR figures across the entire DR were virtually identical. Finally; for the 6th-order Chebyshev 2 based modulator, whose magnitude spectrum is given in Figure 2.61 (b), the SNR figures in Figure 2.63, for the CAFSLRFB significantly outperformed its interpolative counterpart. The marked SNR deterioration in the interpolative case is attributed to the fact that the internal signal levels have larger amplitudes, which cause the quantiser to overload more prematurely. This overloading makes the modulator generate more in-band tones, resulting in inferior resolution.

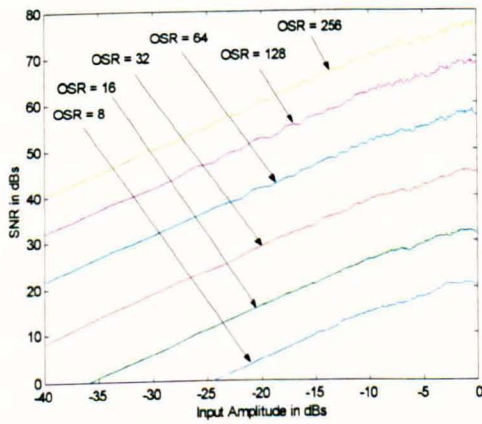


(a)

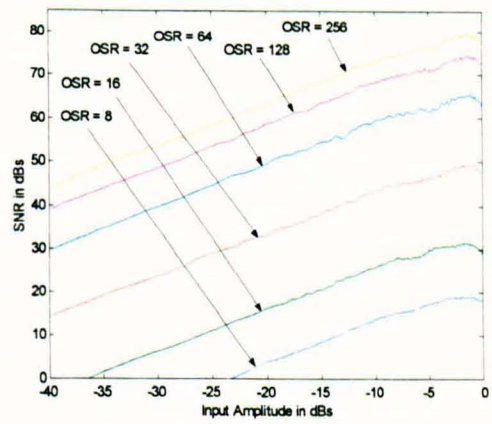


(b)

Figure 2.61 The Sodini Interpolative Magnitude Spectra of a 6th-Order Σ - Δ modulator at $\nu_C = 0.125$ (a) Butterworth, (b) Chebyshev 2.



(a)



(b)

Figure 2.62 SNR Curves at $\nu_C = 0.125$ for (a) 4th-Order, (b) 6th-Order Butterworth Based Variable-Band Bandpass Σ - Δ Modulators.

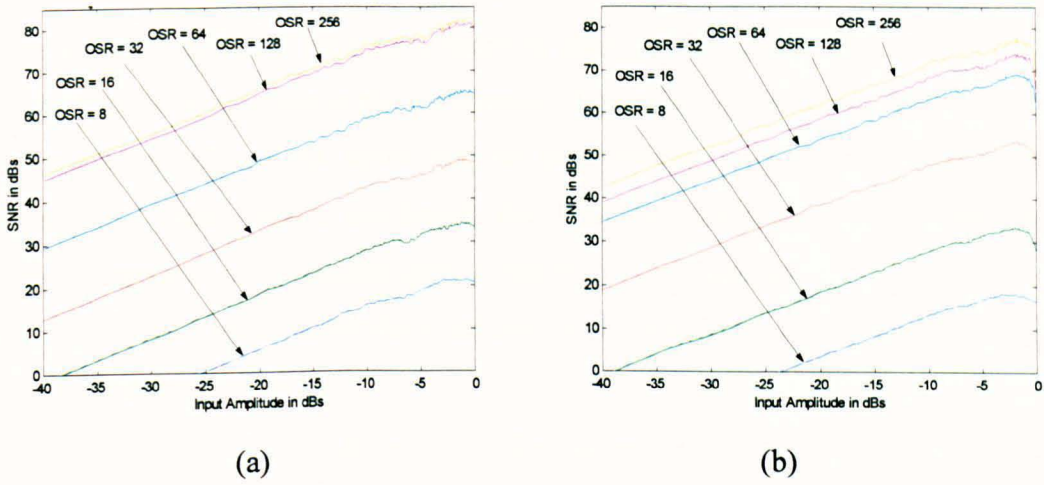


Figure 2.63 SNR Curves at $\nu_C = 0.125$ for (a) 4th-Order, (b) 6th-Order Chebyshev 2 Based Variable-Band Bandpass Σ - Δ Modulators.

2.23 Non-Idealities in Single-Stage Resonator-Based Bandpass Σ - Δ Modulators

This section presents a discussion supported with behavioural-level simulations of the effect of non-idealities on the noise-shaping performance and resolution of a 4th-order variable-band bandpass Σ - Δ modulator. The modulator under investigation was designed using the FIR notch-filter approach to provide variable-band noise-shaping at $\nu_C = 17/64$. These simulations can be broadly divided into two categories.

The first set of simulations investigated the effect of utilising non-unity gain resonators on the modulator resolution for different gain combinations in the 1st and 2nd resonators of the modulator. The transfer function model for this non-unity gain resonator $R_G(z)$ is given:

$$R_G(z) = g/(1 - 2 \cos 2\pi\nu_C z^{-1} + z^{-2}) \quad (2.70)$$

The deductions drawn from the detailed behavioural-level simulation results are summarised as follows. The use of non-unity gain values for the first resonator in the range $0.8 \leq g_1 \leq 1$ has negligible effect on the overall modulator resolution for the different combinations of OSRs. Similarly; the utilisation of non-unity gains for the 2nd-order resonator in the range $0.8 \leq g_2 \leq 1$ has very little effect on the SNR characteristics of the modulator. Moreover, simulations demonstrated that the simultaneous variation of the gains in both resonators had insignificant effect on the overall modulator resolution. It may have been quite surprising to see that in some cases, the peak SNR of this modulator occurred when the resonator gains were below unity. Initially; one is led to believe that a

reduction of resonator gains automatically results in larger in-band quantisation noise. However, moderate gain reductions serve to alleviate the amplitude levels of the internal signals, thus helping to lessen the occurrence of quantiser overloading. This in turn reduces the generation of in-band tones due to overloading, thus yielding better resolution. Furthermore, these results confirmed the fact that single-stage Σ - Δ modulators are relatively insensitive to moderate gain variations in the quantiser.

The second set of simulations utilised leaky resonators in the loop-filter of this 4th-order modulator as given by:

$$R_\rho(z) = 1/1 - 2\rho \cos 2\pi\nu_C z^{-1} + \rho^2 z^{-2} \quad (2.71)$$

The variation of the leakage factor ρ ranged from $0.96 \leq \rho \leq 1$ for each resonator. The use of leaky resonators in either the first or second loop of the modulator demonstrated that there was negligible deterioration in the in-band SNRs for the smaller OSRs of 8 and 16. However, the SNR degradation became significant for the larger OSRs of 32, 64, 128 and 256, where the discrepancy between $\rho = 1$ and $\rho = 0.96$ was as large as 16.5 dB. These observations confirm theoretical expectations, which indicate that the shift of the NTF zeros from the unit-circle towards the origin, causes a reduction of the quantisation noise in the in-band region. This naturally results in inferior resolution. In addition, the simultaneous and equal reduction of the resonator leakage factors below 0.98 produced very shallow noise-shaping responses. These spectra contained many tones especially in the signal region, which inevitably resulted in very poor resolution.

2.24 Concluding Remarks of Chapter 2

This chapter presented a survey of reported publications, an up-to-date review of hardware implementations and a summary of potential applications of bandpass Σ - Δ modulators. The core objective of the chapter was to present, develop and propose different approaches for the system-level design of single-stage bandpass Σ - Δ modulators.

Mid-band resonator-based bandpass Σ - Δ modulators using the $z^{-1} \rightarrow z^{-2}$ frequency transformation technique were relatively easy to design and invariably exhibited symmetrical noise-shaping magnitude spectra. Moreover, this symmetry improved modulator stability and simplified the specification requirements of the decimator. However, there were two constraints associated with this technique. First; it always

required a stable lowpass Σ - Δ modulator prototype. Second, it could only provide noise-shaping for a single frequency at $\nu_c = 0.25$.

The variable-band resonator-based lowpass-to-bandpass frequency transformation technique was simple to apply and allowed noise-shaping to be achieved for any centre frequency across the spectrum. However, it had several limitations. First, a working lowpass Σ - Δ modulator prototype was always needed, whose noise-shaping and stability characteristics were no longer preserved after the transformation. Second, the uneven shoulder gain levels imparted by the variable-band resonator transfer function reduced modulator stability and imposed more stringent specifications on the bandpass decimator. Third, good SNRs and DRs could only be accomplished for extremely narrow bandwidths, normally a single frequency. Fourth, the designer was limited to defining the centre frequency and OSR, having no freedom over specifying the signal bandwidth.

The application of the extended lowpass-to-bandpass frequency transformation approach, which was developed by the author allowed the specification of the signal bandwidth as well as the centre frequency of the noise-shaping band. The main features of this were as follows: First, allowing the designer to specify the signal bandwidth makes this technique more suitable for applications, whose inputs are composed of a multitude of harmonics. This is in contrast to the mid-band and variable-band transformation techniques, which only permitted the specification of the centre frequency, totally disregarding the width of the modulator input signal. Second, the difference in the shoulder gain levels of the loop-filter with this technique was virtually diminished for any band-location in the spectrum. This enhanced stability, especially for higher-order Σ - Δ modulators circumventing the need to use stability scaling factors. Third, this design process required the substitution of each delay element of the lowpass prototype with a generalised lowpass-to-bandpass frequency transformation. An *m-file* was written by the author, which could compute the loop-filter coefficients for a given set of system-level specifications. Fourth, Σ - Δ modulators, which employed this transformation approach contained fewer tones in their magnitude spectra. This was attributed to the more complicated loop-filter, which produced a wider range of state values. Fifth, the coincidental distribution of the poles and zeros of the loop-filter as a result of using this technique helped to simplify the structure of the loop-filter.

The FIR notch filter approach utilised a simpler NTF and was easier to design. However, the uneven shoulder gains of the magnitude spectrum for most centre frequencies was found to reduce modulator stability. Another constraint was that the notch had a

relatively large bandwidth, which implied that unwanted tones close to the input signal might be included in the signal region.

For the IIR notch filter approach, the disparity in the shoulder gain levels for non-mid-band centre frequencies was significantly reduced. This was achieved by placing the NTF poles at the same frequency of the zeros, but with a comparatively smaller magnitude. With this approach, the close proximity of the poles and zeros of the NTF resulted in greater in-band quantisation noise attenuation, but smaller bandwidths. Furthermore, this approach delivered better SNRs, higher DRs, reduced tonality and better stability compared with the FIR case.

The merits and drawbacks of the complex Σ - Δ modulator approach are summarised next. First, the poles and zeros were not restricted to conjugate pairs, which resulted in lower in-band quantisation noise attenuation compared with a real-coefficient modulator of the same order. Second, greater design flexibility and better resolution could be achieved with this approach compared with its real-coefficient counterpart at the cost of an additional quantiser and signal paths for the quadrature components of the input signal to the modulator. Third, these modulators were found to be well-suited for single side-band applications. Fourth, Σ - Δ modulators using this approach were found to be more stable for noise-shaping bands that were very close to dc and Nyquist. This robustness in stability was due to the significantly lower gain of the complex NTF, which consequently produced smaller internal signal levels in the modulator compared with the real FIR notch filter approach.

Complex IIR notch filter based Σ - Δ modulators gave better SNRs, higher DRs, lower tonality and improved stability compared with complex FIR notch filter based Σ - Δ modulators. Moreover, these improvements were accomplished using a lower-order loop-filter compared with the real-coefficient IIR approach, at the price of an extra quantiser and signal path for the imaginary components of the input signal. Once again, complex IIR notch filter based Σ - Δ modulators achieved better stability compared with complex FIR and real-coefficient IIR notch filter based Σ - Δ modulators. However, the design process and loop-filters of these modulators were slightly more complicated.

An alternative novel technique for the design of variable-band bandpass Σ - Δ modulators was proposed by the author, which utilised a first-order sum-filter in conjunction with fractional-delayers to spectrally transfer the noise-shaping band to the desired signal location. This approach was shown to accomplish single-band noise-shaping for any variable centre frequency input signal. In comparison with the transformation based

techniques, FIR sum-filter based Σ - Δ modulators were found to suffer from inadequate noise-shaping at high frequencies due to errors in the amplitude of the FIR filter. For FD requirements other 0.5, the FIR FD filter exhibited small phase errors resulting in minor shifts of the noise-shaping bands towards Nyquist. On the other hand, IIR sum-filter based Σ - Δ modulators yielded enhanced SNRs at the expense of a slightly more complicated design process. Furthermore, Σ - Δ modulators employing this approach contained fewer tones in their magnitude spectra compared with the transformation methods. This was attributed to the more complicated loop-filter transfer function, which resulted in a more diverse range of state values and therefore fewer tones.

A practical step-by-step methodology for the design of bandpass Σ - Δ modulators based on well known filter family types was presented and supported with extensive simulation results. The in-band SNRs that were achieved with a Chebyshev 2 bandpass Σ - Δ modulators outperformed their Butterworth counterparts by as much as 15 dB. This improvement was attributed to the distribution of the NTF zeros across the signal band, which accomplished greater in-band quantisation noise attenuation and therefore better SNRs. On the other hand, the Butterworth based Σ - Δ modulators, whose NTF zeros were coincidentally positioned resulted in a simpler structure of the loop-filter.

Next, several commonly used Σ - Δ modulator topologies were analysed and where appropriate structural modifications were made in order to allow variable-band noise-shaping. Simple-to-use routines, which could compute the required coefficients for any system-level set of specifications as well as a library containing the corresponding Σ - Δ modulator topologies were created in Matlab and Simulink respectively. Analysis showed that the NTF of the chain of resonators with weighted feedforward summation topology was totally independent of the weighting coefficients, thus restricting this topology to achieving noise-shaping at mid-band resonance only. The feedforward coefficients, however, provided flexibility for the positioning of the NTF pole locations in order to reduce if necessary the out-of-band gain of the NTF to allow greater control over modulator stability. The chain of accumulators with feedforward summation and local resonator feedback topology was found to be well-suited for applications that required variable-band noise-shaping. The presence of the internal feedback loop with a suitable coefficient provided the flexibility of moving the loop-filter poles away from dc to any centre frequency up to Nyquist. This structure was found to be suitable for any type of loop-filter irrespective of the pole location unlike its predecessor, which was restricted to mid-band centre frequencies. The chain of resonators with distributed feedback topology

was simple to use for mid-band centre frequency applications. For other centre frequency locations, this topology required the use of variable-band resonators as well as the insertion of additional gain factors prior to these resonators to control the internal amplitude levels in the modulator to ensure stability. The Sodini interpolative Σ - Δ modulator topology was shown to be suitable for any centre frequency specification. However, higher-order interpolative based Σ - Δ modulators produced lower SNRs compared with the other three topologies. This marked SNR deterioration was attributed to the fact that the internal signal levels had larger amplitudes, which caused the quantiser to overload more prematurely. This overloading made the modulator generate more in-band tones, therefore accounting for the poor resolution.

This chapter culminated by presenting detailed simulation results of the effects of non-unity gain and leaky resonators on the overall resolution of a fourth-order variable-band bandpass Σ - Δ modulator. Variations in the gain of either or both resonators by as much as 20% were shown to have negligible effect on the overall modulator resolution for different OSRs. Variations in the leakage factors of either the first or second resonators demonstrated that there was little in-band SNR change for the smaller OSRs of 8 and 16. However, there was significant SNR deterioration for the larger OSRs of 32, 64, 128 and 256 by as much as 16.5 dB for a 4% variation of the leakage factor. In addition, the simultaneous and equal reduction of the resonator leakage factors by as little as 2% exhibited very shallow noise-shaping spectra.

Chapter 3

Multi-Stage (MASH) Bandpass Σ - Δ Modulators

3.1 Overview on Bandpass MASH Σ - Δ Modulators

Multi-stage Noise-Shaping (MASH) Σ - Δ modulators provide an alternative means for achieving low-distortion, high-linearity A/D and D/A conversion on narrow-band low and high frequency input signals [Hay86]-[Mat87]-[Uch88]-[Cho89]-[Kar90]-[Rib91a]-[Rib91b]-[Wil91]-[Wil94]-[Bah95]-[Mar97]. These multi-loop Σ - Δ structures are essentially a cascade of independent lower-order Σ - Δ modulators [Cho89], where the quantisation noise in each stage is fed to the input of the following stage as shown below in Figure 3.1.

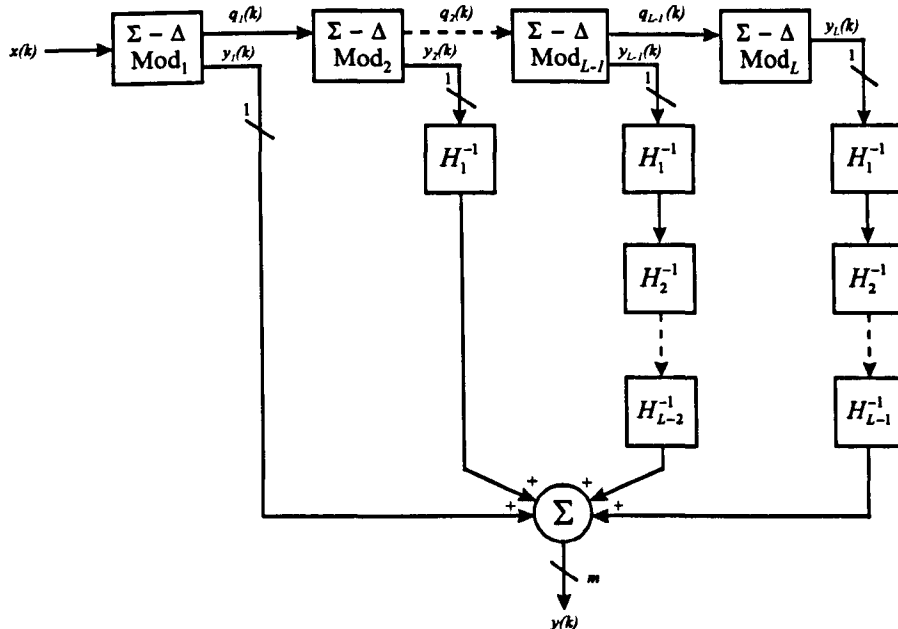


Figure 3.1 Generalised Block Diagram of a Multi-Stage (MASH) Σ - Δ modulator.

The outputs of all the stages are digitally filtered and subsequently combined so as to cancel the quantisation noise of the intermediate stages. The final stage quantisation noise is digitally processed by an L^{th} order filter, where L is the overall order of the modulator [Cho89].

The main advantage of MASH Σ - Δ modulators is that they are guaranteed to be stable to any order under all operating conditions for two important reasons. The first is that the lower-order Σ - Δ modulators that they are composed of are inherently stable,

(normally not exceeding second-order). The second reason is that they only contain feedforward paths between the individual modulator sections [Mat87]-[Uch88]-[Cho89].

A major disadvantage associated with MASH structures is that they are more sensitive to component non-idealities compared with higher-order single-bit Σ - Δ modulators of the same order. Mismatches between the analogue loop-filters and their corresponding digital inverse filters as well as inter-stage mismatches between the analogue stages result in the leakage of the quantisation noise of intermediate stages to the overall modulator output and thus lead to inferior resolution. Improper noise cancellation can also facilitate the propagation of tones from earlier to subsequent stages. For all MASH Σ - Δ modulators, the design of the first-stage is the most critical. The amount of quantisation noise in the in-band region for subsequent stages becomes greatly attenuated by noise-shaping, therefore making the performance requirements of these modulators less stringent [Mat87]-[Cho89]-[Rib91a].

Another drawback of MASH Σ - Δ topologies is increased hardware complexity due to the additional number of quantisers and digital cancellation circuitry at the modulator output stages [Mat87]-[Rib91a]-[Wil91].

Another inherent feature of MASH structures is the presence of multi-bits in its output signal. The cumulative effect of multi-bit outputs depends on the modulator order and its constituent number of internal stages. For example, a 1-1 cascade MASH will produce a final output signal having one of the following values ± 1 and ± 3 . [Cho89]-[Rib91a]-[Wil91]. The linearised model discussed in section 1.8 becomes more accurate for higher-order MASH Σ - Δ modulators, because the quantisation noise components of successive stages become more randomised as a result of more filtering. It could be also intuitively stated that the presence of multi-bit outputs also achieves greater decorrelation of the modulator output signal, thus making the use of the linear analysis more realistic. Assuming identical loop-filters in each modulator stage and unity coefficients throughout, a generalised output expression for the modulator shown in Figure 3.1 is given by:

$$y(k) = y_1(k) + H_1^{-1}y_2(k) + \dots + \sum_{i=1}^{L-2} H_i^{-1}y_{L-1}(k) + \sum_{i=0}^{L-1} H_i^{-1}y_L(k) \quad (3.1)$$

where H represents the loop-filter and L is the overall order of the modulator. Under ideal conditions, this output expression simplifies to

$$y_L(k) = x(k) + H^{-L}q_L(k) \quad (3.2)$$

where $q_L(k)$ is the quantisation noise of the final stage.

A further drawback that is associated with MASH Σ - Δ modulators is that the post digital decimator for A/D applications is complicated by the fact that it must allow for multi-bit inputs [Par92b].

It should be stated that a point is reached where no further improvement in resolution can be accomplished by increasing the number of stages in the modulator. This has been confirmed by simulation results carried out by the author.

Alternative MASH Σ - Δ configurations exist where the loop-filter output of the preceding stage feeds in directly to the following stage instead of feeding in the difference between the quantiser input and output. These modified MASH topologies may use scaling-down factors to control the magnitude of the signal levels from the loop-filters to ensure that the quantisers do not become overloaded [Rib91b].

Chapter 3 provides the design procedure and analysis of variable centre frequency resonator- and non-resonator based bandpass Σ - Δ modulators. The four techniques considered are based on the noise transfer functions of real-coefficient FIR notch-filters, complex FIR notch-filters, fractional-delay filters in conjunction with first-order sum-filters and Butterworth/Chebyshev 2 bandstop filters. A library containing over 33 different combinations of these Σ - Δ modulator topologies is created. The required modulator coefficients to meet any set of specifications can be obtained by running an associated *m-file* prior to simulation. A comparative study based on a mixture of linear modelling and behavioural level simulations of these different topologies is presented. Detailed guidelines for the selection of modulator performance measures are evaluated and shown in tabular and graphical forms.

3.2 Review of Published MASH Σ - Δ Modulators

An extensive literature survey on multi-stage Σ - Δ modulators revealed that 90.4% of all existing conference and journal publications are lowpass-based topologies employing accumulators and differencers for the analogue and digital sections respectively. Of the remaining the 9.6%: 7.7% and 1.9% use the mid-band [Kuo96]-[Mor96]-[Pea94]-[Rib94] and non-mid-band [Ben93] centre frequency low-to-band transformations discussed in sections in 2.5 and 2.7 respectively. These findings confirm the necessity of extending some of the techniques reported in chapter 2 for single-stage and multi-bit modulators to the cascaded MASH Σ - Δ modulators. Table 3.1 provides a chronological summary of all publications to-date on MASH Σ - Δ modulators. The abbreviations used in Table 3.1 are

given by: N is the modulator order, T is the modulator type, NMS represents the Number of Modulator Stages, R_B is the resolution in bits, LP is LowPass and BP is BandPass.

L	T	NMS	Brief Description of the Reported Publication	R_B	Refs
2	LP	1-1	SC 1.5- μ silicon gate CMOS for audio range	14	[Hay86]
3	LP	1-1-1	2- μ CMOS, $f_B = 24$ kHz	16	[Mat87]
L	LP	L	Ergodic Theory for DC inputs	N/A	[He88]
3	LP	2-1	SC 1.5- μ silicon gate CMOS, $f_B = 80$ kHz, $f_S = 2.56$ MHz	13	[Lon88]
3	LP	1-1-1	SC Simulations for Hi-Fi Audio, $f_S = 2.56$ MHz	16	[Uch88]
L	LP	L	Theoretical Analysis for DC and Sinusoids	N/A	[Cho89]
2	LP	1-1	Review of Various Topologies	N/A	[Mat89b]
3	LP	1-1-1	SC 1.5- μ CMOS, $f_B = 80$ kHz, $f_S = 10.24$ MHz	15.6	[Reb89a]
3	LP	1-1-1	SC 1.5- μ CMOS, $f_B = 160$ kHz, $f_S = 10.24$ MHz	14.6	[Reb89b]
2	LP	1-1	Analytical proof that dithered Q_N in 1-1 is White	N/A	[Cho90]
4	LP	2-2	2.5- μ molybdenum gate CMOS, $f_B = 3$ MHz, $OSR = 64$	18	[Kar90]
4	LP	2-2	Robust SC Realisation, $f_B = 32$ kHz, $f_S = 5$ MHz	16	[Mat90]
3	LP	1-1-1	SC 1.5- μ CMOS, $f_B = 80$ kHz, $f_S = 10.24$ MHz	15.2	[Reb90]
2	LP	1-1	Tutorial Survey of Σ - Δ Topologies	N/A	[Tem90]
2	LP	1-1	An extended tutorial on oversampling converters	N/A	[Hau91]
2	LP	1-1	Tutorial Overview on Σ - Δ Topologies	N/A	[Leu91]
3	LP	2-1	Linear Analysis & simulations of two 1-1-1 and 2-1	N/A	[Rib91a]
3	LP	2-1	Robust SC 1.2- μ CMOS, sample rate 80 kHz	15	[Rib91b]
3	LP	2-1	Analytical model & simulations of a 2-1 MASH	N/A	[Wil91]
3	LP	1-1-1	Practical limitations & measurement	N/A	[Hej92]
3	LP	1-1-1	Estimates: $f_S = 3$ MHz, $OSR = 64$, also 1-2 reported	16	[Mat92]
3	LP	2-1	Implemented in 1991 of AT&T DSP16C Codec DSP	-	[Nor92]
4	BP	2-2	Double integrator & bandpass, $v_C = 0.02$, $OSR = 50$	15.5	[Ben93]
3	LP	2-1	Cascade pseudo-multi-bit simulated, $OSR = 64$, $f_C = 4$ kHz	17.5	[Dia93]
4	LP	1-1	Non-accumulator-based 1-1 using Chebyshev	18	[Har93]
3	LP	1-1-1	An overview on A/D Σ - Δ modulators	N/A	[Par93]
4	LP	2-2	Simulated: 1-bit by 3-bit cascade (ideal = 26 b)	20	[Tan93]
6	LP	2-2-2	Implemented 1.2- μ CMOS, $f_B = 100$ kHz, 3-level	15	[Ded94]
4	LP	3-1	Est: $f_S = 22$ MHz, $OSR = 32$, 1.2- μ CMOS, 2 nd stage 5-bit	16	[Har94]
4	BP	2-2	$f_S = 10$ MHz, $f_C = 2.5$ MHz, $f_B = 50$ kHz, CT	-	[Pea94]
6	BP	4-2	SC CMOS, Est: $f_S = 10$ MHz, $f_C = 2.5$ MHz, $OSR = 64$	16	[Rib94]
3	LP	2-1	1- μ CMOS, $f_S = 6.4$ MHz, $f_C = 25$ kHz, $OSR = 128$	17	[Wil94]
4	LP	2-1-1	SC, 2- μ BiCMOS, $f_S = 48$ MHz, $OSR = 32$	16	[Yin94]
4	LP	2-2	SC analysis inc. non-idealities, $OSR = 64$, also 1-1-1-1, 2-1	18.3	[Bah95]
4	LP	1-1-1-1	Multi-stage closed-loop, $OSR = 50$, $v_B = 0.01$, also BP	15	[Ben95]

6	LP	3-3	SC simulations, 3-level, also (3-2 stages, 19.3 b, OSR = 32)	22.6	[Fis96]
4	BP	2-2	Comparative simulations of topologies of same order	17	[Kuo96]
6	BP	4-2	Novel digital FIR compensator to reduce non-idealities	16	[Mor96b]
3	LP	1-1-1	Analysis at circuit-level inc. non-idealities for 2-1, 1-1-1	17.2	[Fis97]
4	LP	mixed	Comparative simulations for 2-1, 2-1-1, 2-2, 3-1	mix	[Mar97]
3	LP	2-1	SC 0.8- μ CMOS, $f_s = 4$ MHz, $f_B = 25$ kHz, OSR = 80	16	[Rab97]
6	LP	3-3	$f_s = 20$ MHz, OSR = 20, digital correction non-idealities	18	[Fis98]
4	LP	2-2	$f_s = 140$ MHz, $f_C = 350$ kHz, multi-bit quantisers, OSR = 16, Stage1 is 2-bit, Stage2 is 6-bit	16	[Got98]
4	LP	mixed	Analysis & simulations of 2-1, 2-1-1, 2-2, 3-1	mix	[Mar98b]
4	LP	2-1-1	Stage3 is 3-bit, OSR = 16, insensitive to non-idealities	13.3	[Med98a]
4	LP	mixed	Investigation inc non-idealities for SC implementation	mix	[Med98b]
4	LP	2-2	SC 3- μ CMOS, $f_s = 3.2$ MHz, OSR = 64	14.7	[Mia98]
3	LP	1-1-1	SC 2- μ CMOS implementation with digital correction	17.8	[Dav99b]
2	LP	1-1	Uni-MASH using time-division concept for architecture	N/A	[Ho99]
2	LP	1-1	Cascade topology with reduced f_s , multi-bit quantiser	15	[Qin99]
2	LP	1-1	Pipelined MASH with inter-stage scaling, SC 2- μ CMOS, OSR = 8, stage2 multi-bit	11.6	[Ram99]
3	LP	1-2	Implementation on Xilinx 3042 FPGA	-	[Sun99]

Table 3.1 Chronological Survey of Publications for MASH Σ - Δ Modulators.

3.3 Design Methodology for MASH Bandpass Σ - Δ Modulators

This section describes a practical step-by-step approach that enables the design of bandpass MASH Σ - Δ modulators using one of the three NTF techniques shown below in Figure 3.2. The first method is based on the Pole-Zero-Placement (PZP) of either real or complex FIR notch-filters for the design of the NTF. The second method employs a first-order sum-filter in cascade with an FIR fractional delayer to spectrally move the NTF notch to the desired centre frequency location. The third technique utilises either Butterworth or Chebyshev 2 bandstop filters, where the stop-bandwidth of the NTF can be specified. The stop-band attenuation can also be specified in the case of Chebyshev 2. Each of the constituent lower-order sections will consist of a chain of resonators with distributed feedback.

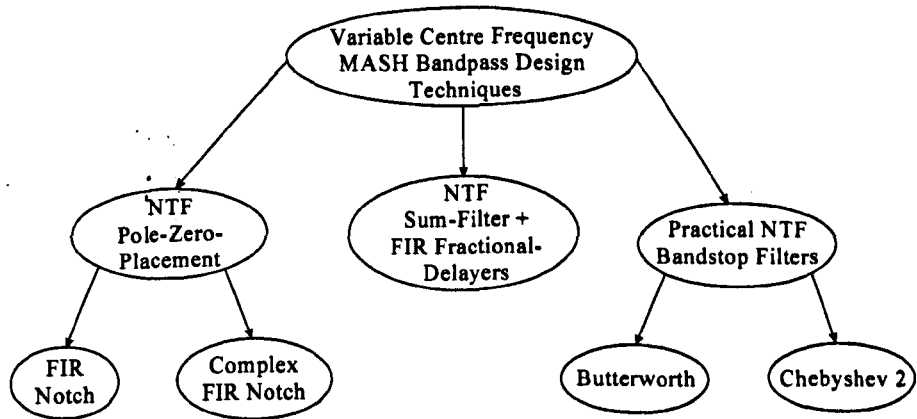


Figure 3.2 Different Techniques for the Design of Bandpass MASH Σ - Δ Modulators.

An algorithmic description of this method is presented in the following steps:

STEP 1: Select a normalised centre frequency ν_C , bandwidth $\Delta\nu$, *OSR*, *DR* and modulator order L .

STEP 2: Select one of three NTF methods.

If NTF PZP method then goto STEP 3,

If NTF Sum Filter + FIR Fractional Delayer Method then goto STEP 12,

If NTF bandstop method then goto STEP 16.

STEP 3: Select one of two sub-methods for NTF PZP,

If real-coefficient FIR notch-filter method then goto STEP 4,

If complex-coefficient FIR notch-filter method then goto STEP 8.

STEP 4: The real-coefficient FIR notch-filter method involves positioning the zeros of the NTF at the desired centre frequency location to provide maximum in-band attenuation. The zeros of the NTF are located at $e^{\pm j2\pi\nu_C}$, where ν_C is the normalised frequency of the input signal. The poles of the NTF, however, are stationed at the origin of the unit-circle. The NTF is given by:

$$NTF = (1 - 2 \cos 2\pi\nu_C z^{-1} + z^{-2})^L \quad (3.3)$$

where L is the modulator order.

STEP 5: The corresponding loop- and feedback filters may be analytically derived using the linear model described in Section 1.8. This linear approximation was found to deliver adequate results as far as depicting the noise-shaping envelope of the modulator.

Therefore, the loop- and feedback transfer functions are analytically obtained by rearranging the expression for the *NTF* as shown below:

$$F(z)L(z) = (1 - NTF)/NTF \quad (3.4)$$

where $F(z)$ and $L(z)$ may be determined by separating the numerator and denominator expressions such that $F(z) = (1 - NTF)$ and $L(z) = 1 / NTF$.

The lowest possible order in the case of real coefficient bandpass Σ - Δ modulators is second-order. Detailed simulations showed that second-order resonator-based single-bit Σ - Δ modulators are guaranteed to be stable for any centre frequency, but that fourth-order resonator-based single-bit bandpass Σ - Δ modulators are stable for a narrow-range of centre frequencies around the mid-band region. The adopted solution was to employ multi-bit quantisers where necessary to ensure that fourth-order resonator-based Σ - Δ modulators are stable for all the centre frequencies. Therefore, in this chapter higher-order bandpass MASH Σ - Δ modulators are constructed by using mixed combinations of second and/or fourth-order independent resonator-based Σ - Δ modulators. The second-order modulators will always contain a single-bit quantiser and the fourth-order modulators will contain either a single- or multi-bit quantiser depending on the centre frequency location.

STEP 6: This step involves confirming the overall MASH modulator order, deciding on the order and number of stages within each MASH topology and hence determining the extra digital filters that are required at the output of each stage to achieve the most effective noise-shaping. Table 3.2 gives a summary of the constituent building blocks of these Σ - Δ MASH topologies. Note that the loop-filter, feedback filters and digital notch-filters are represented by $R(z)$, $F(z)$ and $N(z)$ as shown below:

$$R(z) = \frac{1}{1 - 2 \cos 2\pi\nu_C z^{-1} + z^{-2}} \quad (3.5)$$

$$F(z) = 2 \cos 2\pi\nu_C z^{-1} + z^{-2} \quad (3.6)$$

$$N(z) = 1 - 2 \cos 2\pi\nu_C z^{-1} + z^{-2} \quad (3.7)$$

L	Comb.	Loop-Filters				Feed-back	Notch-Filters		
		Stage1	Stage2	Stage3	Stage4		Stage2	Stage3	Stage4
4	2-2	$R(z)$	$R(z)$	-	-	$F(z)$	$N(z)$	-	-
6	2-2-2	$R(z)$	$R(z)$	$R(z)$	-	$F(z)$	$N(z)$	$N^2(z)$	-
6	4-2	$R^2(z)$	$R(z)$	-	-	$F(z)$	$N^2(z)$	-	-
6	2-4	$R(z)$	$R^2(z)$	-	-	$F(z)$	$N(z)$	-	-
8	2-2-2-2	$R(z)$	$R(z)$	$R(z)$	$R(z)$	$F(z)$	$N(z)$	$N^2(z)$	$N^3(z)$
8	4-2-2	$R^2(z)$	$R(z)$	$R(z)$	-	$F(z)$	$N^2(z)$	$N^3(z)$	-
8	2-4-2	$R(z)$	$R^2(z)$	$R(z)$	-	$F(z)$	$N(z)$	$N^3(z)$	-
8	2-2-4	$R(z)$	$R(z)$	$R^2(z)$	-	$F(z)$	$N(z)$	$N^2(z)$	-
8	4-4	$R^2(z)$	$R^2(z)$	-	-	$F(z)$	$N^2(z)$	-	-

Table 3.2 Constituent Building-Blocks of Bandpass MASH Σ - Δ Modulators.

STEP 7: Run the Matlab m-file *mashdes* first by simply typing it in the Matlab workspace environment. This program requires the user to enter values for ν_c and *OSR*. Then run the simulator using Simulink in Matlab to confirm the correct operation of the chosen modulator. To check SNR and DR values, run another m-file called *snrval*. If the in-band SNR value is not sufficiently high then

- increase the modulator order and repeat STEPS 4-7,
- or increase the *OSR* provided the bandwidth of the in-band region is not violated and repeat STEPS 1-7,
- or increase the number of levels in the quantiser of the first-stage, and repeat STEPS 1-7.

STEP 8: In the complex-coefficient FIR notch-filter method, the zeros of the NTF are placed at the specified positive centre frequency on the unit-circle to accomplish maximum in-band attenuation. The zeros are located at $e^{+j2\pi\nu_c}$. The NTF is given by

$$NTF = (1 - e^{j2\pi\nu_c} z^{-1})^L \quad (3.8)$$

STEP 9: The corresponding loop- and feedback filters may be obtained using the linear model as described in sections 1.8 and STEP 5 respectively.

The lowest possible order in the case of complex-coefficient bandpass Σ - Δ modulators is first-order. Detailed simulations confirmed that both first- and second-order complex resonator-based bandpass Σ - Δ modulators are stable for all centre frequencies up to very high input amplitude levels. Therefore, complex higher-order bandpass MASH Σ - Δ modulators are built using combinations of complex first- and/or second-order resonator-based single-bit Σ - Δ modulators.

STEP 10: This step involves deciding on the order and number of stages within each MASH topology and hence determining the extra digital filters that are needed at the output of each stage to achieve the most effective noise-shaping. Table 3.3 provides a summary of the constituent building blocks of these complex MASH topologies. Note that the complex loop-filters, complex feedback delayers and digital complex notch-filters are depicted by $CR(z)$, $CF(z)$ and $CN(z)$ as shown below:

$$CR(z) = \frac{1}{1 - e^{j2\pi\nu_c} z^{-1}}, \quad CF(z) = e^{j2\pi\nu_c} z^{-1} \quad \text{and} \quad CN(z) = 1 - e^{j2\pi\nu_c} z^{-1} \quad (3.9)$$

L	Comb.	Complex Loop-Filters				Complex Delayers	Complex Notch-Filters		
		Stage1	Stage2	Stage3	Stage4		Stage2	Stage3	Stage4
2	1-1	$CR(z)$	$CR(z)$	-	-	$CF(z)$	$CN(z)$	-	-
3	1-1-1	$CR(z)$	$CR(z)$	$CR(z)$	-	$CF(z)$	$CN(z)$	$CN^2(z)$	-
3	2-1	$CR^2(z)$	$CR(z)$	-	-	$CF(z)$	$N^2(z)$	-	-
3	1-2	$CR(z)$	$CR^2(z)$	-	-	$CF(z)$	$CN(z)$	-	-
4	1-1-1-1	$CR(z)$	$CR(z)$	$CR(z)$		$CF(z)$	$CN(z)$	$CN^2(z)$	$CN(z)$
4	2-1-1	$CR^2(z)$	$CR(z)$	$CR(z)$	-	$CF(z)$	$CN^2(z)$	$CN^3(z)$	-
4	1-2-1	$CR(z)$	$CR^2(z)$	$CR(z)$	-	$CF(z)$	$CN(z)$	$CN^3(z)$	-
4	1-1-2	$CR(z)$	$CR(z)$	$CR^2(z)$	-	$CF(z)$	$CN(z)$	$CN^2(z)$	-
4	2-2	$CR^2(z)$	$CR^2(z)$	-	-	$CF(z)$	$CN^2(z)$	-	-

Table 3.3 Constituent Building-Blocks of Complex Bandpass MASH Σ - Δ Modulators.

STEP 11: Run the Matlab m-file *mashdes* first by simply typing it in the Matlab workspace environment. This program requires the user to enter values for ν_c and *OSR*. Then run the simulator using Simulink in Matlab to confirm the correct operation of the chosen

modulator. To check SNR and DR values, run another m-file called *snrval*. If the in-band SNR value is not sufficiently high then

- a) either increase the modulator order and repeat STEPS 8-10,
- b) or increase the OSR provided the bandwidth of the in-band region is not violated and repeat STEPS 8-10.

STEP 12: The FIR Fractional-Delay-Filter (FDF) method is based on using a first-order sum-filter in cascade with an FDF for the NTF, which is given by,

$$H_N(\nu) = (1 + e^{-j2\pi\nu c D})^L \Rightarrow H_N(\nu) = (1 + e^{-j2\pi\nu c (f+r)})^L \quad (3.10)$$

This implies that an arbitrary normalised centre frequency can be attained by determining the necessary total delay D that must be incorporated in $H_N(z)$, so that the null of the first-order sum-filter is spectrally transferred to the desired signal frequency band. Note that f is the delay of the FD filter itself (including the fractional component) and r is the additional delay required to meet a given specification. Using the Lagrange approximation as detailed in Section 2.15, the NTF becomes:

$$H_N(z) = [1 + z^{-r} (c_0 + c_1 z^{-1} + \dots + c_{(N-1)} z^{-(N-1)} + c_N z^{-N})]^L \quad (3.11)$$

where N is the order of the FDF.

STEP 13: Using linearised analysis, the corresponding loop- and feedback filters become:

$$L(z) = \frac{1}{1 + z^{-r} (c_0 + c_1 z^{-1} + \dots + c_{(N-1)} z^{-(N-1)} + c_N z^{-N})} \quad (3.12)$$

$$C(z) = z^{-r} (c_0 + c_1 z^{-1} + \dots + c_{(N-1)} z^{-(N-1)} + c_N z^{-N}) \quad (3.13)$$

For this technique, higher-order bandpass MASH Σ - Δ modulators are built by using mixed combinations of single-stage single-bit Σ - Δ modulators. The order of the constituent loop-filters depends on the FD order.

STEP 14: This step involves determining the number and order of the digital filters that are required at the output of each stage to achieve the most effective noise-shaping. Table 3.4 gives a summary of all the building blocks contained in these MASH modulators. Note that S refers to the number of stages in this modulator as the order depends on that of FDF.

S	Comb.	Complex Loop-Filters				Feedback filter	Complex Notch-Filters		
		Stage1	Stage2	Stage3	Stage4		Stage2	Stage3	Stage4
2	1-1	$FR(z)$	$FR(z)$	-	-	$FF(z)$	$FN(z)$	-	-
3	1-1-1	$FR(z)$	$FR(z)$	$FR(z)$	-	$FF(z)$	$FN(z)$	$FN^2(z)$	-
4	1-1-1-1	$FR(z)$	$FR(z)$	$FR(z)$	$FR(z)$	$FF(z)$	$FN(z)$	$FN^2(z)$	$FN^3(z)$

Table 3.4 Constituent Building-Blocks of Bandpass FDF-Based MASH Σ - Δ Modulators.

STEP 15: Run the Matlab m-file *mashdes* first by simply typing it in the Matlab workspace environment. This program requires the user to enter values for ν_C and *OSR*. Then run the simulator using Simulink in Matlab to confirm the correct operation of the chosen modulator. To check SNR and DR values, run another m-file called *snrval*. If the in-band SNR value is not sufficiently high then

- a) increase the modulator order and repeat STEPS 11-14,
- b) or increase the OSR provided the bandwidth of the in-band region is not violated and repeat STEPS 11-14,
- c) or increase the number of levels in the quantiser of the first-stage, and repeat STEPS 11-14.

STEP 16: Select a modulator order L , either a Butterworth or Chebyshev 2 bandstop filter for the *NTF*, bandwidth $\Delta\nu$, and stopband ripple (R_S) required for Chebyshev 2. A straightforward procedure for obtaining the *NTF*, for any filter family type involves using the Matlab as indicated below:

For a Butterworth *NTF* :

$$[num, den] = butter(N, [\nu_L \nu_U], 'stop')$$

For a Chebyshev Type 2 *NTF* :

$$[num, den] = cheby2(N, R_S, [\nu_L \nu_U], 'stop')$$

where *num* and *den* refer to the numerator and denominator polynomials of the *NTF*, *stop* refers to a stop-band filter, ν_L and ν_U represent the normalised lower and upper 3dB frequencies and are given by:

$$v_L = v_C - \Delta v/2 \quad \text{and} \quad v_L = v_C + \Delta v/2 \quad (3.14)$$

STEP 17: Scale the *NTF* so that the first sample of the impulse response becomes 1 in order to meet the causality criterion. This can be achieved in Matlab by typing $nums = num / num(1)$, where *nums* contains the newly scaled coefficients of the numerator polynomial of the *NTF*, Ensure that the peak magnitude of the *NTF* spectrum does not exceed 2 to comply with Lee's stability criterion.

STEP 18: The noise, loop-filter and signal transfer functions of an eighth-order Σ - Δ modulator are given by

$$NTF = \frac{1 + b_1 z^{-1} + \dots + b_{(L-1)} z^{-(L-1)} + b_L z^{-L}}{1 + a_1 z^{-1} + \dots + a_{(L-1)} z^{-(L-1)} + a_L z^{-L}} \quad (3.15)$$

$$H(z) = \frac{c_1 z^{-1} + c_2 z^{-2} + \dots + c_{(L-1)} z^{-(L-1)} + c_L z^{-L}}{1 + b_1 z^{-1} + \dots + b_{(L-1)} z^{-(L-1)} + b_L z^{-L}} \quad (3.16)$$

$$STF = \frac{c_1 z^{-1} + c_2 z^{-2} + \dots + c_{(L-1)} z^{-(L-1)} + c_L z^{-L}}{1 + a_1 z^{-1} + \dots + a_{(L-1)} z^{-(L-1)} + a_L z^{-L}} \quad (3.17)$$

where the *b*'s are the most important parameters since they are responsible for controlling the magnitude of the in-band quantisation, the *a*'s for reducing the overall spectral magnitude of the *NTF* so as to avoid overloading the quantiser and the *c*'s are simply given by $c_N = a_N - b_N$.

STEP 19: Run the Matlab m-file *mashdes* first by simply typing it in the Matlab workspace environment. This program requires the user to enter values for v_C and *OSR*. Then run the simulator using Simulink in Matlab to confirm the correct operation of the chosen modulator. To check SNR and DR values, run another m-file called *snrval*. If the in-band SNR value is not sufficiently high then

- a) increase the modulator order and repeat STEPS 16-18,
- b) or increase the *OSR* provided the bandwidth of the in-band region is not violated and repeat STEPS 16-18,
- c) or increase the number of levels in the quantiser of the first-stage, and repeat STEPS 16-18,

- d) resort to an optimisation algorithm, where the poles and zeros of the NTF are shifted to more optimal positions in the z -plane to achieve better resolution.

3.4 Fourth-Order Bandpass 2-2 MASH Σ - Δ Modulator

The double-stage 2-2 MASH Σ - Δ modulator shown in Figure 3.3, is basically a cascade connection of two independent second-order Σ - Δ modulators, which can provide a fourth-order noise-shaping response.

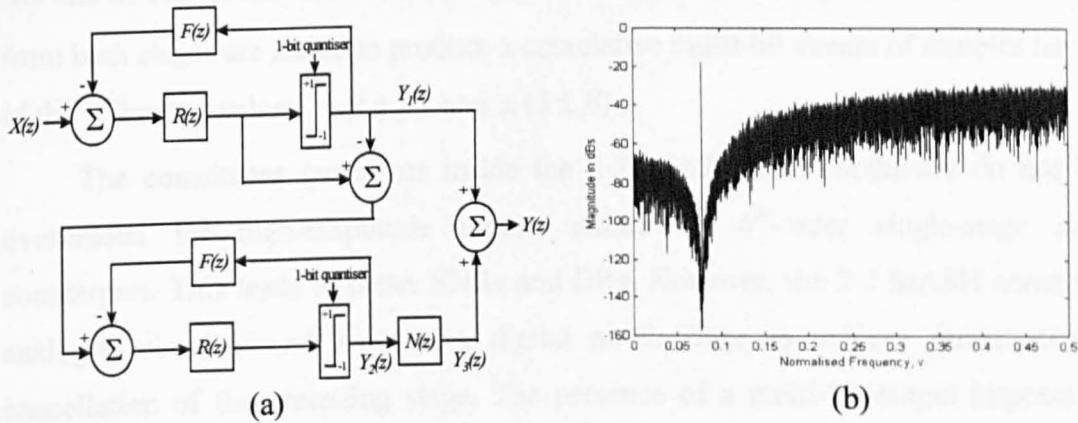


Figure 3.3 Fourth-Order Bandpass 2-2 MASH Σ - Δ Modulator: (a) Block Diagram, (b) Magnitude Spectrum at $\nu_C = 5/64$.

Each of the two modulator sections consists of a second-order variable centre frequency resonator and a single-bit quantiser in the feedforward path as well as a suitable filter in the feedback path to provide effective noise-shaping. The quantisation noise of the first-stage is fed to the input of the second-stage. The resultant outputs of the first $Y_1(z)$ and second $Y_2(z)$ stages are:

$$Y_1(z) = X(z) + (1 - \beta z^{-1} + z^{-2})Q_1(z) \quad (3.18)$$

$$Y_2(z) = \left[-Q_1(z) + (1 - \beta z^{-1} + z^{-2})Q_2(z) \right] N(z) \quad (3.19)$$

The associated quantisation and dither signal of the first-stage can be fully cancelled if the digital notch-filter is $N(z) = (1 - \beta z^{-1} + z^{-2})$, resulting in a final expression for $Y_{22}(z)$ given by:

$$Y_{22}(z) = Y_1(z) + N(z)Y_2(z) = X(z) + (1 - \beta z^{-1} + z^{-2})^2 Q_2(z) \quad (3.20)$$

where $X(z)$ is the input signal, $Q_1(z)$ and $Q_2(z)$ represent the quantisation noise of the first- and second-stages respectively.

The inclusion of a notch-filter at the output of $Y_2(z)$ as well as the summation of the two stages yields a multi-bit output signal in the time-domain. The output signal of the first-stage $y_1(k)$ has values of ± 1 and that of the second-stage after the notch-filter $y_3(k)$ has one of six values $\pm \beta$ and $\pm(2 \pm \beta)$, where $\beta = 2 \cos 2\pi\nu_C$. All output combinations from both stages are added to produce a cumulative multi-bit stream of samples having one of the following values, $\pm(1 \pm \beta)$ and $\pm(3 \pm \beta)$.

The constituent quantisers inside the 2-2 MASH Σ - Δ modulator do not become overloaded for high-amplitude inputs, unlike its 4th-order single-stage single-bit counterpart. This leads to better SNRs and DRs. However, the 2-2 MASH contains more analogue circuitry and requires a digital notch filter to achieve quantisation noise cancellation of the preceding stage. The presence of a multi-bit output imposes further design constraints on the decimator. Furthermore, non-idealities between the analogue stages and digital sections are more critical, because these inaccuracies contribute to the leakage of more quantisation noise and tones to the in-band region.

The 2-2 MASH was evaluated at the behavioural-level in Simulink for an extensive range of centre frequencies to verify its correct operation and the effectiveness of its noise-shaping, where the magnitude spectrum for $\nu_C = 5/64$ is shown in Figure 3.3 (b). The in-band SNRs were determined for three separate examples: a low-frequency ($\nu_C = 5/64$), a medium-frequency ($\nu_C = 17/64$) and a high-frequency ($\nu_C = 29/64$). These in-band SNR curves are illustrated in Figure 3.4 (a), (b) and (c) for different six OSRs.

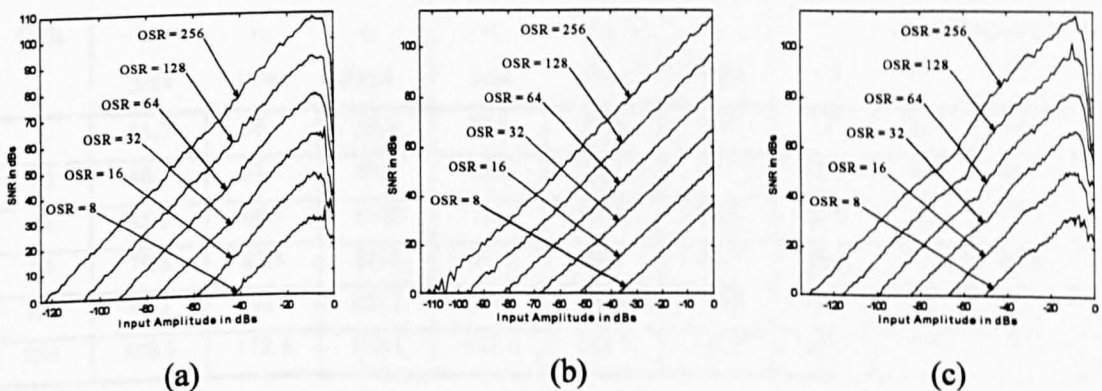


Figure 3.4 SNR Curves for Variable-Band 2-2 MASH Bandpass Σ - Δ Modulators at: (a) $\nu_C = 5/64$, (b) $\nu_C = 17/64$ and (c) $\nu_C = 29/64$.

The in-band SNRs for the normalised frequency range $0.03125 \leq \nu_C \leq 0.46875$ were determined for OSRs of 8, 16, 32, 64, 128 and 256 for four different amplitude levels as demonstrated in Figure 3.5. It is seen from 3.5 that the in-band SNRs deteriorate at very low and very high frequencies for large input amplitudes. This is attributed to quantiser overloading due to the asymmetrical magnitude of the noise transfer function at these frequencies. The in-band SNRs become more constant for moderate input amplitudes. However, for low input amplitudes, the in-band SNRs become more frequency-dependent where better SNRs are accomplished at lower and upper frequencies.

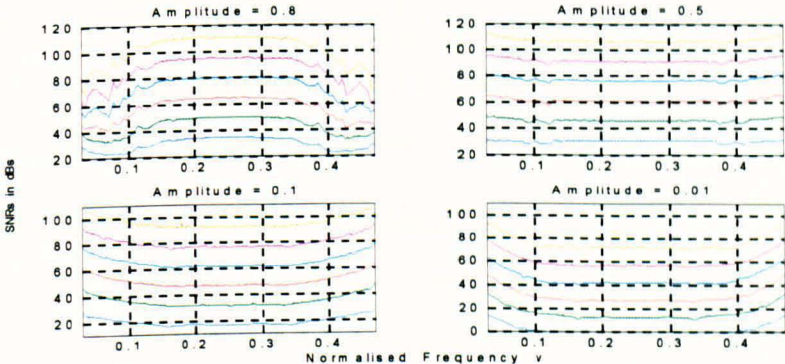


Figure 3.5 SNR curves versus Normalised Input Centre Frequency of a Fourth-Order 2-2 MASH Σ - Δ Modulator for OSRs of 8, 16, 32, 64, 128 and 256 for Input Amplitudes of 0.8, 0.5, 0.1 and 0.01.

The peak SNRs and dynamic ranges for six OSRs for three different normalised centre frequencies are recorded in Table 3.1. The difference between the highest and lowest SNR (Δ SNR) for the normalised frequency range $0.03125 \leq \nu_C \leq 0.46875$ is also recorded for a selection of input amplitudes, where high variations in Δ SNR are measured for large input amplitudes.

OSR	Peak SNRs			Dynamic Ranges			Δ SNR			
	ν_C	ν_C	ν_C	ν_C	ν_C	ν_C	Input Signal Amplitude			
	5/64	17/64	29/64	5/64	17/64	29/64	0.8	0.5	0.1	0.01
8	34.3	36.9	33.6	43.4	36.8	50.6	12	2.9	12.2	18.3
16	48.1	51.7	50.7	59.1	52.1	67.4	17.6	5.9	16.6	21.8
32	65.1	66.9	66.9	76	67.4	84.5	23.8	9.4	17.6	23
64	78.6	82.3	81.7	91.2	81.8	99.7	28.4	7.2	17.8	23.6
128	93.3	97	102.2	106.7	96.5	115.2	36.7	7.7	19.7	23.2
256	108.9	112.4	113.1	122.5	105.2	129.2	41.9	7.7	17.7	23.5

Table 3.5 Peak SNRs, DRs and Δ SNR of the 2-2 MASH for different OSRs.

Table 3.6 reveals that the average SNR and DR increases in relation to the OSRs for the low and high frequencies are noticeably better.

OSR	SNR Increase			DR Increase		
	v_C	v_C	v_C	v_C	v_C	v_C
	5/64	17/64	29/64	5/64	17/64	29/64
8 → 16	8.6	7.5	8.1	15.7	15.3	16.8
16 → 32	8.8	7.6	8.9	16.9	15.3	17.1
32 → 64	8.0	7.3	8.1	15.2	14.4	15.2
64 → 128	7.9	7.1	7.6	15.5	14.7	15.5
128 → 256	7.7	7.2	7.3	15.8	8.7	14
Average SNR Increase	8.2	7.4	8.0	15.8	13.7	15.7

Table 3.6 Average increases in SNR and DR of the 2-2 MASH as a result of doubling OSRs at $v_C = 5/64$, $v_C = 17/64$ and $v_C = 29/64$.

3.5 Sixth-Order Bandpass MASH Σ - Δ Modulator

A sixth-order bandpass MASH Σ - Δ modulator can be built by having cascade combinations of 2-2-2 or 4-2 or 2-4 lower-order modulator sections. The following three sub-sections provide a block diagram, the analysis and the simulation results for each case.

3.5.1 Triple-Stage Sixth-Order 2-2-2 MASH Bandpass Σ - Δ Modulator

This structure is basically a cascade connection of three second-order variable-band resonator-based bandpass Σ - Δ modulators as shown in Figure 3.6 (a), where the quantisation error of the first stage is fed to the input of the second stage.

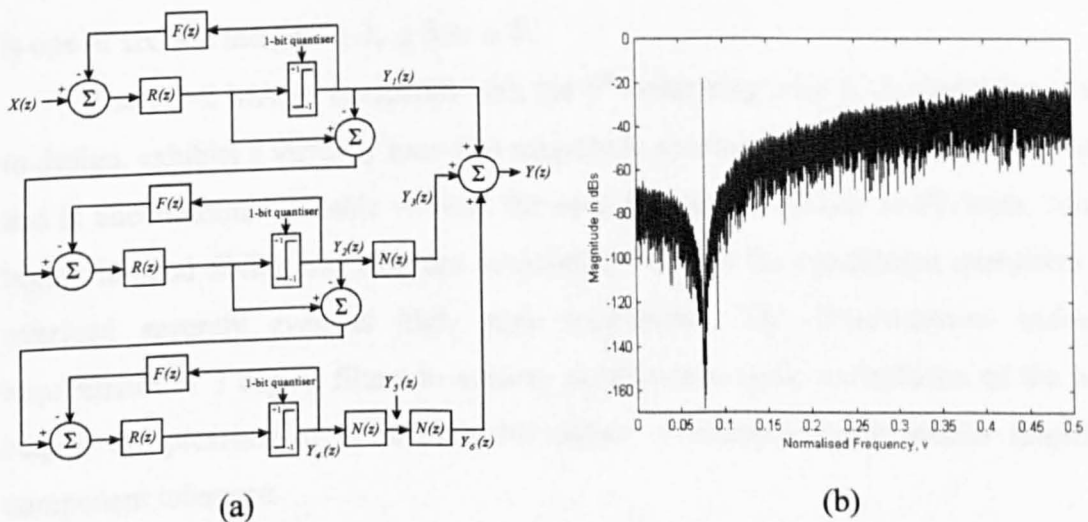


Figure 3.6 Sixth-Order Bandpass 2-2-2 MASH Σ - Δ Modulator: (a) Block Diagram, (b) Magnitude Spectrum at $v_C = 5/64$.

Similarly; the quantisation error of the second stage is fed to the input of the third stage. The output of the modulator is the summation of the first stage $Y_1(z)$, a single notch-filtered output from the second stage $Y_3(z)$ and a double notch-filtered output from the third stage $Y_6(z)$.

These output expressions in the z-domain are given by:

$$Y_1(z) = X(z) + (1 - \beta z^{-1} + z^{-2})Q_1(z) \quad (3.21)$$

$$Y_3(z) = -(1 - \beta z^{-1} + z^{-2}) Q_1(z) + (1 - \beta z^{-1} + z^{-2})^2 Q_2(z) \quad (3.22)$$

$$Y_6(z) = -(1 - \beta z^{-1} + z^{-2})^2 Q_2(z) + (1 - \beta z^{-1} + z^{-2})^3 Q_3(z) \quad (3.23)$$

Therefore, the overall output expression becomes $Y(z)$

$$Y(z) = X(z) + (1 - \beta z^{-1} + z^{-2})^3 Q_3(z) \quad (3.24)$$

where the quantisation noise of the intermediate stages $Q_1(z)$ and $Q_2(z)$ are cancelled out.

The multi-bit output combinations from the 2-2-2 MASH can be determined by examining the modulator amplitude samples in the time-domain. The output signal of the first stage has values of ± 1 and that of the second-stage after the one notch-filter has one of six amplitudes $\pm \beta$ and $\pm (2 \pm \beta)$. Similarly; a double notch-filter yields a signal having values of $\pm (\beta^2 \pm 2m\beta \pm (m+2))$, where m is an integer having one of three values 0 or ± 2 . All the combinations from each of the three stages are added to produce the final output signal, which consists of one of the following values $\pm (\beta^2 \pm p\beta \pm (p+2))$, where p is one of six odd integers $\pm 1, \pm 3$ or ± 5 .

The 2-2-2 MASH compared with the 6th-order single-bit Σ - Δ modulator is simpler to design, exhibits a virtually tone-free magnitude spectrum for ideal component matching and is unconditionally stable without the need for extra feedback coefficients. Moreover, higher in-band SNRs and DRs are achievable, because the constituent quantisers do not overload severely even at high input amplitudes. The disadvantages include, the requirement of 3 digital filters to achieve quantisation noise cancellation of the previous stages, the presence of more multi-bit output combinations and greater sensitivity to component tolerance.

The correct operation of this 2-2-2 MASH is verified for a wide range of frequencies, where the magnitude spectrum for $\nu_c = 5/64$ is shown in Figure 3.6 (b). The in-band SNR curves for three different frequencies for six different OSRs are shown in Figure 3.7.

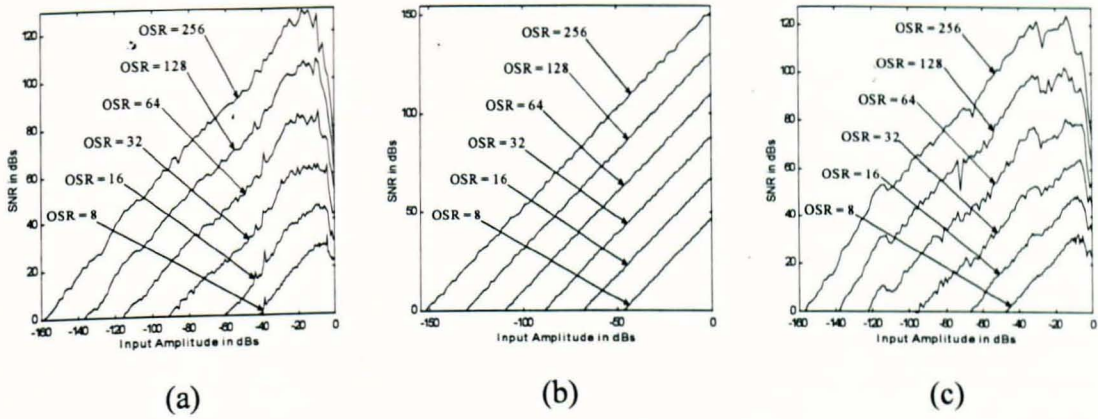


Figure 3.7 SNR Curves for Variable-Band 2-2-2 MASH Bandpass Σ - Δ Modulators at: (a) $\nu_C = 5/64$, (b) $\nu_C = 17/64$ and (c) $\nu_C = 29/64$.

The in-band SNRs for the normalised frequency range $0.03125 \leq \nu_C \leq 0.46875$ were determined for OSRs of 8, 16, 32, 64, 128 and 256 for four different amplitude levels as demonstrated in Figure 3.8. It is seen from 3.8 (a) that the in-band SNRs deteriorate significantly at very low and very high frequencies for large input amplitudes. This is attributed to quantiser overloading due to the asymmetrical magnitude of the noise transfer function at these frequencies. The in-band SNRs become more constant for moderate input amplitudes. However, for low input amplitudes, the in-band SNRs become more frequency-dependent, where better SNRs are accomplished at lower and upper frequencies.

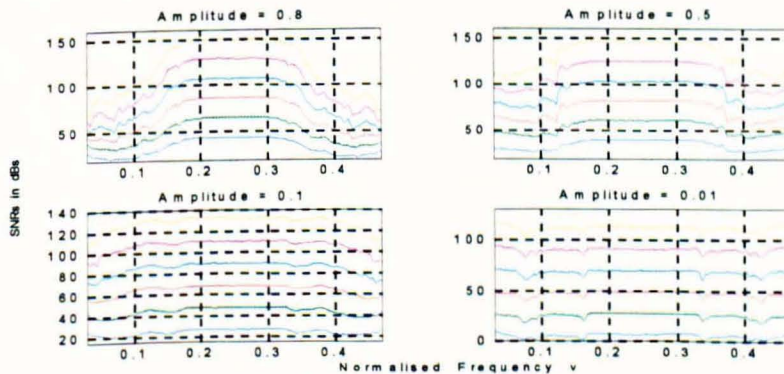


Figure 3.8 SNR curves versus Normalised Input Centre Frequency of a Sixth-Order 2-2-2 MASH Σ - Δ Modulator for OSRs of 8, 16, 32, 64, 128 and 256 for Input Amplitudes of 0.8, 0.5, 0.1 and 0.01.

The peak SNRs and DRs for six OSRs for three different normalised centre frequencies and Δ SNR for different amplitude levels are recorded in Table 3.7. Large variations in SNRs are found for high input amplitude signals.

OSR	Peak SNRs			Dynamic Ranges			Δ SNR			
	ν_c	ν_c	ν_c	ν_c	ν_c	ν_c	Input Signal Amplitude			
	5/64	17/64	29/64	5/64	17/64	29/64	0.8	0.5	0.1	0.01
8	33.2	46.6	32.9	41.9	46.5	47.8	21.7	12.8	6.7	9
16	46.2	67.3	48.8	61.8	67.2	65.9	33.3	18.7	10.3	9.4
32	64.1	88.4	64.1	90.9	88.3	94.3	45.6	24.9	14.8	10
64	86.1	109.5	80.5	116.2	109.2	122.5	56.6	29.7	19.7	10.9
128	108	130.3	102	135.8	129.6	137.7	70.5	35.7	22.9	12
256	129.3	151.3	124.3	158.4	151.9	156.7	81.2	42.3	24.9	12.8

Table 3.7 Peak SNRs, DRs and Δ SNR of the 2-2-2 MASH for different OSRs.

OSR	SNR Increase			DR Increase		
	ν_c	ν_c	ν_c	ν_c	ν_c	ν_c
	5/64	17/64	29/64	5/64	17/64	29/64
8 \rightarrow 16	8.4	11.0	8.9	19.9	20.7	18.1
16 \rightarrow 32	8.8	8.6	7.5	29.1	21.2	28.4
32 \rightarrow 64	11.0	11.0	13.2	25.3	20.9	28.2
64 \rightarrow 128	14.4	11.1	12.5	19.6	20.4	15.2
128 \rightarrow 256	11.8	11.2	11.9	22.6	22.3	19
Average SNR Increase	10.9	10.6	10.8	23.3	21.1	21.8

Table 3.8 Average increases in SNR and DR of the 2-2-2 MASH as a result of doubling OSRs for three different centre frequencies.

3.5.2 Double-Stage Sixth-Order 4-2 MASH Bandpass Σ - Δ Modulator

This structure is a cascade combination of a fourth-order modulator followed by a second-order modulator, thus yielding an overall sixth-order MASH bandpass Σ - Δ modulator. The first stage consists of two second-order variable centre frequency resonator sections and a multi-bit quantiser in the feedforward path. The second-stage contains a second-order resonator and a 1-bit quantiser in the feedforward path. The quantisation noise of the first-stage is fed into the input of the second-stage. The overall output is simply the summation of the first-stage $Y_1(z)$ and a double notch-filtered version of the second-stage $Y_4(z)$ as shown in Figure 3.9.

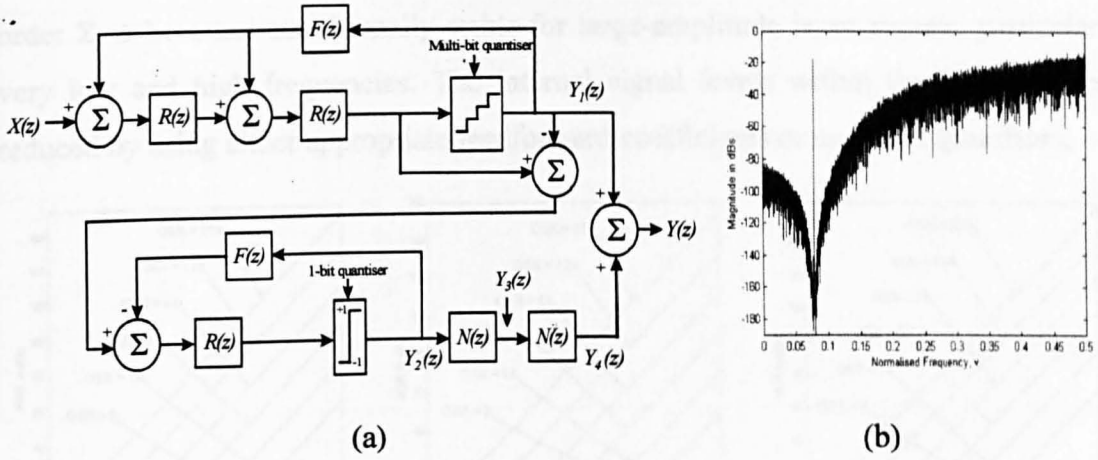


Figure 3.9 Sixth-Order Bandpass 4-2 MASH Σ - Δ Modulator: (a) Block Diagram, (b) Magnitude Spectrum at $\nu_C = 5/64$.

These signals are given by:

$$Y_1(z) = X(z) + (1 - \beta z^{-1} + z^{-2})^2 Q_1(z) \quad (3.25)$$

$$Y_4(z) = -(1 - \beta z^{-1} + z^{-2})^2 Q_1(z) + (1 - \beta z^{-1} + z^{-2})^3 Q_2(z) \quad (3.26)$$

The overall simplified output expression in the z-domain is given by

$$Y(z) = X(z) + (1 - \beta z^{-1} + z^{-2})^3 Q_2(z) \quad (3.27)$$

The multi-bit output combinations from this 4-2 MASH can be established by once again examining the modulator output in the time-domain. The output signal of the first stage has one of fifteen values of $0, \pm 1, \pm 2, \pm 3, \pm 4, \pm 5, \pm 6$ or ± 7 . The output signal of the second stage, which has values of ± 1 after the double notch filter yields one of the following samples $\pm (\beta^2 \pm 2m\beta \pm (m+2))$, where m is an integer having one of three values 0 or ± 2 . Output combinations from both stages are added to produce the final output signal having one of the following values, $\pm (\beta^2 \pm 2m\beta \pm r)$, where r is an integer within the range $0 \leq r \leq 11$. Note that the presence of the 15-level quantiser results in more cumulative multi-bit output combinations.

The main advantage of the 4-2 MASH is that the quantisation noise of the first-stage output produces 4th-order noise-shaping, which is much smaller in magnitude and less tonal. Consequently; the effects of component mismatches on the modulator resolution are less significant. The requirement for 2 instead of 3 notch filters has a twofold advantage in that it reduces the overall modulator complexity, as well as generating fewer multi-bit output combinations compared with the 2-2-2 MASH. The main drawback is that the 4th-

order $\Sigma\text{-}\Delta$ becomes conditionally stable for large-amplitude input signals, particularly for very low and high frequencies. The internal signal levels within the first-stage can be reduced by using either appropriate feedforward coefficients or multi-bit quantisers.

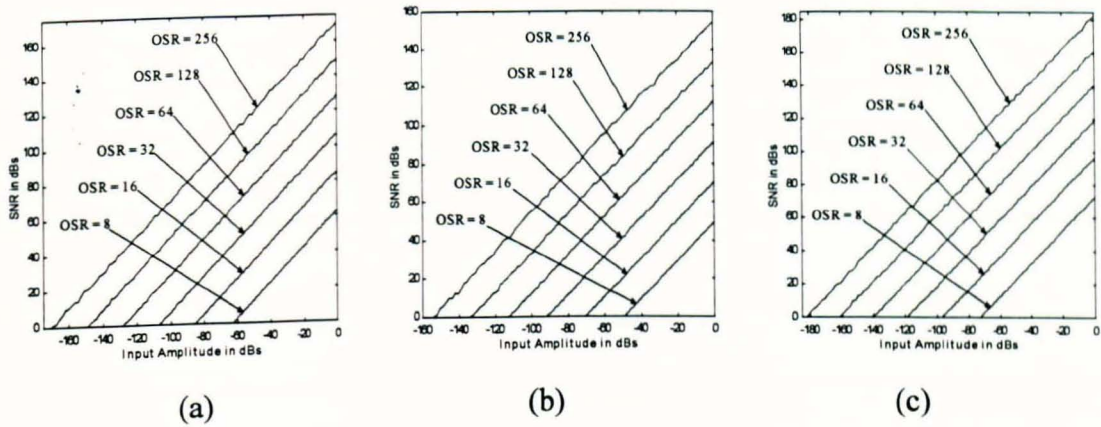


Figure 3.10 SNR Curves for Variable-Band 4-2 MASH Bandpass $\Sigma\text{-}\Delta$ Modulators at: (a) $\nu_C = 5/64$, (b) $\nu_C = 17/64$ and (c) $\nu_C = 29/64$.

In contrast to the magnitude spectra obtained for $\nu_C = 5/64$ and $\nu_C = 17/64$, the simulations for the variable-band modulator at $\nu_C = 29/64$ showed that its in-band region contained smaller-amplitude tones, thus accounting for the better SNR characteristics shown in Figure 3.10. Figure 3.11 shows that this modulator functions correctly for any noise-shaping band location. However, better SNR figures can be achieved for very low and very high frequencies.

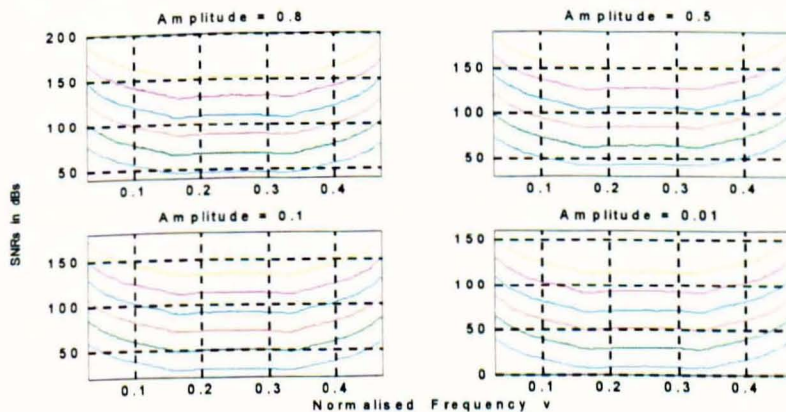


Figure 3.11 SNR curves versus Normalised Input Centre Frequency of a Sixth-Order 4-2 MASH $\Sigma\text{-}\Delta$ Modulator for OSRs of 8, 16, 32, 64, 128 and 256 for Input Amplitudes of 0.8, 0.5, 0.1 and 0.01.

OSR	Peak SNRs			Dynamic Ranges			ΔSNR			
	ν_c	ν_c	ν_c	ν_c	ν_c	ν_c	Input Signal Amplitude			
	5/64	17/64	29/64	5/64	17/64	29/64	0.8	0.5	0.1	0.01
8	62.8	49.3	72.9	62.4	48.9	72	32.6	32.6	32.7	32.7
16	85	70.2	96.8	84.5	69.7	96	37.4	37.6	37.5	37.6
32	106.5	91.2	119.2	106.9	91.2	118.7	39.4	39.8	39.7	40
64	128.7	112.4	140	128.2	112.7	140.6	40.9	40.7	40.5	40.8
128	148.6	133.3	161.3	148.7	132.9	159.7	41.4	40.5	40.9	40.4
256	170.4	154.5	182.8	170.9	153.5	181.3	41.3	41.9	42	40.7

Table 3.9 Peak SNRs, DRs and ΔSNR of the 4-2 MASH for different OSRs.

OSR	SNR Increase			DR Increase		
	ν_c	ν_c	ν_c	ν_c	ν_c	ν_c
	5/64	17/64	29/64	5/64	17/64	29/64
8 → 16	10	11	11.5	22.1	20.8	24
16 → 32	9	11.1	9.6	22.4	21.5	22.7
32 → 64	11.2	11	11.4	21.3	21.5	21.9
64 → 128	11.1	8.6	8.7	20.5	20.2	19.1
128 → 256	8.5	11.1	13.5	22.2	20.6	21.6
Average SNR Increase	10	10.5	10.9	21.7	20.9	21.9

Table 3.10 Average increases in SNR and DR of the 4-2 MASH as a result of doubling OSRs for three different centre frequencies.

3.5.3 Double-Stage Sixth-Order 2-4 MASH Bandpass Σ - Δ Modulator

This structure is a cascade combination of a second-order modulator followed by a fourth-order modulator resulting in an overall sixth-order MASH bandpass Σ - Δ modulator as shown in Figure 3.12. The first-stage consists of a second-order variable centre frequency resonator and a 1-bit quantiser in the feedforward path. The second stage contains two second-order resonators and a 15-level quantiser in the feedforward path. The quantisation noise of the first-stage is the input to the second-stage. The output of the modulator is the summation of the first stage $Y_1(z)$ and a single notched-filtered version of the second stage $Y_3(z)$ as shown below in Figure 3.12.

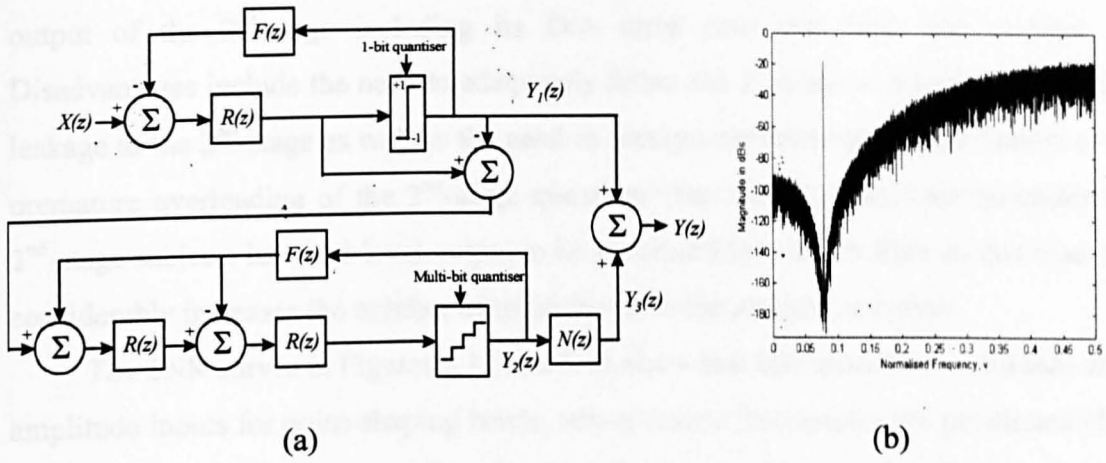


Figure 3.12 Sixth-Order Bandpass 2-4 MASH Σ - Δ Modulator: (a) Block Diagram, (b) Magnitude Spectrum at $\nu_C = 5/64$.

The corresponding output expressions for $Y_1(z)$ and $Y_3(z)$:

$$Y_1(z) = X(z) + (1 - \beta z^{-1} + z^{-2}) Q_1(z) \quad (3.28)$$

$$Y_3(z) = -(1 - \beta z^{-1} + z^{-2}) Q_1(z) + (1 - \beta z^{-1} + z^{-2})^3 Q_2(z) \quad (3.29)$$

The overall simplified output expression in the z-domain is given by

$$Y(z) = X(z) + (1 - \beta z^{-1} + z^{-2})^3 Q_2(z) \quad (3.30)$$

The multi-bit output combinations from this 2-4 MASH can be established by examining the modulator in the time-domain. The output signal of the first stage has one of two values ± 1 . The output of the second stage from the 15-level quantiser has one of fifteen values $0, \pm 1, \pm 2, \pm 3, \pm 4, \pm 5, \pm 6$ or ± 7 , which when going through a notch-filter yields one of the following amplitudes $\pm t\beta \pm (\pm t \pm 7)$, where t is an integer within the range $0 \leq t \leq 7$. Output combinations from both stages are added to produce the final output signal having one of the following values $\pm t\beta \pm (\pm t \pm 8)$, where t is an integer within the range $0 \leq t \leq 7$. Note that the presence of the 15-level quantiser followed by the a notch-filter results in a greater number of cumulative multi-bit output combinations compared with 4-2 MASH topology.

A 2-4 MASH requires a single notch filter and therefore produces fewer multi-levels in its output signal in comparison with 2-2-2 and 4-2 MASH modulators. The main advantage for a 2-4 MASH that employs a multi-bit quantiser in the 2nd-stage is that the effect of distortion due to the non-linearities of the multi-bit D/A are less detrimental to the overall modulator resolution, when compared with the 4-2 MASH. This is because the

output of the 2nd-stage including its D/A error does not feed into another stage. Disadvantages include the need to adequately dither the 1st-stage to alleviate spurious tone leakage to the 2nd-stage as well as the need to incorporate inter-stage scale factors to avoid premature overloading of the 2nd-stage quantiser. The use of a multi-bit quantiser in the 2nd-stage subjects its multi-level output to be processed by a notch filter in this case, which considerably increases the number of multi-levels in the modulator output.

The SNR curves in Figures 3.13 and 3.14 show that this modulator overloads at high-amplitude inputs for noise-shaping bands, whose centre frequencies are positioned close to either dc or Nyquist. This is attributed to the uneven-shoulder gain levels of the loop-filter at these frequencies. This problem can be resolved by increasing the number of levels in the 2nd-stage quantiser adequately to ensure smaller signal amplitudes in the modulator feedforward path.

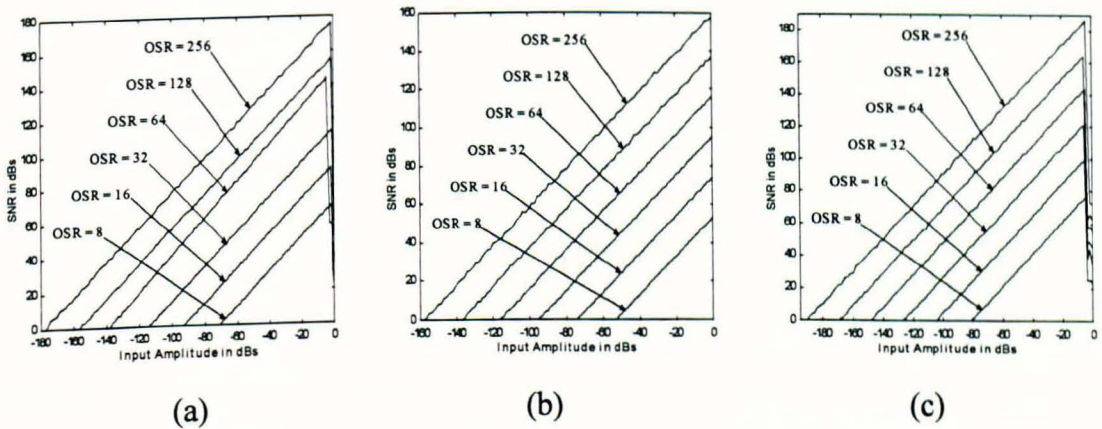


Figure 3.13 SNR Curves for Variable-Band 2-4 MASH Bandpass Σ - Δ Modulators at: (a) $v_C = 5/64$, (b) $v_C = 17/64$ and (c) $v_C = 29/64$.

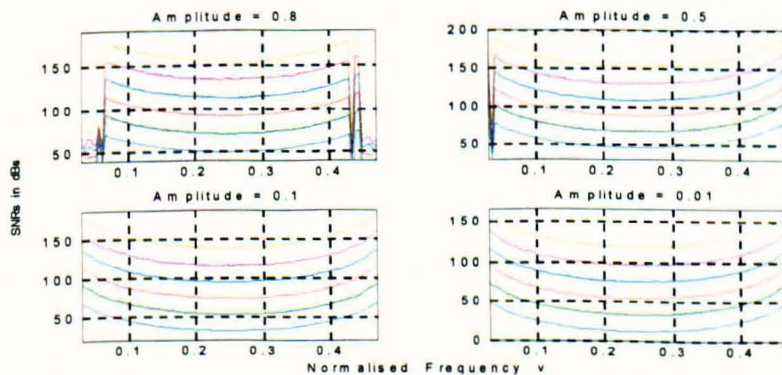


Figure 3.14 SNR curves versus Normalised Input Centre Frequency of a Sixth-Order 2-4 MASH Σ - Δ Modulator for OSRs of 8, 16, 32, 64, 128 and 256 for Input Amplitudes of 0.8, 0.5, 0.1 and 0.01.

OSR	Peak SNRs			Dynamic Ranges			Δ SNR			
	ν_C	ν_C	ν_C	ν_C	ν_C	ν_C	Input Signal Amplitude			
	5/64	17/64	29/64	5/64	17/64	29/64	0.8	0.5	0.1	0.01
8	68.8	52.8	76.9	70.5	52.8	80.7	51.4	53	36.3	36.3
16	90.9	73.8	100.5	91.9	73.5	104.4	64	69.7	40.6	40.2
32	113.1	95.2	121.1	113.9	95	126.8	78.8	87.1	42.3	41.9
64	143.4	116.2	143.4	137.7	115.2	147.2	95.1	104.6	43	42.9
128	155.2	137	164.1	155	135.8	167.9	113.1	120.9	43.9	43.5
256	175.9	158.1	186.4	177.5	156.8	189.1	120.5	133.4	43.9	43.5

Table 3.11 Peak SNRs, DRs and Δ SNR of 2-4 MASH for different OSRs.

OSR	SNR Increase			DR Increase		
	ν_C	ν_C	ν_C	ν_C	ν_C	ν_C
	5/64	17/64	29/64	5/64	17/64	29/64
8 \rightarrow 16	9.4	8.5	11.1	21.4	20.7	23.7
16 \rightarrow 32	11.7	11	8.9	22	21.5	22.4
32 \rightarrow 64	14.3	11.1	11.7	23.8	20.2	20.4
64 \rightarrow 128	5.2	11.1	10.7	17.3	20.6	20.7
128 \rightarrow 256	11	11.1	11.9	22.5	21	21.2
Average SNR Increase	10.3	10.5	10.9	21.4	20.8	21.7

Table 3.12 Average increases in SNR and DR of the 2-4 MASH as a result of doubling OSRs for three different centre frequencies.

3.6 Eighth-Order Bandpass MASH Σ - Δ Modulator

An eighth-order bandpass MASH Σ - Δ modulator can be built by having cascade combinations of 2-2-2-2 or 4-2-2 or 2-4-2 or 2-2-4 or 4-4 lower-order Σ - Δ modulator sections. The following five sub-sections provide a block diagram representation, the necessary analysis and the simulation results for each case.

3.6.1 Quadruple-Stage Eighth-Order 2-2-2-2 MASH Bandpass Σ - Δ Modulator

The modulator in Figure 3.15 (a) is a cascade combination of four second-order variable centre frequency resonator-based bandpass Σ - Δ modulators, where the quantisation error of the first-stage is fed to the input of the second-stage.

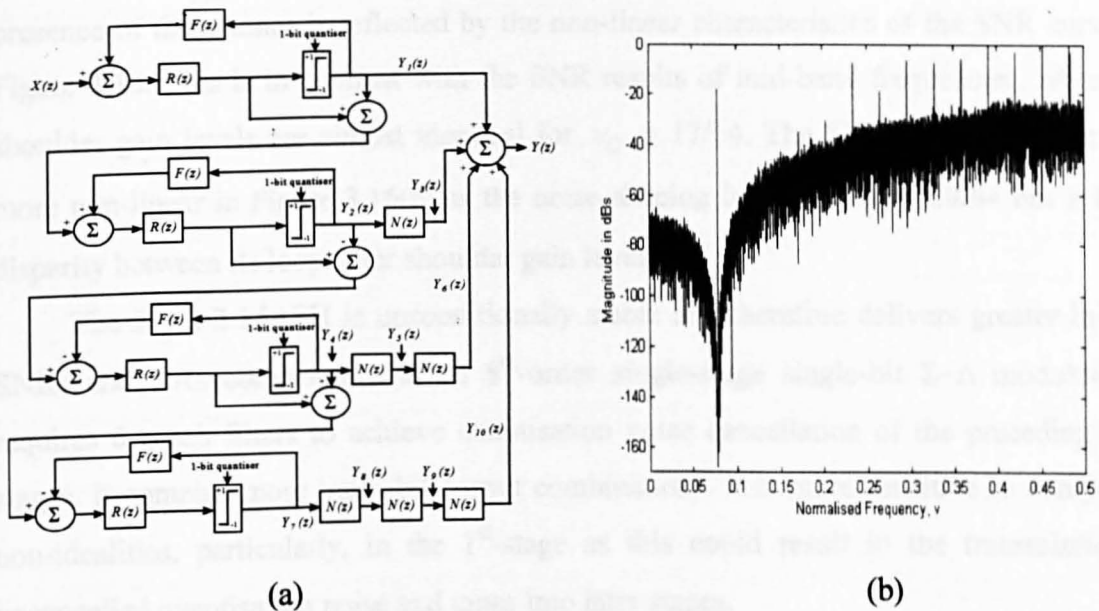


Figure 3.15 Eighth-Order Bandpass 2-2-2-2 MASH Σ - Δ Modulator: (a) Block Diagram, (b) Magnitude Spectrum at $\nu_C = 5/64$.

Similarly; the quantisation error of the second-stage is fed to the input of the third-stage and likewise for the fourth-stage. The output of the modulator is the sum of the first stage $Y_1(z)$, the second stage notch-filtered once $Y_3(z)$, the third stage doubly notch-filtered $Y_6(z)$ and the fourth stage notch-filtered thrice $Y_{10}(z)$. These output expressions corresponding to each stage are given by:

$$Y_1(z) = X(z) + (1 - \beta z^{-1} + z^{-2}) Q_1(z) \quad (3.31)$$

$$Y_3(z) = -(1 - \beta z^{-1} + z^{-2}) Q_1(z) + (1 - \beta z^{-1} + z^{-2})^2 Q_2(z) \quad (3.32)$$

$$Y_6(z) = -(1 - \beta z^{-1} + z^{-2})^2 Q_2(z) + (1 - \beta z^{-1} + z^{-2})^3 Q_3(z) \quad (3.33)$$

$$Y_{10}(z) = -(1 - \beta z^{-1} + z^{-2})^3 Q_3(z) + (1 - \beta z^{-1} + z^{-2})^4 Q_4(z) \quad (3.34)$$

The resultant final output expression $Y(z)$ is given by:

$$Y(z) = X(z) + (1 - \beta z^{-1} + z^{-2})^4 Q_4(z) \quad (3.35)$$

The magnitude spectrum in Figure 3.15(b) of this modulator output at $\nu_C = 5/64$ exhibits some spectral tones, especially at the higher frequencies. These tones, which are caused by overloading, become more persistent as the noise-shaping envelope rises as a result of the imbalance in the shoulder gain levels of the loop-filter as depicted in Figure 3.15 (b). Observation of the magnitude spectra for different input amplitudes showed that this modulator contained a significant number of tones including the in-band region. The

presence of these tones is reflected by the non-linear characteristics of the SNR curves in Figure 3.16. This is in contrast with the SNR results of mid-band frequencies, where the shoulder gain levels are almost identical for $\nu_C = 17/64$. The SNR curves become even more non-linear in Figure 3.16(c) as the noise-shaping band for $\nu_C = 29/64$ has a larger disparity between its loop-filter shoulder gain levels.

The 2-2-2-2 MASH is unconditionally stable and therefore delivers greater in-band SNRs and DRs compared with an 8th-order single-stage single-bit Σ - Δ modulator. It requires 6 notch filters to achieve quantisation noise cancellation of the preceding three stages. It contains more multi-bit output combinations. It is more sensitive to component non-idealities, particularly, in the 1st-stage as this could result in the transmission of uncancelled quantisation noise and tones into later stages.

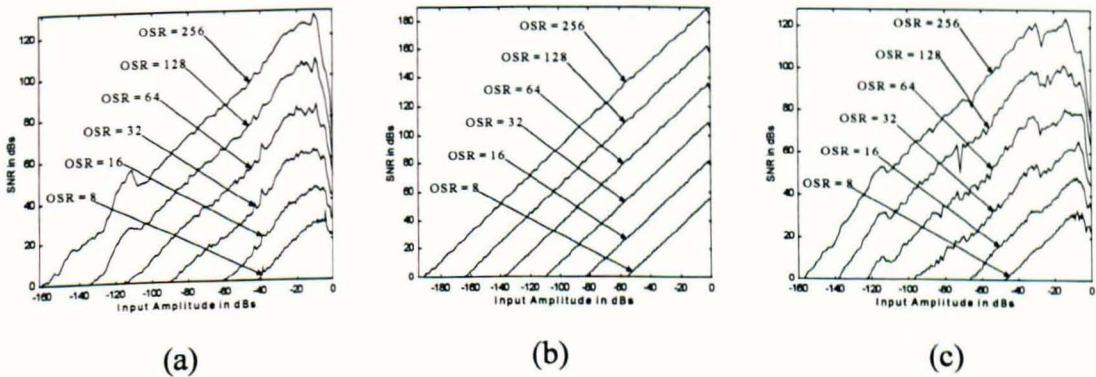


Figure 3.16 SNR Curves for Variable Centre Frequency 2-2-2-2 MASH Bandpass Σ - Δ Modulators at: (a) $\nu_C = 5/64$, (b) $\nu_C = 17/64$ and (c) $\nu_C = 29/64$.

The 2-2-2-2 MASH was evaluated for a whole range of frequencies for different input amplitudes, where the highest SNRs were attained for the mid-band frequencies as illustrated in Figure 3.17, Tables 3.13 and 3.14.

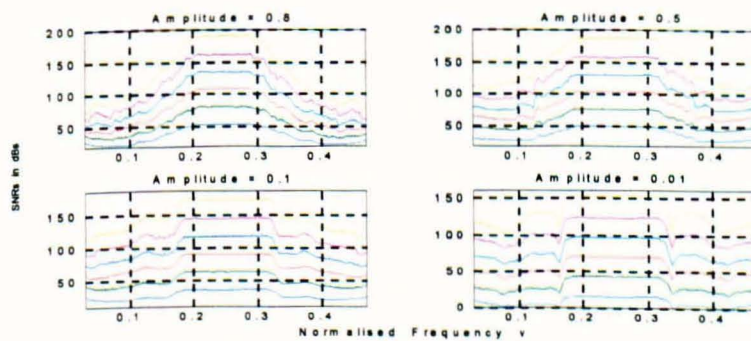


Figure 3.17 SNR curves versus Normalised Input Centre Frequency of a Eighth-Order 2-2-2-2 MASH Σ - Δ Modulator for OSRs of 8, 16, 32, 64, 128 and 256 for Input Amplitudes of 0.8, 0.5, 0.1 and 0.01.

OSR	Peak SNRs			Dynamic Ranges			Δ SNR			
	ν_c	ν_c	ν_c	ν_c	ν_c	ν_c	Input Signal Amplitude			
	5/64	17/64	29/64	5/64	17/64	29/64	0.8	0.5	0.1	0.01
8	33.2	55.5	32.8	41.9	55.8	47.8	31	22.2	16.1	15.1
16	46	82.2	48.8	60.6	82.4	65.9	48.8	34.1	25.6	24.7
32	64.4	108.7	65.6	90.2	109.2	96.7	66.9	46.3	36.4	31.8
64	86.1	136	80.5	114.9	137.2	122.5	83.9	56.9	47.1	37
128	108	162.6	102	134.3	163.1	137.7	104.8	69.5	56.4	43.4
256	129.9	188.7	124.3	160	189.9	156.7	120.7	81.6	64.1	49.7

Table 3.13 Peak SNRs, DRs and Δ SNR of 2-2-2-2 MASH for different OSRs.

OSR	SNR Increase			DR Increase		
	ν_c	ν_c	ν_c	ν_c	ν_c	ν_c
	5/64	17/64	29/64	5/64	17/64	29/64
8 \rightarrow 16	6.3	16.9	8.9	18.7	26.6	18.1
16 \rightarrow 32	8.3	12	5.6	29.6	26.8	30.8
32 \rightarrow 64	12.7	14.6	15.2	24.7	28	25.8
64 \rightarrow 128	14.6	12.2	12.5	19.4	25.9	15.2
128 \rightarrow 256	10.4	12	11.8	25.7	26.8	19
Average SNR Increase	10.5	13.5	10.8	23.6	26.8	21.8

Table 3.14 Average increases in SNR and DR of the 2-2-2-2 MASH as a result of doubling OSRs for three different centre frequencies.

3.6.2 Triple-Stage Eighth-Order 4-2-2 MASH Bandpass Σ - Δ Modulator

This structure is a cascade combination of a fourth-order modulator followed by two further second-order bandpass modulators as shown below in Figure 3.18. The absence of tones in the magnitude spectrum in Figure 3.18(b) is attributed to the use of a multi-level quantiser in the 1st-stage of this 4-2-2 MASH Σ - Δ modulator. This multi-level quantiser also produces sufficiently low-amplitude signals in the modulator, which do not overload the quantiser. This explains why the SNR characteristics in Figure 3.19 appear to be quite linear for all the examined centre frequencies. The multi-bit quantiser also ensures that this modulator functions correctly for all the considered noise-shaping bands for $0.03125 \leq \nu_c \leq 0.46875$.

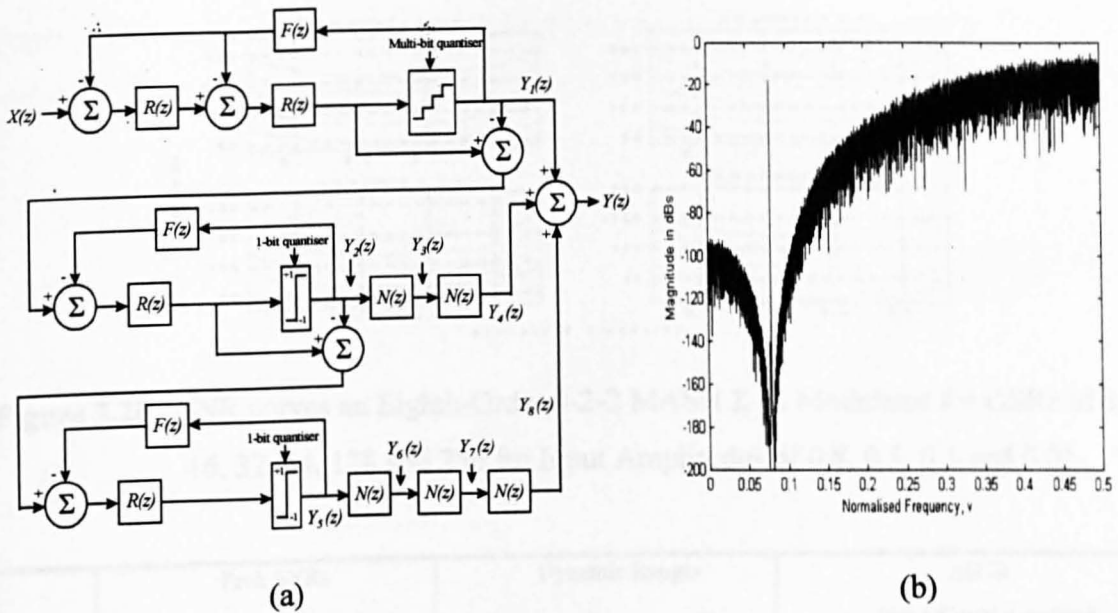


Figure 3.18 Eighth-Order Bandpass 4-2-2 MASH Σ - Δ Modulator: (a) Block Diagram, (b) Magnitude Spectrum at $\nu_C = 5/64$.

Simulations showed that the magnitude spectrum for the mid-band frequencies contained stronger-amplitude in-band tones in comparison with the very low and high frequencies, thus accounting for the better SNR results shown in Figure 3.20, Tables 3.15 and 3.16. The 4-2-2 MASH has greater tolerance to non-idealities in the 1st-stage, requires 5 instead of 6 notch filters and produces fewer multi-bit output combinations (if only 1-bit quantisers are employed in the 1st-stage) compared with the 2-2-2-2 MASH. However, the increased internal signal levels of the 1st-stage overload the quantiser prematurely, thus limiting its DR compared with the 2-2-2-2 MASH.

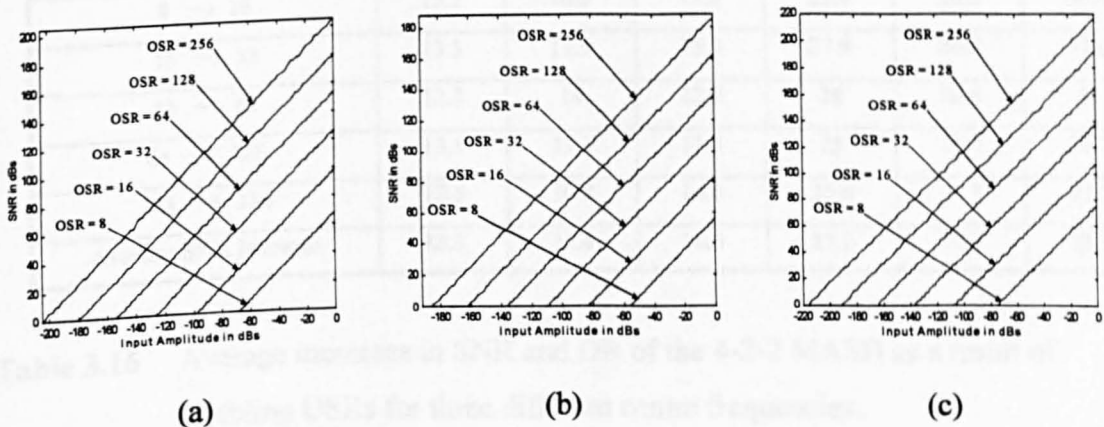


Figure 3.19 SNR Curves for Variable-Band 4-2-2 MASH Bandpass Σ - Δ Modulators at: (a) $\nu_C = 5/64$, (b) $\nu_C = 17/64$ and (c) $\nu_C = 29/64$.

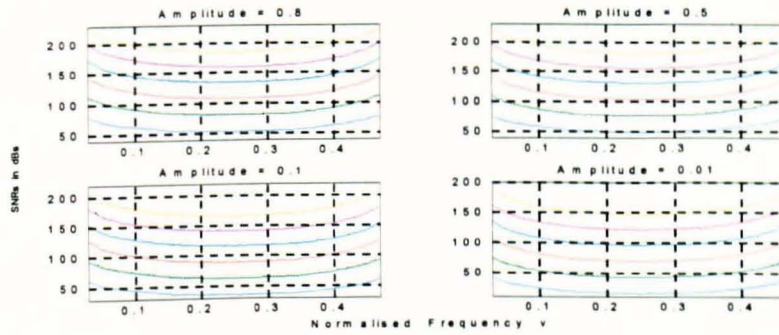


Figure 3.20 SNR curves an Eighth-Order 4-2-2 MASH Σ - Δ Modulator for OSRs of 8, 16, 32, 64, 128 and 256 for Input Amplitudes of 0.8, 0.5, 0.1 and 0.01.

OSR	Peak SNRs			Dynamic Ranges			Δ SNR			
	ν_c	ν_c	ν_c	ν_c	ν_c	ν_c	Input Signal Amplitude			
	5/64	17/64	29/64	5/64	17/64	29/64	0.8	0.5	0.1	0.01
8	68.2	56.1	75.3	68.2	55.8	75.2	25.7	25.9	25.7	25.9
16	98.5	83	107.4	97.6	82.4	105.6	32.6	33.1	31.5	33.2
32	126.9	110.2	138.2	125.5	109.2	137.2	37.2	38.3	36.9	38.2
64	153.9	137	165.5	153.5	135.8	163.2	39.9	40.5	39.6	40.7
128	179.5	162.4	192.6	178.5	161.7	189.9	41.6	41.9	41	41.3
256	204.9	185.9	216.8	204.1	184.2	215.6	42.5	42.9	42.2	44

Table 3.15 Peak SNRs, DRs and Δ SNR of 4-2-2 MASH for different OSRs.

OSR	SNR Increase			DR Increase		
	ν_c	ν_c	ν_c	ν_c	ν_c	ν_c
	5/64	17/64	29/64	5/64	17/64	29/64
8 \rightarrow 16	15.2	16.9	17.2	29.4	26.6	30.4
16 \rightarrow 32	13.3	11.9	15.1	27.9	26.8	31.6
32 \rightarrow 64	12.2	14	12.9	28	26.6	26
64 \rightarrow 128	13.5	13.4	11.4	25	25.9	26.7
128 \rightarrow 256	12.5	10.8	14.8	25.6	22.5	25.7
Average SNR Increase	13.3	13.4	14.3	27.2	25.7	28.1

Table 3.16 Average increases in SNR and DR of the 4-2-2 MASH as a result of doubling OSRs for three different centre frequencies.

3.6.3 Triple-Stage Eighth-Order 2-4-2 MASH Bandpass Σ - Δ Modulator

This structure is a cascade combination of a second-order, a fourth-order and second-order bandpass Σ - Δ modulators respectively as shown below in Figure 3.21 The overall

output of the modulator is the sum of the first stage, the second stage notch filtered twice and the third stage notch filtered three times.

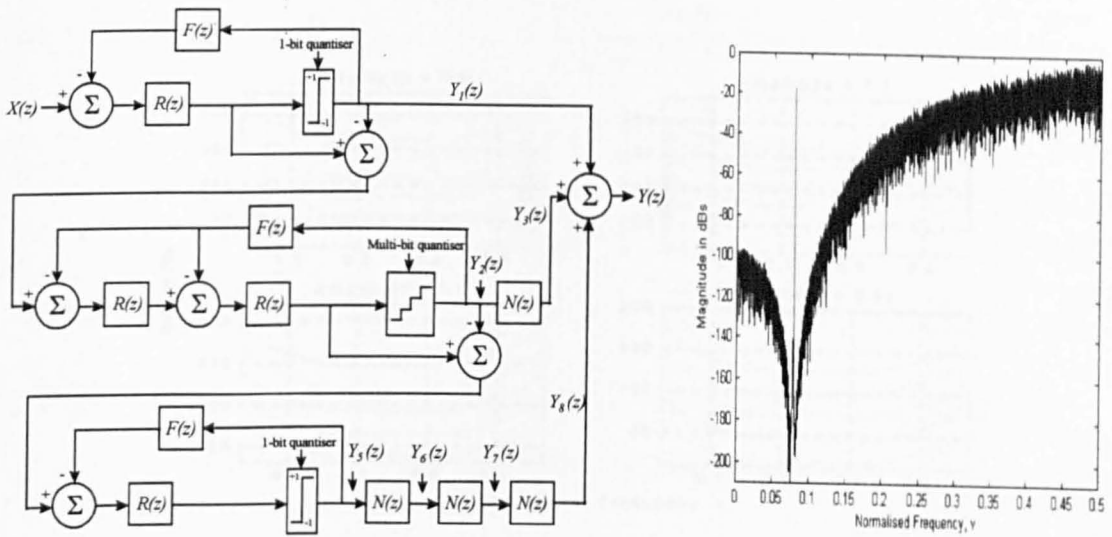


Figure 3.21 Eighth-Order Bandpass 2-4-2 MASH Σ - Δ Modulator: (a) Block Diagram, (b) Magnitude Spectrum at $\nu_C = 5/64$.

The magnitude spectrum in Figure 3.21 corresponding to this modulator is shown to be relatively tone-free. One again, the absence of tones is attributed to the use of multi-bit quantiser in the middle-stage. The SNR characteristics in Figure 3.22 are quite linear. However, this modulator is seen to become unstable for extremely large input-amplitudes for frequencies very close to dc and Nyquist.

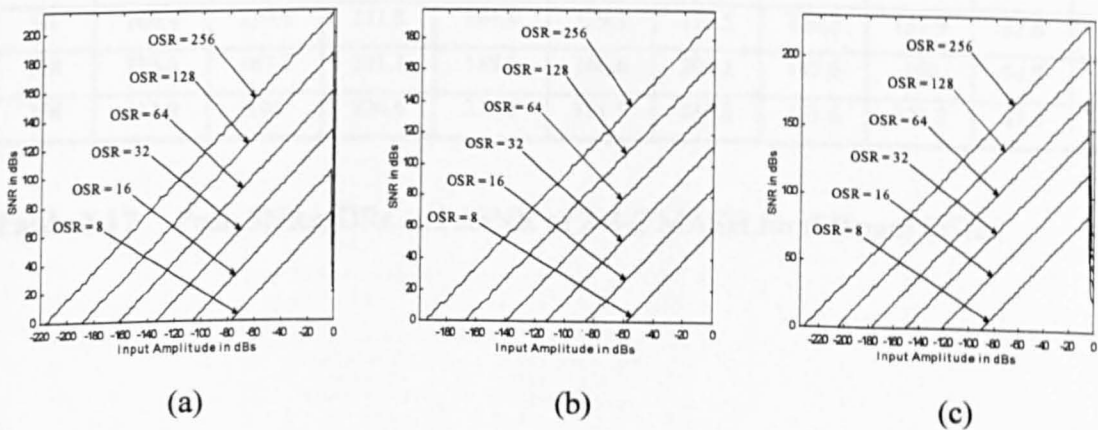


Figure 3.22 SNR Curves for Variable-Band 4-2-2 MASH Bandpass Σ - Δ Modulators at: (a) $\nu_C = 5/64$, (b) $\nu_C = 17/64$ and (c) $\nu_C = 29/64$.

Figure 3.23 verifies the onset of instability when the modulator is subjected to large input-amplitude levels. Tables 3.17 and 3.18 show that better in-band SNRs and DRs are accomplished for very low and very high frequencies.

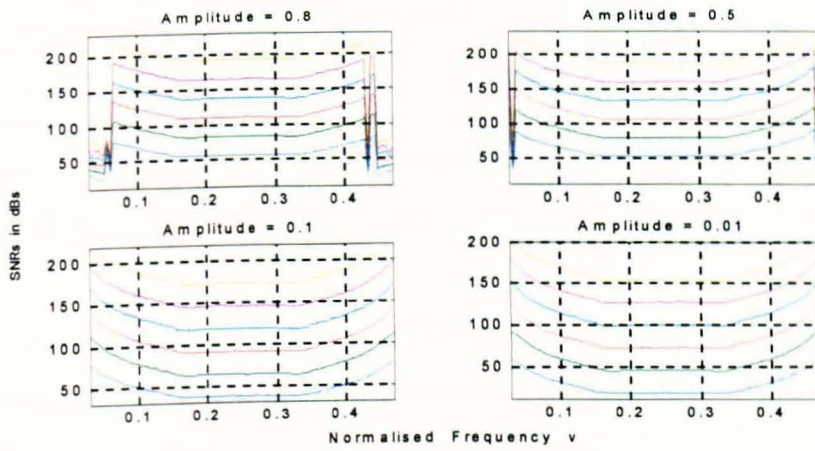


Figure 3.23 SNR curves versus Normalised Input Centre Frequency of a eighth-Order 2-4-2 MASH Σ - Δ Modulator for OSRs of 8, 16, 32, 64, 128 and 256 for Input Amplitudes of 0.8, 0.5, 0.1 and 0.01.

OSR	Peak SNRs			Dynamic Ranges			Δ SNR			
	ν_c	ν_c	ν_c	ν_c	ν_c	ν_c	Input Signal Amplitude			
	5/64	17/64	29/64	5/64	17/64	29/64	0.8	0.5	0.1	0.01
8	75.5	58.5	86.6	77.3	58.4	90.2	59.2	64.3	42.8	42.5
16	104.2	85.8	117.8	105.7	85.5	121.2	79.5	89.2	49	49
32	132.9	112.6	145.9	134.3	111.5	150.3	100.7	114.1	52	52.3
64	160.4	139.5	171.8	161.4	139.1	177.5	124.2	137.9	53.6	53.4
128	186.6	167.2	201.1	189.1	166.6	204.1	147.6	160	54.2	53.4
256	213.9	194	226.6	215.6	191.9	230.3	161.6	171.2	47.4	47

Table 3.17 Peak SNRs, DRs and Δ SNR of 2-4-2 MASH for different OSRs.

OSR	SNR Increase			DR Increase		
	ν_c	ν_c	ν_c	ν_c	ν_c	ν_c
	5/64	17/64	29/64	5/64	17/64	29/64
8 → 16	14	14.4	16.3	28.4	27.1	31
16 → 32	15.9	14.6	13.2	28.6	26	29.1
32 → 64	12.1	12.1	12.1	27.1	27.6	27.2
64 → 128	14.4	14.7	13	27.7	27.5	26.6
128 → 256	14.3	11.9	15.7	26.5	25.3	26.2
Average SNR Increase	14.1	13.5	14.1	27.7	26.7	28

Table 3.18 Average increases in SNR and DR of the 2-4-2 MASH as a result of doubling OSRs for three different centre frequencies.

3.6.4 Triple-Stage Eighth-Order 2-2-4 MASH Bandpass Σ - Δ Modulator

This structure is a cascade combination of a second-order, a second-order and fourth-order bandpass Σ - Δ modulators respectively as shown below in Figure 3.24. Its output magnitude spectrum exhibited several distinct out-of-band tones as shown in Figure 3.25(a). These occurred, because the third-stage contained a 4th-order Σ - Δ modulator, whose quantiser became overloaded. The relatively linear SNR plots in Figure 3.25(b) are attributed to the fact that for the majority of the modulator input amplitudes, the tones occurred outside the signal region.

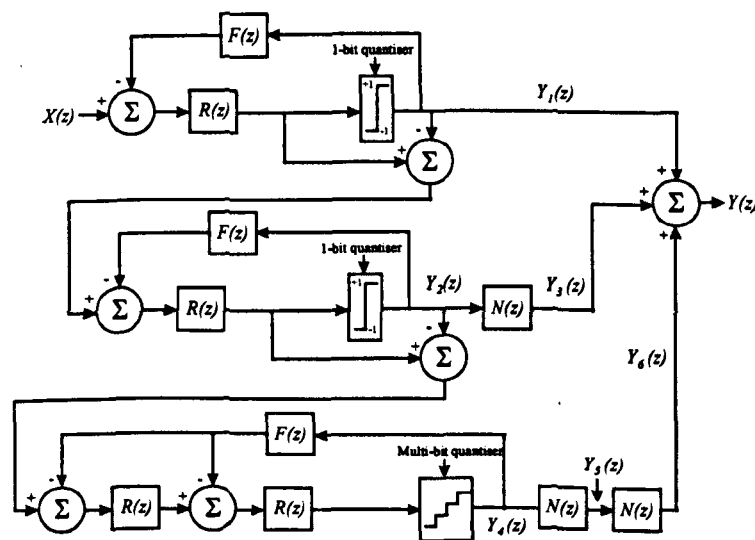


Figure 3.24 Eighth-Order Bandpass 2-2-4 MASH Σ - Δ Modulator: (a) Block Diagram.

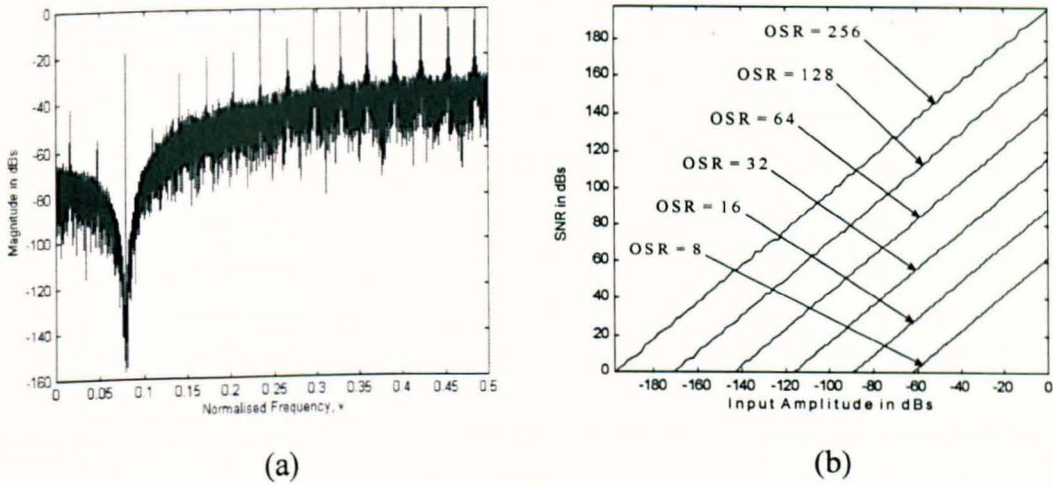


Figure 3.25 Variable-Band 4-2-2 MASH Bandpass $\Sigma\text{-}\Delta$ Modulators at $\nu_C = 5/64$:
 (a) Magnitude Spectrum, (b) SNR Curves.

The simulation results in the form of SNRs and DRs are shown in Figure 3.26, Table 3.19 and Table 3.20 for a combination of centre frequencies and OSRs.

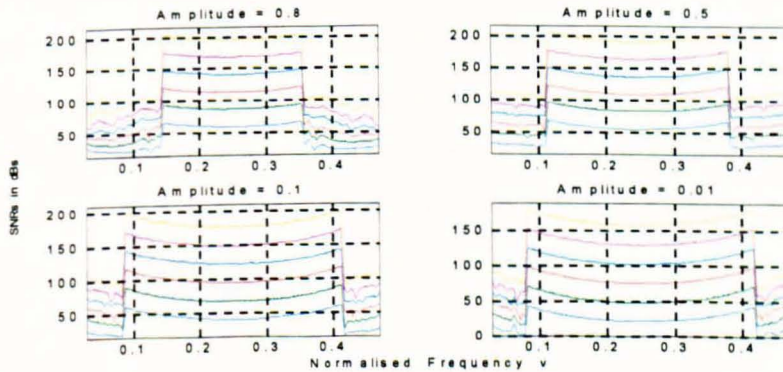


Figure 3.26 SNR curves versus Normalised Input Centre Frequency of a eighth-Order 2-2-4 MASH $\Sigma\text{-}\Delta$ Modulator for OSRs of 8, 16, 32, 64, 128 and 256 for Input Amplitudes of 0.8, 0.5, 0.1 and 0.01.

OSR	Peak SNRs			Dynamic Ranges	Δ SNR			
	ν_C	ν_C	ν_C		Input Signal Amplitude			
	5/64	17/64	29/64	17/64	0.8	0.5	0.1	0.01
8	65.6	62	32.2	61.5	47	46.3	44	41.5
16	89.7	88.9	50.5	88.3	62.4	56.2	62.9	56.5
32	122.2	116.5	66.5	116.4	80.6	70.9	74.1	75.6
64	146	143.4	99.3	142.4	97.2	76.8	82.6	83.2
128	172.5	170.6	144.5	169.1	117.9	94	101.8	103.7
256	175.8	197	128.3	196	134.8	110	113.8	112.6

Table 3.19 Peak SNRs, DRs and Δ SNR of 2-2-4 MASH for different OSRs.

OSR	SNR Increase $v_C = 17/64$	DR $v_C = 17/64$
8 → 16	14.4	26.8
16 → 32	14.6	28.1
32 → 64	12	26
64 → 128	12.1	26.7
128 → 256	17	26.9
Average SNR Increase	14	26.9

Table 3.20 Average increases in SNR and DR of the 2-2-4 MASH as a result of doubling OSRs for three different centre frequencies.

3.6.5 Double-Stage Eighth-Order 4-4 MASH Bandpass Σ - Δ Modulator

This is a cascade combination of two fourth-order modulators yielding an overall eighth-order MASH bandpass Σ - Δ modulator as illustrated in Figure 3.27(a), whose output magnitude spectrum is shown in Figure 3.27(b). The first stage consists of two second-order resonator sections and a one bit quantiser in the feedforward path. The quantisation noise of the first stage is fed to the input of the second stage. The output is the sum of the first stage and the double notch-filtered version of the second stage. The first stage has output values of ± 1 . The second stage which incorporates a double notch filter produces output values of $0, \pm 2$ and ± 4 . Output combinations from both stages are added to produce the final output signal having one of the following values $\pm 1, \pm 3$ and ± 5 . The reduced usage of notch filters results in fewer multi-bit output combinations.

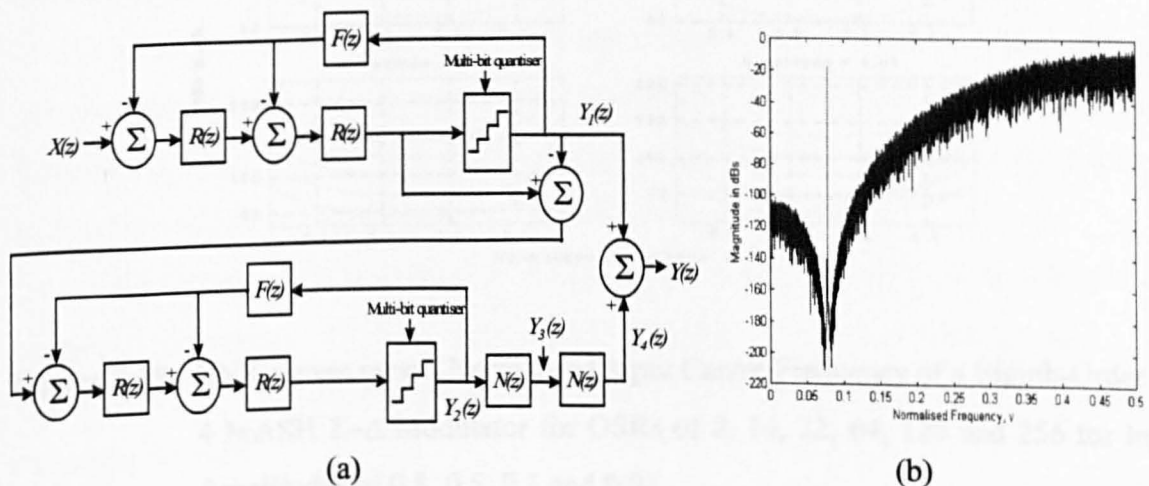


Figure 3.27 Eighth-Order Bandpass 4-4 MASH Σ - Δ Modulator: (a) Block Diagram, (b) Magnitude Spectrum at $v_C = 5/64$.

The 4-4 MASH modulator only requires two notch filters and as a result generates the lowest number of multi-levels in its output signal, when compared with the 2-2-2-2, 4-2-2, 2-4-2 and 2-2-4 MASH modulators. It has greater insensitivity to component non-idealities and is less tonal, because the quantisation noise in both stages is processed by 4th-order noise-shaping. However, it exhibits comparatively lower in-band SNRs and DRs due to the quantiser overloading in both stages for high-amplitude input signals. The SNR curves for different combinations of centre frequencies are illustrated in Figure 3.28 and Figure 3.29. More simulation results are summarised in Tables 3.21 and 3.22.

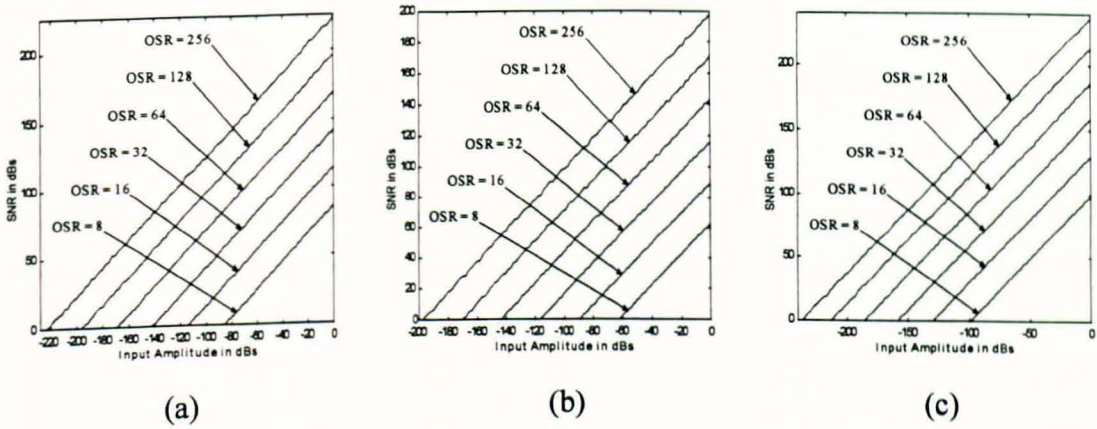


Figure 3.28 SNR Curves for Variable-Band 4-4 MASH Bandpass Σ - Δ Modulators at: (a) $\nu_C = 5/64$, (b) $\nu_C = 17/64$ and (c) $\nu_C = 29/64$.

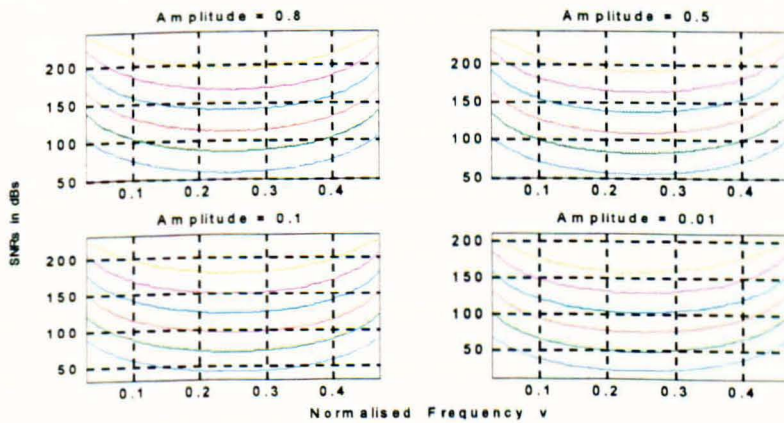


Figure 3.29 SNR curves versus Normalised Input Centre Frequency of a Eighth-Order 4-4 MASH Σ - Δ Modulator for OSRs of 8, 16, 32, 64, 128 and 256 for Input Amplitudes of 0.8, 0.5, 0.1 and 0.01.

OSR	Peak SNRs			Dynamic Ranges			Δ SNR			
	ν_c	ν_c	ν_c	ν_c	ν_c	ν_c	Input Signal Amplitude			
	5/64	17/64	29/64	5/64	17/64	29/64	0.8	0.5	0.1	0.01
8	85.5	62.3	98.9	85.4	61.5	98.6	46.9	47.3	46.7	47.1
16	114.2	89.1	129.8	114	88.3	129.5	53	52.7	52.8	53
32	141.7	116	158.8	140.9	115.2	156.7	55.4	56.1	55.9	55.5
64	168.9	143.2	185.9	167.9	142.4	186.2	56.5	57	56.9	56.6
128	196.1	171.3	212.5	196	169.1	212.9	57.3	57.5	56.9	57.5
256	223.5	198	236.8	222.7	196	235.2	44.6	45.2	45.4	46.1

Table 3.21 Peak SNRs, DRs and Δ SNR of 4-4 MASH for different OSRs.

OSR	SNR Increase			DR Increase		
	5/64	17/64	29/64	5/64	17/64	29/64
8 \rightarrow 16	16.3	14.3	15.8	28.6	26.8	30.9
16 \rightarrow 32	12.6	14.6	13.6	26.9	26.9	27.2
32 \rightarrow 64	14.7	12	15	27	27.2	29.5
64 \rightarrow 128	14.6	12.2	14.7	28.1	26.7	26.7
128 \rightarrow 256	14.3	17.1	11.1	26.7	26.9	22.3
Average SNR Increase	14.5	14.1	14	27.5	26.9	27.3

Table 3.22 Average increases in SNR and DR ranges of the 4-4 MASH as a result of doubling OSRs for three different centre frequencies.

3.7 Complex Second-Order Bandpass MASH Σ - Δ Modulators

The purpose of this section is to present complex MASH variable centre frequency resonator-based bandpass Σ - Δ modulators. The summarised literature survey carried out in Section 3.2 shows that no work has been reported on complex MASH structures with the sole exception of a 1-1 MASH Σ - Δ modulator topology in [Dia96].

The complex 1-1 MASH Σ - Δ modulator shown in Figure 3.30(a) consists of a cascade combination of two independent complex first-order resonator-based Σ - Δ modulators that can accomplish second-order single-band noise-shaping at any centre frequency location.

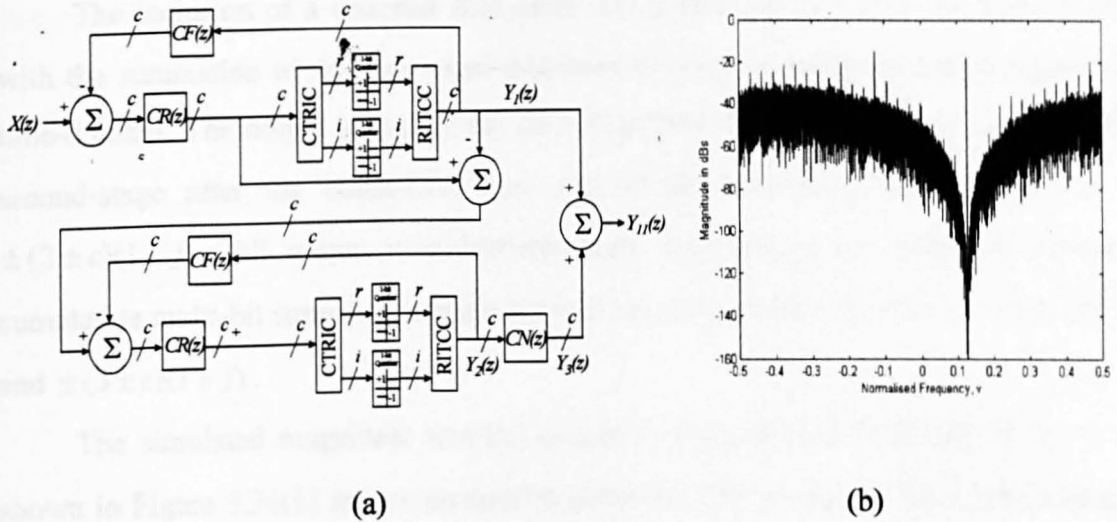


Figure 3.30 Complex Second-Order Bandpass 1-1 MASH Σ - Δ Modulator: (a) Block Diagram, (b) Magnitude Spectrum at $\nu_C = 5/64$.

Each stage comprises a single-pole resonator and two quantisers in the feedforward path as well as a complex delay in the feedback path to achieve effective noise-shaping. The complex quantisation noise of the first-stage is fed to the input of the second-stage. The output of the second-stage is digitally processed by a first-order notch-filter resulting in the cancellation of the quantisation of the first-stage and therefore allowing the second-stage quantisation noise to be noise-shaped by the equivalence of a second-order notch-filter. The resultant outputs of the first $Y_1(z)$ and second $Y_2(z)$ stages are:

$$Y_1(z) = X(z) + (1 - cz^{-1})[Q_{R1}(z) + Q_{I1}(z)] \quad (3.36)$$

$$Y_2(z) = \left[-(Q_1(z)) + (1 - cz^{-1})(Q_{R2}(z) + Q_{I2}(z)) \right] N(z) \quad (3.37)$$

The associated quantisation and dither signal of the first-stage can be fully cancelled if the digital notch-filter is $N(z) = (1 - cz^{-1})$ resulting in a final expression for $Y_{11}(z)$ given by:

$$Y_{11}(z) = Y_1(z) + N(z)Y_2(z) = X(z) + (1 - cz^{-1})^2 [Q_{R2}(z) + Q_{I2}(z)] \quad (3.38)$$

where $c = e^{j\alpha}$, $X(z)$ is the input signal, $Q_{R1}(z)$, $Q_{I1}(z)$, $Q_{R2}(z)$ and $Q_{I2}(z)$ represent the quantisation noise of the first-real, first-imaginary, second-real and second-imaginary quantisers respectively.

The inclusion of a complex first-order notch-filter at the output of $Y_2(z)$ together with the summation of the two stages produces a complex multi-bit output signal in the time-domain. The output signal of the first-stage has values of $\pm(1+j)$ and that of the second-stage after the notch-filter has one of the following values $\pm c(1+j)$ and $\pm(2\pm c)(1+j)$. All output combinations from both stages are added to produce a cumulative multi-bit stream of samples having one of the following values, $\pm(1\pm c)(1+j)$ and $\pm(3\pm c)(1+j)$.

The simulated magnitude spectral output of a complex 2-2 MASH at $\nu_C = 5/64$ shown in Figure 3.30(b) shows asymmetry about dc. The in-band SNRs were determined for three separate examples: a low-frequency ($\nu_C = 5/64$), a medium-frequency ($\nu_C = 17/64$) and a high-frequency ($\nu_C = 29/64$). These in-band SNR curves are illustrated in Figure 3.31 (a), (b) and (c) for different six OSRs.

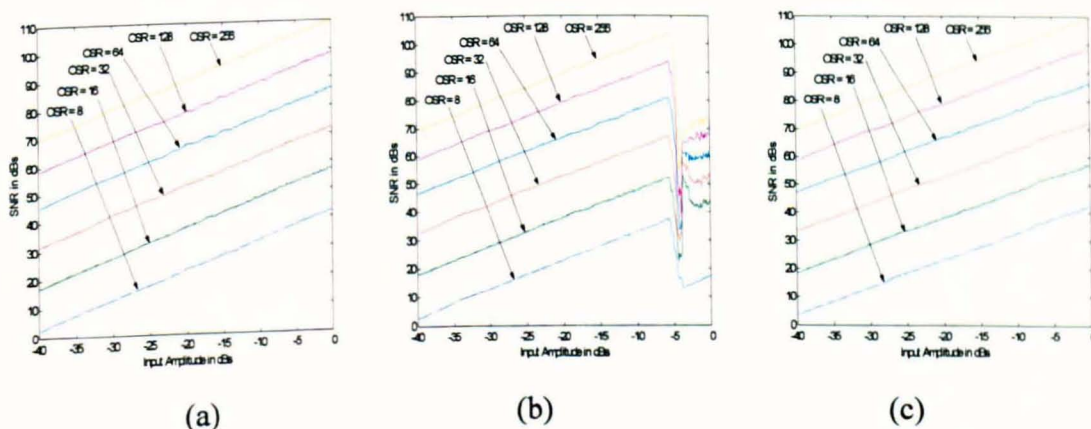


Figure 3.31 SNR Curves for Complex Variable-Band 1-1 MASH Bandpass $\Sigma-\Delta$ Modulators at: (a) $\nu_C = 5/64$, (b) $\nu_C = 17/64$ and (c) $\nu_C = 29/64$.

3.8 Complex Third-Order Bandpass MASH $\Sigma-\Delta$ Modulators

A third-order bandpass MASH $\Sigma-\Delta$ modulator can be constructed by having cascaded combinations of 1-1-1 or 2-1 or 1-2 lower-order complex $\Sigma-\Delta$ modulators. The 1-1-1 and 2-1 will be considered in the following two sub-sections.

3.8.1 Complex Third-Order 1-1-1 Bandpass MASH $\Sigma-\Delta$ Modulators

This topology contains three independent complex first-order variable centre frequency resonator-based $\Sigma-\Delta$ modulators in cascade, where the complex quantisation noise of the first-stage is fed to the input of the second-stage. Likewise; the complex quantisation error of the second-stage is fed to the input of the third-stage. The modulator

output is the summation of the first stage $Y_1(z)$, a single complex notch-filtered output from the second-stage $Y_3(z)$ and a double complex notch-filtered output from the third stage $Y_6(z)$ as shown in Figure 3.32 (a). Its corresponding output magnitude spectrum at $\nu_C = 5/64$ is shown in Figure 3.32(b)

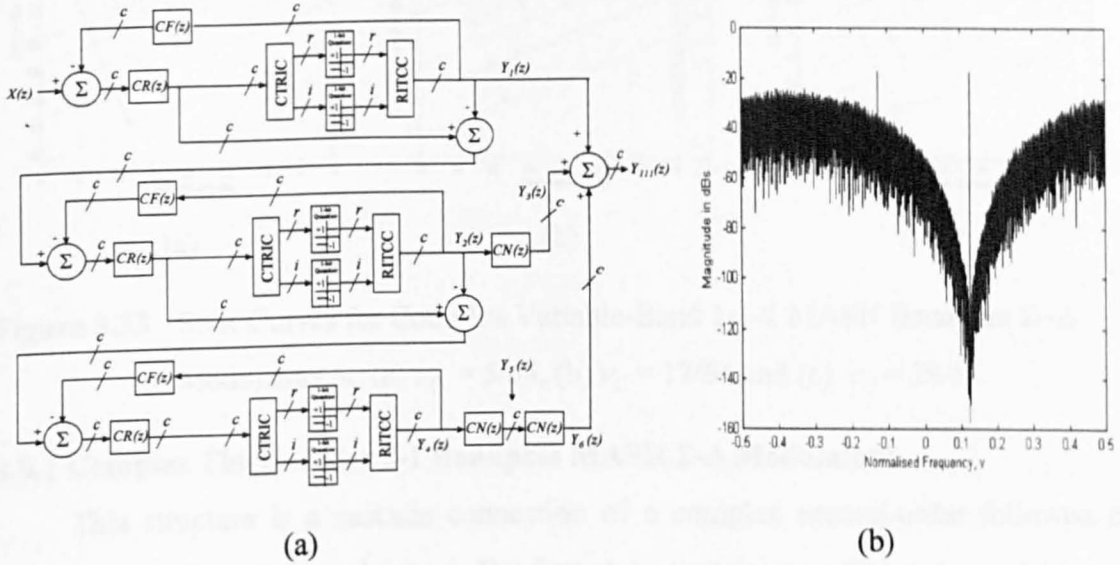


Figure 3.32 Complex Third-Order Bandpass 1-1-1 MASH Σ - Δ Modulator: (a) Block Diagram, (b) Magnitude Spectrum at $\nu_C = 5/64$

These output expressions in the z -domain are given by:

$$Y_1(z) = X(z) + (1 - c z^{-1})[Q_{R1}(z) + Q_{I1}(z)] \quad (3.39)$$

$$Y_3(z) = -(1 - c z^{-1}) [Q_{R1}(z) + Q_{I1}(z)] + (1 - \beta z^{-1} + z^{-2})^2 [Q_{R2}(z) + Q_{I2}(z)] \quad (3.40)$$

$$Y_6(z) = -(1 - c z^{-1})^2 [Q_{R2}(z) + Q_{I2}(z)] + (1 - c z^{-1})^3 [Q_{R3}(z) + Q_{I3}(z)] \quad (3.41)$$

Therefore, the overall output expression becomes $Y(z)$

$$Y_{111}(z) = X(z) + (1 - c z^{-1})^3 [Q_{R3}(z) + Q_{I3}(z)] \quad (3.42)$$

where the quantisation noise of the intermediate stages $Q_{R1}(z)$, $Q_{I1}(z)$, $Q_{R2}(z)$ and $Q_{I2}(z)$ are cancelled out.

The multi-bit output combinations from the 1-1-1 MASH can be determined by examining the modulator amplitude samples in the time-domain. The output signal of the first stage has values of $\pm(1 + j)$ and that of the second-stage after the one notch-filter has one of six amplitudes $\pm c(1 + j)$ and $\pm(2 \pm c)(1 + j)$. Similarly; a double notch-filter yields a signal

having values of $\pm(1+j)(1-e^{j\alpha})^2$. The SNR curves of this modulator for different combinations of centre frequencies and OSRs are presented in Figure 3.33.

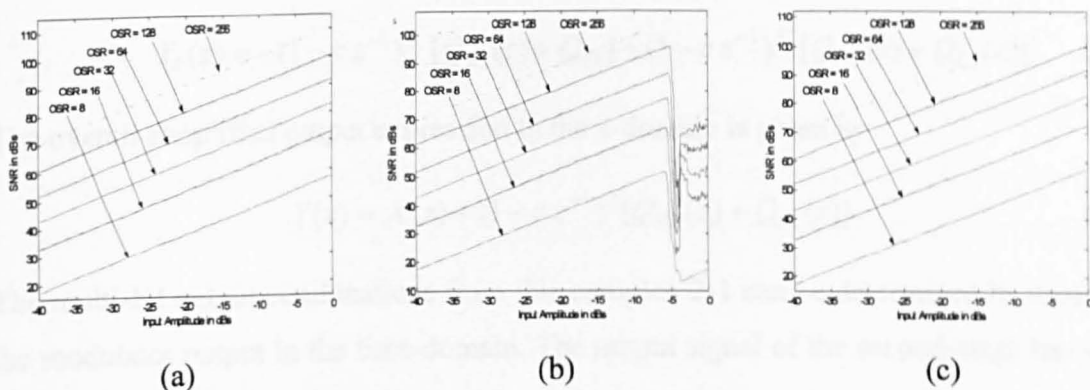


Figure 3.33 SNR Curves for Complex Variable-Band 1-1-1 MASH Bandpass Σ - Δ Modulators at: (a) $\nu_C = 5/64$, (b) $\nu_C = 17/64$ and (c) $\nu_C = 29/64$.

3.8.2 Complex Third-Order 2-1 Bandpass MASH Σ - Δ Modulators

This structure is a cascade connection of a complex second-order followed by a complex first-order Σ - Δ modulators. The first-stage contains two first-order variable centre frequency complex resonator-based sections together with two quantisers for the real and imaginary channels respectively. The complex quantisation noise of the first-stage is fed into the input of the second-stage. The overall complex output signal is simply the summation of the first-stage $Y_1(z)$ and a double complex notch-filtered version of the second-stage $Y_2(z)$ as shown in Figure 3.34(a). Its magnitude spectrum is shown in Figure 3.34 (b).

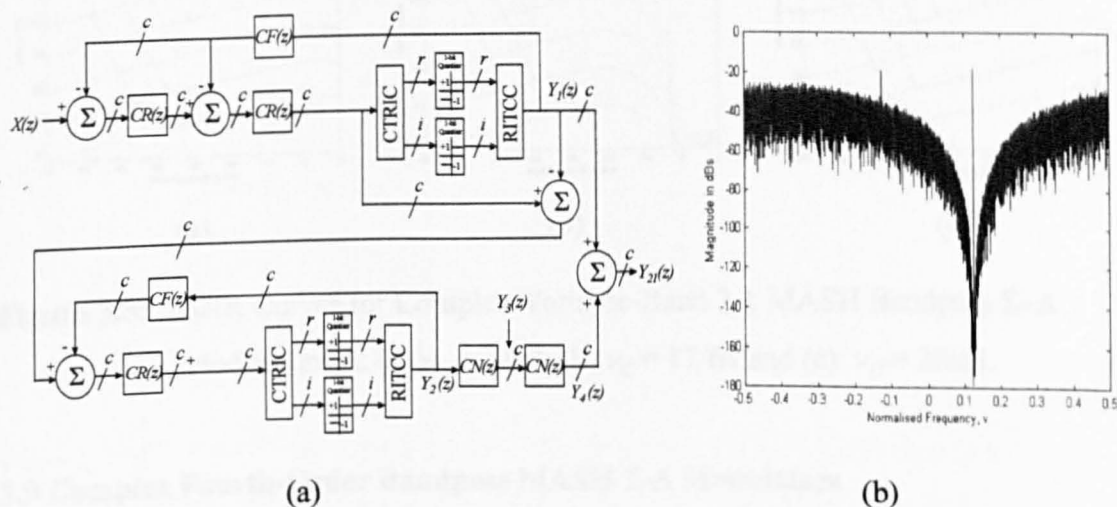


Figure 3.34 Complex Third-Order Bandpass 2-1 MASH Σ - Δ Modulator: (a) Block Diagram, (b) Magnitude Spectrum at $\nu_C = 5/64$.

These are:

$$Y_1(z) = X(z) + (1 - cz^{-1})^2 [Q_{R1}(z) + Q_{I1}(z)] \quad (3.43)$$

$$Y_4(z) = -(1 - cz^{-1})^2 [Q_{R1}(z) + Q_{I1}(z)] + (1 - cz^{-1})^3 [Q_{R2}(z) + Q_{I2}(z)] \quad (3.44)$$

The overall simplified output expression in the z-domain is given by

$$Y(z) = X(z) + (1 - cz^{-1})^3 [Q_{R2}(z) + Q_{I2}(z)] \quad (3.45)$$

The multi-bit output combinations from this complex 2-1 can be determined by examining the modulator output in the time-domain. The output signal of the second-stage has values of $\pm(1+j)(1-e^{j\alpha})^2$, which when summed up with those values of the first-stage $\pm(1+j)$, yield an overall output signal consisting of one of the following samples.

In a complex 2-1 bandpass MASH Σ - Δ modulator, the quantisation noise of the first-stage produces second-order noise-shaping, which is much smaller in amplitude and less tonal compared with a 1-1-1 MASH topology. Therefore, the effects of components mismatches between the first and second stages are less significant, thus achieving better resolution. A second advantage is that this modulator produces fewer multi-bit output combinations compared with a complex 1-1-1, thus simplifying the design of the post decimator filter. The SNR curves of this modulator for different combinations of centre frequencies and OSRs are presented in Figure 3.35.

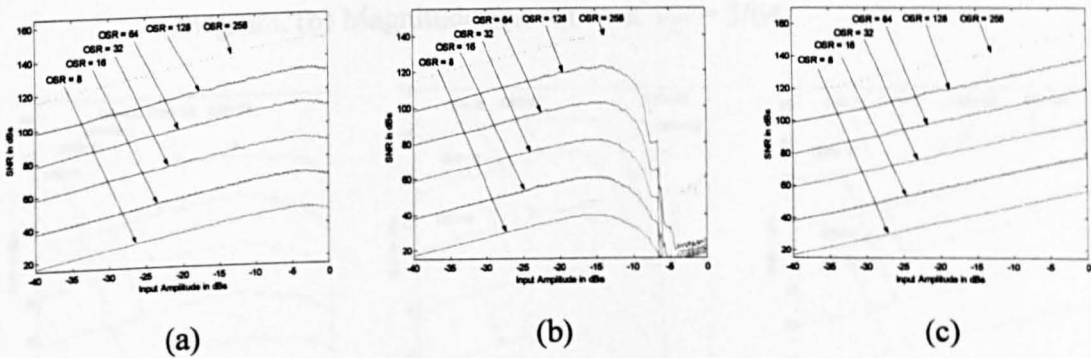


Figure 3.35 SNR Curves for Complex Variable-Band 2-1 MASH Bandpass Σ - Δ Modulators at: (a) $v_C = 5/64$, (b) $v_C = 17/64$ and (c) $v_C = 29/64$.

3.9 Complex Fourth-Order Bandpass MASH Σ - Δ Modulators

A fourth-order complex bandpass MASH Σ - Δ modulator can be constructed by having cascade combinations of 1-1-1-1, or 2-1-1, or 1-2-1, or 1-1-2 or 2-2 complex lower-

order Σ - Δ modulators. The following two sub-sections provide a block diagram as well as the design analysis and simulation results for each case.

3.9.1 Complex Fourth-Order MASH 2-1-1 Bandpass MASH Σ - Δ Modulators

This structure is basically a cascade combination of a complex second-order Σ - Δ modulator followed by two further complex first-order Σ - Δ modulators as shown below in Figure 3.36(a). Its output magnitude spectrum and SNR curves are shown in Figure 3.36 (b) and Figure 3.37 respectively.

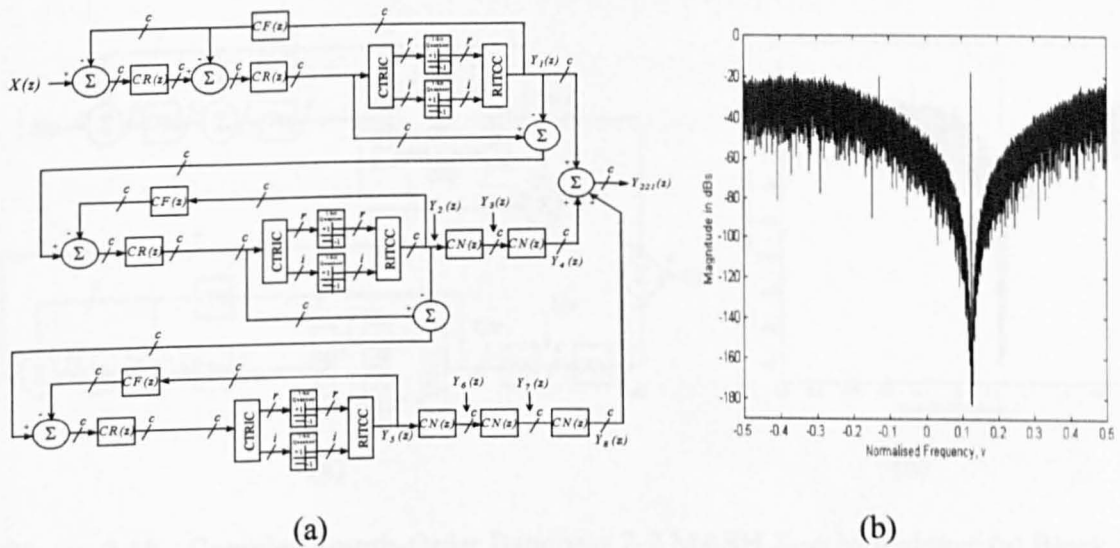


Figure 3.35 Complex Fourth-Order Bandpass 2-1-1 MASH Σ - Δ Modulator: (a) Block Diagram, (b) Magnitude Spectrum at $\nu_C = 5/64$.

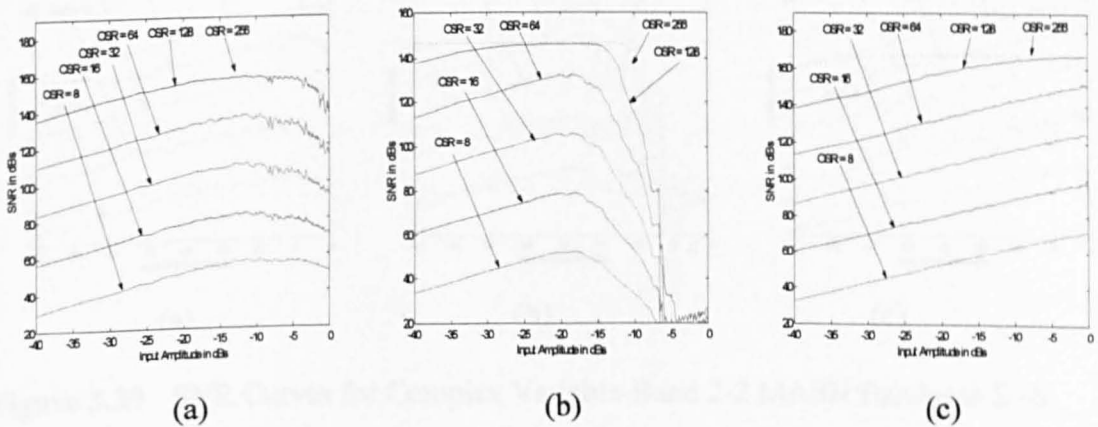


Figure 3.37 SNR Curves for Complex Variable-Band 2-1-1 MASH Bandpass Σ - Δ Modulators at: (a) $\nu_C = 5/64$, (b) $\nu_C = 17/64$ and (c) $\nu_C = 29/64$.

3.9.2 Complex Fourth-Order MASH 2-2 Bandpass MASH Σ - Δ Modulators

This is a cascade combination of two complex second-order Σ - Δ modulators as shown in Figure 3.38(a). Both stages consist of two complex first-order resonators and their associated real and imaginary quantisers in the feedforward paths as well as complex delays in the feedback path to deliver effective noise-shaping. The presence of only two stages coupled with the use of two notch-filters results in fewer multi-bit output combinations. Its magnitude spectrum and SNR curves for different centre frequencies and OSR combinations are given in Figures 3.38(b) and Figure 3.39 respectively.

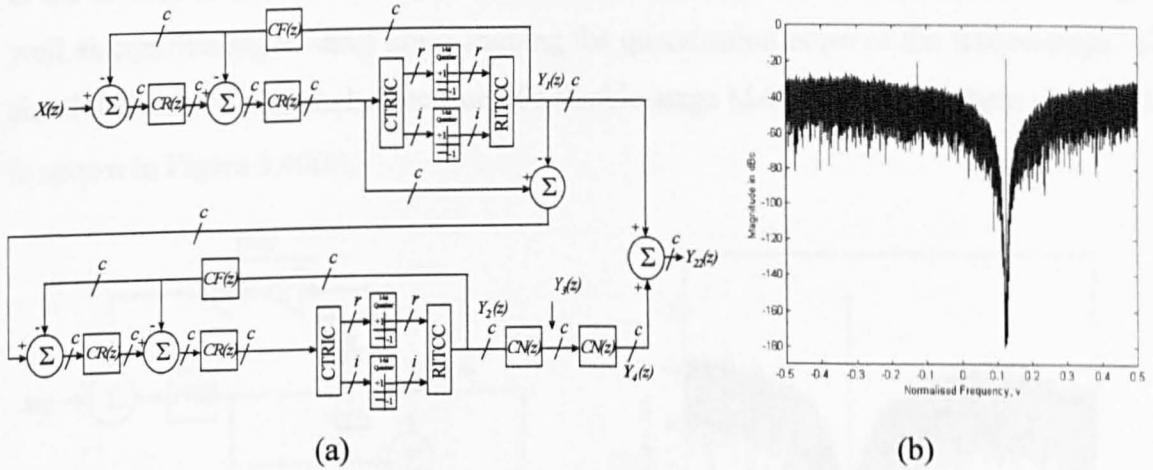


Figure 3.38 Complex Fourth-Order Bandpass 2-2 MASH Σ - Δ Modulator: (a) Block Diagram, (b) Magnitude Spectrum at $\nu_C = 5/64$.

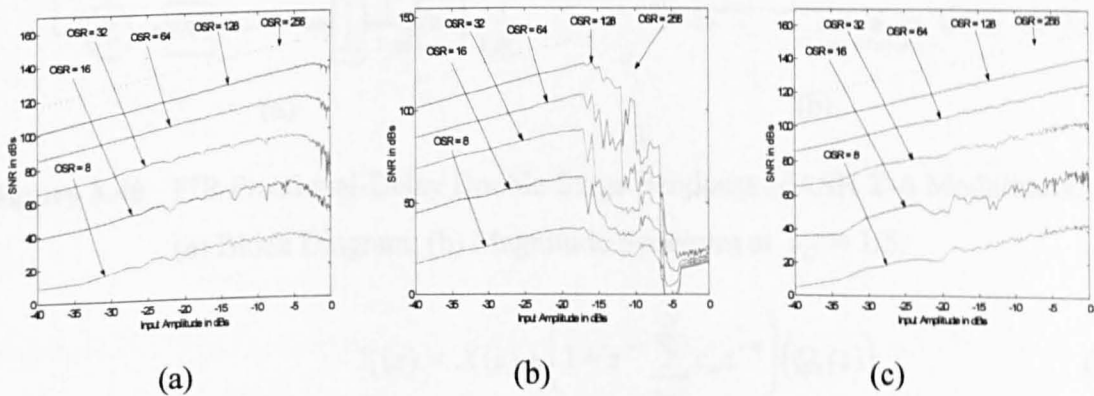


Figure 3.39 SNR Curves for Complex Variable-Band 2-2 MASH Bandpass Σ - Δ Modulators at: (a) $\nu_C = 5/64$, (b) $\nu_C = 17/64$ and (c) $\nu_C = 29/64$.

3.10 FIR Fractional-Delay Double-Stage Bandpass MASH Σ - Δ Modulators

The FIR FD MASH Σ - Δ shown in Figure 3.40(a) consists of a cascade connection of two independent single-stage n^{th} -order FIR FD filter-based Σ - Δ modulators that can

accomplish single-band noise-shaping at any specified centre frequency location. Each stage contains a variable centre frequency loop-filter $FR(z)$ and a 1-bit quantiser in the feedforward path together with two cascaded delays, represented by $FF(z)$, in the feedback path to deliver effective noise-shaping. The variable bulk delayer z^{-r} is responsible for causing coarse spectral shifts, whereas the fractional delayer z^{-f} , takes care of finer frequency adjustments. Note that z^{-r} has to be at least equal to unity to satisfy the causality criterion. The first-stage quantisation noise is fed to the input of the second-stage. The output of the second-stage is processed by a digital filter whose transfer function is the inverse of that of the loop-filter to cancel the quantisation noise of the first-stage as well as contributing towards noise-shaping the quantisation noise of the second-stage. The simulated output magnitude spectrum of a double-stage MASH Σ - Δ modulator at $\nu_C = 1/5$ is shown in Figure 3.40(b).

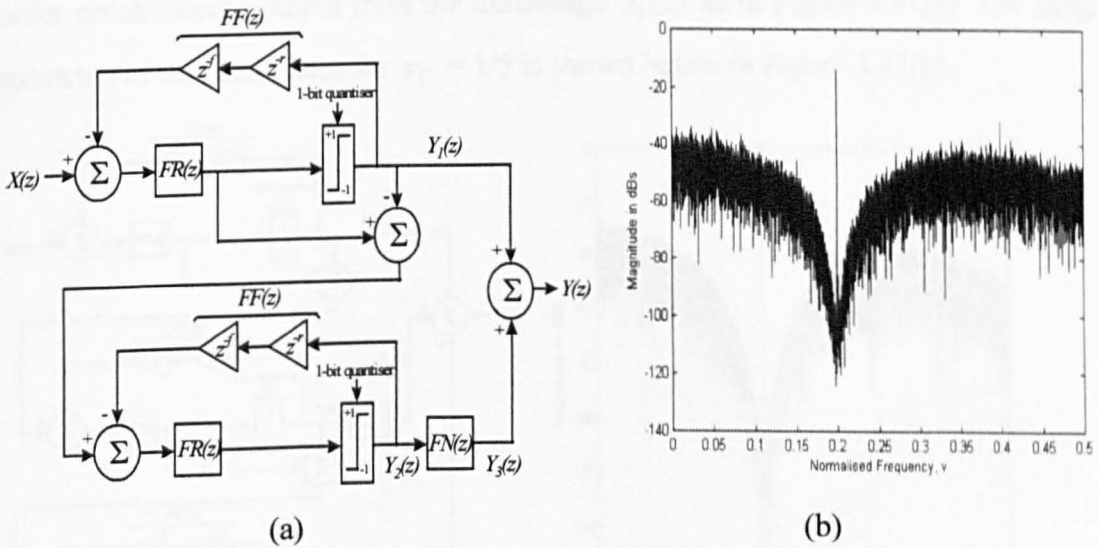


Figure 3.40 FIR Fractional-Delay Double-Stage Bandpass MASH Σ - Δ Modulators: (a) Block Diagram, (b) Magnitude Spectrum at $\nu_C = 1/5$.

$$Y_1(z) = X(z) + \left(1 + z^{-r} \sum_{n=0}^N c_n z^{-n} \right) (Q_1(z)) \quad (3.46)$$

$$Y_2(z) = \left[-(Q_1(z)) + \left(1 + z^{-r} \sum_{n=0}^N c_n z^{-N} \right) (Q_2(z)) \right] N(z) \quad (3.47)$$

The total quantisation noise and dither of the first-stage can be fully cancelled if the digital filter is $N(z) = \left(1 + \sum_{n=0}^N c_n z^{-N} \right)$ resulting in a final expression for $Y_{11}(z)$ given by:-

$$Y_{11}(z) = Y_1(z) + N(z)Y_2(z) = X(z) + \left(1 + z^{-r} \sum_{n=0}^N c_n z^{-N}\right)^2 (Q_2(z)) \quad (3.48)$$

where c 's represent the coefficients of the FD filter.

The inclusion of an n^{th} -order digital filter at the output of $Y_2(z)$ together with the summation of the two stages in the time-domain produces a multi-bit output signal in the time-domain.

3.11 FIR Fractional-Delay Triple-Stage Bandpass MASH Σ - Δ Modulators

This structure contains three independent n^{th} -order variable centre frequency Σ - Δ modulators in cascade, where the first-stage quantisation is fed to the second-stage input and likewise for the third-stage. The modulator output is the summation of the first-stage output $Y_1(z)$, an n^{th} -order notch-filtered output from the second-stage $Y_3(z)$ and a $2n^{\text{th}}$ -order notch-filtered output from the third-stage $Y_6(z)$ as in Figure 3.41(a). The magnitude spectrum of this modulator for $\nu_C = 1/5$ is shown below in Figure 3.41(b).

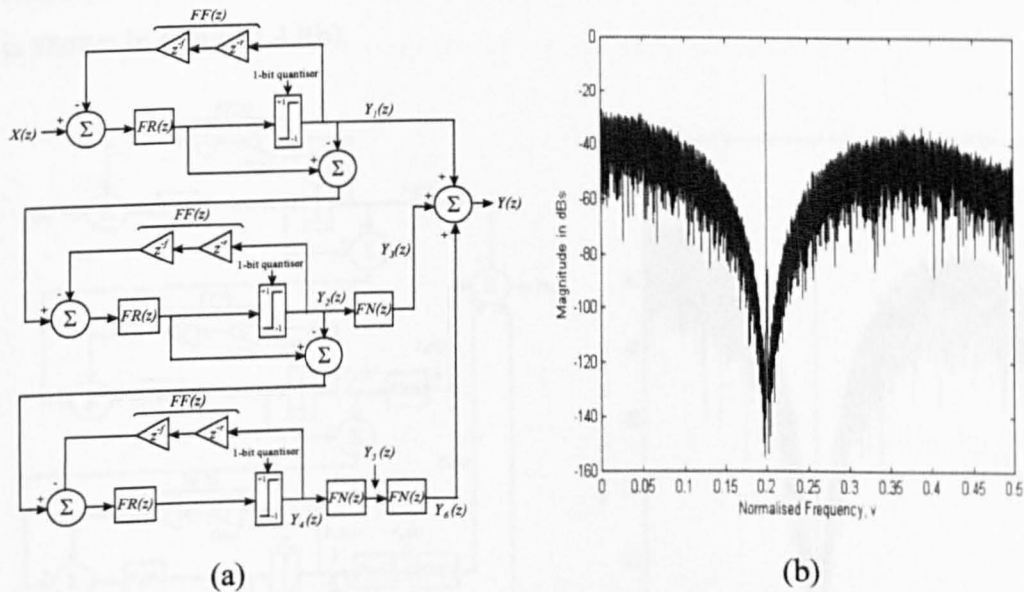


Figure 3.41 FIR Fractional-Delay Triple-Stage Bandpass MASH Σ - Δ Modulators:

(a) Block Diagram, (b) Magnitude Spectrum at $\nu_C = 1/5$.

The output expressions in the z -domain are given by:

$$Y_1(z) = X(z) + \left(1 + z^{-r} \sum_{n=0}^N c_n z^{-N}\right) (Q_1(z)) \quad (3.49)$$

$$Y_3(z) = \left[-(Q_1(z)) + \left(1 + z^{-r} \sum_{n=0}^N c_n z^{-N} \right) (Q_2(z)) \right] N(z) \quad (3.50)$$

$$Y_6(z) = \left[-(Q_2(z)) + \left(1 + z^{-r} \sum_{n=0}^N c_n z^{-N} \right) (Q_3(z)) \right] N^2(z) \quad (3.51)$$

Therefore, the overall output expression becomes $Y_{111}(z)$

$$Y_{111}(z) = Y_1(z) + N(z)Y_2(z) + N(z)Y_4(z) = X(z) + \left(1 + z^{-r} \sum_{n=0}^N c_n z^{-N} \right)^3 (Q_3(z)) \quad (3.52)$$

3.12 FIR Fractional-Delay Quadruple-Stage Bandpass MASH Σ - Δ Modulators

This modulator is a cascade combination of four n th-order variable centre frequency bandpass Σ - Δ modulators as shown in Figure 3.42(a), where the quantisation noise of each-stage is fed to the input of its succeeding-stage. The resulting output is the summation of all stages with the necessary digital filtering so that the quantisation noise of the intermediate stages are all cancelled out. The output magnitude spectrum of this modulator is shown in Figure 3.42(b).

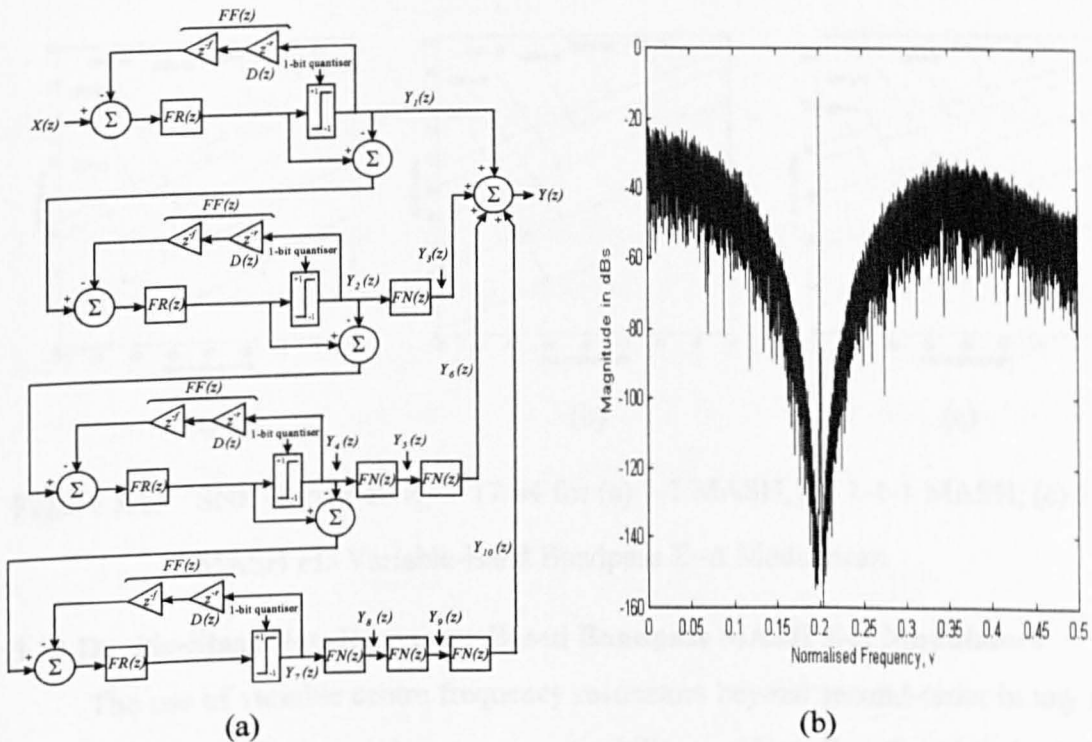


Figure 3.42 FIR Fractional-Delay Quadruple-Stage Bandpass MASH Σ - Δ Modulators: (a) Block Diagram, (b) Magnitude Spectrum at $\nu_C = 1/5$.

The intermediate corresponding output expressions are given by:

$$Y_1(z) = X(z) + \left(1 + z^{-r} \sum_{n=0}^N c_n z^{-n}\right) (Q_1(z)) \quad (3.53)$$

$$Y_3(z) = \left[- (Q_1(z)) + \left(1 + z^{-r} \sum_{n=0}^N c_n z^{-N}\right) (Q_2(z)) \right] N(z) \quad (3.54)$$

$$Y_6(z) = \left[- (Q_2(z)) + \left(1 + z^{-r} \sum_{n=0}^N c_n z^{-N}\right) (Q_3(z)) \right] N^2(z) \quad (3.55)$$

$$Y_{10}(z) = \left[- (Q_3(z)) + \left(1 + z^{-r} \sum_{n=0}^N c_n z^{-N}\right) (Q_4(z)) \right] N^3(z) \quad (3.56)$$

Therefore, the overall output expression becomes $Y_{111}(z)$

$$Y_{1111}(z) = X(z) + \left(1 + z^{-r} \sum_{n=0}^N c_n z^{-N}\right)^4 (Q_4(z)) \quad (3.57)$$

The SNR curves corresponding to the double-, triple- and quadruple-stage MASH FD variable-band bandpass Σ - Δ modulators are illustrated in Figure 3.43.

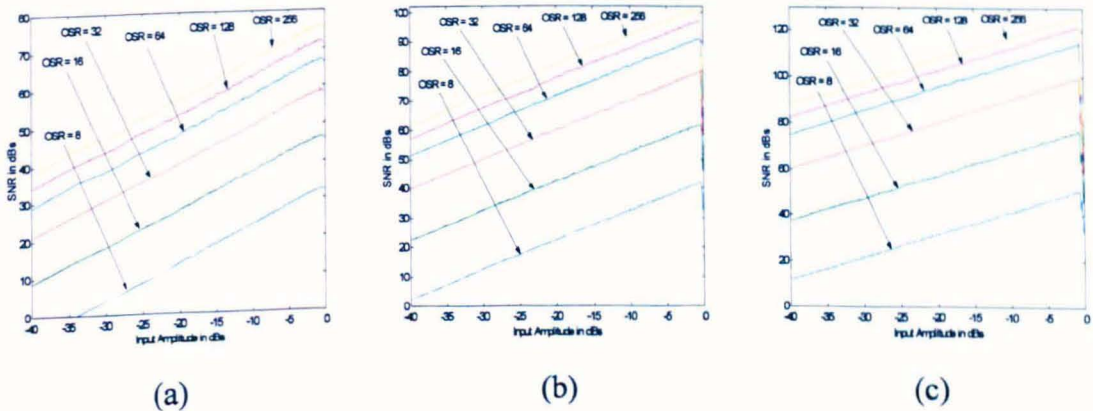


Figure 3.43 SNR Curves at $\nu_C = 17/64$ for (a) 1-1 MASH, (b) 1-1-1 MASH, (c) 1-1-1-1 MASH FD Variable-Band Bandpass Σ - Δ Modulators.

3.13 Double-Stage Non-Resonator-Based Bandpass MASH Σ - Δ Modulators

The use of variable centre frequency resonators beyond second-order in any stage in MASH bandpass Σ - Δ modulators poses a stability problem. Fourth-order single-bit Σ - Δ modulators are conditionally stable due to the uneven shoulder gains of the resonator for non-mid-band centre frequencies. Possible remedies to enhance stability were covered in Section 2.6 such as the use of the multi-bit quantisers, suitable resonator gain factors or feedback coefficients. Another viable choice is to employ non-resonator bandpass

alternatives such as Butterworth or Chebyshev 2 filters, whose zeros can be conveniently exploited to control the internal amplitude level in each stage of the MASH modulator to avert instability. The motivation of this section is to present the design analysis and simulation results of narrow-band bandpass Butterworth- and Chebyshev 2-based Σ - Δ modulators. The two scenarios of employing identical and different loop-filters in each section will be discussed in the following two sub-sections. The double-stage Σ - Δ modulator shown in Figure 3.44 is well-suited for the application and behavioural-level evaluation for both the ensuing stage combinations. Note that the constituent modulator sections are simplified by the embedding the feedback transfer function into that of the loop-filter.

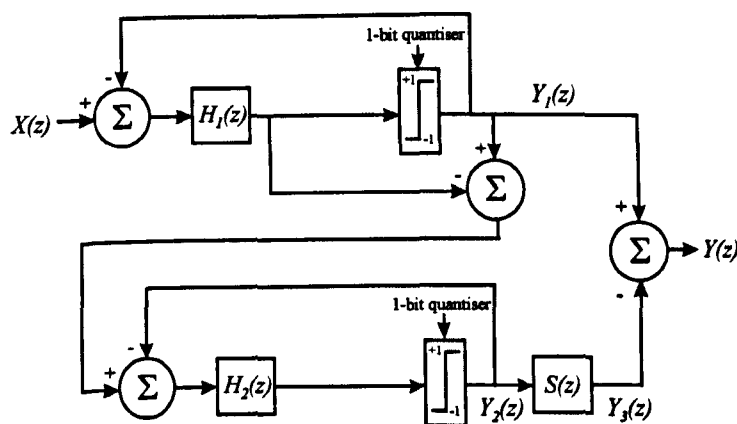


Figure 3.44 Double-Stage Non-Resonator-Based Bandpass MASH Σ - Δ Modulators.

3.13.1 Identical Loop-Filter Stages in Double-Stage Bandpass MASH Σ - Δ Modulators

This section provides the design analysis of identical loop-filter stages for narrow-band bandpass Σ - Δ modulators. The loop-filter $H_1(z)$ is partitioned into a numerator and a denominator polynomial represented by $N_1(z)$ and $D_1(z)$. Given that $H_1(z) = H_2(z)$, the corresponding outputs of both stages $Y_1(z)$ and $Y_3(z)$ are given by

$$Y_1(z) = \frac{N_1(z)}{N_1(z) + D_1(z)} X(z) + \frac{D_1(z)}{N_1(z) + D_1(z)} Q_1(z) \quad (3.58)$$

$$Y_3(z) = \left(\frac{N_1(z)}{N_1(z) + D_1(z)} Q_1(z) + \frac{D_1(z)}{N_1(z) + D_1(z)} Q_2(z) \right) \frac{D_1(z)}{N_1(z) + D_1(z)} \quad (3.59)$$

The resultant output of this modulator after further algebraic simplifications becomes

$$Y(z) = \frac{N_1(z)}{N_1(z) + D_1(z)} X(z) + \left(\frac{D_1(z)}{N_1(z) + D_1(z)} \right)^2 (Q_1(z) - Q_2(z)) \quad (3.60)$$

The SNRs for different combinations of centre frequencies and OSRs are illustrated in Figure 3.45.

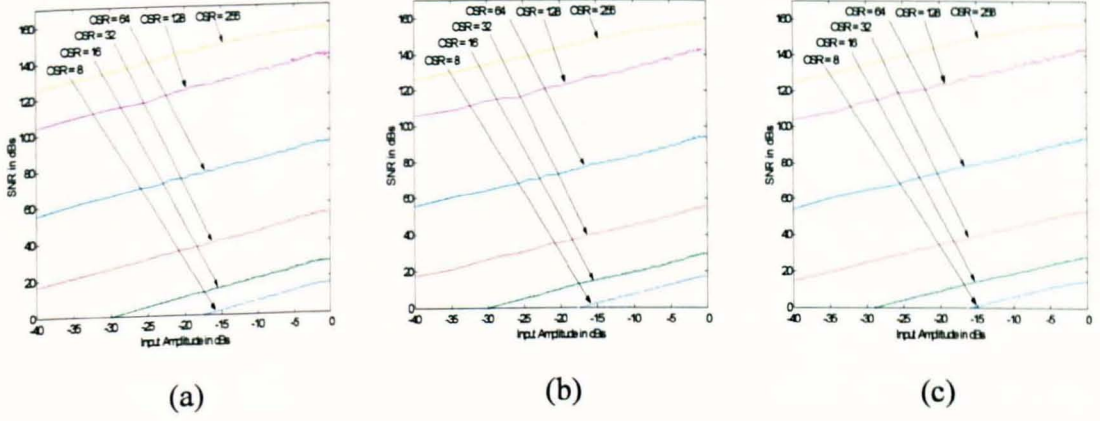


Figure 3.45 SNR Curves for the Identical Loop-Filter Double-Stage Non-Resonator-Based Bandpass MASH Σ - Δ Modulators at: (a) $v_C = 5/64$, (b) $17/64$ and (c) $29/64$.

3.13.2 Dissimilar Loop-Filter Stages in Double-Stage Bandpass Σ - Δ Modulators

This section provides the design analysis of different loop-filter stages for narrow-band bandpass Σ - Δ modulators. The numerator and denominator polynomials of the two loop-filters $H_1(z)$ and $H_2(z)$ are represented by $N_1(z)$, $D_1(z)$, $N_2(z)$ and $D_2(z)$ respectively. The corresponding outputs of both stages $Y_1(z)$ and $Y_3(z)$ are given by

$$Y_1(z) = \frac{N_1(z)}{N_1(z) + D_1(z)} X(z) + \frac{D_1(z)}{N_1(z) + D_1(z)} Q_1(z) \quad (3.61)$$

$$Y_3(z) = \left(\frac{N_2(z)}{N_2(z) + D_2(z)} Q_1(z) + \frac{D_2(z)}{N_2(z) + D_2(z)} Q_2(z) \right) \frac{D_1(z)}{N_1(z) + D_1(z)} \quad (3.62)$$

The resultant output of this modulator after further algebraic simplifications becomes

$$Y(z) = \frac{N_1(z)}{N_1(z) + D_1(z)} X(z) + \left(\frac{D_1(z)D_2(z)}{(N_1(z) + D_1(z)) + (N_2(z) + D_2(z))} \right) (Q_1(z) - Q_2(z)) \quad (3.63)$$

The SNRs of this modulator for different combinations of centre frequencies and OSRs are illustrated in Figure 3.46.

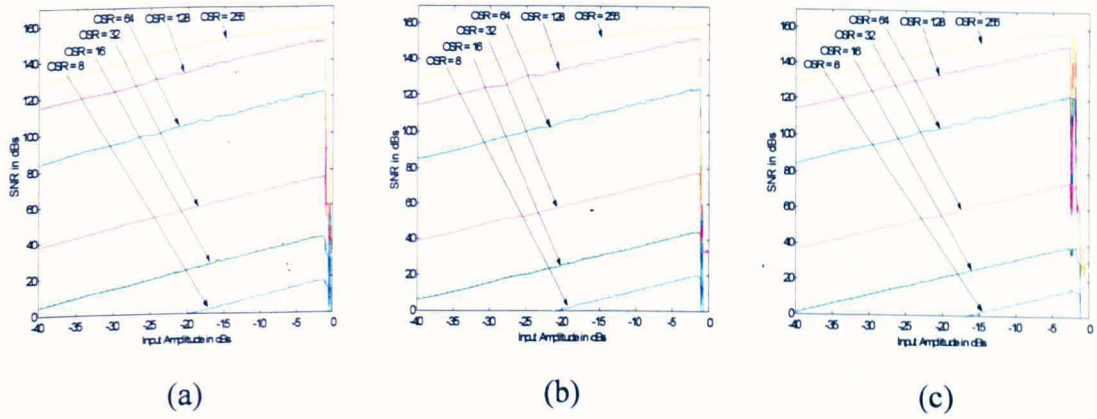


Figure 3.46 SNR Curves for the Dissimilar Loop-Filter Double-Stage Non-Resonator-Based Bandpass MASH Σ - Δ Modulators at: (a) $\nu_C = 5/64$, (b) $\nu_C = 17/64$ and (c) $\nu_C = 29/64$.

3.14 Double-Stage Resonator/Non-Resonator Based Bandpass Σ - Δ Modulators

The novel double-stage Σ - Δ modulator shown below in Figure 3.47 consists of a 4th-order variable centre frequency resonator-based Σ - Δ modulator in the 1st-stage and a 4th-order bandpass Butterworth/Chebyshev 2 Σ - Δ modulator in the 2nd-stage.

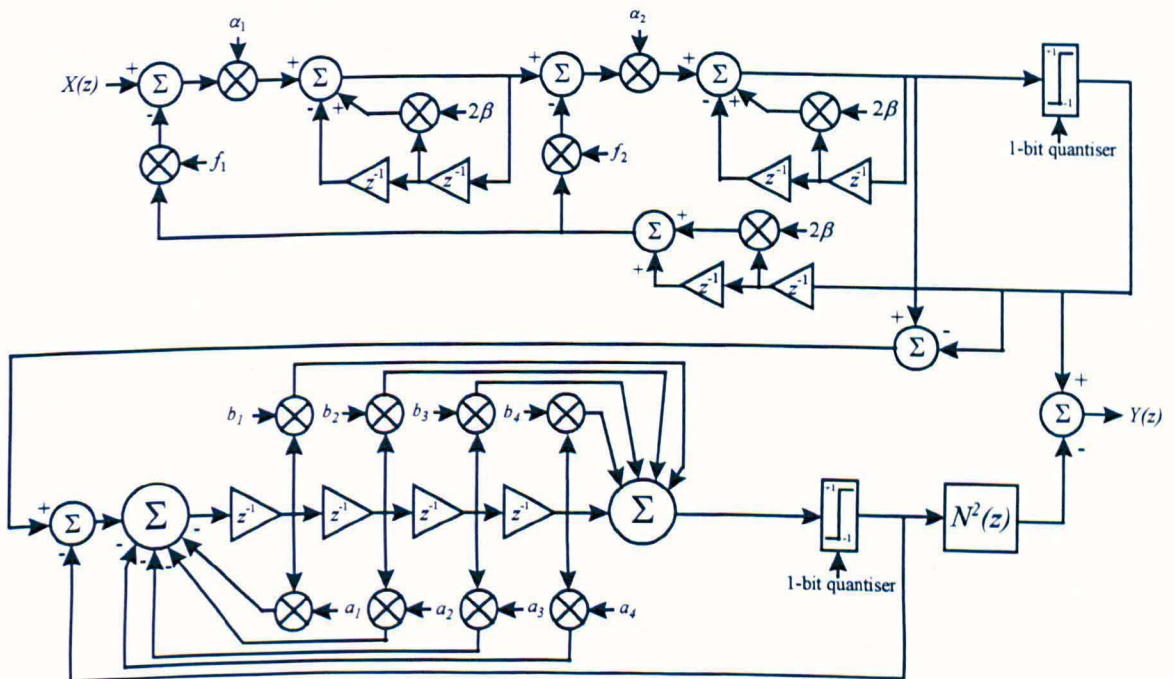


Figure 3.47 Double-Stage Resonator/Non-Resonator-Based Bandpass Σ - Δ Modulators.

The outputs of the 1st-stage $Y_1(z)$ and 2nd-stage $Y_2(z)$ are:

$$Y_1(z) = \frac{g_1 g_2}{D_{S1}(z)} X(z) + \left(\frac{1 - \beta z^{-1} + z^{-2}}{D_{S1}} \right) Q_1(z) \quad (3.64)$$

$$Y_2(z) = \frac{D_{S2}(z) - N_{S2}(z)}{D_{S2}(z)} Q_1(z) + \frac{N_{S2}(z)}{D_{S2}(z)} Q_2(z) \quad (3.65)$$

where $D_{S1}(z)$, $D_{S2}(z)$ and $N_{S2}(z)$ are given by:

$$D_{S1}(z) = 1 + \beta(f_1 g_1 g_2 + f_2 - 2)z^{-1} + (2 + \beta^2(1 - f_2) - f_1 g_1 g_2 - f_2)z^{-2} + 2\beta(f_2 - 1)z^{-3} + (1 - f_2)z^{-4} \quad (3.66)$$

$$D_{S2}(z) = 1 + a_1 z^{-1} + a_2 z^{-2} + a_3 z^{-3} + a_4 z^{-4} \quad (3.67)$$

$$N_{S2}(z) = 1 + b_1 z^{-1} + b_2 z^{-2} + b_3 z^{-3} + b_4 z^{-4} \quad (3.68)$$

The resultant output of this modulator becomes:

$$Y(z) = \frac{g_1 g_2}{D_{S1}(z)} X(z) + \frac{1 - \beta z^{-1} + z^{-2}}{D_{S2}(z)} \left[\frac{Q_1(z)}{D_{S1}(z)} - Q_2(z) \right] \quad (3.69)$$

This topology offers several advantages compared with conventional bandpass MASH Σ - Δ modulators. First; this modulator requires two simple digital notch filters instead of a more complicated band-stop filter at the output of the 2nd-stage to appropriately cancel the quantisation noise of the 1st-stage. Second; the 2nd-stage output undergoes through less digital processing due to the simplicity of the notch filters resulting in fewer cumulative multi-levels in the output signal. This imposes fewer restrictions on the design specifications of the decimation filter. Third; the coincidental zeros of the 1st-stage NTF in combination with the distributed zeros of the 2nd-stage NTF ensure a deep as well as a relatively wide-band notch in the signal region. This has the benefit of providing respectable in-band SNRs for closely-spaced multi-tone input signals as demonstrated in Figure 3.48(a). Fourth; the quantisation noise of the 1st-stage has a smaller magnitude and is less tonal, because it is noise-shaped by a 4th-order Σ - Δ modulator, thus making this topology more immune to component imperfections. Fifth; the 2nd-stage quantiser will not be overloaded for high-amplitude inputs, because of the even distribution of the poles and zeros of the 2nd-stage loop-filter.

The main drawback of this Σ - Δ MASH modulator is that some scaling coefficients are needed in the 1st-stage for non-mid-band centre frequencies to control the internal signal amplitudes in the feedforward path. The SNRs of this modulator significantly outperform those of the 2-2 MASH Σ - Δ modulator as shown below in Figure 3.48.

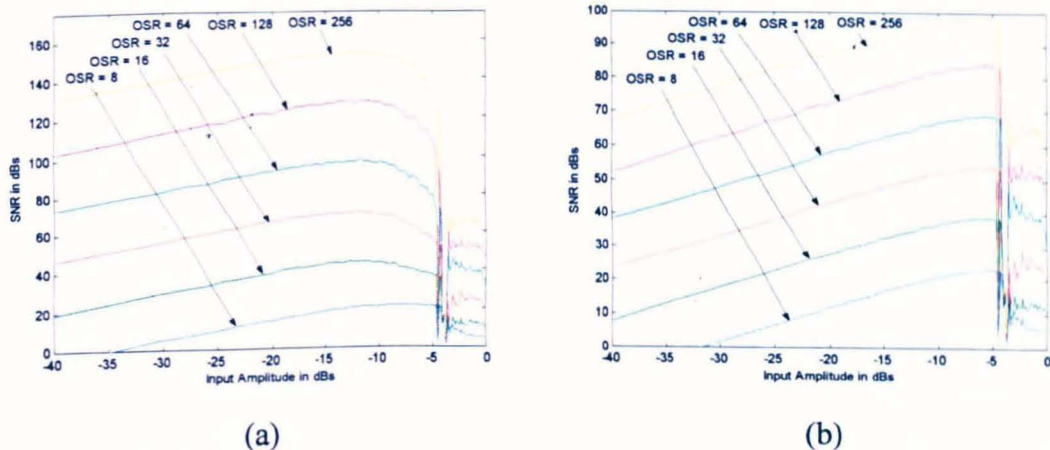


Figure 3.48 SNR Curves of (a) Double-Stage Resonator/Non-Resonator-Based Bandpass Σ - Δ Modulators, (b) 2-2 MASH Bandpass Σ - Δ Modulators at $\nu_c = 17/64$.

3.15 Double-Stage Inverse Comb-Bandpass Filter Based Bandpass Σ - Δ Modulators

3.15.1 Single-Loop Case

This double-stage Σ - Δ modulator employs an L^{th} -order multi-band loop-filter in the 1st-stage that is derived from an L^{th} -order comb filter NTF and an M^{th} -order bandpass Butterworth/Chebyshev 2 filter in the 2nd-stage as shown in Figure 3.48. The bandpass filter in the 2nd-stage acts to concurrently attenuate and widen the notch in the signal region to provide better in-band SNRs. The remaining out-of-band nulls, however, can be subsequently removed by the digital filter in the decimation stage.

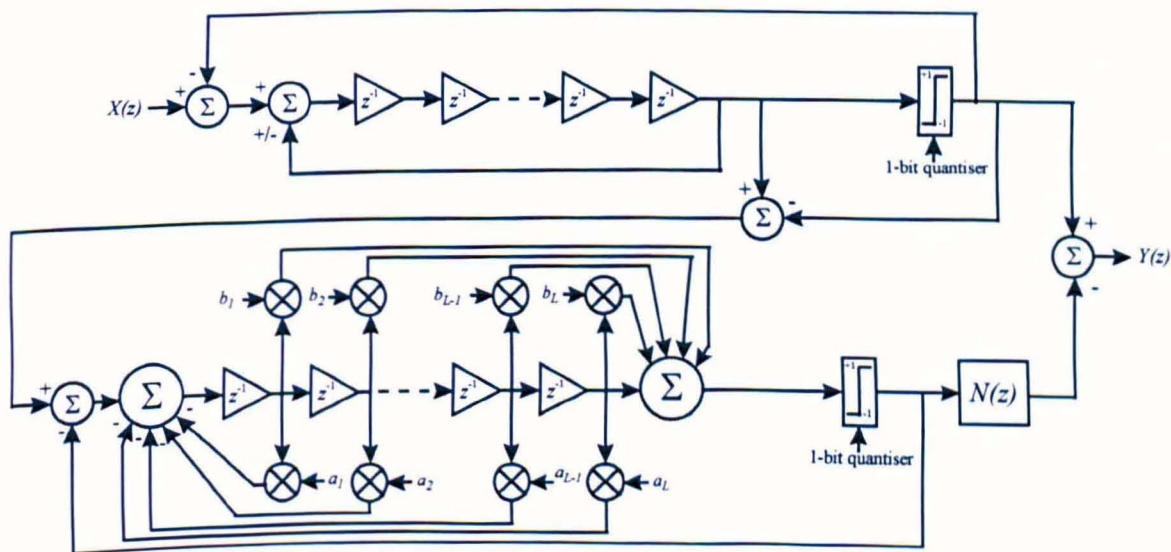


Figure 3.49 Double-Stage Inverse Comb/Non-Resonator-Based Bandpass Σ - Δ Modulator.

The outputs of the 1st $Y_1(z)$ and 2nd-stages $Y_2(z)$ are given by:

$$Y_1(z) = z^{-N} X(z) + (1 + z^{-N})Q_1(z) \quad (3.70)$$

$$Y_2(z) = \left[\frac{N_G(z)}{N_G(z) + D_G(z)} Q_1(z) + \frac{D_G(z)}{N_G(z) + D_G(z)} Q_2(z) \right] (1 + z^{-N}) \quad (3.71)$$

$$Y(z) = z^{-N} X(z) + \frac{D_G(z)(1 + z^{-N})}{N_G(z) + D_G(z)} [Q_1(z) - Q_2(z)] \quad (3.72)$$

The benefits of this novel MASH bandpass $\Sigma\text{-}\Delta$ modulator are summarised as follows: First; it contains a multiplier-free loop-filter in the 1st-stage, which is capable of producing noise-shaping at a variety of centre frequency locations. Second; the digital cancellation filter at the output of 2nd-stage does not use any multipliers. This results in simpler and fewer cumulative multi-levels in the output signal. Third; the quantiser in the 1st-stage does not become overloaded for large-amplitude inputs or non-mid-band centre frequencies, circumventing the need for scaling coefficients to control stability.

The main disadvantage of this MASH topology is that the 1st-stage produces redundant notches. The presence of too many notches due to a high-order loop-filter increase the amplitude level of the out-of-band quantisation noise, making the modulator more susceptible to instability. The output magnitude spectrum of this modulator is shown in Figure 3.50(a), where more effective noise-shaping can be observed for the noise-shaping band of interest. The other notch in the spectrum has occurred as a result of the comb filter in the first stage. The SNR curves for different combinations of centre frequencies and OSRs are shown in Figure 3.50 (b).

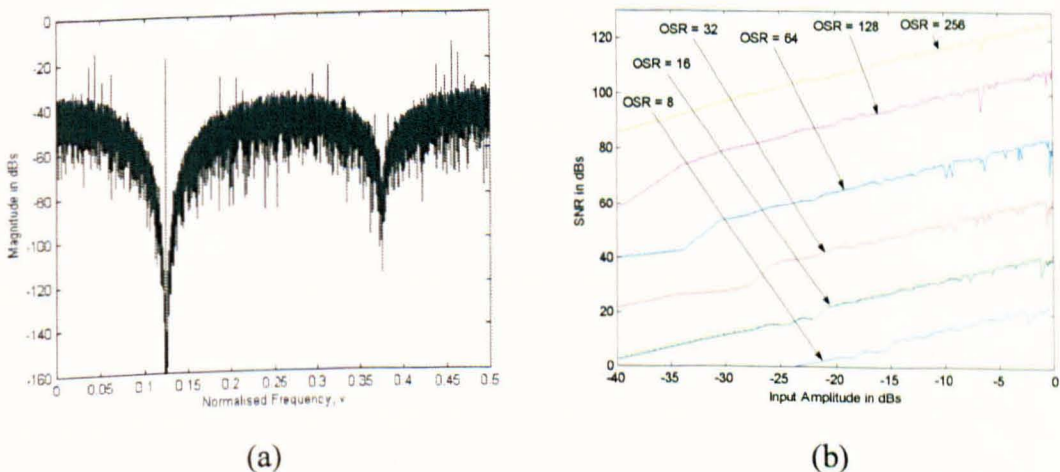


Figure 3.50 Double-Stage Single-Loop Inverse Comb-Bandpass Filter Based Bandpass $\Sigma\text{-}\Delta$ Modulator, (a) Magnitude Spectrum, (b) SNR Curves.

3.15.2 Double-Loop Case

This double-stage $\Sigma\text{-}\Delta$ modulator employs a double-loop inverse-comb filter in the 1st-stage to provide an enhanced noise-shaping response compared with its single-loop

predecessor in 3.15.1 and a bandpass Butterworth/Chebyshev 2 filter in the 2nd-stage as shown in Figure 3.51.

The advantages of this topology are summarised as follows: First; it provides a deeper notch with better resolution without using any multipliers. Second; the presence of a double-loop modulator in the 1st-stage causes the overall modulator output to be less tonal. Third; this modulator is more tolerant to component mismatches; because any leaked quantisation noise that may be transmitted in the 2nd-stage is noise-shaped by twice the order. Fourth; the digital cancellation circuitry does not require any multipliers, thus reducing the hardware complexity of the modulator. Fifth; fewer multi-level outputs are produced with this modulator due to the simplicity of the comb filters.

Two disadvantages exist with this Σ - Δ modulator topology. First; the use of a double-loop inverse comb filter in the 1st-stage results in better resolution for the redundant noise-shaping bands as well as the desired signal-band. Second; the out-of-band quantisation noise magnitude is increased in proportion to the number of noise-shaping bands. As a result, this imposes tighter requirements on the digital decimators.

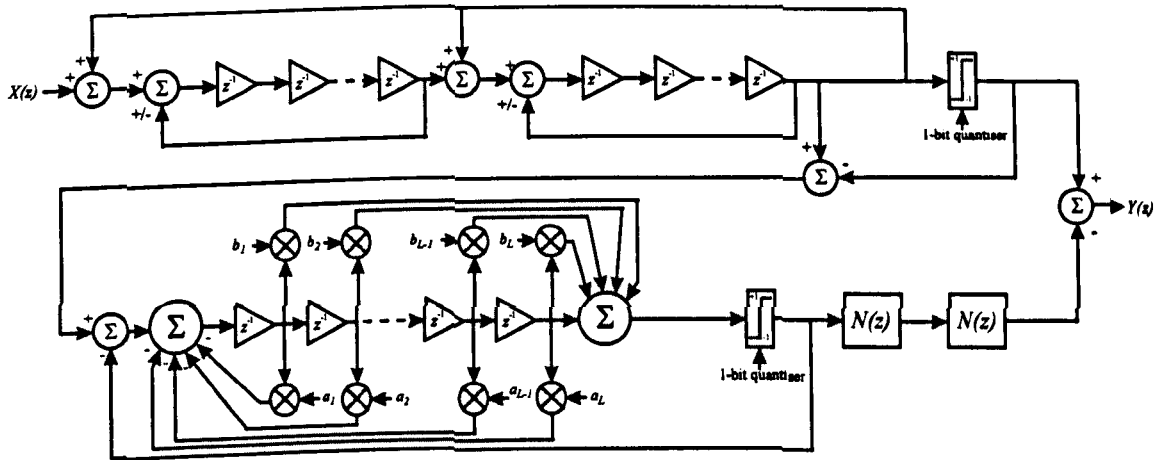


Figure 3.51 Double-Stage Double Inverse Comb/Non-Resonator-Based Bandpass Σ - Δ Modulator.

The intermediate and final outputs of this Σ - Δ modulator are given by:

$$Y_1(z) = z^{-N} X(z) + (1 + z^{-N}) Q_1(z) \quad (3.73)$$

$$Y_2(z) = \left[\frac{N_G(z)}{N_G(z) + D_G(z)} Q_1(z) + \frac{D_G(z)}{N_G(z) + D_G(z)} Q_2(z) \right] (1 + z^{-N})^2 \quad (3.74)$$

$$Y(z) = z^{-N} X(z) + \frac{D_G(z)(1+z^{-N})^2}{N_G(z) + D_G(z)} [Q_1(z) - Q_2(z)] \quad (3.75)$$

The output magnitude spectrum of this modulator is shown in Figure 3.52(a), where significantly better noise-shaping was accomplished. This is reflected by the improved SNR curves shown in Figure 3.52(b) compared with those shown in Figure 3.50(b).

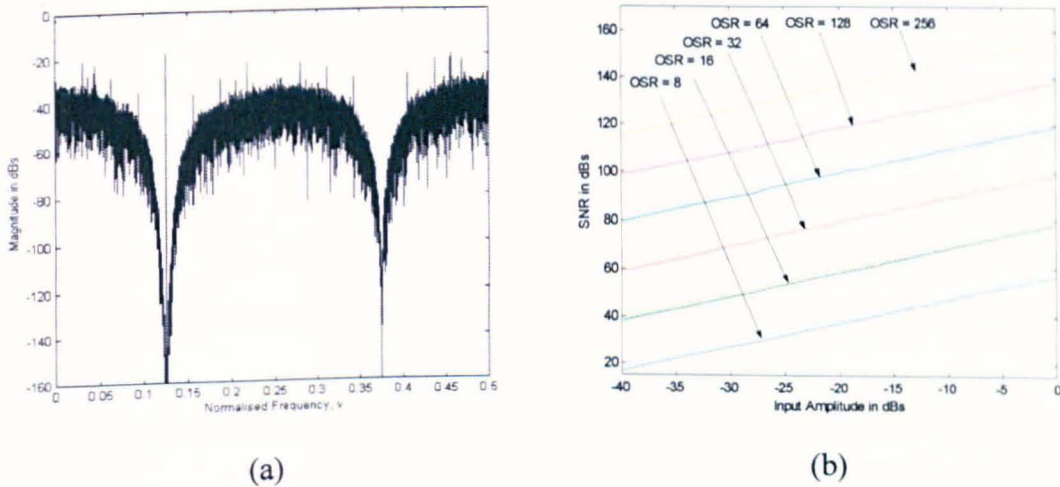


Figure 3.52 Double-Stage Single-Loop Inverse Comb-Bandpass Filter Based Bandpass Σ - Δ Modulator, (a) Magnitude Spectrum, (b) SNR Curves.

3.16 Concluding Remarks to Chapter 3

The design procedure and analysis of variable-band resonator-based MASH bandpass Σ - Δ modulators were presented. The four techniques considered were based on the NTFs of real-coefficient FIR notch filters, complex FIR notch filters, fractional-delay in conjunction with sum filters and Butterworth/Chebyshev 2 bandstop filters.

The stability of the 2-2 MASH bandpass Σ - Δ modulators was maintained for high-amplitude inputs, unlike a fourth-order single-stage single-bit Σ - Δ modulator. This led to better SNRs and DRs. However, the 2-2 MASH contained more analogue circuitry and required a digital notch filter to achieve quantisation noise cancellation of the first stage. The presence of a multi-bit output signal imposed further design constraints on the decimator. Furthermore, non-idealities between the analogue and digital stages were more critical, because these inaccuracies contributed to the leakage of more quantisation noise and tones to the in-band region.

The 2-2-2 MASH was simple to design, exhibited a virtually tone-free magnitude spectrum for ideal component matching and was unconditionally unstable. Moreover, higher in-band SNRs and DRs were achieved, because the constituent quantisers became mildly overloaded for very high input amplitudes. The disadvantages of this modulator

included: the requirement of 3 digital notch filters to achieve the quantisation noise cancellation of the previous stages, the presence of more multi-bit output combinations and greater sensitivity to component tolerance.

The main advantage of the 4-2 MASH was that the quantisation noise of the first-stage output produced fourth-order noise-shaping, which was much smaller in magnitude and less tonal. Consequently; the effects of component mismatches on the modulator resolution were less detrimental. The need for 2 instead of 3 notch filters had a twofold advantage in that it reduced the overall modulator complexity, therefore generating fewer multi-bit output combinations compared with the 2-2-2 MASH. The main drawback was that the fourth-order Σ - Δ modulator in the first-stage, became conditionally stable for large-amplitude input signals, particularly for very low and high frequencies. The stability, however, could be improved by using either suitable feedforward coefficients or multi-bit quantisers.

A 2-4 MASH required a single notch filter and therefore produced fewer multi-levels in its output signal in comparison with the 2-2-2 and 4-2 MASH Σ - Δ modulators. The main advantage for the 2-4 MASH, which used a multi-bit quantiser in the second-stage, was that the effect of distortion due to the non-linearities of the multi-bit D/A were less significant to the overall modulator resolution, when compared with the 4-2 MASH. This was because the output of the second-stage including its D/A error did not feed into another stage. Disadvantages included the need to sufficiently dither the first-stage to reduce spurious tone leakage to the second-stage as well as the need to incorporate inter-stage scale-factors to avert premature overloading of the second-stage quantiser. The use of a multi-bit quantiser in the second-stage subjected its multi-level output to be processed by a notch filter in this case, which considerably increased the number of multi-levels of the modulator output.

The 2-2-2-2 MASH was conditionally stable and therefore delivered greater SNRs and DRs compared with an eighth-order single-stage single-bit Σ - Δ modulator. Compared with other MASH modulators, this required 6 notch filters to achieve quantisation noise cancellation of the preceding three stages. It contained more multi-bit combinations. In addition, it was more sensitive to component non-idealities, especially, in the first-stage, which resulted in the transmission of uncancelled quantisation noise and tones into later stages.

The 4-2-2 MASH had greater tolerance due to non-idealities in the first-stage, requiring 5 instead of 6 notch filters. It also produced fewer multi-bit output combinations

compared with the 2-2-2-2 MASH. However, the increased internal signal levels of the first-stage overloaded the quantiser prematurely, thus limiting its DR compared with the 2-2-2 MASH.

The 4-4 MASH modulator only required two notch filters and a result generated the lowest number of multi-levels in its output signal, when compared with the 2-2-2-2, 4-2-2, 2-4-2 and 2-2-4 MASH modulators. The 4-4 MASH had greater insensitivity to component non-idealities and was less tonal, because the quantisation noise in both stages was processed by fourth-order noise-shaping. However, it exhibited comparatively lower in-band SNRs and DRs due to the quantiser overloading in both stages for high-amplitude input signals.

Several conclusions can be drawn with respect to the arrangement of fourth-order Σ - Δ modulators within these Σ - Δ MASH topologies. The use of a fourth-order modulator in the first-stage makes the overall modulator less sensitive to non-idealities allowing the propagation to subsequent stages quantisation noise that is smaller in magnitude and less tonal. The use of a single-bit fourth-order Σ - Δ modulator in the later stages reduces the number of required notch filters for cancellation purposes resulting in fewer multi-bit output combinations.

MASH Topology	No of levels	Multi-level Combinations
2-2	4	$\pm 1, \pm 3$
2-2-2	8	$\pm 1, \pm 3, \pm 5, \pm 7$
4-2	6	$\pm 1, \pm 3, \pm 5$
2-4	4	$\pm 1, \pm 3$
2-2-2-2	16	$\pm 1, \pm 3, \pm 5, \pm 7, \pm 9, \pm 11, \pm 13, \pm 15$
4-2-2	14	$\pm 1, \pm 3, \pm 5, \pm 7, \pm 9, \pm 11, \pm 13$
2-4-2	12	$\pm 1, \pm 3, \pm 5, \pm 7, \pm 9, \pm 11$
2-2-4	8	$\pm 1, \pm 3, \pm 5, \pm 7$
4-4	6	$\pm 1, \pm 3, \pm 5$

Table 3.23 Multi-Level Output Combinations of Nine-Different Cascades of Mid-Band Resonator-Based Bandpass Σ - Δ Modulators.

The advantages and drawbacks of the complex 1-1 MASH, 1-1-1 MASH, 2-1 MASH, 2-1-1 MASH and 2-2 MASH were very similar to those stated for the real-coefficient 2-2 MASH, 2-2-2 MASH, 4-2 MASH, 4-2-2 MASH and 4-4 MASH bandpass Σ - Δ modulators respectively. In general, the poles and zeros of the loop-filters in complex MASH Σ - Δ modulators were not restricted to conjugate pairs, implying that better in-band

quantisation noise attenuation could be attained, compared with a real-coefficient MASH modulator of the same order. Greater resolution and design flexibility were provided by complex MASH modulators at the expense of an extra quantiser and signal paths for the imaginary components of the signals in the modulator. The constituent second-order modulators were stable compared with their real-coefficient fourth-order counterparts especially for non-mid-band centre frequencies. Complex MASH Σ - Δ modulators did not exhibit symmetrical noise-shaping spectra and were thus viable candidates for the generation of single side-band noise-shaping.

The FIR fractional delay double-, triple- and quadruple-stage bandpass MASH Σ - Δ modulators achieved similar SNRs and DRs in comparison with their real-coefficient FIR notch filter based counterparts. Moreover, they exhibited smoother magnitude spectra that contained fewer tones. This improvement, however, was accomplished at the price of slightly more complicated analogue loop-filters and digital cancellation circuitry.

The double-stage resonator/non-resonator based bandpass Σ - Δ modulator had several advantages compared with conventional bandpass MASH Σ - Δ modulators. First, this modulator required two simple digital notch filters instead of a more complicated bandstop filter at the output of the second-stage to suitably cancel the quantisation noise of the first-stage. Second, the second-stage output went through less digital processing due to the simplicity of the notch filters resulting in fewer cumulative multi-levels in the output signal. This imposed fewer restrictions on the design specifications of the decimation filter. Third, the coincidental zeros of the first-stage NTF in combination with the distributed zeros of the second-stage NTF ensured a deep as well as a relatively wide-band notch in the signal region. This had the benefit of providing respectable in-band SNRs for closely-spaced multi-tone input signals. Fourth, the quantisation noise of the first-stage had a smaller magnitude and was less tonal, because it was noise-shaped by a fourth-order Σ - Δ modulator, thus making this topology more immune to component imperfections. Fifth, the second-stage quantiser would not be overloaded for high-amplitude inputs, because of the even distribution of the poles and zeros of the second-stage loop-filter. The main drawback of this Σ - Δ MASH modulator was that some scaling coefficients were needed in the first-stage for non-mid-band centre frequencies to control the internal signal amplitudes in the feedforward path. The SNRs of this modulator were shown to significantly outperform those of the 2-2 MASH Σ - Δ modulator.

The advantages of the double-stage single-loop inverse comb-bandpass filter based Σ - Δ modulators were: First, it contained a multiplier-free loop-filter in the first-stage, which was capable of producing noise-shaping at a variety of centre frequency locations.

Second, the digital cancellation filter at the output of second-stage did not use any multipliers. This resulted in simpler and fewer cumulative multi-levels in the output signal. Third, the quantiser in the first-stage did not become overloaded for large-amplitude inputs or non-mid-band centre frequencies, circumventing the need for scaling coefficients to control stability. The main disadvantage of this MASH topology was that the first-stage produced redundant notches. The presence of too many notches due to a high-order loop-filter increased the amplitude level of the out-of-band quantisation noise, making the modulator more susceptible to instability.

The benefits of the double-stage double-loop inverse comb-bandpass based Σ - Δ modulators were: First, it provided a deeper notch with better resolution without using any multipliers. Second, the presence of a double-loop modulator in the first-stage caused the overall modulator output to be less tonal. Third, this modulator was more tolerant to component mismatches, because any leaked quantisation noise that might be transmitted in the second-stage was noise-shaped by twice the order. Fourth, the digital cancellation circuitry did not require any multipliers, thus simplifying the hardware structure of the modulator. Fifth, fewer multi-level outputs were produced with this modulator due to the simplicity of the comb filters. However, two drawbacks existed with this Σ - Δ modulator topology. First, the use of a double-loop inverse comb filter in the first-stage resulted in better resolution for the redundant noise-shaping bands as well as the desired signal-band. Second, the out-of-band quantisation noise magnitude was increased in proportion to the number of noise-shaping bands. As a result, this imposed tighter requirements on the digital decimators.

In summary, a comparative study was given based on a mixture of linear modelling, behavioural level simulations as well as SNRs and DRs. In addition, a library in Simulink containing over 33 different combinations of these Σ - Δ modulator topologies was created. The required modulator coefficients to meet any set of specifications were obtained by running an associated *m-file*, which was written by the author.

Chapter 4

Multi-Band Bandpass Σ - Δ Modulators

4.1 Introduction to Multi-Band Σ - Δ Modulators

Work reported to-date has focused on single-band noise-shaping Σ - Δ modulators. This chapter provides the design analysis and detailed behavioural-level simulations of a novel class of programmable narrow-band bandpass Σ - Δ modulators, that can achieve concurrent multiple noise-shaping bands for multi-tone input signals. Five different design methodologies based on the noise transfer functions of comb filters, slink filters, fractional-delay comb filters, FIR multi-notch filters and IIR multi-bandstop filters, are applied for the design of these multiple-band Σ - Δ modulators. A tree structure summarising all these techniques is shown below in Figure 4.1.

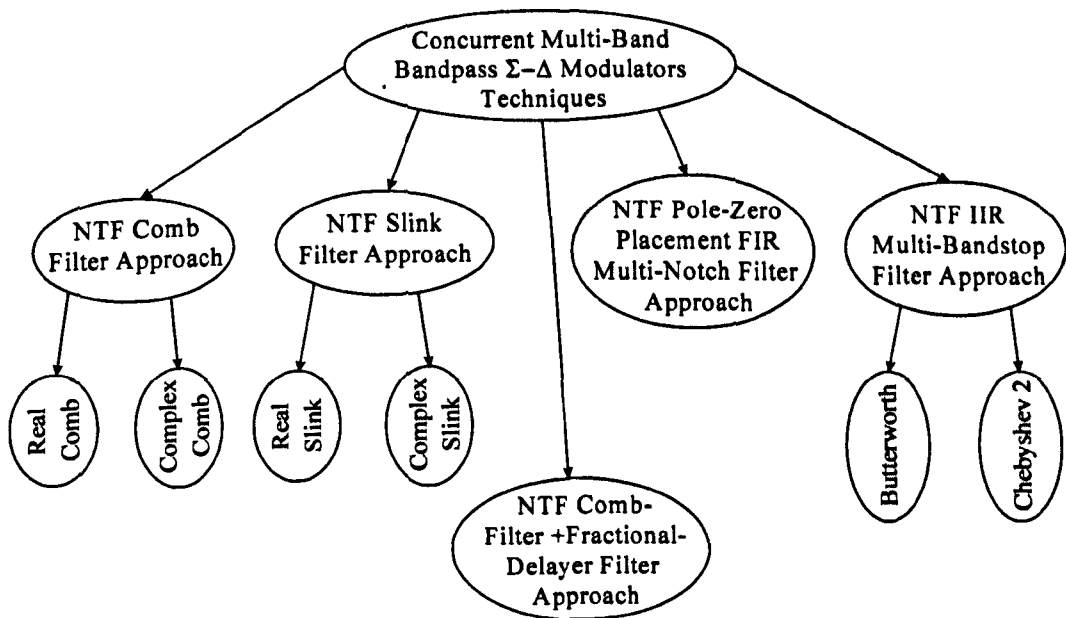


Figure 4.1 Different Techniques for the Design of Multi-Band Bandpass Σ - Δ Modulators

Comb filters [Cun92]-[Pro92] provide both a simple and cheap option of generating concurrent multiple noise-shaping bands when employed in the design of Σ - Δ modulators. The number and location of these bands is dependent on the order of the comb filter.

However, their main drawback is that only a limited range of multiple noise-shaping band combinations is attainable.

The second technique circumvents this limitation to a certain extent by substituting comb filters with slink filters, with the latter containing more adjustable multiplier-free parameters. This has the advantage of accomplishing more null combinations for the NTF without employing any multipliers.

The use of FIR or allpass IIR fractional delay filters in conjunction with comb filters can achieve multi-band noise-shaping for any equi-spaced combination of centre frequencies, overcoming the constraints imposed by the comb or slink filter approaches. This improvement, however, is achieved at the expense of using multipliers for the fractional delay filters.

The fourth technique utilises single-block multiple notch-filters to generate the necessary nulls for any combination of non-equi-spaced as well as equi-distant noise-shaping bands.

In the fifth technique, bandstop Butterworth or Chebyshev 2 filters are used to characterise the NTFs. These have the benefit of enabling the designer to specify the signal bandwidths, the stop-band attenuation together with the provision for non-equi-spaced band locations.

The merits and drawbacks of each technique for a variety of Σ - Δ modulator topologies are assessed in terms of in-band SNRs, accuracy of the noise-shaping band location and coefficient complexity for ease of implementation.

The SNR routine discussed in Section 1.13.2 was developed so as to allow it to simultaneously determine the in-band SNR for each band in these Σ - Δ modulators. This involved subtracting the input signals from the modulator output, thus retaining the quantisation noise in the in-band region for each signal band. If this method did not work properly, then a second procedure was employed, where the bins that represented the input signal in each band were removed. The SNR for each band was then calculated by simply evaluating the ratio of the signal power to that of the in-band quantisation noise power.

4.2 Applications for Multi-Band Σ - Δ Modulators

Multi-band A/D converters may be well suited for the simultaneous A/D conversion of multi-tone input signals for telecommunication and commercial broadcasting systems, for both medium to high resolution applications, so that all subsequent signal processing

operations can be performed digitally. This leads to cheaper, more robust and easily testable communications systems.

A further promising application is in specialist high-quality instrumentation to yield accurate reproductions of signals with their periodic and aperiodic harmonics. In general, potential applications include systems, which require closely spaced filter banks [Nor93b].

4.3 Comb Filter Approach

This multiple noise-shaping technique employs comb-filters, whose conjugate zero-pairs are distributed around the unit-circle in the z -domain, to provide maximum in-band attenuation. The nulls of the comb filter are equi-spaced along the unit-circle and separated by frequency gaps of $1/m$ in width, where m is the filter order [Cun92]-[Pro92]. The Comb Filter noise transfer function $H_{CF}(z)$ is defined as

$$H_{CF}(z) = 1 + d z^{-m} \quad (4.1)$$

where d is a constant value that is set to ± 1 . The resultant loop $M_{CF}(z)$ and feedback $C_{CF}(z)$ transfer functions are:

$$M_{CF}(z) = \frac{1}{1 + d z^{-m}} \quad \text{and} \quad C_{CF}(z) = -d z^{-m} \quad (4.2)$$

The number of nulls for the NTF corresponds to the number of noise-shaping bands that are provided by the loop-filter. The Number of Bands (NB) is governed by the comb filter order and is given by

$$(2NB - 1) < m < (1 + 2NB) \quad (4.3)$$

The locations of these bands can be determined by finding the roots of the comb filter expression in (4.2). When d is $+1$, the zero positions are at $e^{j\pi(1+2k)/m}$, and when d is -1 , the zeros are located at $e^{\pm j2\pi k/m}$, where k is a positive integer. For example, selecting $m = 8$ and $d = 1$ result in four normalised frequency nulls at $1/16$, $3/16$, $5/16$ and $7/16$. These nulls are repeated at the corresponding conjugate frequencies, since only real filters are being considered in this section. The outcome is a total of eight symmetrical notches across the entire normalised frequency spectrum, which are positioned at $(\pm 1/16, \pm 3/16, \pm 5/16$ and $\pm 7/16)$. Similarly, when $m = 8$ and $d = -1$, the outcome is a total of eight equi-spaced nulls positioned at $(0, \pm 1/8, \pm 1/4, \pm 3/8$ and $1/2)$. Several combinations of narrow multi-bands can be obtained by choosing different values for m and d as shown in Table 4.1. Positive values of d result in equi-spaced centre frequency locations having odd multiples

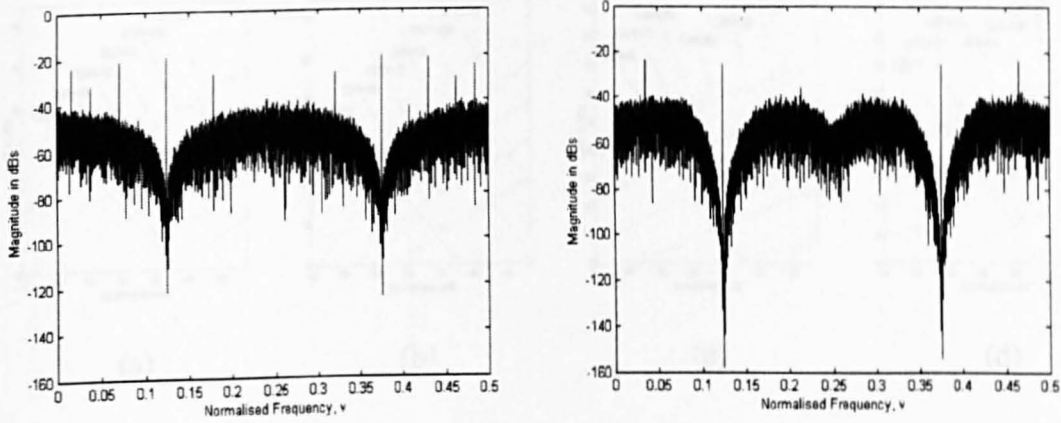
of $2m$, whereas negative values of d yield equi-distant centre frequency positions at even multiples of $2m$.

m	d	ν_c	d	ν_c
2	1	$\pm 1/4$	-1	0, 1/2
3	1	$\pm 1/6, 1/2$	-1	0, $\pm 1/3$
4	1	$\pm 1/8, \pm 3/8$	-1	0, $\pm 1/4, 1/2$
5	1	$\pm 1/10, \pm 3/10, 1/2$	-1	0, $\pm 1/5, \pm 2/5$
6	1	$\pm 1/12, \pm 1/4, \pm 5/12$	-1	0, $\pm 1/6, \pm 1/3, 1/2$
7	1	$\pm 1/14, \pm 3/14, \pm 5/14, 1/2$	-1	0, $\pm 1/7, \pm 2/7, \pm 3/7$
8	1	$\pm 1/16, \pm 3/16, \pm 5/16, \pm 7/16$	-1	0, $\pm 1/8, \pm 1/4, \pm 3/8$ & 1/2
9	1	$\pm 1/18, \pm 1/6, \pm 5/18, \pm 7/18, 1/2$	-1	0, $\pm 1/9, \pm 2/9, \pm 1/3, \pm 4/9$
10	1	$\pm 1/20, \pm 3/20, \pm 1/4, \pm 7/20, \pm 9/20$	-1	0, $\pm 1/10, \pm 1/5, \pm 3/10, \pm 2/5, 1/2$

Table 4.1 Loop-Filter and Feedback Filter Parameters for a Combination of Centre Frequencies for the Comb Filter Approach.

A closer inspection of Table 4.1 reveals that when $d = -1$ and m is an odd integer, one of the centre frequency bands is invariably positioned at dc. On the other hand, when $d = -1$ and m is an even integer, two of the noise-shaping bands always occur at both dc and Nyquist. Multi-band conventional comb filter based Σ - Δ modulators may be simpler to implement as they do not require any multipliers. Their main limitation, however, lies in the fact that only a finite number of noise-shaping bands is attainable.

A 4th-order double-band comb filter based Σ - Δ modulator was simulated using two sinusoids, whose input and dither amplitudes were 0.1 and 0.01 respectively. The magnitude spectrum of this modulator shown in Figure 4.2 exhibited several dominant tones, whose locations, amplitude and mode of repetition were related to the modulator input amplitudes.



(a)

(b)

Figure 4.2 Magnitude Spectrum of a Double-Band Comb Filter Based Σ - Δ Modulator Centred at $1/8$ & $3/8$, (a) Fourth-Order, (b) Eighth -Order.

Simulations showed that the amplitude level and concentration of these tones decreased as the dither amplitude increased. This particular modulator was tonal, because it contained a simple loop-filter that generated fewer state values. This enabled the modulator to generate identical patterns for its output signal in the time-domain. This corresponded to distinct spectral tones in the frequency-domain. The application of a large amount of dither significantly reduced the tonality content, but at the price of reducing the SNR. The SNRs in Figure 4.3 (a) exhibited non-linear characteristics, which were primarily attributed to the number and power of the tones, whose properties varied with respect to the input amplitudes. This comb filter approach was then extended to higher-order Σ - Δ modulators, where better SNRs were accomplished. The magnitude spectrum of an 8th-order double-loop single-bit comb filter based Σ - Δ modulator is shown in Figure 4.2(b). This spectrum exhibited fewer tones in the spectrum due to the presence of the extra loop-filter, which was responsible for causing greater quantisation noise de-correlation. The SNR characteristics of this modulator in Figure 4.3 show that the curves become non-linear for large-input amplitudes. This was caused by the excessive quantiser overloading, which resulted in the occurrence of more tones, especially in the signal region.

Figure 4.2 coupled with the simulation results shown in Figure 4.3, Figure 4.4 and Figure 4.5 indicate that performance improvements in terms of in-band SNRs and DRs are attained for both noise-shaping bands (i.e. $1/8$ and $3/8$) at the expense of more complicated loop-filters, feedback filters and multi-level quantisers.

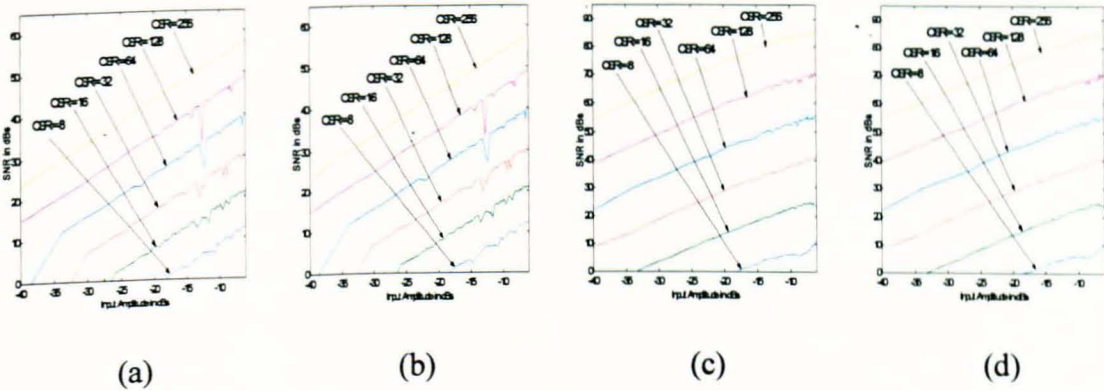


Figure 4.3 SNR Curves for Single-Bit Double-Band Comb Filter Based Σ - Δ Modulator (a) Single-Loop at $\nu_C = 1/8$, (b) Single-Loop at $\nu_C = 3/8$, (c) Double-Loop at $\nu_C = 1/8$, (d) Double-Loop at $\nu_C = 3/8$.

The SNR curves for the triple-band single-loop and double-loop comb filter based Σ - Δ modulators are shown in Figure 4.4 and Figure 4.5 respectively for all three bands. Simulations as well as the SNR curves in Figure 4.4 show that the single-loop modulator becomes unstable, when the amplitude of each of the three sinusoids exceeds -8 dB. The non-linearities at these amplitude are attributed to tones due to quantiser overloading. Moreover, simulation results showed that the occurrence of instability for the double-loop modulator was sharper. This is confirmed by the steep drop of the SNR values as soon as the modulator reaches its maximum stable input amplitude.

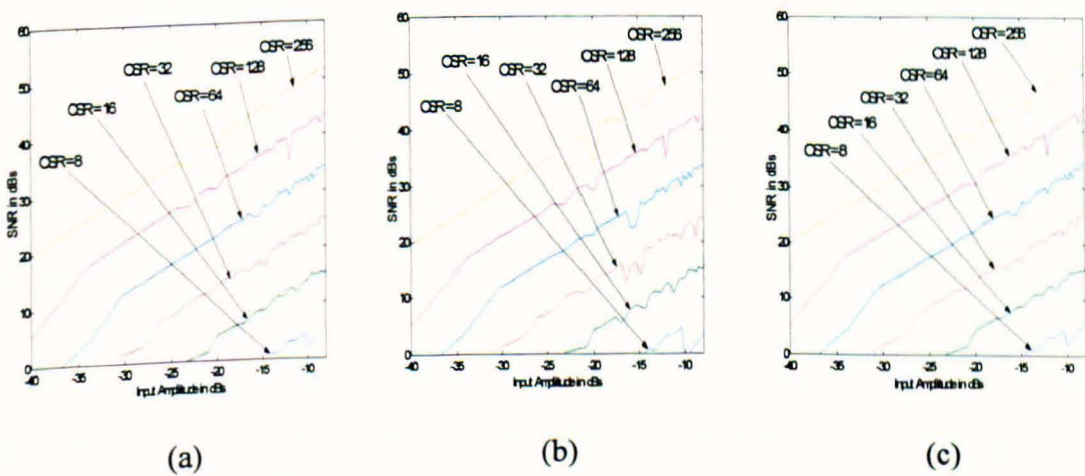


Figure 4.4 SNR Curves for Single-Loop Single-Bit Triple-Band Comb Filter Based Σ - Δ Modulator at (a) $\nu_C = 1/12$, (b) $\nu_C = 1/4$, (c) $\nu_C = 5/12$.

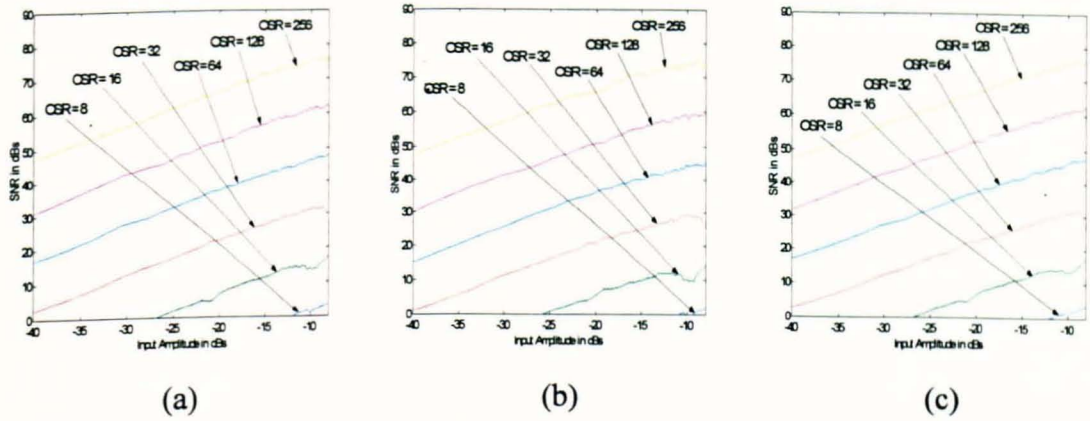


Figure 4.5 SNR Curves for Double-Loop Single-Bit Triple-Band Comb Filter Based Σ - Δ Modulator at (a) $\nu_C = 1/12$, (b) $\nu_C = 1/4$, (c) $\nu_C = 5/12$.

4.4 Complex Comb Filter Approach (CCFA)

Alternative sets of noise-shaping bands can be accomplished by employing Complex Comb Filters for the noise transfer function $H_{CCF}(z)$. The zeros of $H_{CCF}(z)$ are equi-distanced along the unit-circle and segregated by frequency gaps of $1/m$ in width, where m is the filter order [Cun92]-[Pro92]. $H_{CCF}(z)$ is given by:

$$H_{CCF}(z) = 1 - j d z^{-m} \quad (4.4)$$

where d is a constant value that can be set to $+1$, -1 , $+j$ or $-j$. The resultant loop $L_{CCF}(z)$ and feedback $F_{CCF}(z)$ transfer functions are:

$$L_{CCF}(z) = \frac{1}{1 - j d z^{-m}} \quad \text{and} \quad B_{CCF}(z) = j d z^{-m} \quad (4.5)$$

Complex comb filters cause their spectral null locations to be spectrally shifted by $\pm(\pi m/2)$ compared with real comb filters, thus creating new multi-band combinations. For the d values -1 , $+1$, $-j$ and $+j$, the corresponding zeros of $H_{CCF}(z)$ are located at $e^{j(1+4k)\pi/2m}$, $e^{-j(1+4k)\pi/2m}$, $e^{\pm j2\pi k/m}$ and $e^{j\pi(1+2k)/m}$ respectively, where k is an integer.

For example, selecting $m = 3$ and $d = 1$ result in three normalised frequency nulls at $(1/12$, $5/12$ and $-1/4)$ as can be seen from Table 4.2.

m	d	v_c	d	v_c
3	1	1/12, 5/12, -1/4	-1	1/4, -1/12, -5/12
3	j	$\pm 1/6, 1/2$	-j	0, $\pm 1/3$
4	1	1/16, 5/16, -3/16, -7/16	-1	3/16, 7/16, -1/16, -5/16
4	j	$\pm 1/8, \pm 3/8$	-j	0, $\pm 1/4, 1/2$
5	1	1/20, 1/4, 9/20, 3/20, -7/20	-1	3/20, 7/20, -1/20, 1/4, -9/20
5	j	$\pm 1/10, \pm 3/10, 1/2$	-j	$\pm 1/5, \pm 2/5$
6	1	1/24, 5/24, 9/24, -3/24, -7/24, -11/24	-1	3/24, 7/24, 11/24, -1/24, -5/24, -9/24
6	j	$\pm 1/12, \pm 1/4, \pm 5/12$	-j	0, $\pm 1/6, \pm 1/3, 1/2$

Table 4.2 Loop-Filter & Feedback Filter Parameters for a Combination of Centre Frequencies for CCFA.

Similarly, when $m = 3$ and $d = -1$, the outcome is a total of three different equi-spaced nulls positioned at (1/4, -1/12 and -5/12). When $d = \pm j$, $H_{CCF}(z)$ becomes a real-coefficient comb filter, which can deliver a different set of centre frequency bands (only restricted to conjugate pairs). Several more multi-band combinations can be obtained by choosing suitable values for m and d as shown in Table 4.2, where a complex-coefficient comb filter is seen to offer a wider range of distinct centre frequency nulls for the same filter order compared with its real-coefficient counterpart.

The magnitude spectra of a second-order and fourth-order double-band complex comb filter based Σ - Δ modulator centred at -1/8 & 3/8 are shown below in Figure 4.6.

The spectrum of the complex 2nd-order Σ - Δ modulator shown in Figure 4.6 (a) contained many tones. The power of these tones decreased as the amplitude of the injected dither at the quantiser inputs was increased. However, this modulator exhibited more tones than its real coefficient counterpart and required significantly more dither to suppress these tones. The spectrum of the complex 4th-order Σ - Δ modulator shown in Figure 4.6 (b) contained fewer tones and was shown to provide greater quantisation noise attenuation in the in-band region.

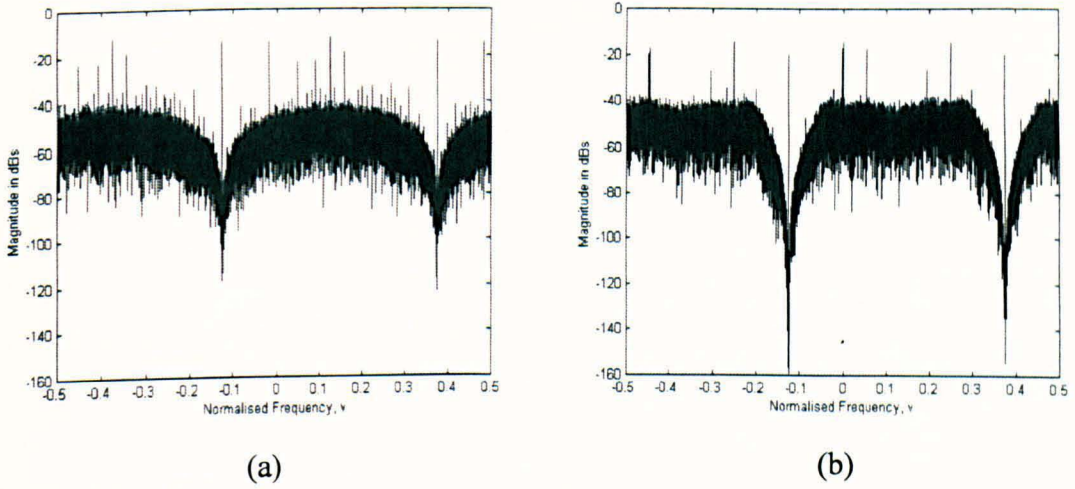


Figure 4.6 Magnitude Spectra of a Double-Band Complex Comb Filter Based $\Sigma-\Delta$ Modulator Centred at $-1/8$ & $3/8$, (a) Second-Order, (b) Fourth-Order.

The non-linear characteristics of the SNR curves for the single-loop modulator in Figure 4.7 demonstrated once again the effect of tones. These tones were shown to diminish in both amplitude and number for the double-loop case as was shown in Figure 4.6(b). The SNR characteristics verified that this observation by showing greater linearity until the quantiser became overloaded due to the large amplitude modulator inputs. The non-linearities in Figure 4.8 are attributed to the emergence of tones due to quantiser overloading. However, the SNR curves in Figure 4.9 display fewer non-linearities as a result of the larger de-correlation of the quantisation noise.

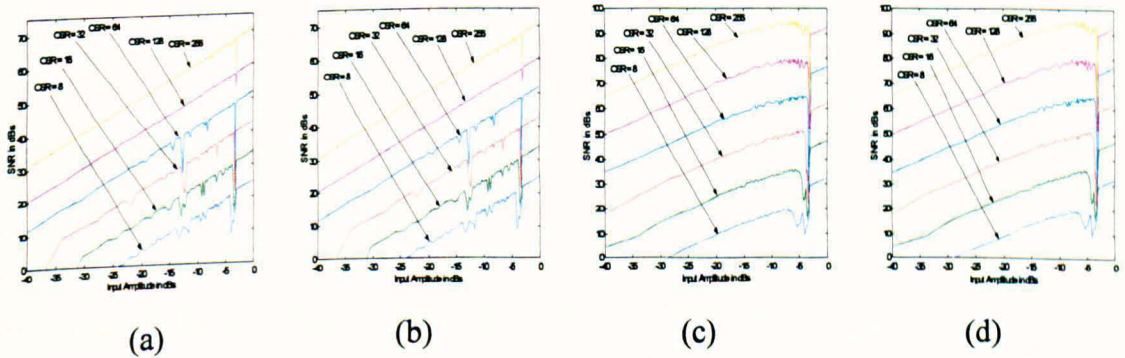


Figure 4.7 SNR Curves for Single-Bit Double-Band Complex Comb Filter Based $\Sigma-\Delta$ Modulator (a) Single-Loop at $\nu_C = -1/8$, (b) Single-Loop at $\nu_C = 3/8$, (c) Double-Loop at $\nu_C = -1/8$, (d) Double-Loop at $\nu_C = 3/8$.

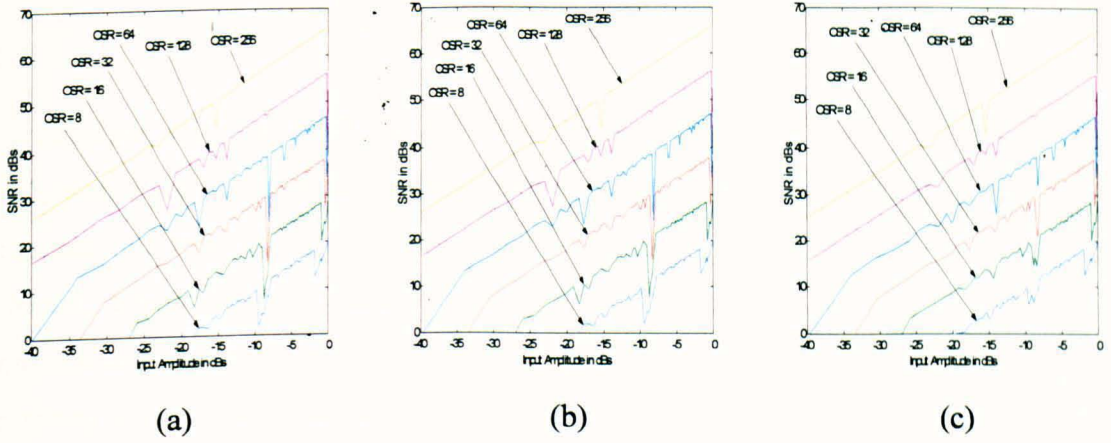


Figure 4.8 SNR Curves for Single-Loop Single-Bit Triple-Band Comb Filter Based Σ - Δ Modulator at (a) $\nu_C = 1/12$, (b) $\nu_C = 5/12$, (c) $\nu_C = -1/4$.

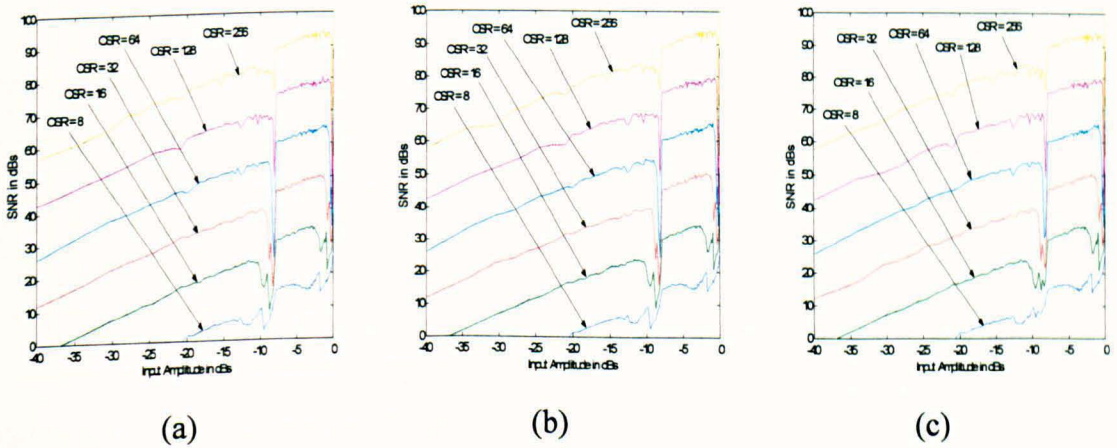


Figure 4.9 SNR Curves for Double-Loop Single-Bit Triple-Band Comb Filter Based Σ - Δ Modulator at (a) $\nu_C = 1/12$, (b) $\nu_C = 5/12$, (c) $\nu_C = -1/4$.

4.5 Slink Filter Approach

The second multiple noise-shaping approach employs slink filters [Cun92]-[Mor94] in which the nulls occur periodically across the frequency band of the Slink Filter based noise transfer function $H_{SF}(z)$. This is given by

$$H_{SF}(z) = \frac{1 - s z^{-L(R+1)}}{1 - t z^{-L}} \quad (4.6)$$

where R is the number of nulls and L is the order of null repetition in the normalised frequency range $-0.5 \leq \nu \leq 0.5$. The resultant loop-filter $M_{SF}(z)$ and feedback filter $C_{SF}(z)$ transfer functions are:

$$M_{SF}(z) = \frac{1 - z^{-LR}}{1 - z^{-L(R+1)}} \quad \text{and} \quad C_{SF}(z) = z^{-L} \quad (4.7)$$

For example, selecting $R = 2$ and $L = 4$ result in two fundamental nulls centred at $1/12$ and $2/12$, which are then repeated at the corresponding image and conjugate frequencies. The outcome is a total of eight symmetrical notches across the entire normalised frequency interval, which are positioned at $(\pm 1/12, \pm 2/12, \pm 4/12$ and $\pm 5/12)$. This example demonstrates that many combinations of multi-band centre frequencies can be obtained by choosing appropriate values for R and L . More examples are presented in Table 4.3.

m	R	L	s	t	ν_C	m	R	L	s	t	ν_C
4	3	1	-1	-1	$\pm 1/4, 1/2$	9	2	3	-1	-1	$\pm 1/9, \pm 2/9, \pm 3/9$
4	3	1	-1	1	$0, \pm 1/4$	9	2	3	1	1	$\pm 1/18, \pm 5/18, \pm 7/18$
5	4	1	-1	-1	$\pm 1/5, \pm 2/5$	8	3	2	-1	-1	$\pm 1/8, \pm 1/4, \pm 3/8$
5	4	1	1	1	$\pm 1/10, \pm 3/10$	6	5	1	-1	1	$0, \pm 1/6, \pm 1/3$
6	2	2	-1	-1	$\pm 1/6, \pm 1/3$	6	5	1	1	-1	$\pm 1/6, \pm 1/3, 1/2$
6	2	2	1	1	$\pm 1/12, \pm 5/12$	12	1	6	-1	-1	$\pm 1/12, \pm 1/4, \pm 5/12$
-	-	-	-	-	-	7	6	1	-1	-1	$\pm 1/7, \pm 2/7, \pm 3/7$

Table 4.3 Loop-Filter and Feedback Filter Parameters for a Combination of Centre Frequencies for the Slink Filter Approach.

More equi-spaced noise-shaping band combinations can be achieved using this approach, because slink filters contain more adjustable multiplier free parameters compared with comb filters. This improvement is achieved at the price of having to use higher-order loop-filters in some cases. For instance, a ninth-order loop-filter is needed to perform noise-shaping at $\nu_C = \pm 1/9$, $\nu_C = \pm 2/9$ and $\nu_C = \pm 3/9$. On the other hand, an equi-spaced three-band specification such as $\nu_C = \pm 1/7$, $\nu_C = \pm 2/7$ and $\nu_C = \pm 3/7$ only requires a sixth-order loop-filter.

Figure 4.10 shows that the magnitude spectrum of a fifth-order double-band slink filter based Σ - Δ modulator for sinusoidal inputs and dither amplitudes of 0.1 and 0.01 respectively. The uneven distribution of the out-of-band quantisation noise is attributed to the ratio of the peak amplitudes of the main-to-side lobes of the slink filter.

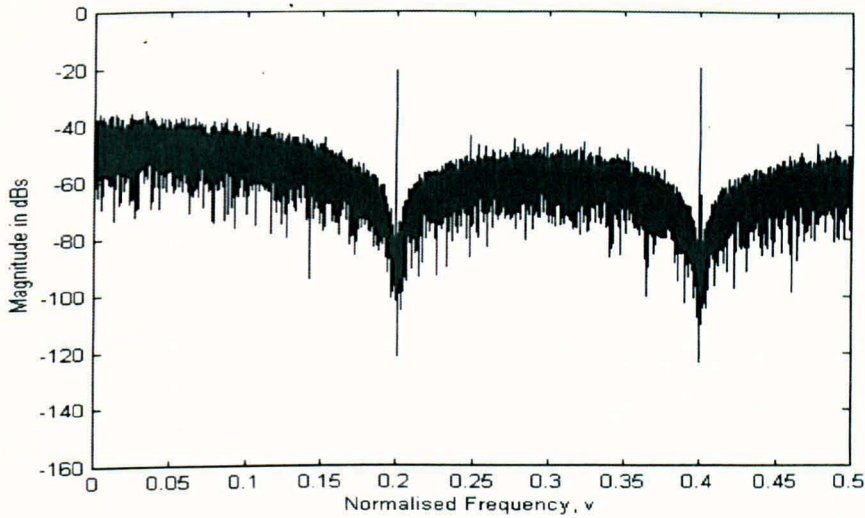


Figure 4.10 Magnitude Spectra of a Fifth-Order Double-Band Slink Filter Based Σ - Δ Modulator Centred at $1/5$ & $2/5$.

The in-band SNR curves corresponding to the double-band double-loop slink filter based Σ - Δ modulator are shown in Figure 4.11. The modulator became unstable for input amplitudes exceeding -8 dB. This is attributed to the quantiser overloading. This modulator produced fewer tones compared with the single-loop case.

This technique was then extended to design triple-band slink filter based modulators to achieve noise-shaping at $\nu_c = 1/9$, $\nu_c = 2/9$ and $\nu_c = 4/9$ respectively. The SNR curves for this triple-band Σ - Δ modulator are illustrated in Figure 4.12.

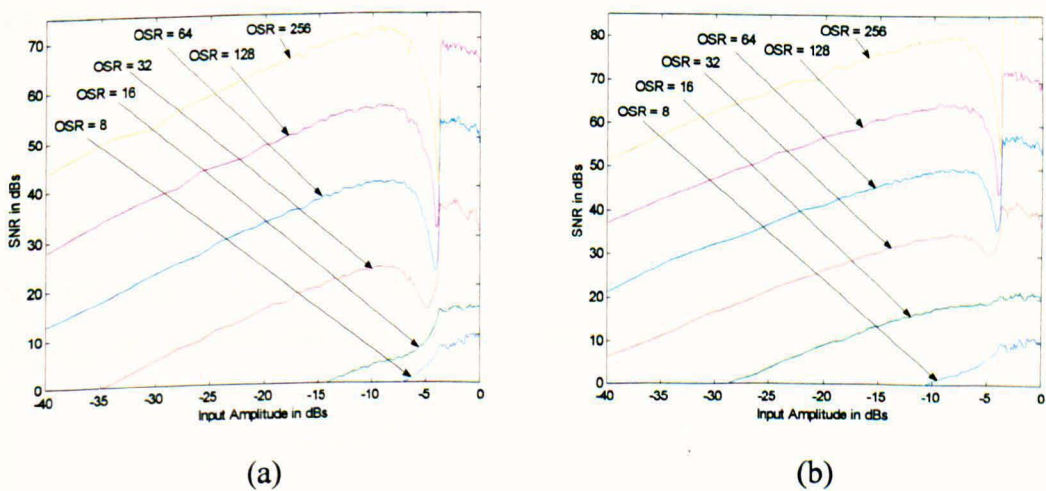


Figure 4.11 SNR Curves for Single-Bit Double-Band Slink Filter Based Σ - Δ Modulator (a) Single-Loop at $\nu_c = 1/5$, (b) Single-Loop at $\nu_c = 2/5$, (c) Double-Loop at $\nu_c = 1/5$, (d) Double-Loop at $\nu_c = 2/5$.

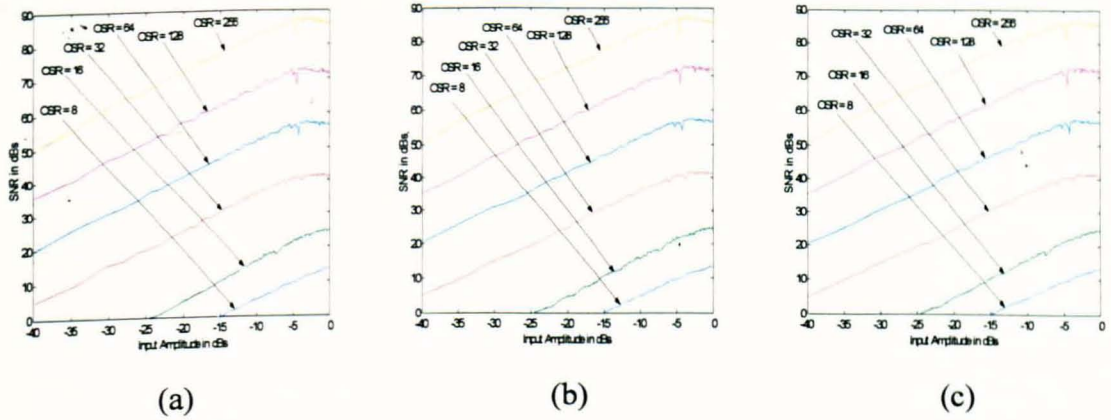


Figure 4.12 SNR Curves for Double-Loop Single-Bit Triple-Band Comb Filter Based Σ - Δ Modulator at (a) $\nu_C = 1/9$, (b) $\nu_C = 2/9$, (c) $\nu_C = 4/9$.

It should be stated that the uneven distribution of the out-of-band quantisation noise in Figure 4.10 is attributed to the ratio of the peak amplitudes of the main-to-side lobes of the slink filter. Further simulations demonstrate that an almost 2-bit improvement in resolution can be obtained by raising the number of levels of the quantiser from 2 to 5.

Unfortunately; comb and slink filter based Σ - Δ modulators can only be used for equi-spaced multi-band applications.

4.6 Complex Slink Filter Approach (CSFA)

This multiple noise-shaping approach employs Complex Slink Filters [Mor94]-[Cun92]-[Pro92], in which the nulls occur at periodic intervals across the frequency spectrum of the noise transfer function $H_{CSF}(z)$. This is given by

$$H_{CSF}(z) = \frac{1 - j s z^{-L(R+1)}}{1 + j s z^{-L}} \quad (4.8)$$

where R is the number of nulls, L is the order of null repetition in the normalised frequency range $-0.5 \leq \nu \leq 0.5$ and s could be set to either +1 or -1. The resultant loop-filter $L_{CSF}(z)$ and feedback filter $B_{CSF}(z)$ transfer functions are:

$$L_{CSF}(z) = \frac{1 + z^{-LR}}{1 - j s z^{-L(R+1)}} \quad \text{and} \quad B_{CSF}(z) = j s z^{-L} \quad (4.9)$$

Extra positioning of centre-frequency bands is achieved by controlling an additional parameter L as well as R and s of $H_{CSF}(z)$. For example, selecting $L = 4$, $R = 2$ and $s = 1$

result in four equi-spaced nulls centred at $1/24$, $5/24$, $-7/24$ and $-11/24$. More examples are given in Table 4.4.

L	R	s	ν_C
1	2	1	$1/12, 5/12$
1	4	1	$1/20, 9/20, -3/20, -7/20$
2	2	1	$1/24, 5/24, -7/24, -11/24$
2	2	-1	$7/24, 11/24, -1/24, -5/24$
3	2	1	$1/36, 5/36, 13/36, 17/36, -7/36, -11/36$

Table 4.4 Loop-Filter & Feedback Filter Parameters for a Combination of Centre Frequencies for CSFA.

Extensive simulations have shown that greater flexibility in the selection of noise-shaping bands is accomplished by employing complex slink filters for the noise transfer function, where an example demonstrating the correct operation of this approach is shown in Figure 4.13.

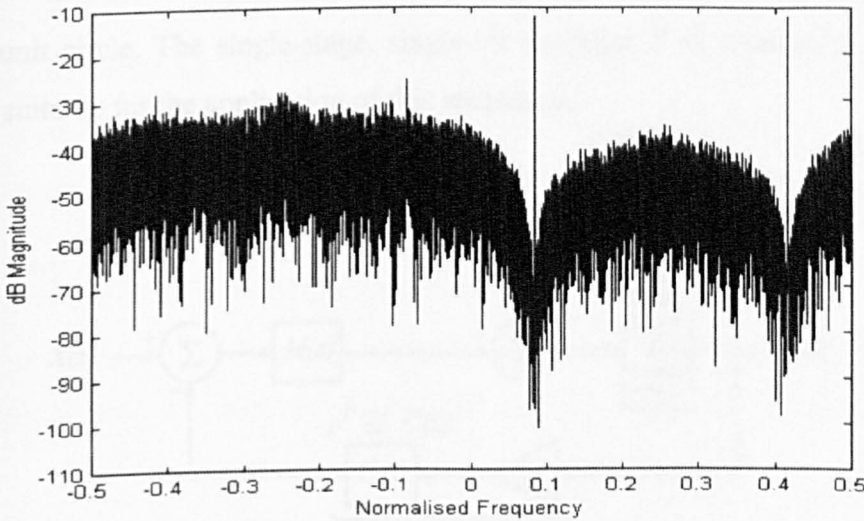


Figure 4.13 Magnitude Spectra of a Fifth-Order Double-Band Complex Slink Filter Based Σ - Δ Modulator Centred at $1/5$ & $2/5$.

The in-band SNRs corresponding to single-loop and double-loop complex slink-filter based Σ - Δ modulators are shown in Figure 4.14. The complex single-loop slink filter based Σ - Δ modulator exhibited more in-band tones as reflected by the non-linearity of the SNR curves in Figure 4.14. On the other hand, the complex double-loop Σ - Δ modulator

displayed smoother SNR curves due to the presence of fewer tones. However, the modulator became unstable more abruptly. This was due to the larger amplitudes of the internal signals of the modulator.

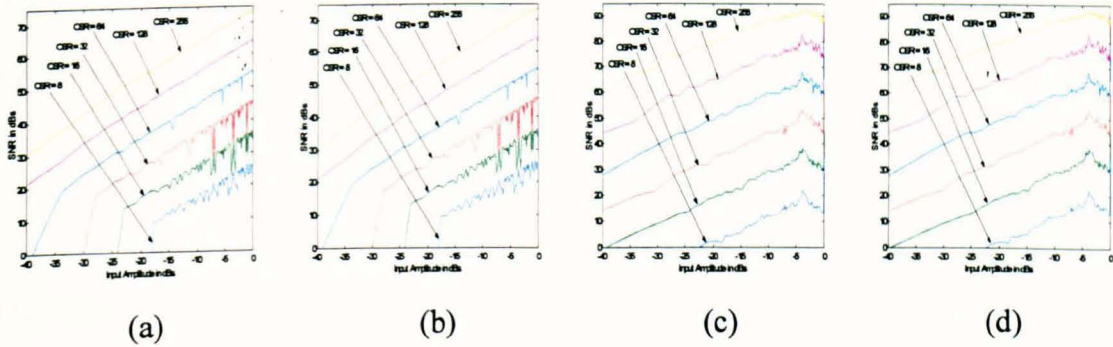


Figure 4.14 SNR Curves for Single-Bit Double-Band Complex Slink Filter Based Σ - Δ Modulator (a) Single-Loop at $\nu_C = 1/12$, (b) Single-Loop at $\nu_C = 5/12$, (c) Double-Loop at $\nu_C = 1/12$, (d) Double-Loop at $\nu_C = 5/12$.

4.7 Comb Filter Fractional-Delay Approach

Comb filters combined with fractional delays [Laa96]-[Pei98] form the new Fractional Delay noise transfer function $H_{FD}(z)$, whose zeros can be distributed anywhere in the unit circle. The single-stage, single-bit bandpass Σ - Δ modulator shown in Figure 4.15 is suitable for the application of this technique.

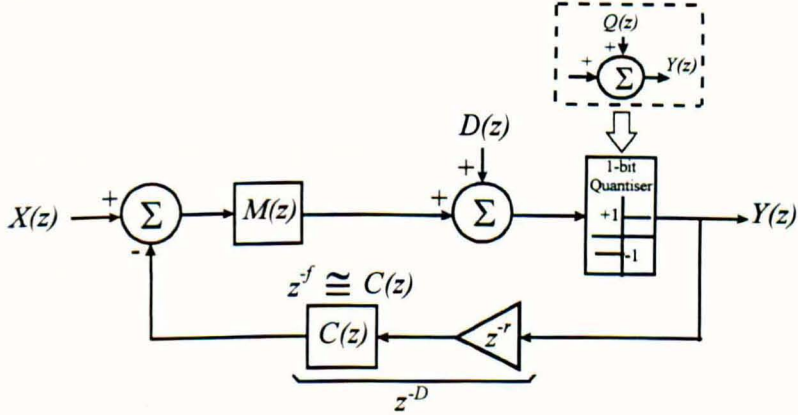


Figure 4.15 Proposed FDF based Multi-Band Σ - Δ Modulator.

This structure consists of a multi-variable centre frequency loop-filter $M(z)$ and a 1-bit quantiser in the feedforward path as well as a cascade combination of a variable bulk delay z^{-r} and FD filter $T(z) \cong z^{-f}$ in the feedback path. Also, an amplitude of 0.1 of random dither $D(z)$ is added prior to the quantiser input to reduce spurious tones [Dun96a]. The conventional means of analysing the noise-shaping properties of dithered Σ - Δ

modulators involve modelling the 1-bit non-linear quantiser by an equivalent additive white noise source that is statistically independent of the input. This linearised approach though not very accurate, delivers results which are representative [Can92]-[Azi96]-[Jan96b]. The signal $H_S(z)$ and noise $H_N(z)$ transfer functions of this dithered linearised system are:

$$H_S(z) = \frac{M(z)}{1 + z^{-r} T(z) M(z)} \quad \text{and} \quad H_N(z) = \frac{1}{1 + z^{-r} T(z) M(z)} \quad (4.10)$$

The filter order m of $H_N(z)$ is replaced by a generalised non-integer value D . The parameter D can be expressed as the summation of two variables (i.e. $D = f + r$), where f is the delay of the FD filter itself (including the fractional component) and r is the additional integer delay required to satisfy the design specification. The new expression for $H_N(z)$ is

$$H_N(z) = 1 + cz^{-(r+f)} \quad (4.11)$$

Simple mathematical analysis demonstrates that when $c = -1$, the zeros of $H_N(z)$ are placed at $e^{\pm 2\pi k/(r+f)}$ and when $c = +1$, the zeros are located at $e^{\pm \pi(1+2k)/(r+f)}$. This implies that any equi-distanced combination of centre frequencies can be obtained by determining the necessary total delay D that must be incorporated in $H_N(z)$, so that the nulls of the modified comb filter are spectrally shifted to the corresponding signal bands.

4.8 FIR Fractional-Delay Multi-Band Σ - Δ Modulator

The maximally flat Lagrange interpolation method is used here to design an FIR filter for approximating the fractional-delay filter [Laa96], whose coefficients $h(k)$ are defined as:

$$h(k) = \prod_{n=0, n \neq k}^N \frac{D-n}{k-n}, \quad k = 0, 1, \dots, N. \quad (4.12)$$

The Lagrange approximation is the most suitable for use in Σ - Δ modulators, because the peak of its magnitude never exceeds unity [Laa96]. This particular feature substantially alleviates the occurrence of instability. The new expression for $H_N(z)$ including the FIR FD filter becomes:

$$H_N(z) = 1 + cz^{-r} H_{FIR}(z) \quad (4.13)$$

The resultant loop and feedback filters are:

$$M(z) = \frac{1}{1 + cz^{-r} H_{FIR}(z)} \quad \text{and} \quad T(z) = -cz^{-r} H_{FIR}(z) \quad (4.14)$$

The order of the numerator and denominator of these FD approximations are the same, which means that r must have a minimum value of 1 to satisfy the causality criterion [Jan91]. For example, there are six feasible alternatives of representing D when it is equal to 6.4, two of which are shown in Table 4.5. When $D = 6.4$, the FIR FD approximation is given by,

$$H_{FIR}(z) = h_0 + h_1 z^{-1} + h_2 z^{-2} + \dots + h_{10} z^{-10} + h_{11} z^{-11} \quad (4.15)$$

A distinction must be made between the actual order of the FD filter and its associated group delay [Laa96]. It is seen from Table 4.4 that an FD specification of 4.4 can be achieved with a tenth-order FIR filter. Note that the FIR FD filter does not have a linear phase (except when $FD = 0.5$) due to the asymmetry of the coefficients of $H_{FIR}(z)$. The coefficients for some of the FIR FD filter approximations are shown in Table 4.4.

f	4.4	5.4	f	4.4	5.4
r	2	1	r	2	1
h_0	0.0005	-0.0001	h_6	-0.1202	0.4848
h_1	-0.0061	0.0016	h_7	0.0317	-0.1299
h_2	0.0344	-0.0102	h_8	-0.0057	0.040
h_3	-0.1374	0.0433	h_9	0.0005	-0.0096
h_4	0.7214	-0.1484	h_{10}	0	0.0015
h_5	0.4809	0.7272	h_{11}	0	-0.0001

Table 4.5 Loop & feedback filter coefficients for the FIR FD approach for ($D = 6.4$).

Extensive behavioural level simulations as will be seen in Section 4.10 demonstrate that a significant amount of quantisation noise is retained in the in-band signal region at frequencies close to Nyquist. This noise-shaping degradation is attributed to an inherent large magnitude error associated with FIR FD approximations at high frequencies. This error can be reduced by increasing the order of the FD approximation at the cost of large values of f and consequently using more coefficients.

4.9 Allpass IIR Fractional-Delay Multi-Band Σ - Δ Modulators

Alternatively; fractional delayers can be represented by the IIR allpass maximally flat group-delay approximation [Laa96]. The advantage being that an IIR digital filter can provide the same or even better specifications with fewer coefficients compared with FIR filters [Laa96]. Allpass filters have unity magnitude and much improved group delay responses for the entire frequency range [Laa96]. The filter coefficients of an N^{th} -order FD filter are:

$$\alpha_k = (-1)^k C_k^N \prod_{n=0}^N \frac{D-N+n}{D-N+k+n} \quad k = 0, 1, 2, \dots, N \quad (4.16)$$

The resultant loop and feedback filters are:

$$M(z) = \frac{1 + b_1 z^{-1} + \dots + b_{(N-2)} z^{-(N-2)} + b_{(N-1)} z^{-(N-1)}}{1 + a_1 z^{-1} + \dots + a_{(N-1)} z^{-(N-1)} + z^{-N}} \quad (4.17)$$

$$T(z) = -c z^{-r} \frac{\alpha_N + \alpha_{N-1} z^{-1} + \dots + \alpha_1 z^{-(N-1)} + z^{-N}}{1 + \alpha_1 z^{-1} + \dots + \alpha_{(N-1)} z^{-(N-1)} + \alpha_N z^{-N}} \quad (4.18)$$

Some of these coefficients are given below in Table 4.6:

f	1.4	2.4	3.4	4.4	5.4
r	5	4	3	2	1
α_1	-0.1667	-0.2353	-0.2727	-0.2963	-0.3125
α_2	0	0.0374	0.0707	0.0972	0.1182
α_3	0	0	-0.0088	-0.021	-0.0388
α_4	0	0	0	0.0021	0.0061
α_5	0	0	0	0	-0.0005
b_1	-0.1667	-0.2353	-0.2727	-0.2963	-0.3125
b_2	0	0.0374	0.0707	0.0972	0.1182
b_3	0	0	-0.0088	-0.021	-0.0388
b_4	0	0	0	0.0021	0.0061
b_5	0	0	0	0	-0.0005
a_1	-0.1667	-0.2353	-0.2727	-0.2963	-0.313
a_2	0	0.0374	0.0707	0.0993	0.1243
a_3	0	0	-0.0176	-0.042	-0.0776
a_4	0	0.0374	0.0707	0.0993	0.1243
a_5	-0.1667	-0.2353	-0.2727	-0.2963	-0.313

Table 4.6 Loop & Feedback Filter Coefficients for the Allpass IIR FD Approach for ($D = 6.4$).

Behavioural level simulations conducted for the fourth approach showed that the use of either FIR or IIR allpass FD filters combined with comb filters accomplish noise-shaping

for any combination of equi-spaced centre-frequency locations. The magnitude spectrum of a 12th-order triple-band FIR FD filter Σ - Δ modulator centred at 5/64, 15/64 & 25/64 is shown in Figure 4.16.

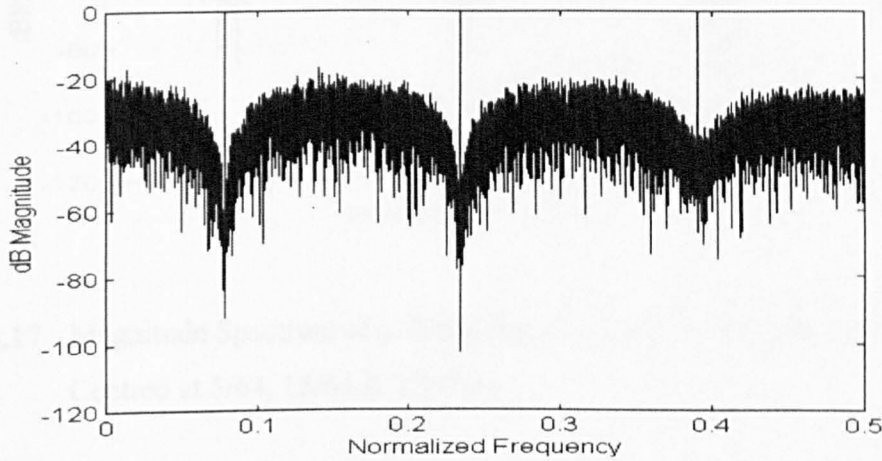


Figure 4.16 Magnitude Spectrum of a Twelfth-Order Triple-Band FIR FD Filter Σ - Δ Modulator Centred at 5/64, 15/64 & 25/64.

It is seen from Figure 4.16 that a significant amount of quantisation noise is retained in the in-band region at $f_c = 25/64$. This noise-shaping degradation is attributed to an inherent large magnitude error associated with FIR FD approximations at high frequencies. This error can be reduced by employing allpass IIR FD filter approximations.

Figure 4.17 shows that better noise-shaping is accomplished across the entire spectrum including high frequencies, when an allpass FD filter is employed. This improvement is attributed to the unity gain magnitude of the allpass FD filter. The third centre-frequency band, however, is marginally shifted to a slightly higher frequency. This inaccuracy can be attributed to an inferior group delay approximation at very high frequencies. Tunability at high frequencies can be more accurately represented by encompassing high-order allpass FD approximations.

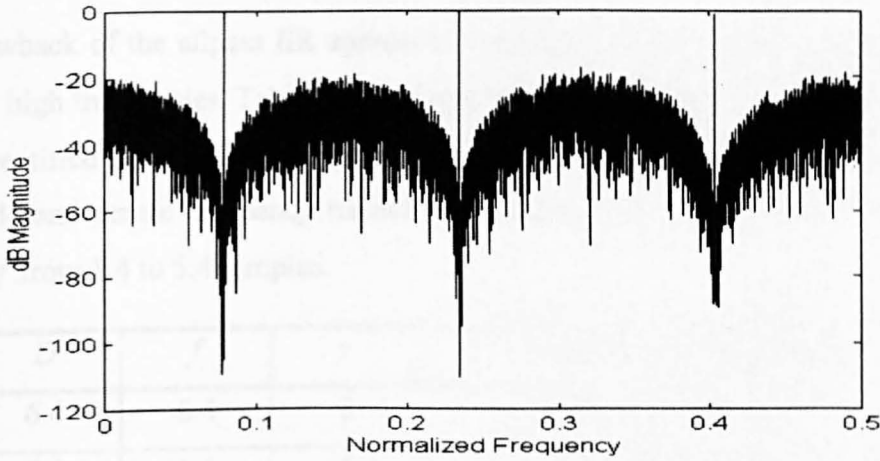


Figure 4.17 Magnitude Spectrum of a Triple-Band Allpass IIR FD Filter Σ - Δ Modulator Centred at $5/64$, $15/64$ & $129/320$.

Table 4.7 provides a comparison of the quantisation noise power in dBs between FIR and IIR allpass filters for different f and r permutations when $D = 6.4$.

f	r	$QF1$	$QA1$	$QF2$	$QA2$	$QF3$	$QA3$
1.4	5	-59.5	-58.4	-46.9	-44.6	-31.9	-40.7
2.4	4	-59.4	-59.9	-55.2	-50.0	-35.6	-45.1
3.4	3	-60.1	-59.2	-58.3	-55.8	-37.3	-48.2
4.4	2	-57.7	-56.9	-59.7	-57.1	-38.9	-53.3
5.4	1	-59.7	-56.4	-59.4	-57.6	-41.0	-60.8

Table 4.7 Quantisation Noise Power Comparison in dBs between Single-Stage FIR and Allpass IIR FD Filters Based Σ - Δ Modulators.

$QF1$, $QF2$ and $QF3$ are the in-band quantisation noise powers of the FIR FD approximation for the first, second and third bands respectively. Similarly, $QA1$, $QA2$ and $QA3$ represent the corresponding quantisation noise powers for the allpass IIR case. The in-band noise using the allpass IIR FD approximation decreases at a faster rate compared with the FIR FD case especially at high frequencies. For example, $QA3$ reduces by as much as 20 dBs when f increases from 1.4 to 5.4 samples confirming that superior signal-to-noise ratios are achieved with the allpass IIR case.

The drawback of the allpass IIR approach is the slight displacement of the noise-shaping bands at high frequencies. Table 4.8 confirms that this improper centre frequency tunability can be rectified by employing higher-order allpass IIR FD approximations. For instance, the third-band centre frequency tunability percentage error drops from 5.6% to 3% by raising f from 1.4 to 5.4 samples.

D	f	r	Normalised Frequencies
6.4	6.4	0	0.078, 0.234 and 0.391
6.4	1.4	5	0.078, 0.241 and 0.413
6.4	2.4	4	0.078, 0.237 and 0.410
6.4	3.4	3	0.078, 0.236 and 0.407
6.4	4.4	2	0.078, 0.235 and 0.405
6.4	5.4	1	0.078, 0.234 and 0.403

Table 4.8 Comparison of Centre Frequency Locations for Different Allpass IIR FD Approximations.

4.10 Multi-Notch Filter Approach

In multiple narrow-band bandpass Σ - Δ modulators, the noise-shaped band centres are designed by positioning the zeros of the Multi-Notch [Pro92] noise transfer function $H_{MN}(z)$ at the desired centre frequencies to provide maximum in-band attenuation. The zeros of $H_{MN}(z)$ are located at $e^{\pm j\alpha_1}$, $e^{\pm j\alpha_2}$... $e^{\pm j\alpha_P}$, where the α coefficients are chosen to centre the signal passbands. Note that $\alpha = 2\pi f_C / f_S$, where f_C is the designated centre frequency, f_S is the sampling frequency and P is the number of signal bands. The generalised case of $H_{MN}(z)$ for any number of bands is:

$$H_{MN}(z) = \prod_{i=0}^P (1 - c_i z^{-1} + z^{-2}) \quad (4.19)$$

where $c_i = 2 \cos \alpha_i$. For example, for a single-stage triple-band Σ - Δ modulator, it can be analytically shown that $M(z)$ and $C(z)$ for the Multi-Notch filter case are:

$$M_{MN}(z) = \frac{1}{1 - \beta_1 z^{-1} + \beta_2 z^{-2} - \beta_3 z^{-3} + \beta_2 z^{-4} - \beta_1 z^{-5} + z^{-6}} \quad (4.20)$$

$$C_{MN}(z) = -\beta_1 z^{-1} + \beta_2 z^{-2} - \beta_3 z^{-3} + \beta_2 z^{-4} - \beta_1 z^{-5} + z^{-6} \quad (4.21)$$

where $\beta_1 = (c_1 + c_2 + c_3)$, $\beta_2 = (3 + c_1 c_2 + c_1 c_3 + c_2 c_3)$ and $\beta_3 = 2(c_1 + c_2 + c_3) + c_1 c_2 c_3$. This analysis reveals that the coefficients of the feedback filter $C_{MN}(z)$ are dependent on the centre frequency. Concurrent multiple tunability of the modulator centre frequencies is achieved by varying the zero locations of $H_{MN}(z)$. This process is equivalent to the movement of the loop-filter poles along the unit circle to the chosen frequency locations. Table 4.9 presents the modulator coefficients for a combination of centre frequencies, showing this approach requires the use of multipliers for non-equi-spaced noise-shaping bands, which may complicate modulator implementation.

Normalised Centre Frequencies, ν_C	β_1	β_2	β_3
$\pm 1/7, \pm 2/7 \text{ \& } \pm 3/7$	1	1	1
$\pm 1/9, \pm 2/9 \text{ \& } \pm 4/9$	0	0	1
$\pm 1/8, \pm 2/8 \text{ \& } \pm 2/5$	-0.2	0.71	-0.41
$\pm 1/10, \pm 4/16 \text{ \& } \pm 7/16$	-0.23	0.01	-0.46
$\pm 1/16, \pm 4/16 \text{ \& } \pm 15/32$	-0.11	-0.63	-0.22

Table 4.9 Loop-Filter and Feedback Filter Coefficients for a Combination of Centre Frequencies using the Multi-Notch Approach.

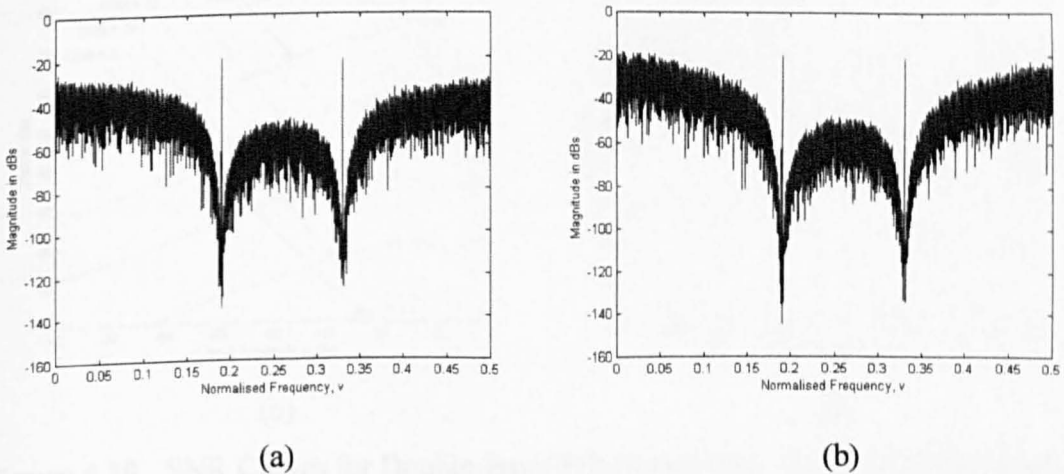


Figure 4.18 Magnitude Spectrum of a Double-Band Multi-Notch Filter Based Σ - Δ Modulator Centred at $\nu_C = 0.19$ and $\nu_C = 0.33$, (a) 1-1 MASH, (b) 1-1-1 MASH.

Simulations have verified that the multi-notch approach can achieve simultaneous multiple noise-shaping for any combination of equi-spaced and non-equi-spaced centre frequencies. This approach was extended to multi-stage topologies, where the magnitude spectrum of the double-stage and triple-stage MASH Σ - Δ modulators are shown in Figure 4.18. The complexity of the loop-filter as well as the presence of more than one stage resulted in substantial quantisation noise randomisation. This is reflected by the near absence of tones in the spectra shown in Figure 4.18.

The SNR plots shown in Figure 4.19 remained quite linear until the modulator reached its maximum stable input amplitude. The sharp drop in the SNR values is the result of modulator instability for large input-amplitude signals.

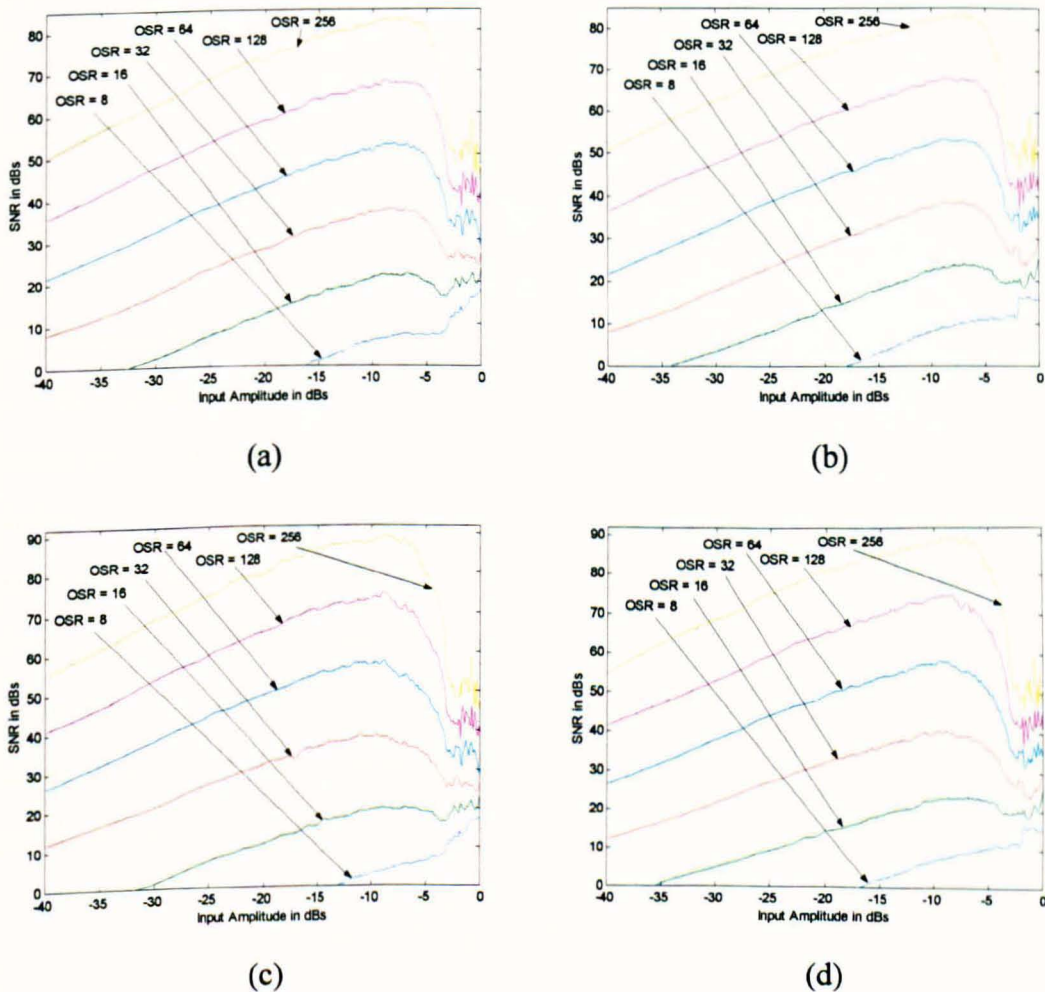


Figure 4.19 SNR Curves for Double-Band FIR Notch Filter Based Σ - Δ Modulator (a) 11 MASH at $\nu_C = 0.19$, (b) 11 MASH at $\nu_C = 0.33$, (c) 111 MASH at $\nu_C = 0.19$, (d) 111 MASH at $\nu_C = 0.33$.

Alternatively; the SNRs can be improved by increasing the number of levels in the quantiser of these multi-notch based Σ - Δ modulators. Quantisers with an odd number of

levels outperform those with an even number of levels, because of the presence of the zero threshold, which reduces the occurrence of oscillations for small amplitude signals. Nearly 2-bits in resolution are gained by increasing the number of levels from 2 to 5 for ν_C of 1/10 and 1/4. Furthermore, the dynamic range of this modulator was increased with the use of more quantiser levels.

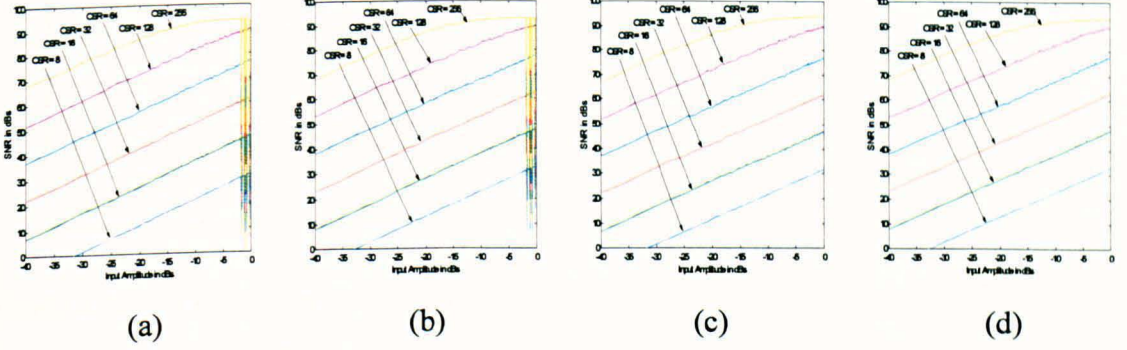


Figure 4.20 SNR Curves for Double-Loop Single-Bit Double-Band FIR Notch Filter Based Σ - Δ Modulator (a) 11-levels at $\nu_C = 0.19$, (b) 11-levels at $\nu_C = 0.33$, (c) 16-levels at $\nu_C = 0.19$, (d) 16-levels at $\nu_C = 0.33$.

4.11 Complex Multi-Notch Filter Approach (CMNFA)

The noise-shaped band centres in complex multiple narrow-band bandpass Σ - Δ modulators are designed by placing the zeros of the Complex Multi-Notch noise transfer function $H_{CMN}(z)$ at the specified centre frequencies on the unit circle, so as to ensure maximum in-band attenuation. This implies that the zeros of $H_{CMN}(z)$ are positioned at $e^{j2\pi\nu_1}$, $e^{j2\pi\nu_2}$... $e^{j2\pi\nu_P}$, where ν is the normalised centre-frequency of interest and P is the number of notches in $H_{CMN}(z)$. Since $H_{CMN}(z)$ is complex, ν could be either positive or negative. The general expression for $H_{CMN}(z)$ for any number of concurrent signal bands is:

$$H_{CMN}(z) = \prod_{i=0}^P (1 - \beta_i z^{-1}) \quad (4.22)$$

where $\beta_i = e^{j2\pi\nu_i}$. For example, the resulting transfer functions, for $L_{CMN}(z)$ and $B_{CMN}(z)$ for a single-loop triple-band multi-notch based Σ - Δ modulator are given by:

$$L_{CMN}(z) = \frac{1}{1 - (\beta_1 + \beta_2 + \beta_3) z^{-1} + (\beta_1\beta_2 + \beta_1\beta_3 + \beta_2\beta_3) z^{-2} - (\beta_1\beta_2\beta_3) z^{-3}} \quad (4.23)$$

$$B_{CMN}(z) = -(\beta_1 + \beta_2 + \beta_3) z^{-1} + (\beta_1\beta_2 + \beta_1\beta_3 + \beta_2\beta_3) z^{-2} - (\beta_1\beta_2\beta_3) z^{-3} \quad (4.24)$$

This analysis demonstrates that the complex coefficients of $L_{CMN}(z)$ and $B_{CMN}(z)$ are directly related to the centre frequency locations where some examples are given in Table 4.10.

	β_1	β_2	β_3
1/10, 3/10	-0.809 - j0.588	0.309 - j0.951	0
1/8, 2/8, 3/8	-j0.707 - j0.707	-j	0.707 - j0.707
1/16, 5/16, 7/16	-0.924 - j0.383	0.383 - j0.924	0.924 - j0.383
-1/4, 3/20, 23/50	+j	-0.588 - j0.809	0.969 - j0.249

Table 4.10 Loop-Filter & Feedback Filter Coefficients for a Combination of Equi-Spaced & Non-Equi-Spaced Centre Frequencies for CMNA.

The complex multi-notch approach demonstrated multi-band noise-shaping for any combination of equi-spaced as well as non-equi-spaced centre frequency locations, where two examples for double-band 1-1 MASH complex Σ - Δ modulators are shown in Figure 4.21. The absence of tones in the magnitude spectrum of these modulators is attributed to the more complicated loop-filter and the extra stages, which achieve a sufficient amount of quantisation noise decorrelation.

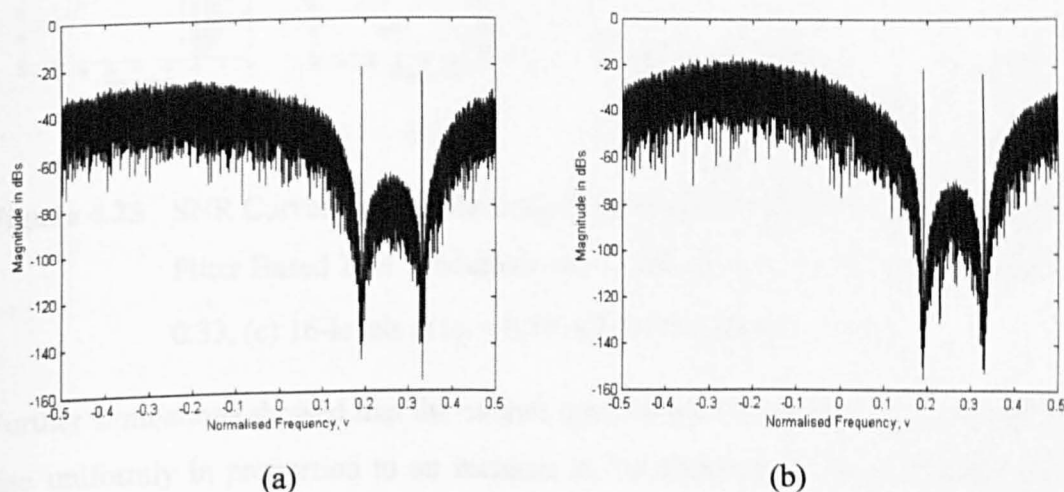


Figure 4.21 Magnitude Spectrum of a Double-Band Complex Multi-Notch Filter Based Σ - Δ Modulator Centred at $\nu_C = 0.19$ and $\nu_C = 0.33$, (a) 1-1 MASH, (b) 1-1-1 MASH.

Figure 4.21(b) shows that the 1-1-1 MASH modulator was capable of pushing away more in-band quantisation noise to the out-of-band regions, compared with the 1-1 MASH modulator.

Figure 4.22 presents the SNR curves for single- and double-stage Σ - Δ modulators, where better SNRs are achieved with the latter due to more effective quantisation noise-shaping in the in-band region.

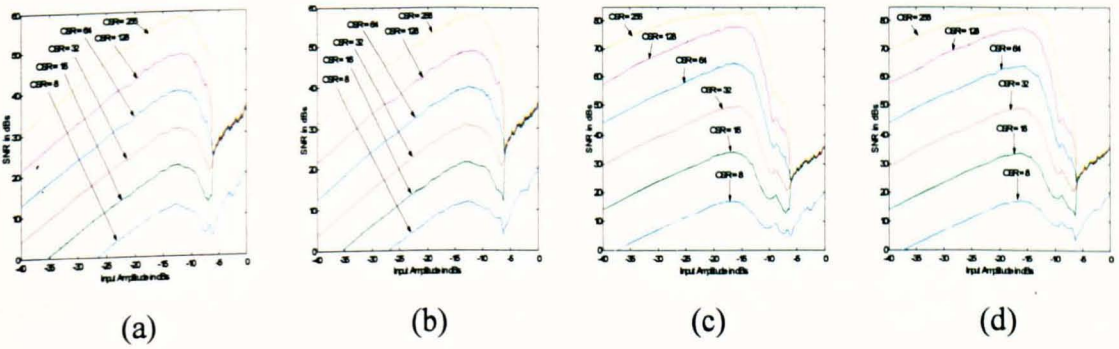


Figure 4.22 SNR Curves for Double-Band Complex FIR Notch Filter Based Σ - Δ Modulator (a) Single-Stage at $\nu_C = 0.19$, (b) Single-Stage at $\nu_C = 0.33$, (c) Double-Stage at $\nu_C = 0.19$, (d) Double-Stage at $\nu_C = 0.33$.

Figure 4.23 illustrates the SNR curves of a double-loop multi-bit Σ - Δ modulator, where the use of more quantiser levels is shown to significantly increase the DR of the modulator.

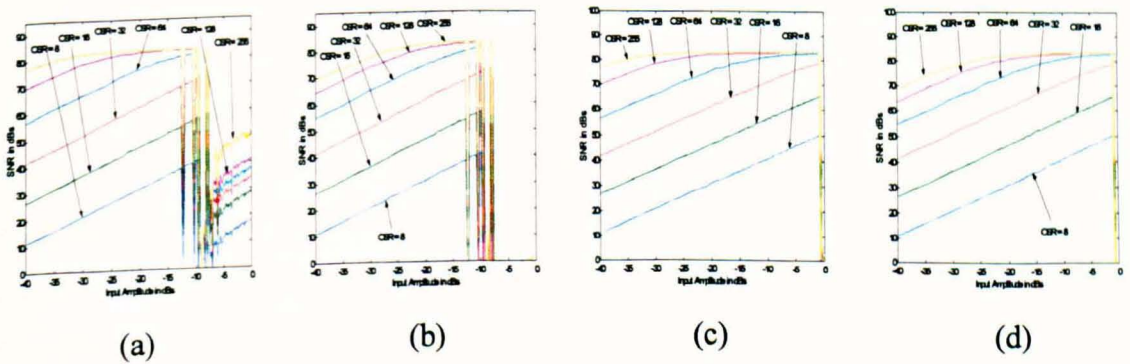


Figure 4.23 SNR Curves for Double-Loop Single-Bit Double-Band Complex FIR Notch Filter Based Σ - Δ Modulator (a) 13-levels at $\nu_C = 0.19$, (b) 13-levels at $\nu_C = 0.33$, (c) 16-levels at $\nu_C = 0.19$, (d) 16-levels at $\nu_C = 0.33$.

Further simulations showed that the overall quantisation noise floor level was observed to rise uniformly in proportion to an increase in the number of noise-shaping bands. This feature inevitably imposes tighter constraints for the digital decimator, particularly, in the case of too many and/or very closely located adjacent signal bands. Moreover, a sharp rise in the level of quantisation noise may lead to modulator instability.

4.12 IIR Multi-Notch Filter Approach (IMNFA)

In this technique, a bank of lower-order IIR notch filters are cascaded to provide an overall multiple-notch NTF. The normalised centre frequency, bandwidth and stop-band

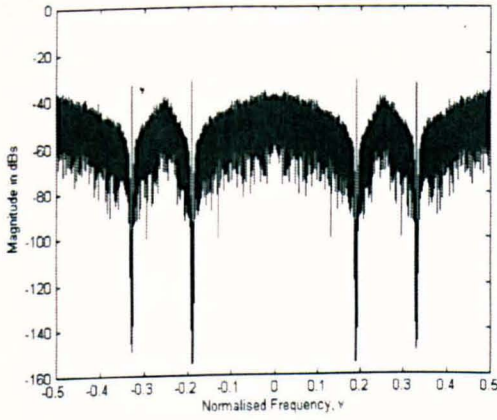
attenuation (in the case of Chebyshev 2) for each signal band need to be specified initially. These individual NTFs, which can have the same or different orders are then multiplied together to provide a single-block multi-notch NTF as shown below:

$$H_N(z) = \prod_{i=0}^P \frac{b_{i0} + b_{i1}z^{-1} + b_{i2}z^{-2} + \dots + b_{i(L-1)}z^{-(L-1)} + b_{iL}z^{-L}}{1 + a_{i1}z^{-1} + a_{i2}z^{-2} + \dots + a_{i(L-1)}z^{-(L-1)} + a_{iL}z^{-L}} \quad (4.25)$$

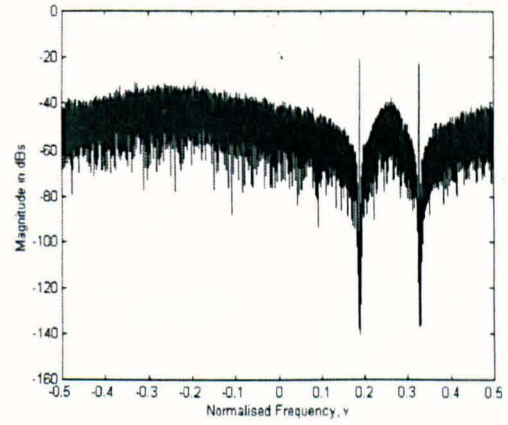
It should be pointed out that the leading coefficient of the overall NTF need to be scaled up to unity to satisfy the causality criterion. Also, the maximum gain of the NTF needs to comply with Lee's rule to ensure modulator stability.

This method offers several advantages compared with its predecessors. First; the signal bandwidth can be adjusted to meet any given specification. Second; the signal bands are not restricted to having identical widths. Third; the signal bands can be assigned to non-equi-distant locations in the frequency-domain. Fourth; the notch depth for the in-band region can be modified in the case of Chebyshev 2. Fifth; higher-order bandpass Σ - Δ modulators can be more easily stabilised as the freedom of the movement of the poles within the unit-circle given by an IIR NTF helps to substantially reduce the out-of-band gain. Six; the greater flexibility in the distribution of the poles and zeros of the NTF result in significant improvements to the noise-shaping symmetry and modulator resolution. Seven; the particular locations of signal bands do not unnecessarily increase the modulator order as was the case with the comb and slink filter NTF based modulators. Eight; smaller amounts of dither are deemed necessary with this approach, because the more complicated loop-filter produces a wider variation in state values resulting in more quantisation noise variation and ultimately fewer tones across the spectrum.

Figure 4.24 shows that magnitude spectra of a real and a complex sixth-order double-band Σ - Δ modulators. Figure 4.25 shows the SNR curves for different quantiser levels for the 6th-order double-band IIR notch-filter based Σ - Δ modulator.

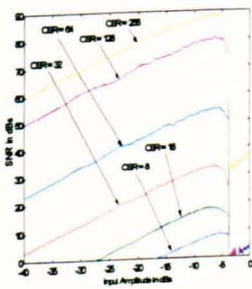


(a)

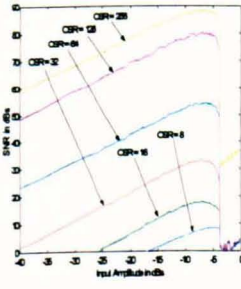


(b)

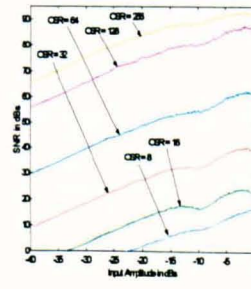
Figure 4.24 Magnitude Spectrum of a Sixth-Order Double-Band Multi-Notch Filter Based Σ - Δ Modulator Centred at $\nu_C = 0.19$ and $\nu_C = 0.33$,
(a) Real Coefficient, (b) Complex Coefficient.



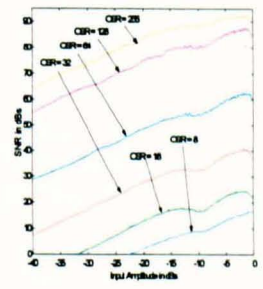
(a)



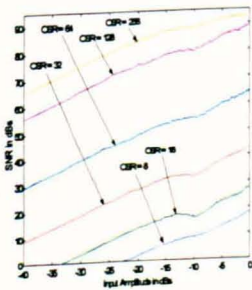
(b)



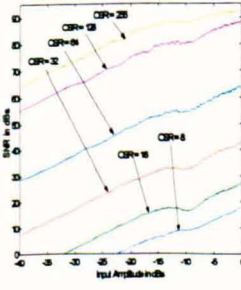
(c)



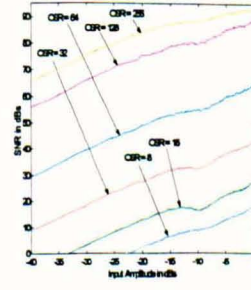
(d)



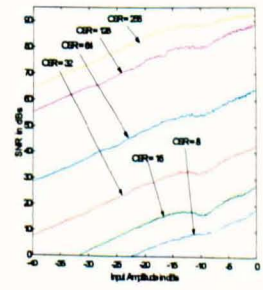
(e)



(f)



(g)



(h)

Figure 4.25 SNR Curves for Sixth-Order Double-Band IIR Notch Filter Based Σ - Δ Modulator (a) 2-level at $\nu_C = 0.19$, (b) 2-level at $\nu_C = 0.33$, (c) 4-level at $\nu_C = 0.19$, (d) 4-level at $\nu_C = 0.33$, (e) 8-level at $\nu_C = 0.19$, (f) 8-level at $\nu_C = 0.33$, (g) 16-level at $\nu_C = 0.19$, (h) 16-level at $\nu_C = 0.33$.

Figure 4.26 shows the SNR curves for different quantiser levels for the 6th-order double-band complex IIR notch-filter based Σ - Δ modulator.

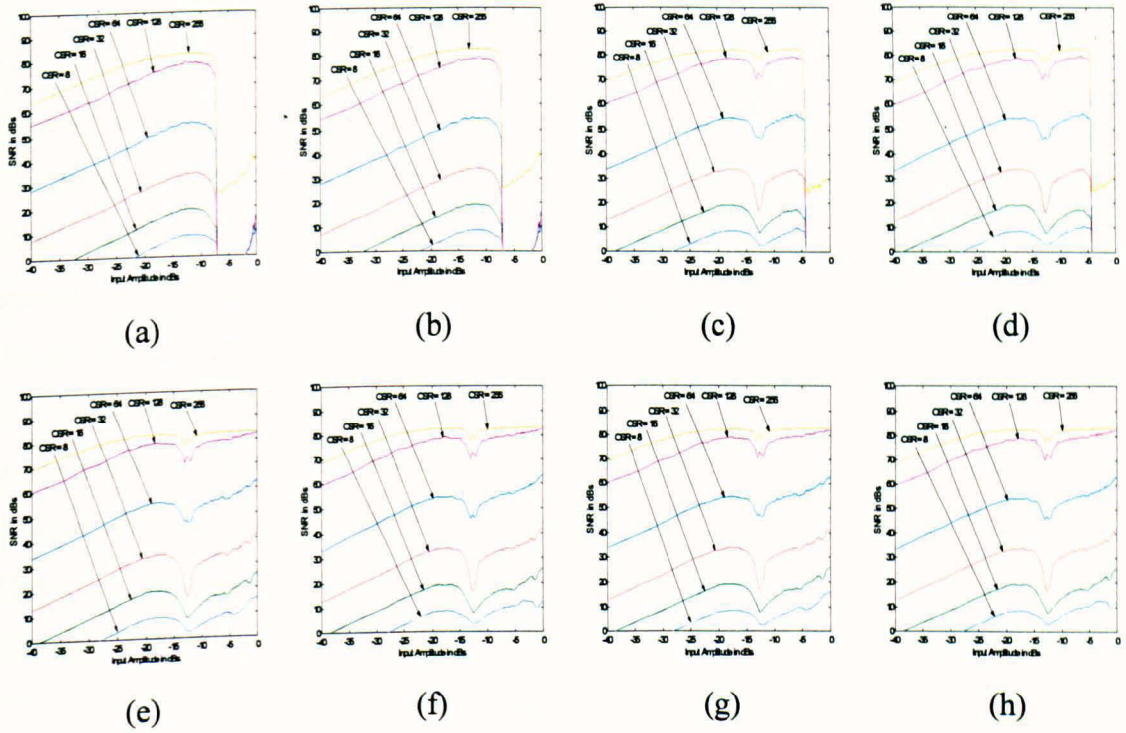


Figure 4.26 SNR Curves for Sixth-Order Double-Band Complex IIR Notch Filter Based Σ - Δ Modulator (a) 2-level at $\nu_C = 0.19$, (b) 2-level at $\nu_C = 0.33$, (c) 4-level at $\nu_C = 0.19$, (d) 4-level at $\nu_C = 0.33$, (e) 8-level at $\nu_C = 0.19$, (f) 8-level at $\nu_C = 0.33$, (g) 16-level at $\nu_C = 0.19$, (h) 16-level at $\nu_C = 0.33$.

4.13 Concluding Remarks to Chapter 4

Comb filter based Σ - Δ modulators provided a simple and cheap option of generating concurrent multiple noise-shaping bands, when used in Σ - Δ modulators. The number and location of these bands was dependent on the order of the comb filter. The main drawback associated with this technique was that only a limited range of multiple noise-shaping band combinations was attainable. Simulations also showed that the magnitude spectra of these modulators exhibited several dominant tones, because they contained relatively simple loop-filters that generated fewer state values. The SNR curves of the double- and triple-band became non-linear for large-amplitude inputs. This was caused by the excessive quantiser overloading, which resulted in the occurrence of more tones in the in-band region. Alternative noise-shaping bands were accomplished by using complex comb filters

for the NTFs. The magnitude spectra of the complex comb filter modulators contained more tones compared with their real-coefficient counterparts and required more dither to alleviate these tones.

For the slink filter approach, more equi-spaced noise-shaping band combinations could be achieved, because slink filters contained more adjustable multiplier free parameters compared with comb filters. This improvement was accomplished at the cost of having to use higher-order loop-filters in some cases. The uneven distribution of the out-of-band quantisation noise exhibited by the magnitude spectra of slink filter based Σ - Δ modulators was attributed to the ratio of the peak amplitudes of the main-to-side lobes of the slink filter. Once again, different combinations in the selection of noise-shaping bands was accomplished by employing complex slink filters for the NTF. Slink filter based Σ - Δ modulators were seen to become unstable more abruptly compared with their comb counterparts, because of the disparity of the shoulder gains levels of the slink filter. However, simulations demonstrated that slink filter based Σ - Δ modulators were less tonal, because of the slight complexity in the loop-filter.

Fractional delay filters in conjunction with comb filters were shown to accomplish concurrent noise-shaping for any equi-spaced combination of multi-tone input signals, overcoming the limitations imposed by the comb or slink filter approaches. This improvement, however, was achieved at the expense of using multipliers for the fractional delayer filters. FIR FD comb filter based Σ - Δ modulators were found to suffer from inadequate noise-shaping performance at high frequencies (due to errors in the amplitude of the FIR filter). For FD requirements other 0.5, the FIR FD filter exhibited small phase errors resulting in minor shifts of the noise-shaping bands near Nyquist. On the other hand, IIR allpass comb filter based Σ - Δ modulators yielded enhanced resolution at slightly displaced noise-shaping bands at high frequencies (due to errors in the phase of the allpass filter).

In order to enable multi-band noise-shaping for any arbitrary combination of centre frequencies, FIR multi-notch based Σ - Δ modulators were designed and evaluated at the behavioural level. The main features of this approach were: First, these modulators were shown to accomplish multiple-band noise-shaping for any combination of equi-spaced as well as non-equi-spaced centre frequencies. Second, the signal bands were not constrained to having the same bandwidths. Third, the designated locations of the signal bands did not increase the modulator order unnecessarily as was the case with the previous three

approaches. Fourth, care had to be taken to ensure that the disparity of the shoulder gain levels of the composite loop-filter did not reduce modulator stability.

The IIR multi-bandstop filter approach offered several advantages compared with the above four techniques. First, the signal bandwidth could be adjusted to meet any given specification. Second, the signal bands were not restricted to having identical widths. Third, the signal bands could be allocated to non-equi-distant locations in the frequency-domain. Fourth, the notch depth for the in-band region could be modified in the case of the Chebyshev 2. Fifth, higher-order bandpass Σ - Δ modulators could be more easily stabilised as the flexibility in the distribution of the poles within the unit-circle helped to substantially reduce the out-of-band gain. Sixth, the increased freedom to disperse the poles and zeros of the NTF led to enhanced noise-shaping symmetry and SNRs. Seventh, the particular locations of the signal bands did not unnecessarily increase the modulator order as was the case with the comb-, slink and FD comb-filter based modulators. Eighth, smaller amplitudes of dither were deemed necessary with this approach, because the more complicated loop-filter produced a more diverse range of state values resulting in greater quantisation noise randomisation and consequently fewer spectral tones.

Chapter 5

Stability of Bandpass Σ - Δ Modulators

5.1 An Overview on Stability

It is well established that higher-order single-bit Σ - Δ modulators provide better signal-to-noise ratios, increased dynamic ranges, have inherent linearity and are easier to implement. On the other hand, the fact that these modulators are susceptible to instability coupled with the harsh non-linearity of the 1-bit quantiser have made the identification of the conditions for modulator stability a crucial part of the design process [Bai93].

There does not exist a complete theory to-date that can with complete accuracy predict stability in Σ - Δ modulators. The endeavours to theoretically determine the stability of single-bit Σ - Δ modulators in [Ken88]-[Ana89]-[Hei91]-[Wan92] were shown to be correct, but modulator-specific. The techniques proposed in [Ard87]-[Rit90] are useful, but unfortunately approximate. Furthermore, it is shown that the stability rules-of-thumb presented in [Agr83]-[Lee87] give unreliable results for certain Σ - Δ modulator topologies.

The design of stable high-order Σ - Δ modulators is a non-trivial task. A major challenge faced by all Σ - Δ designers and practitioners involves selecting a suitable noise transfer function and hence a loop-filter that will result in stable operation. Root locus techniques, non-linear optimisation approaches, exhaustive searching routines, extensive simulations as well as procedures based on intuition have all been attempted in order to facilitate the design of stable high-order single-bit Σ - Δ modulators.

A literature survey is presented at the outset of this chapter, whose purpose is to summarise all the publications related to stability in Σ - Δ modulators, in order to highlight areas that merit further investigations. A brief categorisation of the different interpretations of stability as well as a critical review of existing rules-of-thumb, which have been widely employed by leading practitioners are presented in Sections 5.3 and 5.4 respectively. The Root Locus Technique, behavioural-level simulations as well as highly intuitive approaches are used to understand, design and evaluate the behaviour of high-order single-bit and multi-bit bandpass Σ - Δ modulators. The factors that directly and indirectly control stability in Σ - Δ modulators are considered carefully. Some of these attributes reinforce what is intuitively expected and their impact on stability is supported, where appropriate by a plethora of simulation results. The ultimate, but yet the most important objective of this

chapter is to provide more accurate guidelines for the design of single- and multi-bit bandpass Σ - Δ modulators.

5.2 Survey of Publications Related to Stability in Σ - Δ Modulation

Publications, which deal with aspects related to stability in Σ - Δ modulation are summarised below in Table 5.1. These cover rigorous theoretical analysis, detailed behavioural investigations of new techniques as well as actual experimental results obtained from hardware implementations.

Brief Description of the Reported Publication	Ref
Derivation of stability constraints for lowpass single-bit limiter-based Σ - Δ modulators using root locus techniques.	[Sti88]
Linearised analysis, simulation and intuitive explanation of the stability in lowpass second- and third-order single-bit Σ - Δ modulators.	[Sim89]
Development of a Markov model to calculate the quantiser gain curve, stability ranges, SNRs & harmonic distortion content in lowpass single-bit Σ - Δ modulators.	[Wol89]
Techniques based on limit cycle analysis for constant inputs which guarantee the design of stabilised higher-order interpolative Σ - Δ modulators.	[Hei91]
Stability analysis coupled with detailed simulations of lowpass third-order Σ - Δ modulators. Popular rules-of-thumb proposed by other practitioners in the field are shown to be invalid for certain topologies.	[Sch91b]
A variable gain model for the quantiser is proposed that allows the stability analysis of various third-order Σ - Δ modulator combinations using root locus techniques.	[Bai93]
A novel FIR spectrum distribution technique is proposed for improving the stability of higher-order Σ - Δ modulators. Stability is verified using the root locus method.	[Oka93]
Detailed simulations to establish the stability input limits and SNR curves of non-optimised and optimised lowpass higher-order single-bit Σ - Δ modulators.	[Sch93b]
Root locus analysis of higher-order Σ - Δ modulators showing the effect of resonator gains, input amplitudes, number of delayers & initial conditions on stability.	[Bai94]
An improved linear model for determining the quantiser gain is proposed which recognises the constant power criterion & explains some of the non-linear features of Σ - Δ modulators.	[Mag94]
A new method for stabilising higher-order single-bit Σ - Δ modulators is proposed which limits the amplitude of the internal signals through the insertion of local feedback loops inside the modulator.	[Mou94]
A method based on quasi-linear modelling is proposed for predicting the stability	[Ris94]

and quantisation noise properties of higher-order single-bit Σ - Δ modulators.	
A technique is proposed based on state-space division into regions to analyse & derive simpler equations that characterise the stability of 2 nd -order Σ - Δ modulators.	[Ste94]
Conditions for the stability of continuous-time 2 nd & 3 rd -order Σ - Δ modulators are derived and compared with the results provided by other authors.	[Ush94]
The stability analysis of a lowpass 4 th -order multi-bit Σ - Δ modulator using root locus techniques. A description of the complete design process is also included.	[Bai96]
A novel analytical approach using a mixture of non-linear dynamics & geometrical techniques is proposed to identify the stability bounds of 2 nd -order Σ - Δ modulators.	[Far96]
Evaluation of the stability limits of lowpass third-order single-bit Σ - Δ modulators based on modulation depth and feedback coefficients.	[Mor96a]
Derivation of the stability boundaries for the max. internal signal levels in double-loop Σ - Δ modulators. Effect of chaos on tone reduction & stability is investigated.	[Mot96a]
The effectiveness of a new optimised reduced sample rate technique on the stability of 2 nd - & 3 rd -order Σ - Δ modulators is investigated using root locus techniques.	[Bir97]
A new model depicting both the gain and phase of the quantiser is described for the root locus stability analysis of lowpass Σ - Δ modulators.	[Eng97]
An extensive simulation study of single-bit & multi-bit Σ - Δ modulators based on the effect of loop-filter coefficients & input amplitude on stability & SNRs.	[Pel97]
A novel highly-accurate approach that analytically models the accumulator output signal levels of 2 nd -order lowpass Σ - Δ modulators for constant input signals.	[Far98]
Section 4 of this paper discusses the stability analysis of 2 nd - & 3 rd -order lowpass Σ - Δ modulators using root locus techniques.	[Ben99]
Stability analysis based on modelling the gain & phase of the quantiser of continuous-time higher-order bandpass Σ - Δ modulators using root locus methods.	[Eng99a]
The effect of coefficient quantisation on the stability and resolution of higher-order lowpass Σ - Δ modulators is evaluated in this paper.	[Gil99]
A novel stabilisation method based on detecting quantiser input overload which subsequently reduces the modulator order to ensure stability.	[Pne99]

Table 5.1 Summarised Survey of Publications Related to Stability in Σ - Δ Modulators.

5.3 Different Definitions and Interpretations of Stability

The most common interpretations of the occurrence of instability in Σ - Δ modulators are summarised next. First; a Σ - Δ modulator is described as being unstable if it has a persistent pattern of large-amplitude internal signals, especially at the quantiser input

accompanied by poor SNR performance [Nor97]-[Hei91]. Second; a Σ - Δ modulator is declared unstable if it exhibits a very low-frequency output signal that contains an alternating long sequence of 1's and -1's [Nor97]. Third; a Σ - Δ modulator is considered unstable if the SNR decreases significantly even though all the internal signals within the modulator are bounded [Hei91]. Fourth; a Σ - Δ modulator is pronounced unstable when its quantiser input or output signal stays at a very high positive or negative value indefinitely [Kar94]. Fifth; a modulator is defined as unstable if the error signal and/or output voltages emanating from the resonators keep growing until the quantiser becomes continuously saturated [Mou94]-[Sch91b]. Sixth; a modulator is defined as unstable if the average value of its output signal is no longer a close approximation of the amplitude of the input signal.

5.4 Review of Existing Rules-of-Thumb

This section demonstrates that all the existing rules-of-thumb proposed to-date are neither sufficient nor necessary to entirely and accurately predict the stability of single-bit Σ - Δ modulators. Extensive simulations have shown that excessive out-of-band quantisation noise gains leads to instability in Σ - Δ modulators.

Lee's criterion states that a Σ - Δ modulator is guaranteed to be stable provided the peak gain of the noise-shaping spectral magnitude at any frequency does not exceed 2, i.e. $|H_N(z)| < 2$ [Lee87].

It is stated in [Agr83] that the power gain of the NTF should be less than 3 to ensure modulator stability. This power criterion assumes that the quantisation noise signal is white and uniformly distributed having a power value of 1/3. Given that the output signal for a single-bit Σ - Δ modulator is unity, this implies that the power gain of the NTF has to satisfy $\|H\|_2^2 \leq 3$. It should be pointed out that the power gain criterion is more conservative as the equivalent power gain proposed by Lee implies that $\|H\|_2^2 \leq 4$.

A third alternative stability criterion is proposed by Anastassiou [Ana89]-[Sch91b] requires that the condition given below to be satisfied in order to ensure stability:

$$\sum_{i=1}^{\infty} |h(i)| \leq 2 - \|u\|_{\infty} \quad (5.1)$$

where u is the input to the modulator and $h(i)$ is the impulse response of the NTF.

Despite the popular use and reliability of these ad-hoc criteria in numerous situations, Schreier in [Sch91b] shows through rigorous simulations that the maximum gain and

power gain criteria are neither necessary nor sufficient in certain cases to guarantee stability.

5.5 Stability using the Root Locus Techniques

It has already been discussed that modelling the 1-bit quantiser by an additive White noise source only provides useful information about the noise transfer function envelope of Σ - Δ modulators. The technique reported here is based on Kalman's Theorem [Tha62], which simply states that most types of non-linearities including saturation may be represented by an arbitrary range of linear gain values. Thus, the quantiser is modelled by a variable gain, whose value is adjusted depending upon the previous states of the modulator and the input signal. This variable gain method facilitates the stability analysis of Σ - Δ modulator structures. Theoretically, the gain value can lie anywhere between zero and infinity for any given input. However, behavioural simulations and practical implementations demonstrate that this gain has a finite value. The quantiser gain may be simply defined as the ratio of the quantiser output to the quantiser input voltages as given by:

$$H(z, k) = \frac{N(z, k)}{D(z, k)} \quad (5.2)$$

where $N(z, k)$ and $D(z, k)$ represent the numerator and denominator polynomials of the Σ - Δ modulator transfer function. The quantiser gain has a constant value during each clock period and only varies in magnitude from one sample to another. The well known Root Locus Techniques are employed to illustrate the movement of the poles of a Σ - Δ modulator as the quantiser gain varies [Bai93]-[Oka93]-[Bai94]. A transfer function incorporating this variable gain is derived from first principles, where the *Jury Criterion* is applied in order to determine the range of stable quantiser gain values.

The root locus of $D(z, k)$ can provide valuable information regarding the stability behaviour of a Σ - Δ modulator. A modulator is described as being unconditionally stable if the locus of all its poles reside inside the unit circle. If one or more of its poles leave the unit-circle without coming back, then the modulator becomes unstable. The in-between cases refer to modulators, which are conditionally stable meaning that these modulators will be stable for a given range of input signals [Bai94]-[Ben99].

If the poles of $H(z, k)$ remain inside the unit-circle for all values of k , then the modulator is said to be unconditionally stable. When one or more poles move outside the unit-circle for a given quantiser value, the internal signal levels in the modulator begin to

diverge in amplitude causing k to change its value. If the new k causes the pole to return to the unit-circle, then the modulator is described as having a stable limit cycle and therefore stable. On the other hand, if the change in k results in a pole staying outside the unit-circle, then the limit cycle is said to be unstable. Behavioural level simulations showed that under this condition, the internal signal levels of the constituent resonators continued to grow in an uncontrollable manner. This eventually causes the modulator to lock itself into endless low-frequency, high-amplitude oscillations which can only be terminated through external stabilisation techniques.

5.5.1 Root Locus Analysis of Fourth-Order Bandpass Σ - Δ Modulators

This section presents the stability analysis of a variable-band fourth-order bandpass Σ - Δ modulator using root locus techniques. The 1-bit quantiser is represented by a variable gain to enable the application of linear theory so that a closed-loop transfer function that characterises the Σ - Δ modulator can be obtained. This is given by:

$$\frac{Y(z)}{X(z)} = \frac{k R^2(z)}{1 - k R^2(z)F(z) - k R(z)F(z)} \quad (5.3)$$

where k is the quantiser gain, $R(z)$ is the variable-band resonator transfer function of both stages and $F(z)$ is a feedback filter to provide effective noise-shaping. Algebraic manipulations demonstrate that

$$R(z) = \frac{g}{1 - 2 \cos \alpha z^{-1} + z^{-2}} \quad \text{and} \quad F(z) = 2 \cos \alpha z^{-1} + z^{-2} \quad (5.4)$$

in order to provide maximum attenuation in the in-band region. Note that g is the resonator gain and α is chosen to centre the signal band at any frequency given by $\alpha = 2\pi\nu_C$, where ν_C is the normalised centre frequency of interest.

5.5.2 Ideal Fourth-Order Mid-Band Resonator Σ - Δ Modulator

This Σ - Δ modulator structure is cheap to implement, because it does not require any multipliers, since α is zero for the mid-band resonance case. Furthermore, it assumes both resonator gains g_1 and g_2 to be unity. Analysis of this fourth-order Σ - Δ modulator yields a system transfer function given by

$$\frac{Y(z)}{X(z)} = \frac{k}{1 + (2 - 2k)z^{-2} + (1 - k)z^{-4}} \quad (5.5)$$

It can be seen from the above expression that pole locations are dependent on the quantiser gain k . This variable gain, whose value is governed by the modulator input signal and the previous error samples, makes the poles move along the root locus during normal operation. A well known stability criterion for sampled-data systems in the z -domain is the *Jury Test* [Phi96]. The *Jury Test* was applied to (5.3) to establish the quantiser gain values for which this ideal modulator is stable. The range of quantiser gains that must be satisfied to ensure modulator stability is given by

$$0 < k < \frac{4}{3} \quad (5.6)$$

All the internal voltages of the modulator including the maximum voltage attained by the resonators depend on the amplitude of the input signal. This implies that the quantiser input voltage is directly proportional to the signal input to the modulator and inversely proportional to the quantiser gain since the output is a constant. Therefore, when the quantiser gain value exceeds $4/3$, the two poles on the real axis exit the unit circle in opposite directions, one towards the positive real axis and the other towards the negative real axis. The other two poles remain permanently inside the unit circle for the entire range of quantiser gains.

5.5.3 Variable-Band Resonator-Based Bandpass Σ - Δ Modulators

This fourth-order Σ - Δ modulator can accommodate a variety of centre frequencies overcoming the $f_s/4$ restriction. The internal configuration of this structure is identical to that considered earlier with the exception that the resonators are not necessarily multiplier-free. The corresponding closed-loop transfer function of this modulator becomes:

$$\frac{Y(z)}{X(z)} = \frac{k}{1 + 2\beta(k-1)z^{-1} + (2 + \beta^2 - (2 + \beta^2)k)z^{-2} + 2\beta(k-1)z^{-3} + (1-k)z^{-4}} \quad (5.7)$$

where $\beta = 2 \cos \alpha$. By application of the *Jury Test*, the ranges of quantiser that must be satisfied to ensure modulator stability are as follows:

$$\text{for normalised centre frequencies, } 0 < \nu_c < 0.25, \quad \frac{\beta^2}{\beta^2 + 1} < k < \frac{\beta^2 + 4\beta + 4}{\beta^2 + 4\beta + 3} \quad (5.8)$$

for normalised centre frequencies, $0.25 < \nu_C < 0.5$, $\frac{\beta^2}{\beta^2 + 1} < k < \frac{\beta^2 - 4\beta + 4}{\beta^2 - 4\beta + 3}$ (5.9)

The poles may exit the unit circle for two different ranges of k and therefore modulator stability should be considered for each case. Furthermore, there are two separate cases depending on the resonator normalised centre frequencies, when k has a high value. For the range, $0 < \nu_C < 0.25$, the pole on the negative real axis exits the unit circle, while the two conjugate poles and the other pole on the positive real axis remain inside the unit circle. The pole on the negative real axis should not result in continued instability due to the small amplitude internal voltages. After a number of samples, the signal levels within the modulator increase in amplitude. This amplification includes the quantiser input, which consequently reduces the quantiser gain and hence this real pole returns into the unit circle. Note that for modulators, whose centre frequencies lie between $0.25 < \nu_C < 0.5$, the pole that leaves the unit circle is the one on the positive real axis, while the pole on the negative real axis and the conjugate pair remain inside the unit circle. The internal signal levels including the quantiser input begin to rise, which result in a reduction in quantiser gain. Consequently, the pole returns to the unit circle. Unlike the ideal case, a quantiser gain less than $\beta^2 / (\beta^2 + 1)$ for the normalised centre frequency range $0 < \nu_C < 0.5$ will inevitably lead to instability. When the value of k goes below this threshold, the quantiser saturates, which leads to permanent large-amplitude low-frequency limit cycle oscillations. The internal signal levels within the modulator become excessively large as a result of the small quantiser gain and thereby force the two conjugate poles to go outside the unit circle and cause permanent instability. This modulator can be stabilised by either using a multi-bit quantiser or suitably clipping the resonator outputs [Bai94].

5.5.4 Non-Ideal Variable-Band Frequency Bandpass Σ - Δ Modulator

It is useful to consider the effect of employing non-unity gain resonators on the stability of variable-band fourth-order bandpass Σ - Δ modulators. The root locus plots of the poles of a fourth-order bandpass Σ - Δ modulator for two centre frequencies for different resonator gains are given in Figure 5.1. The two resonator gains g_1 and g_2 are assumed to be scalar and less than unity. The use of lower gains, particularly in the first-stage controls the level of the internal signals in the feedforward path and thus protects the quantiser from becoming overloaded. The resultant closed-loop transfer function including these two non-unity gains is given by

$$\frac{Y(z)}{X(z)} = \frac{k g_1 g_2}{1 + \beta(g_1 g_2 k + g_2 k - 2)z^{-1} + (\beta^2 + 2 - g_2 k(\beta^2 + g_1 + 1))z^{-2} + 2\beta(kg_2 - 1)z^{-3} + (1 - kg_2)z^{-4}} \quad (5.10)$$

By application of the *Jury Test*, the range of quantiser gain values that must be satisfied to ensure modulator stability are as follows:

$$\text{for } 0 < v_C < 0.25 \quad \frac{g_1 \beta^2}{g_2 (g_1 \beta^2 + 1)} < k < \frac{\beta^2 + 4\beta + 4}{g_2 (\beta^2 + (3 + g_1)\beta + (2 + g_1))} \quad (5.11)$$

$$\text{for } 0.25 < v_C < 0.5 \quad \frac{g_1 \beta^2}{g_2 (g_1 \beta^2 + 1)} < k < \frac{\beta^2 - 4\beta + 4}{g_2 (\beta^2 - (3 + g_1)\beta + (2 + g_1))} \quad (5.12)$$

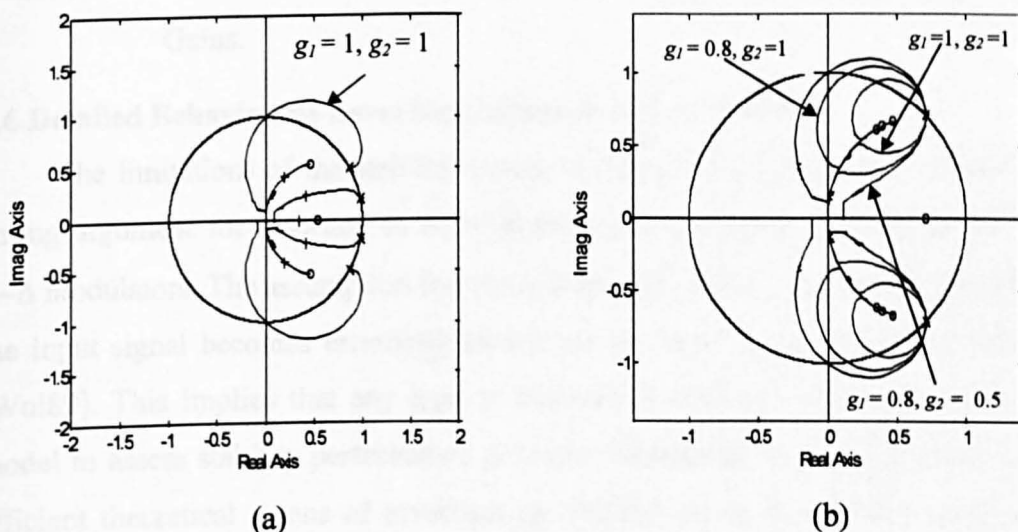


Figure 5.1 Root Locus of the Poles of 4th-Order Bandpass Σ - Δ Modulator Centred at (a) $v_C = 1/16$, b) $v_C = 1/8$ for Different Resonator Gains.

Once again, the poles may exit the unit-circle for two different ranges of k . Furthermore, large values of k have two separate cases depending on the locality of the centre frequency. The movement of the poles due to small and large quantiser gain values is very similar to the explanations provided in the above section. However, extra care must be exercised to ensure that the resonator gains are not significantly reduced, because this will push the poles closer to the zeros on the unit-circle. This results in a flatter response as opposed to the desired valley-shaped notch response. Often a compromise has to be made to satisfy both requirements. Table 5.2 gives the results of the Critical Quantiser Gain Range (*CQGR*) for various combinations of resonator gains.

$f_c : f_s$	$CQGR g_1 = 1, g_2 = 1$	$CQGR g_1 = 0.1, g_2 = 1$	$CQGR g_1 = 0.1, g_2 = 0.5$
1:10	$0.72 < k < 1.08$	$0.21 < k < 1.34$	$0.41 < k < 2.69$
1:8	$0.67 < k < 1.09$	$0.17 < k < 1.37$	$0.33 < k < 2.75$
1:6	$0.5 < k < 1.13$	$0.09 < k < 1.45$	$0.18 < k < 2.9$
1:5	$0.28 < k < 1.17$	$0.04 < k < 1.56$	$0.07 < k < 3.12$
1:4	$0 < k < 1.33$	$0 < k < 1.9$	$0 < k < 3.81$
1:3	$0.5 < k < 1.13$	$0.09 < k < 1.45$	$0.18 < k < 2.9$
3:8	$0.67 < k < 1.09$	$0.17 < k < 1.37$	$0.33 < k < 2.75$
2:5	$0.72 < k < 1.08$	$0.21 < k < 1.34$	$0.41 < k < 2.69$

Table 5.2 The Different Critical Quantiser Gain Ranges for Different Resonator Gains.

5.6 Detailed Behavioural-Level Simulations to Assess Stability

The limitations of the stability criteria discussed in the previous section provides a strong argument for resorting to simulations when evaluating the stability of high-order Σ - Δ modulators. The assumption that the quantisation noise is white and uncorrelated with the input signal becomes especially inaccurate for large or very small amplitude signals [Wol89]. This implies that any type of theoretical analysis that employs this simplified model to assess stability performance produces incomplete results. The most reliable and efficient theoretical means of investigating stability is via behavioural level simulations compared with other types of low level and architectural simulations. [Mor94]-[Wol89]. Floating point simulations provide a reliable means of verifying the overall operation and choice of filter coefficients [Mor94]. The behavioural simulations can be run for a larger number of samples for a given time interval compared with architectural simulations thus allowing the detailed investigation of limit cycle oscillations and long term stability behaviour to be evaluated more thoroughly. The generation of 3D plots, which provide valuable description of the stability behaviour of these modulators require an extremely large number of sampling points. These can only be practically achieved using behavioural-level simulations.

The stability a fourth-order single-bit Σ - Δ modulator was investigated using Matlab and Simulink based behavioural level simulations. Simulations were performed to provide adequately reliable 2D and 3D plots of the maximum amplitude input signal with respect to modulator order. It was found that the point of instability was sensitive to the initial conditions of the Σ - Δ modulator. The procedure adopted was to increase the input level in steps of 0.01 with zero initial conditions at first. This procedure was then repeated for

random initial conditions over the range ± 0.1 . The simulation length was 272144 samples for each point, where the initial 10000 points were discarded as transient samples. The stability of this Σ - Δ modulator was assessed by verifying the amplitude level of the input signal to the quantiser $q_{IN}(k)$. Knee plots similar to those found in [Sch93] were employed. The modulator was not considered to be stable and its quantiser input amplitude was not plotted, unless it satisfied the stability criterion $|q_{IN}(k)| \leq 10$ for $k \in [0..272144]$ for the random choice of initial conditions within ± 0.1 . All quantiser amplitude levels exceeding 10 were replaced with 0 and subsequently plotted on the stability charts to represent the unstable region of the modulator. This process was repeated several times with a different set of random initial conditions, where the worst-case value was always kept.

5.7 Factors that Affect Modulator Stability

This section discusses the various factors that affect stability in bandpass Σ - Δ modulators. These include the amplitude, phase and frequency of the sine input signal, the initial conditions of the loop-filter, the number of delayers in the loop, the number of levels in the quantiser, the modulator order as well as the feedforward and feedback coefficients of the modulator [Bai93]. The simultaneous requirements of maximum in-band noise suppression as well as maximum modulator stability are not possible. Given that both requirements need to be fulfilled, a trade-off has to be made to ensure stability as well as sufficiently high SNR values [Hei91]-[Bai94]. The degree of stability for a given Σ - Δ modulator topology should be defined in the early stages of the design process together with the other specification parameters [Hei91].

5.7.1 Amplitude and Type of Input Signal

An extremely important parameter in the design of Σ - Δ modulators is the modulation depth stability limit given by the maximum input value for which the modulator remains stable. The properties of the input signal have a considerable effect on the stability of higher-order Σ - Δ modulators [Bai93]-[Bai94]. The amplitude of the input signal limits the stability boundaries and the dynamic range of a Σ - Δ modulator [Wol89]. It is vital that the maximum stable input amplitude is determined in the early stages of the design process to establish whether it meets the design specifications [Wol89]. Behavioural-level simulations have shown that higher-order Σ - Δ modulators are conditionally stable meaning that a Σ - Δ

modulator becomes unstable beyond a certain input amplitude. For example, the sixth-order mid-band resonator-based bandpass Σ - Δ modulator is driven into instability when its input amplitude signal level exceeds 0.7. This is in contrast to the sixth-order Butterworth based bandpass Σ - Δ modulator, whose maximum input amplitude, before the onset of instability is 0.88. These results demonstrate that for the same modulator order and type of input signal, the maximum input for which this modulator remains stable is dependent on the NTF. A Butterworth based filter exhibits a NTF with a lower out-of-band gain making it more tolerant to higher input-amplitudes. On the other hand, the significantly higher-order out-of-band gains coupled with the sharper rise of notch filter based NTFs explain why modulators employing notch filters have a lower stable input-amplitude threshold.

A large-amplitude input signal to the Σ - Δ modulator invariably results in high-amplitude internal signals within the modulator, including the quantiser input signal. A point is reached, depending on the order, where the quantiser input amplitude rises very sharply, almost vertically as verified by the knee plots overleaf in Figure 5.3. This signifies severe quantiser overloading and therefore leads to instability [Sti88]. Furthermore, the input amplitude needs to be confined to the limits ± 1 , otherwise the average value of the Σ - Δ modulator output would not be able to track the input.

For large OSRs, the input signal to a Σ - Δ modulators appears to be relatively constant, thus providing good justification for evaluating the stability behaviour of Σ - Δ modulators with dc inputs [Hei91] for lowpass applications. It is stated in [Hei91] that any Σ - Δ modulator designed for dynamic inputs must be capable of handling dc input signals. It is recommended in [Sch91b] that any useful Σ - Δ modulator should be stable with zero input. Another recommendation is to ensure that the input amplitude does not exceed 80-90% of the peak input amplitude as a safety margin. This precaution becomes more significant in the case of aggressive NTF, e.g. Chebyshev as opposed Butterworth NTF [Nor97, pp. 141].

5.7.2 Modulator Order

This section presents stability input limit plots for different orders of Σ - Δ modulators. These are checked against the ad-hoc criteria proposed in [Agr83-[Lee87] to check their accuracy. It is shown that the input stability limits have significant variations for different Σ - Δ modulator orders for a given topology. The use of several loop-filters in cascade in the feedforward path of Σ - Δ modulators, as is the case in the distributed resonator feedback topology, results in large phase-shifts as well as huge-amplitude signal

levels (especially from the outputs of the later stages) leading to inevitable stability [Sim89]-[Bai94]. The effect of increasing the loop-filter order on the stability of bandpass Σ - Δ modulators is investigated. Second-, fourth-, sixth-, eighth-, tenth-, twelfth- and fourteenth-order bandpass Butterworth based Σ - Δ modulators were designed and evaluated at the behavioural level. Figure 5.2 illustrates the topology under consideration, whose feedforward coefficients (i.e. the g 's) are listed in Table 5.3 for each modulator order. These simulations involved subjecting the modulator to a single-tone sinusoid at $\nu_C = 0.25$, whose input amplitude was swept from 0 to 1 in steps of 0.01.

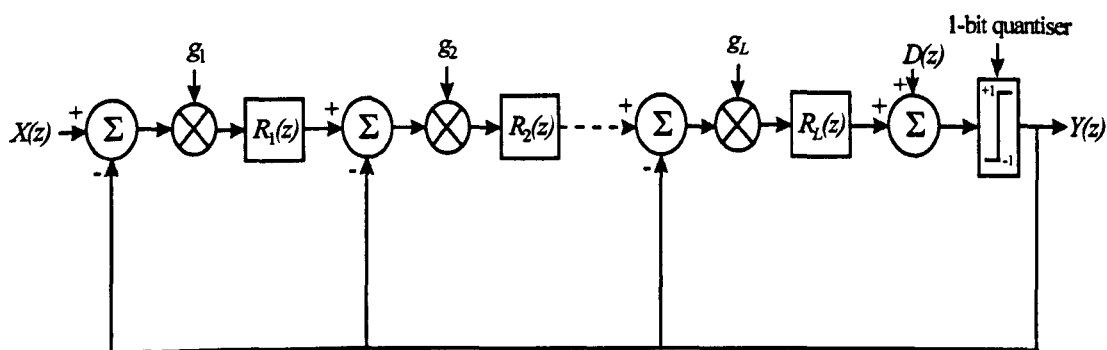


Figure 5.2 Chain of Resonators with Distributed Feedback.

Order	g_1	g_2	g_3	g_4	g_5	g_6	g_7
2 nd	-0.1988	-	-	-	-	-	-
4 th	-0.1350	-0.3090	-	-	-	-	-
6 th	-0.0947	-0.2077	-0.4390	-	-	-	-
8 th	-0.0723	-0.1550	-0.2771	-0.5741	-	-	-
10 th	-0.0583	-0.1232	-0.2075	-0.3464	-0.7112	-	-
12 th	-0.0488	-0.1022	-0.1669	-0.2575	-0.4159	-0.8493	-
14 th	-0.0419	-0.0872	-0.1399	-0.2074	-0.3063	-0.4854	-0.9880

Table 5.3 Coefficients of Different Orders of Butterworth Based Σ - Δ Modulators.

The knee plots in Figure 5.3 show the maximum output-amplitude signal of each resonator stage for different orders of this modulator. It is quite apparent from the curves in Figure 5.3 and the results in Table 5.4 that the maximum modulator input amplitude is reduced as the modulator order is increased. For the lower order modulators, the rate at which the resonator output diverges towards instability varies, especially for the fourth- and sixth-order modulators. However, the onset of instability for the tenth-, twelfth- and fourteenth-order modulators becomes almost concurrent as shown in Figure 5.3. In

addition, massive fluctuations in the output signal amplitude of these resonators very close to the maximum modulator input amplitude were observed for the twelfth- and fourteenth-order modulators.

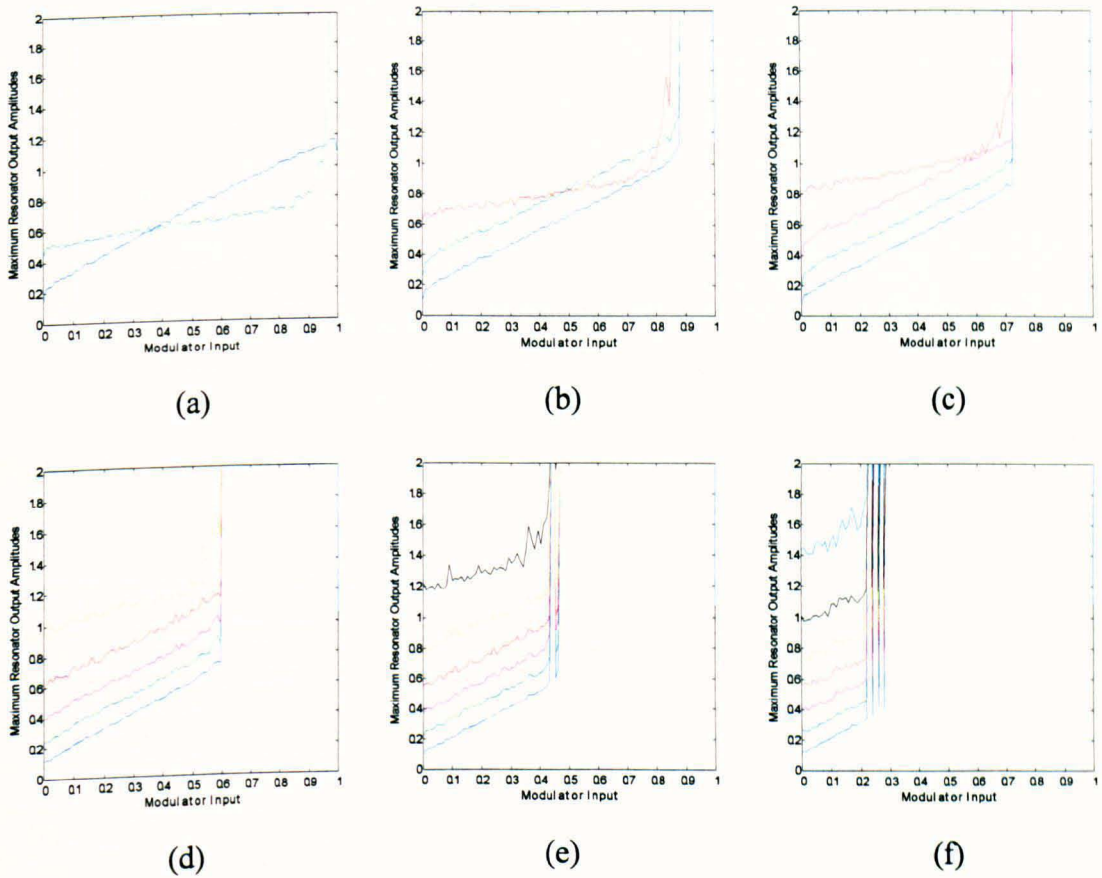


Figure 5.3 Knee Plots Depicting Resonator Output Amplitudes for Different $\Sigma\text{-}\Delta$ Modulator Orders for Zero Initial Conditions.

Figure 5.4 compares the maximum quantiser input levels versus the modulator input amplitude, where all the resonator initial conditions are set to zero. The second-order modulator, as expected remained unconditionally stable for all input amplitudes. However, the remaining modulators become unstable for input amplitudes below unity as can be shown in Table 5.4. Note that all the simulations for this topology were carried out for a dither amplitude of 0.01 and an OSR of 128. The most significant feature of these curves is the vertical rise (i.e. sharp knee), which segregates the stable and unstable regions for a given modulator order.

Also, the ripples exhibited by the curves in Figure 5.4 show that the rise of the quantiser input with respect to the modulator input is not always monotonic. Simulations which were run for many input values and a large number of time steps showed a significant reduction in this ‘non-monotonicity phenomenon’. This suggested that these

ripples were attributed to the finite number of time-steps. These results and remarks comply with the observations made in [Sch93b].

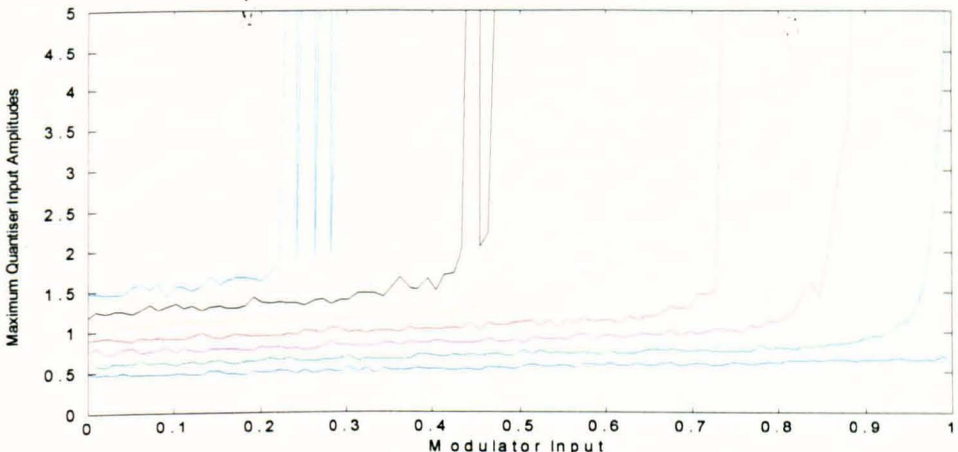


Figure 5.4 Knee Plots Depicting Quantiser Input Amplitudes for Different $\Sigma\text{-}\Delta$ Modulator Orders for Zero Initial Conditions.

Modulator Order	2	4	6	8	10	12	14
Max Quantiser Input	0.607	4.303	3.546	1.520	1.56	2.22	1.931
Max Modulator Input	1	0.990	0.879	0.727	0.596	0.465	0.283
SNR before Instability	60.84	61.84	83.11	112.16	128.04	144.54	154.04
Max SNR	60.84	77.64	95.20	112.62	129.53	144.96	154.04
Input Amp. - Max SNR	1	0.828	0.737	0.657	0.576	0.434	0.283
Peak NTF Magnitude	1.11	1.17	1.25	1.33	1.429	1.531	1.641
Max Reson 1 Amp.	0.398	1.08	1.136	1.157	1.049	1.074	1.089
Max Reson 2 Amp.	-	4.177	1.315	1.040	0.859	0.834	0.522
Max Reson 3 Amp.	-	-	3.510	1.165	0.994	0.981	0.651
Max Reson 4 Amp.	-	-	-	1.550	1.154	1.059	0.801
Max Reson 5 Amp.	-	-	-	-	1.558	1.228	0.974
Max Reson 6 Amp.	-	-	-	-	-	2.240	1.187
Max Reson 7 Amp.	-	-	-	-	-	-	1.898

Table 5.4 Maximum Quantiser Input and Peak Resonator Output Amplitudes for Different $\Sigma\text{-}\Delta$ Modulator Orders for Zero Initial Conditions.

The same set of simulations were repeated, but this time with the resonators containing random initial conditions, whose values lied between +0.1 and -0.1. Figure 5.5 shows the maximum resonator amplitude versus the modulator input amplitude for different modulator orders. These plots as well as the results presented in Table 5.5 indicated that the internal signal levels in the modulator, including those of the modulator outputs were

not always larger compared with the zero initial conditions' case. This variation could be attributed to the mixed use of positive and negative random initial conditions.

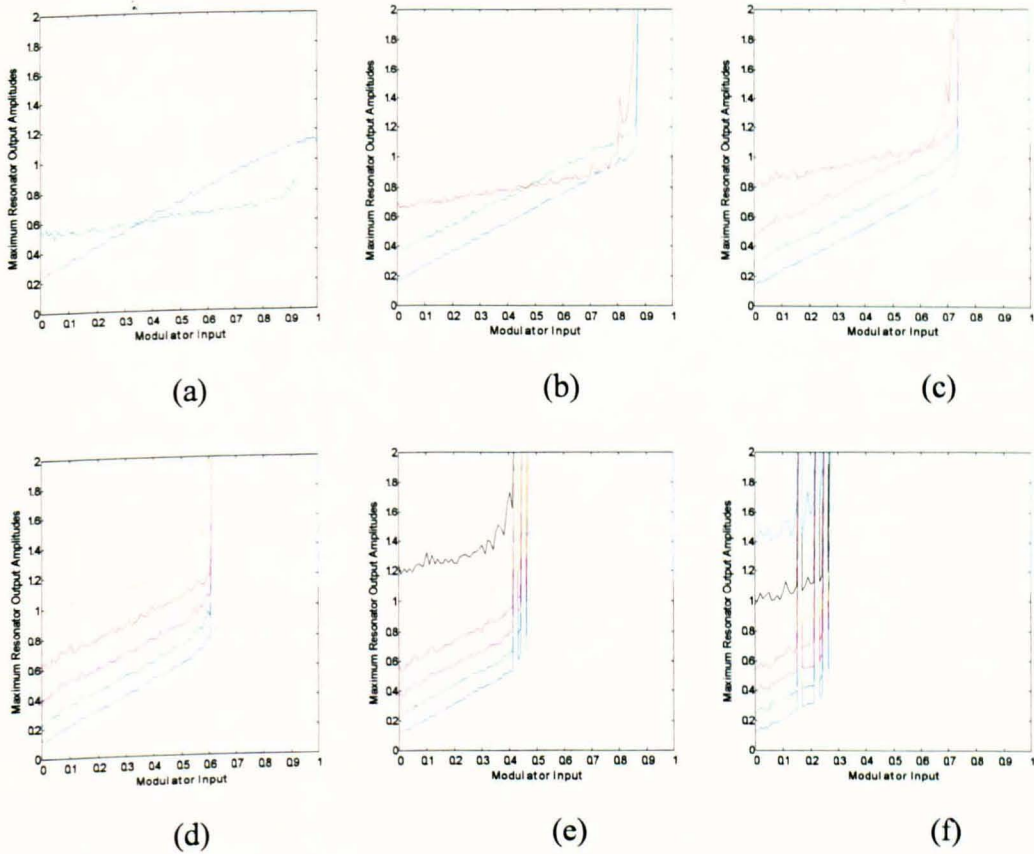


Figure 5.5 Knee Plots Depicting Resonator Output Amplitudes for Different $\Sigma-\Delta$ Modulator Orders for Random Initial Conditions

Modulator Order	2	4	6	8	10	12	14
Max Quantiser Input	0.649	3.027	2.693	2.155	1.942	2.806	1.937
Max Modulator Input	1	0.990	0.869	0.737	0.606	0.465	0.263
SNR before Instability	62.93	60.36	88.17	109.83	128.42	143.21	153.9
Max SNR	62.93	77.23	95.32	112.94	129.57	143.87	153.9
Input Amp. - Max SNR	1	0.778	0.677	0.616	0.556	0.44	0.263
Peak NTF Magnitude	1.11	1.17	1.25	1.33	1.429	1.531	1.641
Max Reson 1 Amp.	0.440	1.11	1.017	1.102	1.11	1.136	1.059
Max Reson 2 Amp.	-	2.92	1.262	1.093	0.931	0.86	0.571
Max Reson 3 Amp.	-	-	2.649	1.209	1.061	1.012	0.727
Max Reson 4 Amp.	-	-	-	2.087	1.201	1.077	0.877
Max Reson 5 Amp.	-	-	-	-	1.927	1.285	1.004
Max Reson 6 Amp.	-	-	-	-	-	2.72	1.191
Max Reson 7 Amp.	-	-	-	-	-	-	1.923

Table 5.5 Maximum Quantiser Input and Peak Resonator Output Amplitudes for Different $\Sigma-\Delta$ Modulator Orders for Random Initial Conditions.

Figure 5.6 showed that the quantiser input amplitude versus the modulator input amplitude for different modulator orders, whose constituent resonators contained random initial conditions. The maximum modulator input amplitudes were shown to be the same for 2nd, 4th and 12th order modulators, lower for 6th- and 14th-order modulators and slightly higher for the 8th- and 10th-order modulators, as can be seen from Table 5.5.

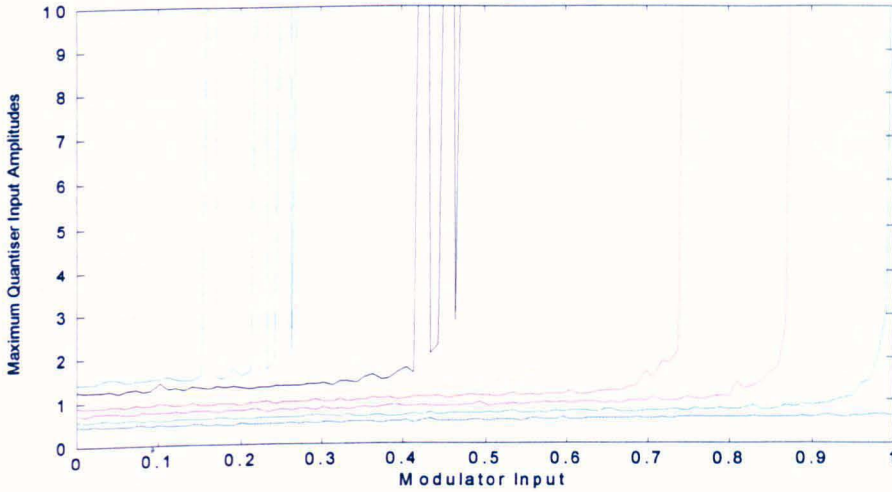


Figure 5.6 Knee Plots Depicting Quantiser Input Amplitudes for Different Σ - Δ Modulator Orders for Random Initial Conditions.

5.7.3 Feedback Coefficients

In this section, the maximum stable limits on the modulator input as a function of the feedback coefficients are established, for the distributed feedback topology shown in Figure 5.7. A relationship between the two feedback coefficients to maximise the DR of the fourth-order mid-band resonator-based Σ - Δ modulator is empirically determined via behavioural level simulations.

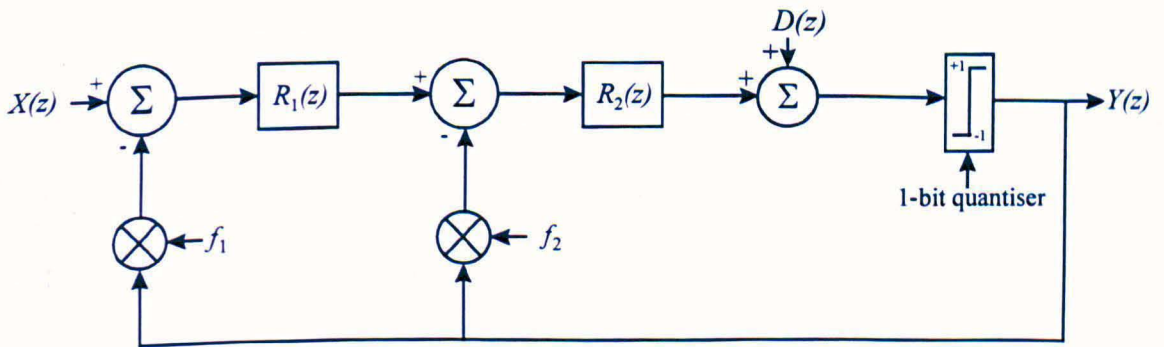


Figure 5.7 Chain of Resonators with Distributed Feedback.

It is well known that the cascaded arrangement of the resonators in higher-order single-bit Σ - Δ modulators considerably increases the amplitude of the internal signals in the feedforward path, thus overloading the 1-bit quantiser and resulting in instability [Sim89]. The accumulative effect of the phase shifts imparted by these resonators is another hazardous contributor to instability [Sim89]. One simple heuristic solution is to choose suitable values for the feedback coefficients to make the magnitude of the feedback signals comparable to those circulating in the feedforward path as discussed in Section 2.6. Intuitively, these coefficient values should be increased in powers comparable in value with the peak amplitude increase of the modulator-order NTF. For a fourth-order mid-band resonator-based Σ - Δ modulator, these feedback coefficients are numbered f_2 and f_1 respectively from the resonator nearest the quantiser as shown below in Figure 5.7.

Detailed simulations have confirmed that this increase is proportional to $(L-1)$ for feedback coefficients closest to the quantiser decreasing in successive powers for consecutive feedback coefficients away from the quantiser. Integer coefficient combinations are easier to use, e.g. 1 and 3 or 1 and 4 for f_1 and f_2 respectively.

The 3D plots shown in Figure 5.8(a) were obtained by sweeping the input amplitude and f_1 feedback coefficient from 0 to 1 and 1 to 10 for 100 equi-spaced divisions respectively, while keeping f_2 fixed to unity. A modulator was not considered stable unless it satisfied the 'empirically-set' stability criterion of $|q_{IN}(k)| \leq 10$ for $k \in [0, 272144]$ for zero initial conditions.

A careful examination of Figure 5.8(a) showed that the modulator remained stable up to an amplitude level of 0.9, provided f_1 did not exceed 3. Beyond that value, the modulator remained stable for a very small range of input amplitudes. These results quantitatively confirm that there is little point in increasing the f_1 coefficients above unity as this makes the feedback signal to the first differencer significantly higher than the feedforward signal. The error signal, as a result becomes very large, thus overloading the quantiser and rendering the modulator unstable.

These simulations results were repeated for random initial conditions in the resonators, whose values were between the range +0.1 and -0.1. The modulator remained

stable for nearly the same DR as for the zero initial conditions' case as long as f_1 did not exceed 3. However, the modulator stability for $f_1 > 3$ became rather unpredictable even for the smaller input-amplitudes as can be seen in Figure 5.8(b).

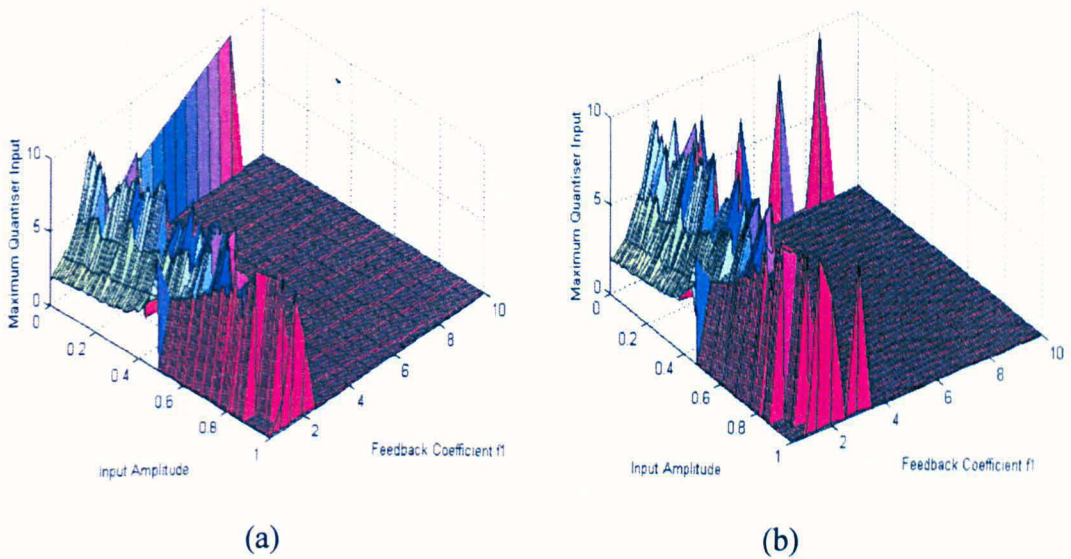


Figure 5.8 Maximum Quantiser Input Amplitude versus Feedback Coefficient f_1 versus Input Amplitude for $f_2 = 1$ and $v_C = 0.25$ under (a) Zero Initial Conditions, (b) Random Initial Conditions.

In a similar way, the 3D plots in Figure 5.9(a) were generated by sweeping the input amplitudes and f_2 feedback coefficients through the same number of points, while keeping f_1 set to unity. A careful examination of Figure 5.9(a) shows that the variation of the f_2 coefficient is more effective in allowing the modulator to remain stable for a much wider range of input amplitude levels. This can be explained by the fact that the amplitude levels of the later signals become inevitably large, because of the amplification imparted by the resonators. This makes it more appropriate to use an f_2 value greater than 1, to control the amplitude level of the internal signals. This plot also shows that when $f_2 > 4$, the maximum stable input amplitude to the modulator begins to decrease. In other words, the f_2 coefficient is shown to be a function of the input amplitude to the modulator. The 'red carpet' pattern shown represents the unstable region of the modulator. These results show that this modulator becomes permanently unstable by making $f_2 > 8$.

Simulations were repeated for a similar set of random initial conditions. The major difference between the two plots in Figure 5.9 was the more decisive onset of instability for

input amplitudes higher than 0.8. This is in contrast to Figure 5.9(a), where the modulator produced quantiser inputs, whose amplitudes were below 10.

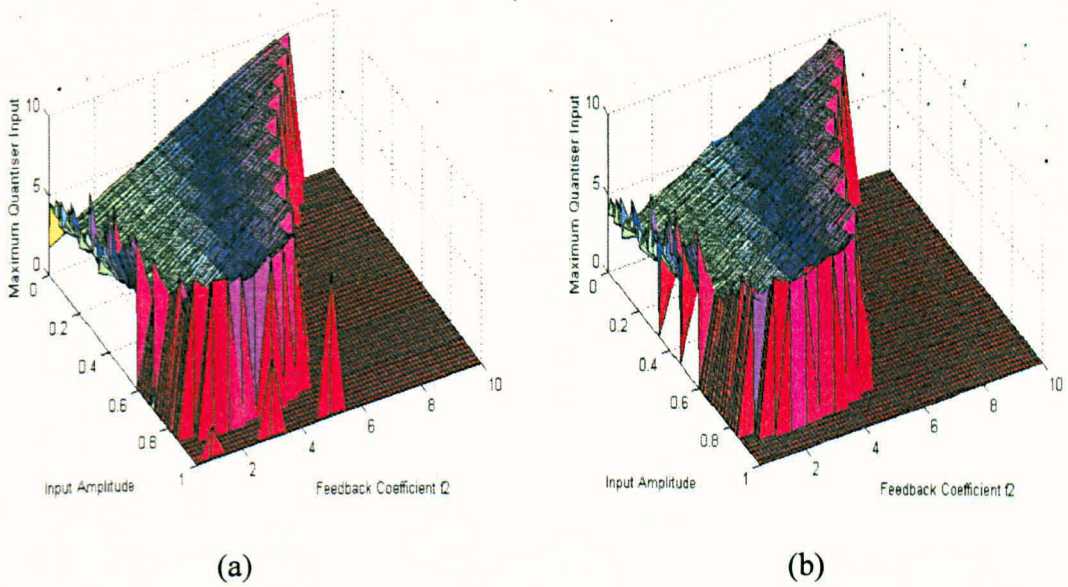


Figure 5.9 Maximum Quantiser Input Amplitude versus Feedback Coefficient f_2 versus Input Amplitude for $f_1 = 1$ and $v_C = 0.25$ under (a) Zero Initial Conditions, (b) Random Initial Conditions.

The 3D plots in Figure 5.10 were obtained by sweeping the input amplitudes and feedback coefficients from 0 to 1, 1 to 10 and 1 to 10 respectively for 100 equi-spaced divisions. The motivation here was to evaluate the effect of modulator stability versus input amplitude by simultaneously changing the two feedback coefficients f_1 and f_2 for zero initial conditions, an OSR of 128 and an input amplitude of 0.01. The following conclusions can be drawn from these plots. First; increasing the value of f_2 from 1 to 5 helps to improve the modulator stability as long as f_1 remains below 4. Second; the modulator stability deteriorates as f_2 exceeds 5, resulting in smaller DRs. Third; the modulator becomes permanently unstable when $f_2 > 8$. Fourth; better stability is always achieved when the values of f_1 are always smaller than f_2 . Fifth; when f_2 exceeds 5, the modulator begins to have sporadic regions of stability. Sixth; these plots show that the input levels, size and shape of the stability regions of this modulator are a function of f_1 and f_2 . Seventh; the input signals, which have low-amplitudes tend to span over a wider stable region compared with large-amplitude inputs.

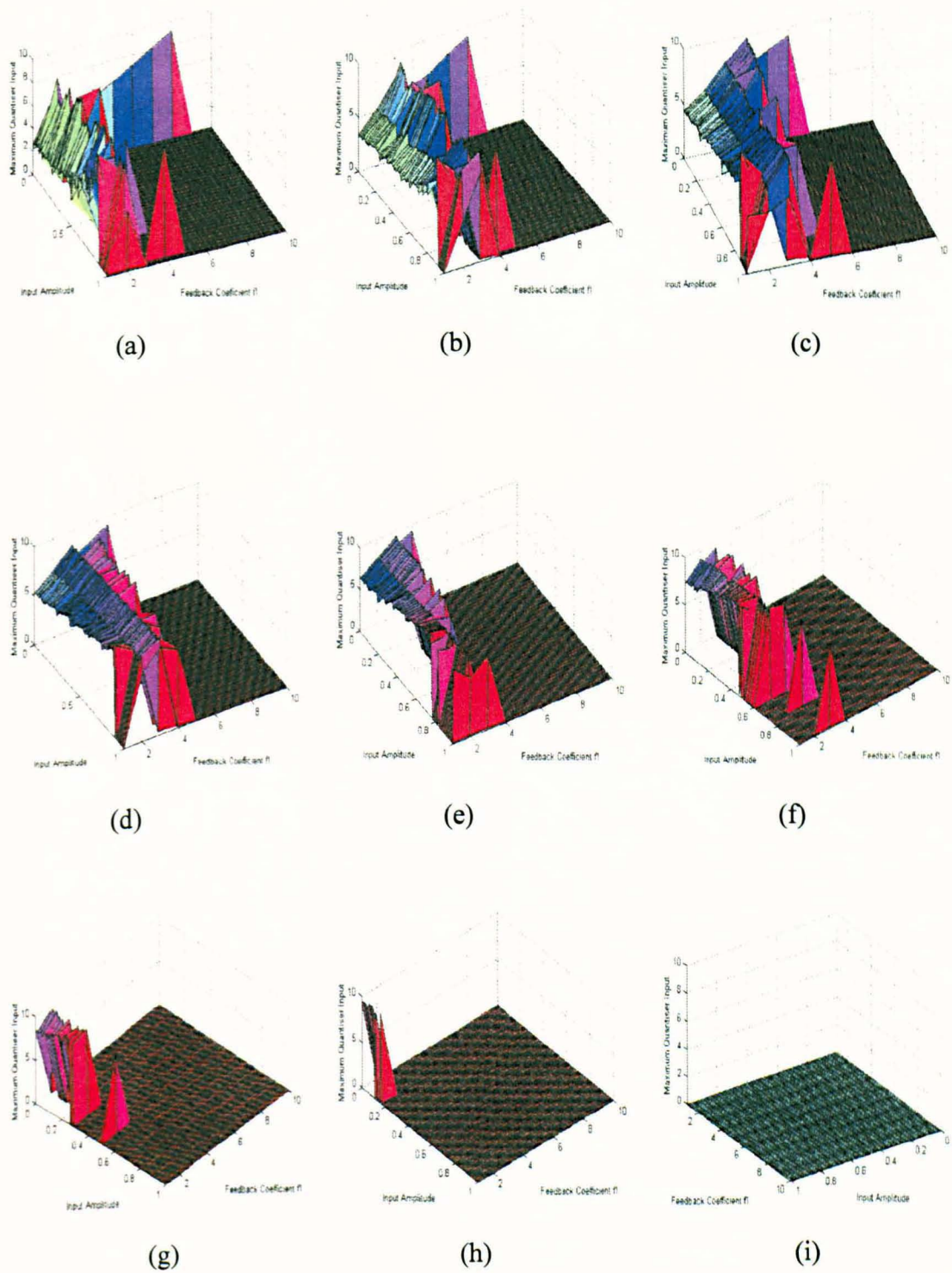
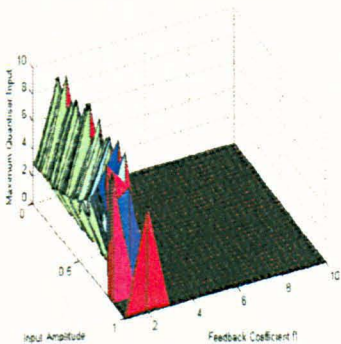
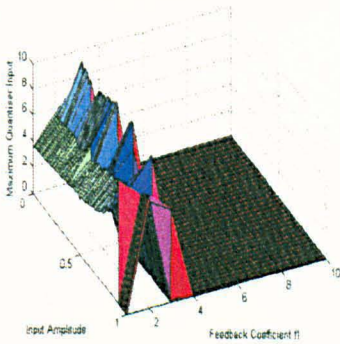


Figure 5.10 Maximum Quantiser Input Amplitude versus Feedback Coefficient f_1 versus Input Amplitude for $v_C = 0.25$ under Zero Initial Conditions, (a) $f_2 = 1$, (b) $f_2 = 2$, (c) $f_2 = 3$, (d) $f_2 = 4$, (e) $f_2 = 5$, (f) $f_2 = 6$, (g) $f_2 = 7$, (h) $f_2 = 8$ and (i) $f_2 = 9$.

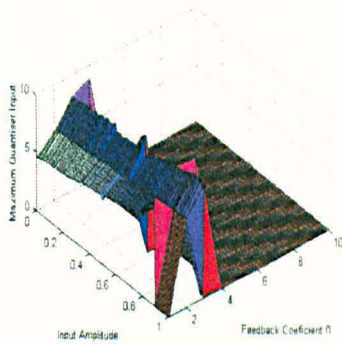
The plots in Figure 5.11 were generated for the same modulator parameters, but this time for a random set of initial conditions. First; the ‘a’ plot shows that this modulator became unstable for all input levels, when $f_1 > 3$. Second; the region of modulator stability especially for the low input-amplitudes was shown to be sensitive to the random initial conditions of the resonators as well as the feedback coefficients of the modulator.



(a)



(b)



(c)

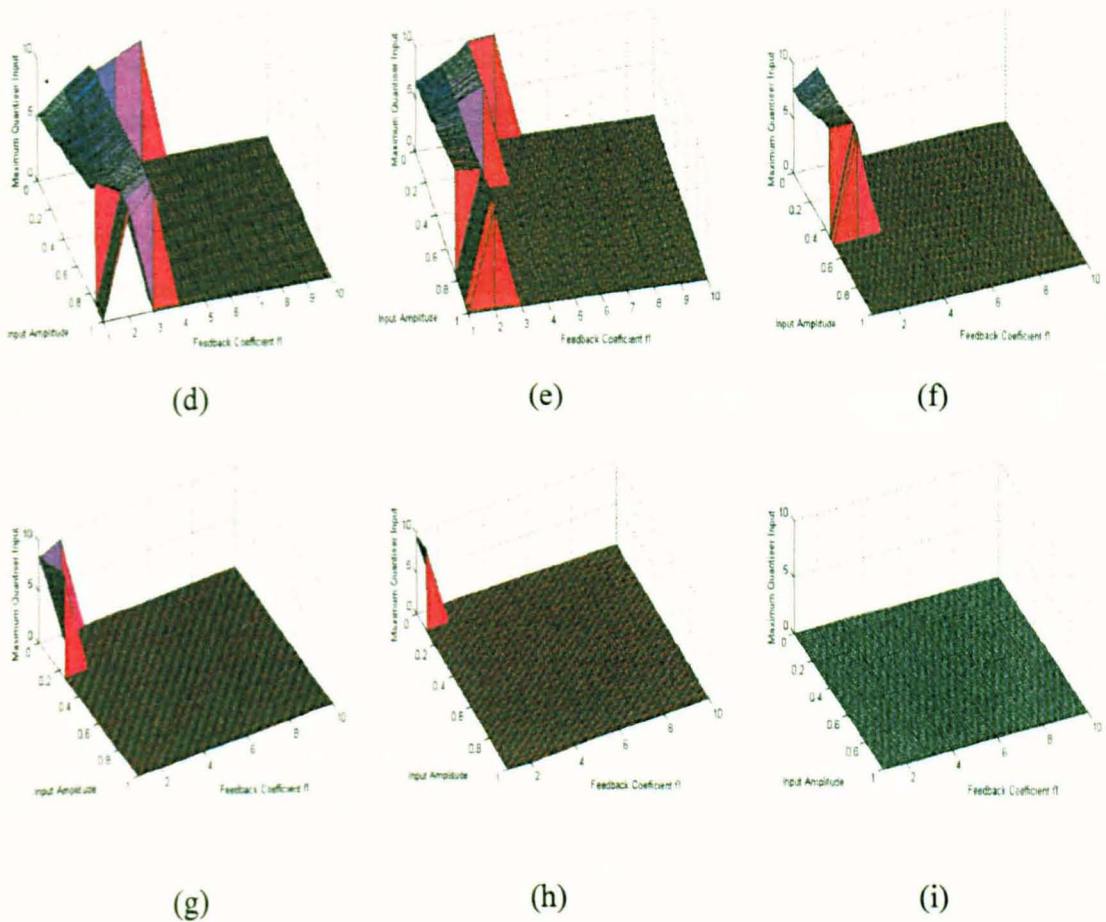


Figure 5.11 Maximum Quantiser Input Amplitude versus Feedback Coefficient f_1 versus Input Amplitude for $v_c = 0.25$ for Random Initial Conditions, (a) $f_2 = 1$, (b) $f_2 = 2$, (c) $f_2 = 3$, (d) $f_2 = 4$, (e) $f_2 = 5$, (f) $f_2 = 6$, (g) $f_2 = 7$, (h) $f_2 = 8$ and (i) $f_2 = 9$.

5.7.4 Feedforward Loop-Filter Gains

An alternative approach to stabilise higher-order single-bit Σ - Δ modulators is to employ small gains for the loop-filter resonators in order to reduce the magnitude of the signals circulating in the feedforward path [Bai93]. This lowers the noise suppression in the in-band region, thus relaxing the steep rise in the out-of-band quantisation noise and thereby maintaining modulator stability. The price paid for this stabilisation improvement is lower SNRs [Hei91]. A compromise has to be reached, where these values must be sufficiently low to ensure modulator stability. However, they should not be excessively small as this causes the NTF poles to be shifted close to the NTF zeros, thereby degrading the noise-shaping response of the modulator [Bai94]. Intuitively, the resonator furthest away from the quantiser should have the smallest gain value in order to control the

amplitude level of the first-stage signal components before they become amplified by the gains of subsequent resonator stages. It makes good common sense to have coefficients whose values increase from the first to the last resonator to adequately control the internal signal levels of the modulator. A useful rule-of-thumb based on extensive simulations is to double the resonator gain value for each consecutive succeeding resonator. Care should be taken to ensure that the first resonator gain is not made unnecessarily low, as this will result in degraded noise-shaping performance and lower in-band SNRs. Therefore, a compromise has to be reached for choosing suitable gain values that will ensure stability without significant penalties in SNR and DR.

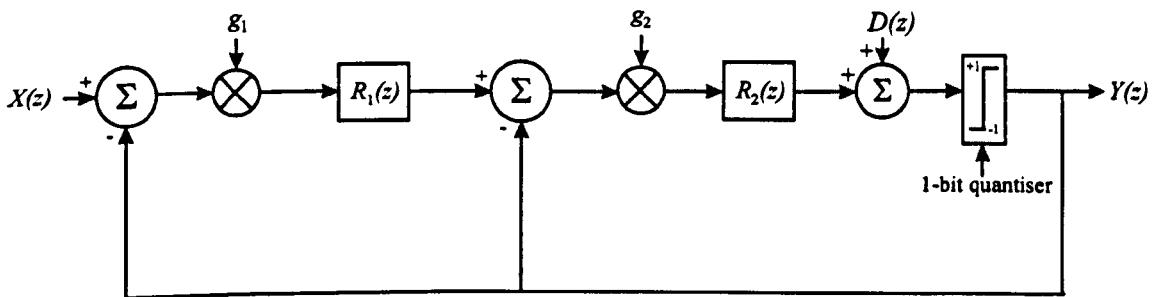


Figure 5.12 Chain of Resonators with Distributed Feedback.

The 3D plots in Figure 5.13 were generated by sweeping the input amplitude and resonator gain of the first stage g_1 in steps of 0.01 and 0.1 respectively, while keeping the second stage resonator gain g_2 set to unity. The two 3D plots in Figure 5.13 show the maximum quantiser input amplitude versus the modulator input and g_1 for zero and random initial conditions respectively. The plots in Figure 5.14 were generated using the same number of points, but this time g_2 was varied, while g_1 was set to unity. The following observations were made. First; the modulator remained stable for almost all the input amplitude levels. Second; the amplitude of the quantiser input increased with respect to the modulator input amplitude. The quantiser inputs in Figure 5.13 had larger input amplitudes, because only g_2 was scaled down. This is in contrast to Figure 5.14, where all the internal signals in the modulator including the quantiser input signal had much smaller amplitudes, because of the gain reduction in the first stage, which had greater control over all the internal signals in the modulator. In addition, the use of random initial conditions resulted in modulators, whose amplitudes increased more rapidly.

The 3D plots in Figure 5.13 were generated by simultaneously varying g_1 and g_2 in steps of 0.1 to evaluate their effect on modulator stability. The following observations were made. First; the quantiser input amplitude progressively increased as g_2 became larger. Second; a rise in g_1 caused the quantiser input amplitude to increase as well. However, this increase became more significant with both g_1 and g_2 increasing as depicted in Figure 5.15 by the more frequent occurrence of peaks for the higher-amplitude input signals. Also, the modulator remained stable for almost the entire DR, until g_2 exceeded 0.9, where it began to exhibit tones as a result of substantial quantiser overloading. The simulations showed that there are diminishing returns in SNR improvement as the resonator gains are increased too much. As the Σ - Δ modulator is driven close to the edge of its stability threshold as a result of very high resonator gains, both the SNR and DR are reduced.

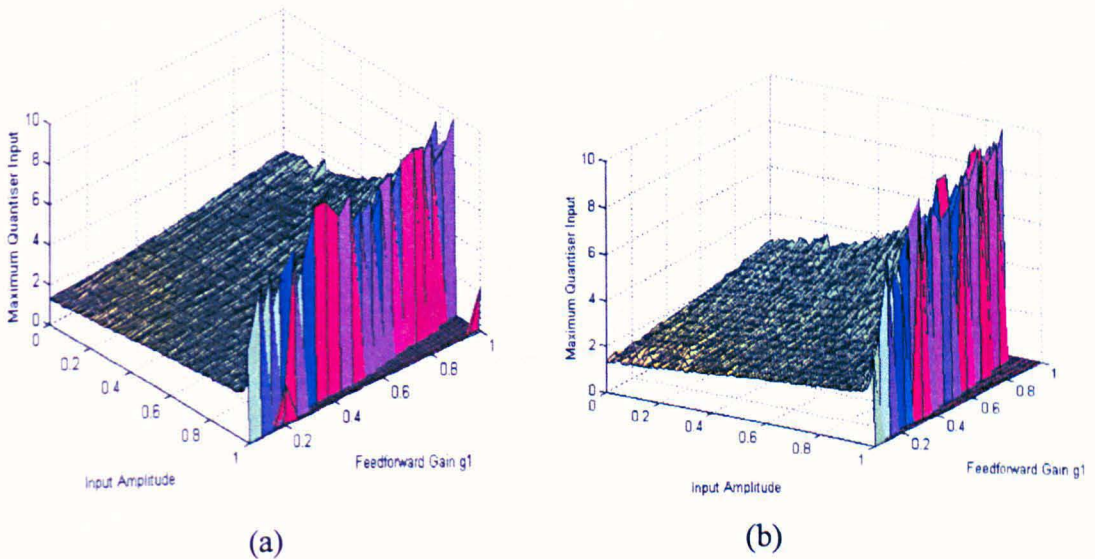
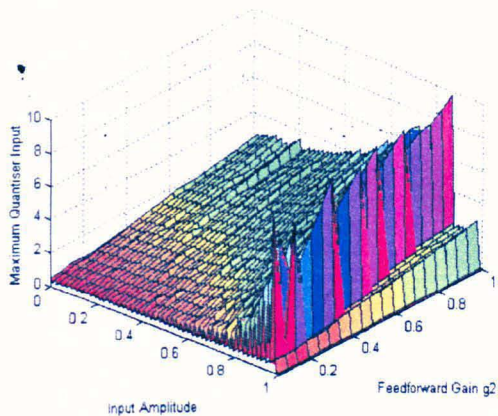
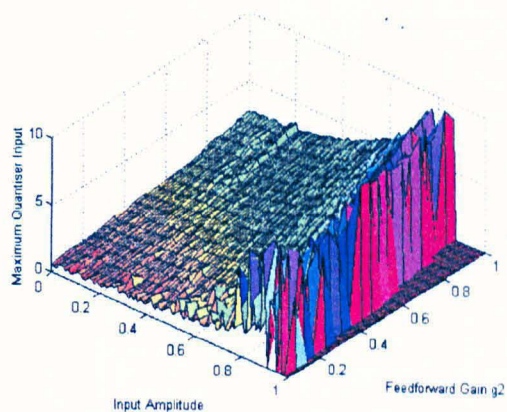


Figure 5.13 Maximum Quantiser Input Amplitude versus Feedback Coefficient g_1 versus Input Amplitude for $g_2 = 1$ and $v_C = 0.25$ under (a) Zero Initial Conditions, (b) Random Initial Conditions.

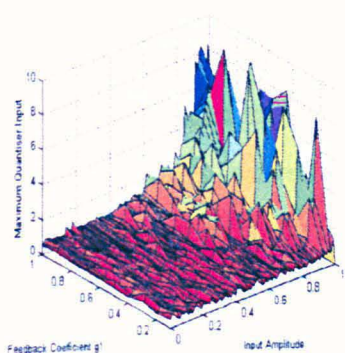


(a)

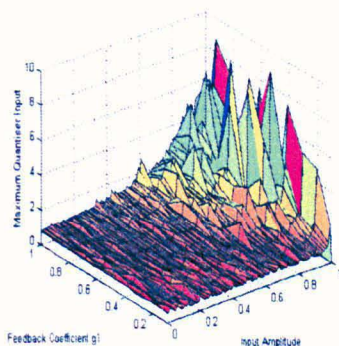


(b)

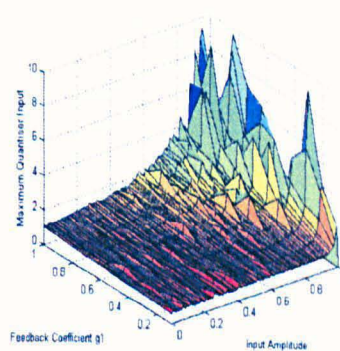
Figure 5.14 Maximum Quantiser Input Amplitude versus Feedback Coefficient g_2 versus Input Amplitude for $g_1 = 1$ and $v_C = 0.25$ under (a) Zero Initial Conditions, (b) Random Initial Conditions.



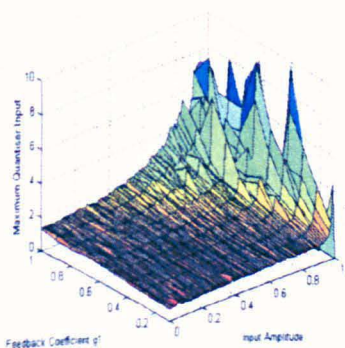
(a)



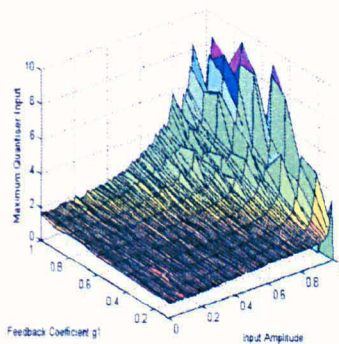
(b)



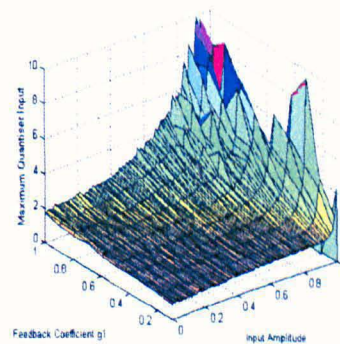
(c)



(d)



(e)



(f)

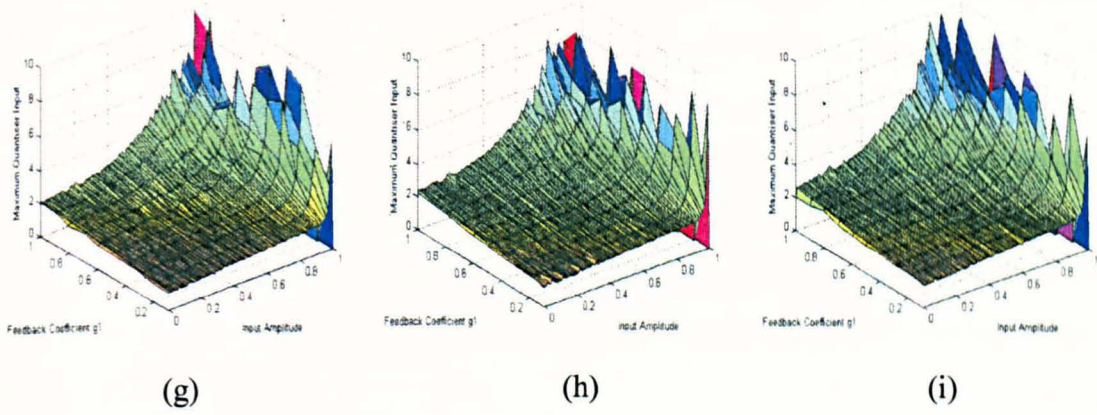


Figure 5.15 Maximum Quantiser Input Amplitude versus Feedback Coefficient g_1 versus Input Amplitude for $v_C = 0.25$ for Random Initial Conditions, (a) $g_2 = 0.1$, (b) $g_2 = 0.2$, (c) $g_2 = 0.3$, (d) $g_2 = 0.4$, (e) $g_2 = 0.5$, (f) $g_2 = 0.6$, (g) $g_2 = 0.7$, (h) $g_2 = 0.8$ and (i) $g_2 = 0.9$.

5.7.5 Number of Delayers

The sixth- and eighth-order Σ - Δ modulators based upon a cascade of resonators with distributed feedback to each stage are popular topologies for A/D conversion applications due to their inherent ease of hardware implementation [Ada91]. This section starts by examining three variants for the sixth-order Σ - Δ modulator: the first with a double delay associated with only the final resonator, the second with delays in the latter stages and the third with all three resonators providing delay.

Previous work reported in [Bai94] showed that the number of delayers in the feedforward path had a significant effect on the stability and DR of the modulator. A conventional third-order lowpass Σ - Δ modulator with a single-delayer in its third stage remained stable until the modulator input reached 0.7. This was in contrast to another third-order modulator, whose constituent accumulators were all delayed, which remained stable up to an input amplitude of 0.5.

Sixth- and eighth-order Σ - Δ modulators were designed using Butterworth filters, whose coefficients for different delayer combinations are listed in Table 5.6. The knee plots in Figure 5.16 and Figure 5.17 as well as the results shown in Table 5.7 and Table 5.8, indicated that the number of delayers has virtually no effect on the modulator stability or indeed on its DR. These simulations were repeated, but with the resonators containing random initial conditions. Once again, there was little discrepancy in the maximum stable input amplitudes for the different delayer combinations. This is attributed to the fact that

the arbitrary selection of resonator gains as was the case in [Bai94] resulted in significantly different modulator transfer functions, whose stability robustness varied according to the modulator input. In this case, however, the gains of the modulator were varied so as to preserve the modulator transfer function. It should be pointed out that the substitution of delayed accumulators with delayed resonators for the same modulator coefficients as used in [Bai94] did not preserve the stability properties of the modulator. Figure 5.18 and Figure 5.19 show the knee plots for the resonator outputs and quantiser input, but this time using random initial conditions.

Order	g_1	g_2	g_3	g_4
Sixth-Order Single-Delay	0.1169	0.2074	-0.3564	-
Sixth-Order Double-Delay	0.1064	-0.1880	-0.4390	-
Sixth-Order Triple-Delay	-0.0947	-0.2077	-0.4390	-
Eighth-Order Single-Delay	0.0923	0.1677	0.2630	-0.4379
Eighth-Order Double-Delay	0.0845	0.1548	-0.2373	-0.5741
Eighth-Order Triple-Delay	0.0779	-0.1438	-0.2771	-0.5741
Eighth-Order Quadruple-Delay	-0.0723	-0.1550	-0.2771	-0.5741

Table 5.6 Coefficients of Sixth- and Eighth- Order Butterworth Based Σ - Δ Modulators for Different Delayer Combinations.

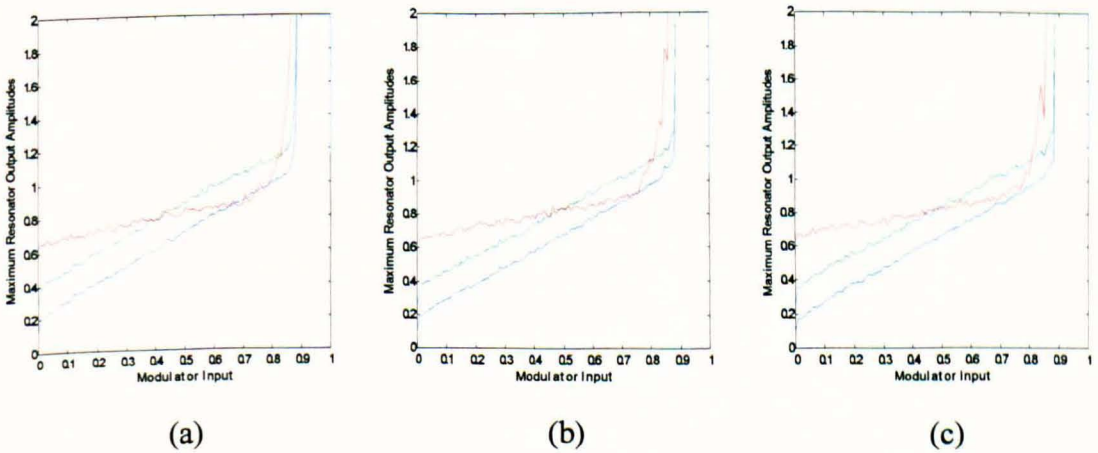


Figure 5.16 Knee Plots Depicting Resonator Output Amplitudes for Different Delayer Combinations of 6th-Order Σ - Δ Modulators for Zero Initial Conditions.

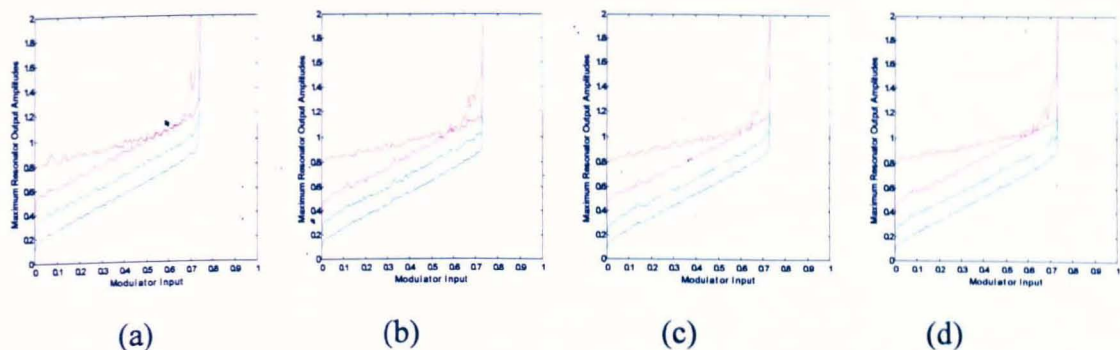
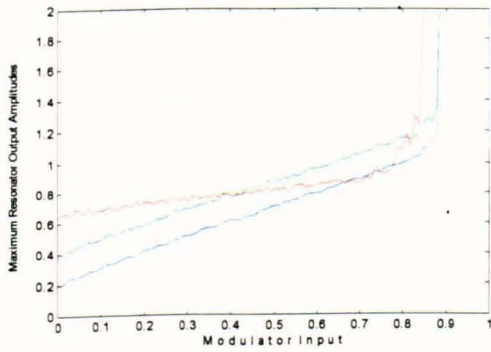


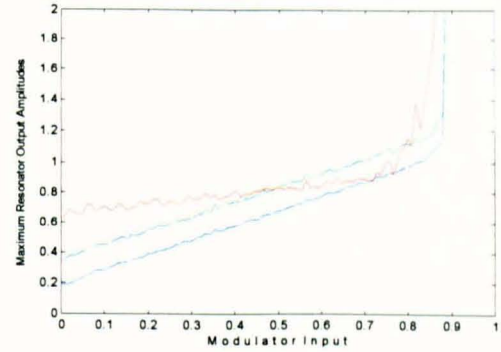
Figure 5.17 Knee Plots Depicting Resonator Output Amplitudes for Different Delayer Combinations of 8th-Order Σ - Δ Modulators for Zero Initial Conditions.

Modulator Order	Sixth-Order			Eighth-Order			
	z^{-1}	z^{-2}	z^{-3}	z^{-1}	z^{-2}	z^{-3}	z^{-4}
Max Quantiser Input	6.71	3.297	3.546	2.253	1.493	1.794	1.52
Max Modulator Input	0.879	0.879	0.879	0.737	0.727	0.727	0.727
SNR before Instability	83.11	85.3	83.11	109.97	111.08	110.78	112.16
Max SNR	95.2	95.19	95.2	112.96	112.86	112.83	112.62
Input Amp. - Max SNR	0.737	0.758	0.737	0.646	0.677	0.677	0.657
Peak NTF Magnitude	1.25	1.25	1.25	1.33	1.33	1.33	1.33
Max Reson 1 Amp.	1.169	1.046	1.136	1.108	1.183	1.091	1.157
Max Reson 2 Amp.	1.64	1.303	1.315	1.14	1.043	1.054	1.041
Max Reson 3 Amp.	6.68	3.286	3.510	1.297	1.156	1.188	1.165
Max Reson 4 Amp.	-	-	-	2.142	1.506	1.806	1.546

Table 5.7 Maximum Quantiser Input and Peak Resonator Output Amplitudes for Different Delayer Combinations of 6th- and 8th-Order Σ - Δ Modulators for Zero Initial Conditions.

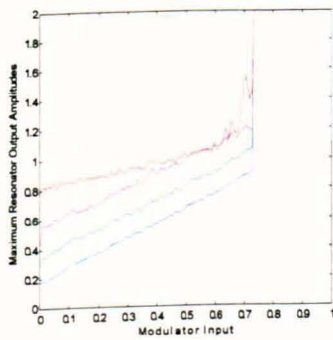


(a)

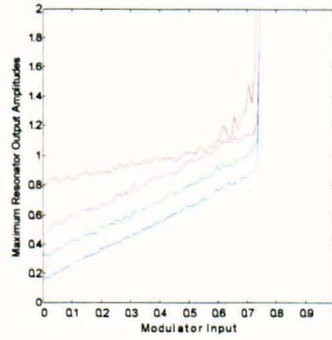


(b)

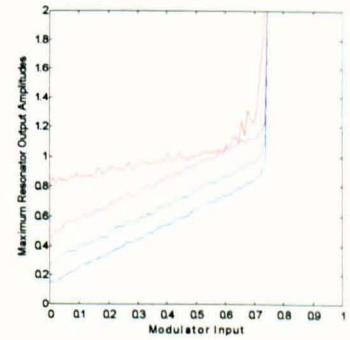
Figure 5.18 Knee Plots Depicting Resonator Output Amplitudes for Different Delayer Combinations of 6th-Order Σ - Δ Modulators for Random Initial Conditions.



(a)



(b)



(c)

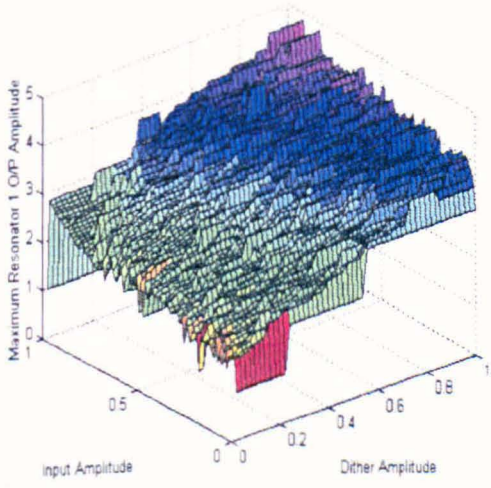
Figure 5.19 Knee Plots Depicting Resonator Output Amplitudes for Different Delayer Combinations of 8th-Order Σ - Δ Modulators for Random Initial Conditions.

Modulator Order	Sixth-Order			Eighth-Order			
	z^{-1}	z^{-2}	z^{-3}	z^{-1}	z^{-2}	z^{-3}	z^{-4}
Max Quantiser Input	3.351	3.584	2.693	1.579	2.389	2.382	2.155
Max Modulator Input	0.879	0.879	0.869	0.727	0.737	0.737	0.737
SNR before Instability	85.17	84.03	88.17	109.2	110.45	109.51	109.83
Max SNR	95.61	95.51	95.32	112.52	112.75	112.17	112.94
Input Amp. - Max SNR	0.697	0.758	0.677	0.687	0.677	0.636	0.616
Peak NTF Magnitude	1.25	1.25	1.25	1.33	1.33	1.33	1.33
Max Reson 1 Amp.	1.095	1.192	1.017	1.106	1.182	1.18	1.102
Max Reson 2 Amp.	1.362	1.307	1.262	1.075	1.125	1.09	1.09
Max Reson 3 Amp.	3.282	3.58	2.649	1.183	1.227	1.246	1.209
Max Reson 4 Amp.	-	-	-	1.455	2.29	2.352	2.087

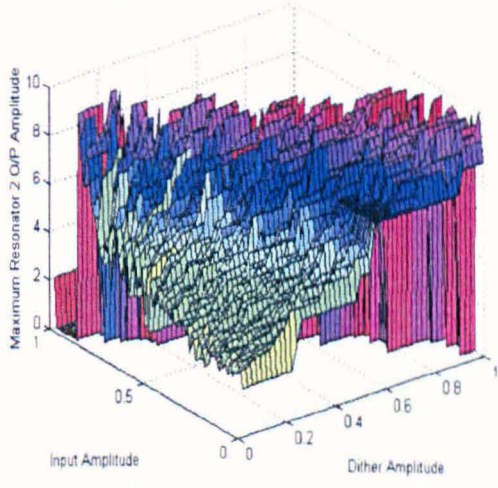
Table 5.8 Maximum Quantiser Input and Peak Resonator Output Amplitudes for Different Delayer Combinations of 6th- and 8th-Order Σ - Δ Modulators for Random Initial Conditions.

5.7.6 Effect of Dither on Stability

As already discussed in Chapter 1, the injection of dither prior to the quantiser input serves to alleviate the tonal content from the output of a Σ - Δ modulator. However, this is achieved at the expense of an increase of in-band quantisation noise. Another shortcoming, which becomes more apparent with higher-order Σ - Δ modulators is the reduction in DR, which is further degraded due to the utilisation of dither. This section presents simulation results of a special-case 4th-order resonator-based Σ - Δ modulator. It is demonstrated that the amplitude of the internal signal levels rise in proportion to the amplitude of the dither signal. The maximum amplitudes from the outputs of the first and second resonators are recorded for a single-tone input signal ranging from 0 to 1, as shown in Figure 5.20 (a) and (b). The peak amplitude quantiser input signal, which is connected after the additive dither signal and prior to the quantiser is recorded and compared with the output of the second resonator as shown in Figure 5.20(c). A simultaneous variation of the modulator input and dither amplitude with respect to the in-band SNR for this modulator is shown In Figure 5.20(d).



(a)



(b)

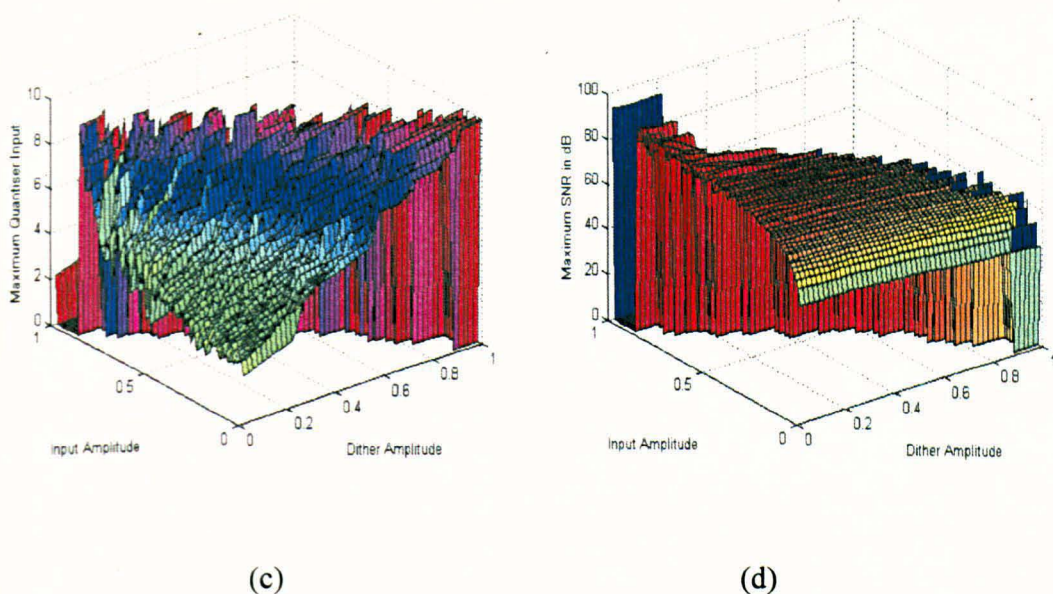


Figure 5.20 (a) Maximum Resonator 1 Output Amplitude, (b) Maximum Resonator 2 Output Amplitude, (c) Maximum Quantiser Input Amplitude, (d) Maximum SNR, versus Input Signal Amplitude versus Dither.

The four plots in Figure 5.20 demonstrate that the injection of dither at the quantiser input serves to reduce tonal content especially in the signal region, but at the same time lower the SNRs and DRs of Σ - Δ modulators. Simulations also confirmed that relatively high-amplitude dithers were needed, particularly, in the case of lower-order Σ - Δ modulators to sufficiently dilute in-band tones. Needless to say, the best location for the inclusion of dither was at the quantiser input, because that took advantage of noise-shaping, which ensured that the bulk of the added dither was shifted to the out-of-band region leaving as little as possible in the signal band. Furthermore, higher-order Σ - Δ modulators were found to require smaller amounts of dither to alleviate in-band signal content, due to the randomisation effect of the extra loop-filters. It was also shown that MASH Σ - Δ modulators required dither in all their constituent stages, so as to avert the propagation of tones into the latter stages in order to preserve the overall resolution of the modulator.

5.7.7 Dependence of Modulator Stability on the Number of Quantisation Levels

The cumulative magnitude imparted by a higher-order loop-filter amplifies the intermediate signal levels of a Σ - Δ modulator causing the 1-bit quantiser to prematurely overload and rendering modulator instability. One means of enhancing stability is to replace the 1-bit quantiser with a multi-level quantiser which results in the generation of comparatively smaller-amplitude signals. The knee plots in Figure 5.21 demonstrate that

the stability of a tenth-order $\Sigma\text{-}\Delta$ modulator improves as the number of quantiser levels is increased.

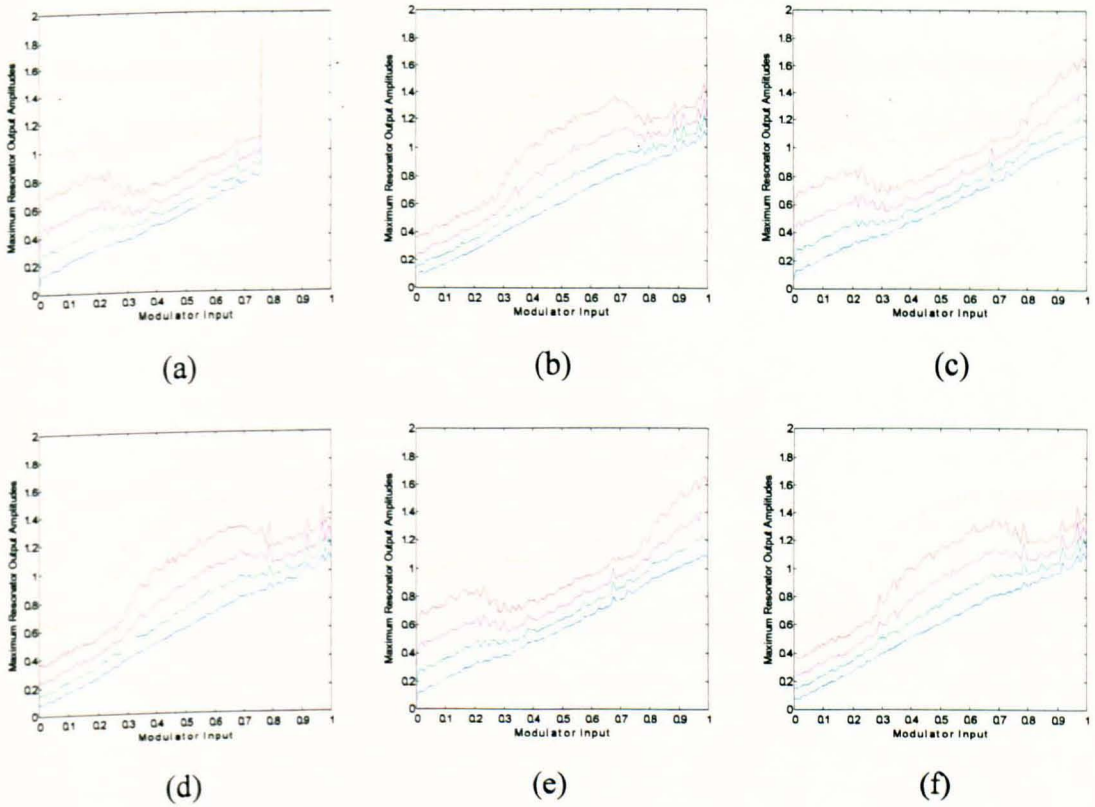


Figure 5.21 Knee Plots Depicting Resonator Output Amplitudes for a 10th-Order $\Sigma\text{-}\Delta$ Modulator for Various Multi-Level Quantisers for Random Initial Conditions (a) 3-Level, (b) 4-Level, (c) 5-Level, (d) 6-Level, (e) 7-Level and (f) 8-Level.

The use of multi-bit quantisers in $\Sigma\text{-}\Delta$ modulators decreases the magnitude of the quantisation noise, consequently reducing quantiser overloading [Bai94]-[Bai96]. This improvement in stability relaxes the constraints on other design parameters, which can be exploited to enhance SNRs and DRs.

5.7.8 Dependence of Modulator Stability on Multi-Sinusoidal Inputs

The effect of closely-adjointing multi-tone sinusoids on the stability of higher-order $\Sigma\text{-}\Delta$ modulators is quantitatively evaluated at the behavioural level. A sixth-order distributed feedback $\Sigma\text{-}\Delta$ modulator is empirically tested with 2-Input, 3-input, 4-input and 5-Input sinusoidal combinations given by:

$$X_2(\nu) = \sin 1.99\pi\nu + \sin 2.01\pi\nu \tag{5.13}$$

$$X_3(\nu) = \sin 1.99\pi\nu + \sin 2\pi\nu + \sin 2.01\pi\nu \tag{5.14}$$

$$X_4(\nu) = \sin 1.99\pi\nu + \sin 1.995\pi\nu + \sin 2.005\pi\nu + \sin 2.01\pi\nu \quad (5.15)$$

$$X_5(\nu) = \sin 1.99\pi\nu + \sin 1.995\pi\nu + \sin 2\pi\nu + \sin 2.005\pi\nu + \sin 2.01\pi\nu \quad (5.16)$$

The knee-plots presented in Figure 5.22 and results Table 5.9 confirm that the stability of this Σ - Δ modulator is decreased as the number and amplitude level of the input signals increased.

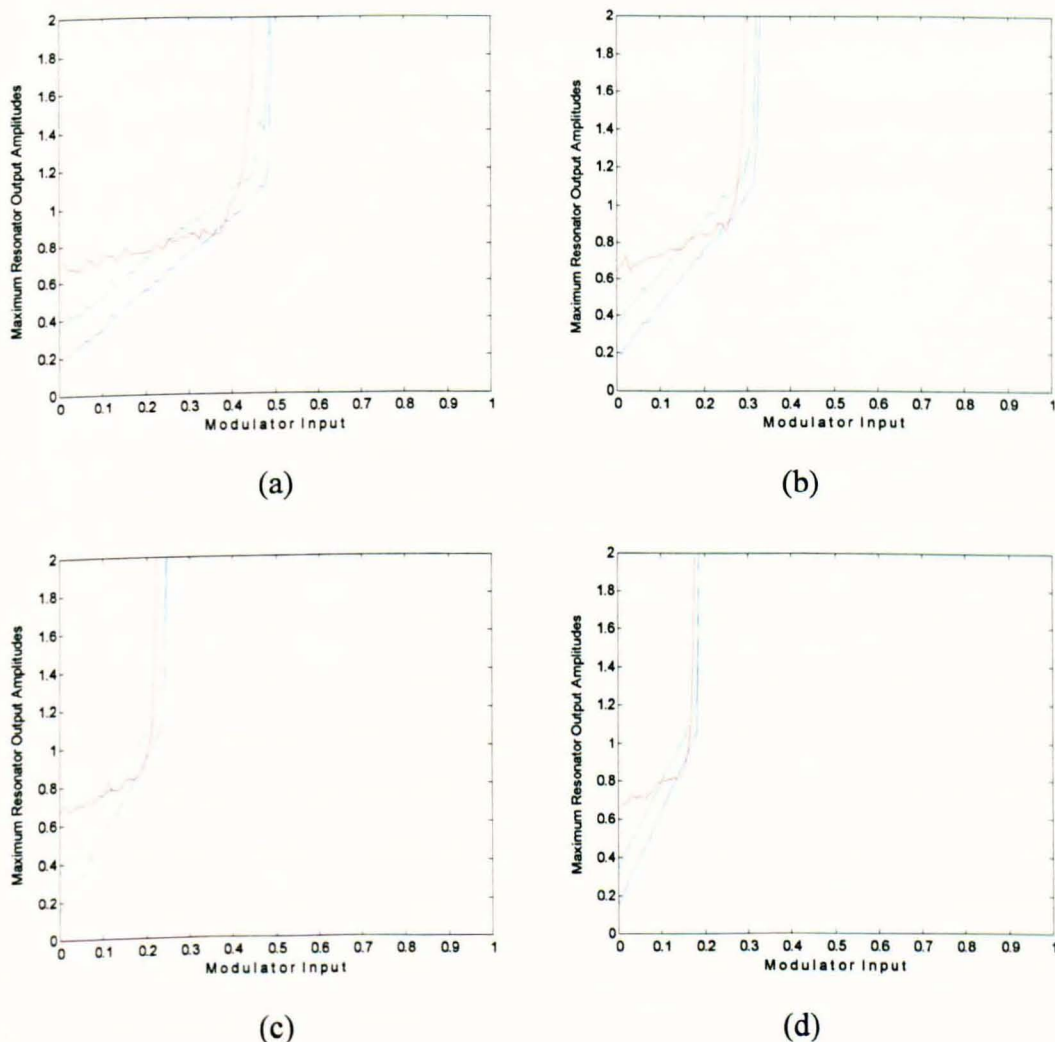


Figure 5.22 Knee Plots Depicting Resonator Output Amplitudes for a 6th-Order Σ - Δ Modulator for Multi-Tone Input Sinusoids under Random Initial Conditions (a) 2-Tones, (b) 3-Tones, (c) 4-Tones and (d) 5-Tones.

Modulator Order	Zero Initial Conditions				Random Initial Conditions			
	2 I/P	3 I/P	4 I/P	5 I/P	2 I/P	3 I/P	4 I/P	5 I/P
Max Quantiser Input	8.606	6.068	4.694	3.315	6.239	5.025	9.042	2.462
Max Modulator Input	0.485	0.313	0.232	0.182	0.475	0.313	0.242	0.182
Max Reson 1 Amp.	1.207	1.119	1.103	1.084	1.224	1.38	1.274	1.069
Max Reson 2 Amp.	1.777	1.438	1.363	1.29	1.93	2.112	1.814	1.236
Max Reson 3 Amp.	8.576	6.031	4.636	3.201	6.168	4.998	9.041	2.383

Table 5.9 Maximum Quantiser Input and Peak Resonator Output Amplitudes for Different Delayer Combinations of 6th- and 8th-Order Σ - Δ Modulators for Zero and random Initial Conditions.

Concluding Remarks to Chapter 5

In this chapter, a brief categorisation of the different interpretations of stability as well as a review of existing stability rules-of-thumb were presented. An analytical method employing the Jury Criterion was proposed, which could be used to identify the stable range of quantiser gains for ideal and non-unity-gain variable-band fourth-order resonator-based bandpass Σ - Δ modulators. It was demonstrated that the critical quantiser gain range was increased as the centre frequency approached half-Nyquist culminating in a peak value for mid-band resonance. It was shown that lowering the resonator gains resulted in a higher stable quantiser gain range and therefore more stable modulators. However, the resonator gains should not be reduced more than necessary in order to control the noise level in the in-band region. Theoretical findings coupled with root locus plots demonstrated that identical quantiser gain ranges and symmetrical plots about the real axes were obtained for all conjugal quartet centre frequencies.

The factors that directly control stability in Σ - Δ modulators were investigated at the behavioural level. Some of these reinforced, what was intuitively expected and their effect on stability was supported, where appropriate by simulation results. First, simulations showed that the maximum stable input amplitude to the modulator decreased as the modulator order was increased. It was shown that the maximum input amplitudes were 1, 0.99, 0.88, 0.73, 0.60, 0.47 and 0.28 for the 2nd-, 4th-, 6th-, 8th-, 10th-, 12th- and 14th-order variable-band bandpass Σ - Δ modulators. Second, it was empirically confirmed that modulator stability could be enhanced by progressively increasing the feedback coefficients such that the one closest to the quantiser had the highest value. Integer coefficient

combinations were recommended as these were easier to implement. Third, an alternative stability approach was to use small gains for the loop-filter resonators in order to reduce the magnitudes circulating in the feedforward path. Intuitively; the resonator furthest away from the quantiser should have the smallest gain value in order to control the amplitude level of the first-stage signal components before they were amplified by the gains of the later resonator stages. Fourth, the relationship between the number of delayers and stability was examined for different Butterworth filters, whose coefficients varied for different delayer combinations. There was little difference in the maximum stable input amplitudes for different delayer combinations. This was attributed to the fact that the gains of the modulator were varied so as to preserve the modulator transfer function. Fifth, it was shown that the inclusion of a dither signal at the quantiser input reduced the tonal content of the modulator output. However, this resulted in increased in-band quantisation noise and a lower DR. This result implied that a trade-off should be made between the stability, tonality and SNRs in Σ - Δ modulators. Sixth, it was shown through detailed simulations that modulator stability was enhanced as the number of levels in the quantiser increased, because multi-level quantisers produced comparatively smaller-amplitude signals. It was also shown that this stability improvement relaxed the other constraints on other design parameters, which could be exploited to improve SNRs and DRs. Seventh, the type of input signal on the stability of Σ - Δ modulators was examined for closely-adjointing multi-tone sinusoids, where it was shown that modulator stability was reduced as the number of tones was increased. It was also shown that when the number of tones increased, it was necessary to reduce their amplitudes in order to ensure modulator stability.

Chapter 6

Conclusions and Suggestions for Future Research

6.1 Concluding Remarks

In chapter 1, the fundamental principles of Σ - Δ modulation were reviewed and compared with Nyquist rate and conventional oversampling A/D converters. A discussion addressing some of the problems associated with the design analysis and evaluation of these Σ - Δ modulators was presented. A major literature survey at the time showed that there was a considerable vacuum in the area of bandpass Σ - Δ modulation. This in conjunction with the continued demand for high-resolution A/D converters represented the prime motivation behind this work. Chapter 1 provided a detailed explanation of the operation of a first- and higher-order lowpass Σ - Δ modulators, including the popular distributed feedback topology. The chapter culminated by explaining the simulation approach and defining specifically the performance criteria that were used for the evaluation of all the Σ - Δ modulators in this thesis.

Chapter 2 started by reviewing the fundamental principles of bandpass Σ - Δ modulation. A system-level description of a typical bandpass A/D converter was given, where the operation of each constituent building-block was briefly described. This was followed by a chronological survey of reported publications, an up-to-date review of hardware implementations and a summary of potential applications of bandpass Σ - Δ modulators. The lowpass-to-bandpass frequency transformation $z^{-1} \rightarrow -z^{-2}$, for the design of mid-band resonator-based bandpass Σ - Δ modulators was explained and analysed in greater depth. Several methods, based on the author's experience, of enabling the modulator to function correctly in a simulation environment were discussed. This transformation was extended to higher-order mid-band resonator-based bandpass Σ - Δ modulators. The noise-shaping properties and the SNR characteristics were evaluated for the fourth-, sixth- and eighth-order bandpass Σ - Δ modulators. The peculiar appearance of unexpected notches in the magnitude spectra of the higher-order modulators, which had not been accounted for in the open literature, was explained and supported with detailed simulation results. A heuristic solution based on the appropriate selection of modulator feedback coefficients was provided, which enabled the stabilisation of higher-order Σ - Δ modulators.

The lowpass-to-bandpass frequency transformation technique proposed by Harris [Har93] for the design of variable-band bandpass Σ - Δ modulators was discussed and mathematically analysed. Simulation results were provided to indicate the correct operation for the second-order variable-centre frequency bandpass Σ - Δ modulator. However, the analysis in [Har93] were extended to the fourth-order case, where it was shown with the aid of simulations that the noise-shaping properties were no longer preserved due to the asymmetrical magnitude spectrum of the loop-filter. Detailed behavioural-level simulations were carried out for this fourth-order variable-band Σ - Δ modulator, where the stability of the modulator was examined for each noise-shaping band-location across the spectrum for the entire dynamic range of the modulator. This showed that when all its coefficients were set to unity, this modulator remained stable for the narrow-range $0.22 \leq \nu_c \leq 0.28$. Despite its relatively straightforward application, this technique had several drawbacks. Firstly; a working lowpass Σ - Δ modulator prototype was always needed, whose noise-shaping properties and stability were not maintained after the transformation. Secondly; the unequal shoulder-gain levels imparted by the loop-filter worsened modulator stability and imposed tighter specifications on the post bandpass decimator. Thirdly; good SNR figures were only attainable for extremely narrow-bandwidths. Fourthly; the designer was limited to only specifying the central location of the noise-shaping band and OSR, having no freedom over setting other parameters that govern the stability and tonality properties of the modulator. These limitations coupled with the accelerating demand for easy-to-design variable-band bandpass Σ - Δ modulators provided ample justification for the further development of existing techniques and the search of alternative novel approaches that could deliver improved noise-shaping spectra and better resolution.

Based upon the above comments, a starting-point involved developing the Harris lowpass-to-bandpass frequency transformation technique so as to allow the designer to specify the bandwidth as well as the centre frequency location for any NTF specification. A simple algorithm incorporating this transformation to facilitate the design of variable-band Σ - Δ modulators was presented. This algorithm was coded into Matlab to provide the rapid derivation of the loop-filter coefficients for any differencer-based NTF. This approach was verified using behavioural-level simulations for the first-, second- and third-order accumulator-based Σ - Δ modulators.

Another technique, which was developed involved utilising variable-centre frequency notch filters for the NTF of these modulators to achieve maximum quantisation noise attenuation in the signal region. The design criteria in combination with linear

mathematical analysis and empirical deductions were carried out for modulators, whose NTFs employed FIR notch-filters, IIR notch-filters, complex FIR notch-filters and complex IIR notch-filters. The salient features for each NTF method were discussed, and where appropriate supported with simulation results. The fourth-order variable-band Σ - Δ modulator using the FIR notch-filter method was shown to remain stable for a slightly wider range of frequencies. This was attributed to the larger coefficient in the modulator feedback, which delivered more effective noise-shaping. The effect of the uneven shoulder gain levels of the FIR notch-filter for non-mid-band centre frequencies was analysed and was deduced to be the primary cause behind the destabilisation of this fourth-order Σ - Δ modulator. The variable FIR notch filter was replaced with a suitable IIR notch filter that was capable of delivering variable-band noise-shaping in the signal region, but for a broader stable range of centre frequencies. An alternative stabilisation mechanism for this modulator involved utilising multi-level quantisers. These helped reduce the quantisation errors, therefore lessening the occurrence of quantiser overloading. The results detailing the quantitative relationships between the stable range of normalised centre frequencies and the number of quantiser levels for a fourth-order variable-band bandpass Σ - Δ modulator were empirically verified via behavioural-level simulations and documented.

An alternative novel technique for the design of bandpass Σ - Δ modulators with an embedded tuneable centre frequency mechanism was proposed, where the mathematical model for its NTF was derived from first principles. This method demonstrated that the use of a sum-filter combined with fractional-delayers provided the flexibility of spectrally transferring the noise-shaping band to the desired centre frequency location. FIR and allpass IIR filter representations of these fractional-delayers were applied and evaluated to establish their suitability. The FIR FD approach was found to suffer from inadequate noise-shaping performance at high frequencies due to errors in the amplitude of the FIR filter. For non-mid-array FD requirements, the FIR FD filter exhibited small phase errors, which caused small shifts of the noise-shaping bands towards Nyquist. The IIR allpass approach, on the other hand, gave better resolution at the expense of a more complicated loop-filter. The SNR results were comparable to those obtained from the FIR and IIR notch filter approaches, but the magnitude spectra of the FD based Σ - Δ modulators contained fewer tones. This is attributed to the more complicated loop-filter structure, which served to generate a more diverse range of state values. These naturally lessened the periodicity of the Σ - Δ modulator output signal resulting in fewer spectral tones.

A practical step-by-step method for the design of variable-band bandpass Σ - Δ modulators based on Butterworth and Chebyshev 2 filters was presented with extensive analysis and behavioural-level simulation results. Guidelines to facilitate the design and enhance the resolution of these Σ - Δ modulators were given as well. This was followed by an analysis in conjunction with structural modifications, where appropriate to allow variable-band noise-shaping. The author's contribution specifically included structural modifications to the 'chain of weighted accumulators with feedforward summation' and the 'chain of accumulators with distributed feedback' topologies to make them provide noise-shaping for mid-band centre frequencies. The latter topology was further modified to enable it to accomplish variable-band noise-shaping. Simple-to-use routines, which could compute the required coefficients for the FIR notch filter, IIR notch filter, complex FIR notch filter and complex IIR notch filter, FIR and allpass IIR FD as well as the practical bandstop NTF approaches were written in Matlab to compute the required coefficients for any system-level set of specifications. These routines could be easily operated in conjunction with a large Simulink library created by the author, which contained a myriad of real and complex single-bit and multi-bit bandpass Σ - Δ modulator topologies.

This chapter culminated by establishing via behavioural-level simulations, the effect of non-idealities on the noise-shaping performance and SNRs of a variable-band fourth-order single-bit Σ - Δ modulator. The simulation results demonstrated that this modulator was relatively insensitive to gain variations of the order of 10% to 20% in its loop-filter. In fact, moderate gain variations were shown to be beneficial in that they controlled the amplitude level of the internal signals propagating in the modulator. This reduced the occurrence of quantiser overloading and thus resulted in less tonal magnitude spectra. On the other hand, the use of leaky resonators was shown to impact the SNR characteristics in a significant way for the higher OSRs. This was attributed to the migration of the NTF zeros away from the unit-circle. The simultaneous and equal reductions of both resonator leakage factors below 0.98 produced very shallow noise-shaping responses, which helped to strengthen the power of the tones in the in-band region. The double effect of leakage in the resonators prevented the complete cancellation of the quantisation noise from the preceding samples. This resulted in the progressive build-up of noise as well as tones in the in-band region, which regrettably delivered inferior resolution, by as much as 16.5 dB for $\rho_1 = \rho_2 = 0.96$ for an OSR of 256.

In chapter 3, the underlining principles together with an explanation of the functionality of MASH Σ - Δ modulators was provided at the start. A chronological survey

showed that over 90% of all the reported publications to-date on MASH Σ - Δ modulators were designed for lowpass applications. The few papers on bandpass Σ - Δ modulators with the exception of [Ben93] utilised the $z^{-1} \rightarrow -z^{-2}$ frequency transformation, thus restricting their suitability to the popular $\nu_C = 0.25$. The clear deficiency of bandpass MASH Σ - Δ modulators coupled with the massive demand for stable high-resolution bandpass Σ - Δ modulators provided sufficient ammunition for the development of the work in this chapter.

A novel practical step-by-step approach was developed, which enabled the design of variable-band bandpass Σ - Δ modulators using one of three NTF techniques. The first method utilised either real or complex FIR notch filters for its NTF design. The second method employed a first-order sum-filter in cascade with a FIR FD filter to spectrally shift the NTF notch to the desired band location. The third method used Butterworth and Chebyshev 2 bandstop filters, to accomplish noise-shaping responses with slightly larger bandwidths. Numerous novel variable-band bandpass Σ - Δ modulators were designed, analysed and evaluated to verify their correct operation. These included the 2-2, 2-2-2, 4-2, 2-4, 2-2-2-2, 4-2-2, 2-4-2, 2-2-4 and 4-4 MASH topologies. Novel complex MASH variable-band bandpass Σ - Δ modulators were also designed and simulation-tested such as the complex 1-1, 1-1-1, 2-1, 2-1-1 and 2-2 MASH topologies. Moreover, new double-, triple and quadruple-stage FD filter based MASH Σ - Δ modulator topologies were also designed and evaluated.

The double-stage Σ - Δ modulator was modified and analysed to allow it to use bandpass filters in stead of resonators in its loop-filters. This allowed the design of stable higher-order Σ - Δ modulators having more symmetrical magnitude spectra and better resolution. Two versions of this topology were designed: the first employed identical loop-filters in each section, whereas the second was capable of using different loop-filters in each stage. Another novel bandpass MASH topology was developed, which contained a fourth-order variable resonator based Σ - Δ modulator in its first stage and a bandpass filter in its second stage. This cascade modulator had many advantages and was shown to deliver very good SNR figures. The double-stage inverse comb/bandpass filter based Σ - Δ modulator, which was absolutely novel was proposed, analysed and simulated at the behavioural level. Two versions of this modulator were developed containing either a single-loop or a double-loop inverse comb filters in the first stage followed by a bandpass

filter in the second stage. The main benefits of this topology were the simpler first-stage loop-filter and multiplier-free digital filter for the cancellation circuitry.

Chapter 4 presented the design, mathematical analysis and evaluation of a novel class of narrow-band bandpass Σ - Δ modulators, which could accomplish concurrent multiple noise-shaping bands for multi-tone input signals. Specifically; the analyses and behavioural-level simulations for equi-distant and non-equi-spaced double- and triple-band bandpass Σ - Δ modulators were presented. Five different techniques based on the NTFs of comb filters, slink filters, fractional-delay comb filters, FIR multi-notch filters and IIR multi-bandstop filters were employed to design these multi-band Σ - Δ modulators. These analyses were subsequently extended to design complex multi-band noise-shaping Σ - Δ modulators using the NTFs of complex comb filters, complex slink filters, complex FIR multi-notch filters and complex IIR multi-bandstop filters. All these complex multi-band bandpass Σ - Δ modulator topologies were verified via behavioural-level simulations. Routines in Matlab were written in order to facilitate the computation of the coefficients for all the above designs. These were used in conjunction with a library created in Simulink that contained a multitude of these multi-band topologies for evaluation purposes.

In chapter 5, a survey containing all the major publications, which address stability in Σ - Δ modulation was initially presented. This was followed by a review of the different interpretations of stability. A brief discussion containing all the well-known ad-hoc criteria for assessing stability in Σ - Δ modulators was presented. The stability of bandpass Σ - Δ modulators was evaluated by using a variable gain model for the quantiser. Root locus techniques in combination with the Jury Criterion were employed to determine the stable range of quantiser gain values. The chapter discussed and presented detailed simulation results of the main factors that affected stability in Σ - Δ modulators. These included the input amplitude, modulator order, feedback coefficients, feedforward loop-filter gains, number of delayers, initial conditions and the composition of the input signal. The overall goal of the chapter was to provide more accurate guidelines for the design of single- and multi-bit bandpass Σ - Δ modulators.

6.2 Suggestions for Future Research

Based on the work carried out and the results obtained from this research programme, the following present suggestions for future research.

- Investigate the use of other types of FD filters in conjunction with sum-filters to find out, whether better accuracy in tunability and resolution can be obtained, especially for noise-shaping bands located at high frequencies.
- Design FD filters, which impart small phase delays (including the delay of the inherent filter) in order to enable the design of bandpass Σ - Δ modulators that can deliver good SNR figures at high frequencies.
- Evaluate at the behavioural level the effect of non-unity gain resonators, leaky resonators and mismatches between the analogue and digital sections on the resolution in MASH bandpass Σ - Δ modulators.
- Determine the effect of incorporating inter-stage coupling coefficients on the SNR, DR and tonal content of MASH bandpass Σ - Δ modulators, whose constituent stages contain a mixture of single- and multi-bit quantisers.
- Develop and compare two types of tonality indexes, which can assess the degree of tonality in the spectrum of Σ - Δ modulators. The first quantifying tonality in the in-band region and the second quantitatively evaluating the power of tones across the entire spectrum, including in-band tones.
- Investigate the advantages gained in utilising non-equi-spaced quantisation levels in single-stage bandpass Σ - Δ modulators, paying particular attention to improvements to resolution, tonality content and modulator stability.
- Conduct a detailed comparative study of the effect of windowing on the spectral characteristics of bandpass Σ - Δ modulators, to determine whether any SNR improvements can be achieved in the in-band region.

References

- [Abc97] Abcarius, J., L. Louis and G.W. Roberts, "The design of high-order delta-sigma modulators for bandpass A/D conversion", *Midwest Symposium on Circuits and Systems*, vol. 1, pp. 272-275, 1998.
- [Ada91] Adams, R.W., "Theory and practical implementation of a fifth-order sigma-delta A/D converter", *Journal of the Audio Engineering Society*, vol. 39, no. 7/8, pp. 515-528, July 1991.
- [Agr83] Agrawal, B. P. and K. Sheno, "Design methodology for $\Delta\Sigma$ ", *IEEE Transactions on Communications*, vol. 31, no. 3, pp. 360-369, March 1983.
- [Ana89] Anastassiou, D., "Error diffusion coding for A/D conversion", *IEEE Transactions on Circuits and Systems*, vol. 36, no. 9, pp. 1175-1186, September 1989.
- [And96] Andre, E., D. Morche, F. Balestro and P. Senn, "A 2-path Σ - Δ modulator for bandpass application", *Workshop on Analog and Mixed IC Design*, pp. 87-91, 1996.
- [Ard87] Ardalan, S.H. and J.J. Paulous, "An analysis of nonlinear behaviour in delta-sigma modulators", *IEEE Transactions on Circuits and Systems*, vol. cas. 34, no. 6, pp. 593-603, June 1987.
- [Azi95] Aziz, P.M., H.V. Sorensen and J. Van der Spiegel, "Performance of complex noise transfer functions in bandpass and multi-band sigma-delta systems", *ISCAS*, Seattle, pp. 641-644, April 1995.
- [Azi96] Aziz, P.M., H.V. Sorensen and J. Van der Spiegel, "An overview of sigma-delta converters", *IEEE Signal Processing Magazine*, pp. 61-84, January 1996.
- [Bah95] Baher, H. and E. Afifi, "A fourth-order switched capacitor cascade structure for sigma-delta converters", *International Journal of Circuit Theory and Applications*, vol. 23, pp. 3-21, 1995.
- [Ben95] Benabes, P., A. Gauthier and R. Kielbasa, "New high-order universal Σ - Δ modulator", *Electronic Letters*, vol. 31, no. 1, pp. 8-9, January 1995.
- [Bai93] Baird, R.T. and T.S. Fiez, "Stability analysis of high-order modulators for delta-sigma ADCs", *ISCAS*, vol. 2, pp. 1361-1364, Chicago, May 1993.
- [Bai94] Baird, R.T. and T.S. Fiez, "Stability analysis of high-order delta-sigma modulation for ADCs", *IEEE Transactions on Circuits and Systems II: Analog and Digital Signal Processing*, vol. 41, no. 1, pp. 59-62, January 1994.
- [Bai96] Baird, R.T. and T.S. Fiez, "A low oversampling ratio 14-b 500 kHz $\Delta\Sigma$ ADC with a self-calibrated multibit DAC", *IEEE Journal of Solid-State Circuits*, vol. 31, no. 3, pp. 312-320, March 1996.

[Baz95] Bazarjani, S. and M. Snelgrove, "A 4th order SC bandpass Σ - Δ modulator designed on a digital CMOS Process", *38th Midwest Symposium on Circuits and Systems*, vol. 2, pp. 1345-1348, Rio de Janeiro, August 1995.

[Baz97] Bazarjani, S. and M. Snelgrove, "A 40 MHz IF fourth-order double-sampled SC Bandpass Σ - Δ modulator", *ISCAS*, vol. I, pp. 73-76, Hong Kong, June 1997.

[Baz98] Bazarjani, S. and M. Snelgrove, "A 160-MHz fourth-order double-sampled SC bandpass sigma-delta modulator", *IEEE Transactions on Circuits and Systems II: Analog and Digital Signal Processing*, vol. 45, no. 5, pp. 547-555, May 1998.

[Bel95] Bellanger, M., "A DSP perspective of sigma-delta techniques and applications in communications" *International Symposium on Signals, Systems and Electronics*, pp. 195-198, 1995.

[Ben93] Benabes, P., A. Gauthier and D. Billet, "New wideband sigma-delta converter", *Electronic Letters*, vol. 29, no. 17, pp. 1575-1577, August 1993.

[Ben99] Benabes, P., P. Aldebert and R. Kielbasa, "Analog-to-digital sigma-delta converters modeling for simulation and synthesis", *IMEKO Workshop on ADC Modelling and Testing*, pp. 3-14, Bordeaux, September 1999.

[Bos88b] Boser, B.E. and B. A. Wooley, "The design of sigma-delta modulation analog-to-digital converters", *Journal of Solid-State Circuits*, vol. SC-23, pp. 1298-1308, December 1988.

[Bot97] Botteron, Y. And B. Nowrouzian, "An investigation of bandpass sigma-delta A/D converters", *Midwest Symposium on Circuits and Systems*, vol. 1, pp. 293-296, 1998.

[Bot99] Botteron, Y., B. Nowrouzian and A. T. G. Fuller, "design and switched-capacitor implementation of a new cascade-of-resonators Σ - Δ converter configuration", *ISCAS*, vol. II, pp. 45-49, Florida, 1999.

[Bry94] Bryant, J.M., "Bandpass sigma-delta ADCs for direct IF conversion", *Analog Devices*, pp. 5.4.1-5.4.10, USA, 1994.

[Can74] Candy, J.C., "A use of limit cycle oscillations to obtain robust analog-to-digital converters", *IEEE Trans. Commun.*, vol. COM-22, pp. 298-305, March 1974.

[Can76] Candy, J.C., "Using triangularly weighted interpolation to get 13-bit PCM from a sigma-delta", *IEEE Trans. Commun.*, vol. COM-24, pp. 1268-1275, November 1976.

[Can85] Candy, J.C., "A use of double integration in sigma delta modulation", *Transactions on Communications*, vol. 33, no. 3, pp. 249-258, March 1985.

[Can92] Candy, J.C. and G.C. Temes, "Oversampling Delta-sigma Data Converters - Theory, Design and Simulation", *IEEE Press*, pp. 1-25, 1992.

[Cha90] Chao, K.C.H., S. Nadeem, W.L. Lee and C.G. Sodini, "A higher order topology for interpolative modulators for oversampling A/D converters", *IEEE Transactions on Circuits and Systems*, vol. 37, no. 3, pp. 309-318, March 1990.

- [Cha99] Chang, T. and S. B. Bibyk, "Exact analysis of second-order bandpass delta-sigma modulator with sinusoidal inputs", *ISCAS*, vol. II, pp. 372-375, Florida, 1999.
- [Ché99] Cherry, J. A. and W. M. Snelgrove, "Excess loop-delay in continuous-time delta-sigma modulators", *IEEE Transactions on Circuits & Systems -II: Analog and Digital Signal Processing*, vol. 46, no. 4, pp. 376-389, April 1999.
- [Cho89] Chou, W., P.W. Wong and R.M. Gray, "Multistage sigma-delta modulation", *IEEE Transactions on Information Theory*, vol. 35, no. 4, pp. 784-796, July 1989.
- [Cho90] Chou, W. and R. M. Gray, "Dithering and its effects on sigma-delta and multi-stage sigma-delta modulation", *ISCAS*, pp. 368-371, August 1990.
- [Chu97] Chuang, S., X. Yu, T. Sculley and R. Bamberger, "Design and implementation of a sixth-order bandpass delta-sigma A/D converter with single quantiser", *ISCAS*, vol. I, Hong Kong, pp. 381-384, June 1997.
- [Chu98] Chuang, S., L. Huining, X. Yu, T.L. Sculley and R. Bamberger, "Design and implementation of bandpass delta-sigma modulators using half-delay integrators", *IEEE Transactions on Circuits and Systems II: Analog and Digital Signal Processing*, vol. 45, no. 5, pp. 535-546, May 1998.
- [Cor94] Cormier, R.F., T.L. Sculley and R.H. Bamberger, "Combining subband decomposition and sigma-delta modulation for wideband A/D conversion", *ISCAS*, London, pp. 357-360, May 1994.
- [Cor97] Cormier Jr, R. F., T. L. Sculley and R. H. Bamberger, "A fourth-order bandpass delta-sigma modulator with digitally programmable passband frequency", *Analog Integrated Circuits and Signal Processing*, vol. 12, pp. 217-229, 1997.
- [Cun92] Cunningham, E. P., "Digital Filtering: An Introduction", Houghton Mifflin Company, pp. 244-256, 1992.
- [Cut60] Cutler, C. C., "Transmission system employing quantisation", U.S. Patent No. 2,927,962, filed (1954), March, 1960.
- [Dav96] Davies, A., "Periodic non-linear oscillations from bandpass Σ - Δ modulators", *ISCAS '96*, vol. 2, Atlanta, pp. 469-472, May 1996.
- [Dav97] Davies, A. C. and G. P. Petkov, "Zero-input oscillation bounds in a bandpass Σ - Δ modulator", *Electronic Letters*, vol. 33, no. 1, pp. 28-29, January 1997.
- [Dav99b] Davies, A. J., G. Fischer, H. H. Albrecht and J. Hess, "Digital correction of circuit imperfections in the 1-1-1 cascaded Σ - Δ modulator", *IMEKO Workshop on ADC Modeling and Testing*, pp. 153-158, Bordeaux, September 1999.
- [Ded94] Dedic, I., "A sixth-order triple-loop sigma-delta CMOS ADC with 90dB SNR and 100 kHz Bandwidth", *IEEE International Solid-State Circuits Conference*, session 11, pp. 188-189, February 1994.

- [Dia93] Dias, V.F. and V. Liberali, "Cascade pseudomultibit noise shaping modulators", *IEE Proceedings-G*, vol. 140, no. 4, pp. 237-246, August 1994.
- [Dia96] Dias, V., "Complex-signal sigma-delta modulators for quadrature bandpass A/D conversion", *Microelectronics Journal*, no. 27, pp. 505-524, 1996.
- [Dre90] Dressler, H.J., "Interpolative bandpass A/D conversion-experimental results", *Electronics Letters*, vol. 26, no. 23, 1941-1942, 1990.
- [Dre91] Dressler, H. J., "Interpolative bandpass A/D conversion", *Signal Processing*, vol. 22, no. 2, pp. 139-151, February 1991.
- [Dun96a] Dunn, C. and M. Sandler, "A comparison of dithered and chaotic sigma-delta modulators", *Journal of Audio Engineering Society*, vol. 44, no. 4, pp. 227-244, April, 1996.
- [Eng99a] Engelen, J. and R. Plassche, "Stability and design of continuous-time bandpass sigma-delta modulators", *ISCAS'99*, vol. II, pp. 355-359, Florida, 1999.
- [Eng99b] Engelen, J. and R. Plassche, "A sixth-order continuous-time bandpass sigma-delta modulator for digital Radio IF", *IEEE Journal of Solid-State Circuits*, vol. 34, no. 12, pp. 1753-1764, December 1999.
- [Fee96] Feely, O. and D. Fitzgerald, "Bandpass sigma-delta modulation - an analysis from the perspective of non-linear dynamics", *ISCAS*, vol. 3, Atlanta, pp. 146-149, May 1996.
- [Fis96] Fischer, G. and A.J., Davis, "A sigma-delta modulator architecture for wide bandwidth applications", *ISCAS*, vol. 1, pp. 25-28, May 1996.
- [Fis97] Fischer, G. and A. J. Davis, "Alternative topologies for sigma-delta modulators-a comparative study", *IEEE Transactions on Circuits & Systems -II: Analog and Digital Signal Processing*, vol. 44, no. 10, pp. 789-797, October, 1997.
- [Fis98] Fischer, G. and A.J. Davies, "Wideband cascade delta-sigma modulators with digital correction for finite amplifier gain offsets", *Electronics Letters*, vol. 34, no. 6, pp. 511-512, March 1998.
- [Fra95] Francesconi, F., V. Liberali and F. Maloberti, "A bandpass sigma-delta modulator architecture for digital radio", *38th Midwest Symposium on Circuits and Systems*, vol. 2, pp. 885-888, Rio de Janeiro, August 1995.
- [Gai89] Gailus, P. H., W. J. Turney and F. R. Yester Jr, "Method and arrangement for a sigma-delta converter for bandpass signals", US patent no. 4857928, August 1989.
- [Gao98] Gao, W. and W. M. Snelgrove, "A 950-MHz IF second-order integrated LC bandpass delta-sigma modulator", *IEEE Journal of Solid-State Circuits*, vol. 33, no. 5, pp. 723-732, May 1998.
- [Gar99] Garcia, J. C. and A.G. Armada, "Effects of bandpass sigma-delta modulation on OFDM signals", *IEEE Transactions on Consumer Electronics*, vol. 45, no. 2, pp. 318-326, May 1999.

- [Got98] Gothenberg, A. A. and H. Tenhunen, "Performance analysis of low oversampling ratio sigma-delta noise-shapers for RF applications", *ISCAS'98*, vol. 1, pp. 410-404, 1998.
- [Gou94] Gourgue, F. and M. Bellanger, "A bandpass subsampled delta-sigma modulator for narrowband cellular mobile communications", *ISCAS*, vol. 5, pp. 353-356, London, May 1994.
- [Gra89a] Gray, R.M., "Spectral analysis of quantisation noise in a single-loop sigma-delta modulator with dc input", *IEEE Transactions on Communications*, vol. 37, no. 6, pp. 588-599, June 1989.
- [Gra89b] Gray, R. M., W. Chou and P. W. Wong, "Quantisation noise in single-loop sigma-delta modulation with sinusoidal inputs", *IEEE Transactions on Communications*, vol. 37, no. 9, pp. 956-967, September 1989.
- [Gra90b] Gray, R.M., "Quantisation noise spectra", *IEEE Transactions on Information Theory*, vol. 36, no. 6, pp. 1220-1244, November 1990.
- [Har93a] Harris, F., B. Caulfield and B. McKnight, "Use of allpass networks to tune the centre frequency of sigma-delta modulators", *27th Asilomar Conference on Signals, Systems & Computers*, vol. 2, pp. 1230-1234, November 1993.
- [Hau91] Hauser, M. W., "Principles of oversampling A/D conversion", *Journal Audio Engineering Society*, vol. 39, no. 1, pp. 3-26, January/February 1991.
- [Hau95] Haurie, X. And G. W. Roberts, "A multiplier-free structure for 1-bit high-order delta-sigma modulators", *38th Midwest Symposium on Circuits and Systems*, vol. 2, pp. 889-892, Rio de Janeiro, August 1995.
- [Hay86] Hayashi, T., Y. Inabe, K. Uchimura and T. Kimura, "A multistage delta-sigma modulator without double integration loop", *ISSCC*, pp. 182-183, February 1986.
- [He88] He, N., A. Buzo and F. Kuhlmann, "Multi-loop sigma-delta quantisation: spectral analysis", *IEEE*, pp. 1870-1873, 1988.
- [Hei91] Hein, S. and A. Zakhor, "On the stability of interpolative sigma delta modulators", *ISCAS*, vol. 3, pp. 1621-1624, Singapore, June 1991.
- [Hej92] Hejn, K., P. Murphy and I. Kale, "Measurement and enhancement of multistage sigma-delta modulators", *IEEE IMTC'92*, 1992.
- [Her96] Hernandez, L., "Frequency synthesis based on bandpass sigma-delta modulation", *Electronics Letters*, vol. 32, no. 18, pp. 1642-1643, August 1996.
- [Ho99] Ho, C. C. and C. J. Kuo, "Gain mismatch effect of cascaded sigma-delta modulator reduced by serial technique", *ISCAS*, vol. II, pp. 9-12, Florida, 1999.
- [Hor91] Horrocks, D.H., "A second-order oversampled sigma-delta modulator for bandpass signals", *ISCAS*, pp. 1653-1656, 1991.

- [Ino63] Inose, H. and Y. Yasuda, "A unity bit coding method by negative feedback", *IEEE*, vol. 51, pp. 1524-1535, November 1963.
- [Ism94] Ismail, M., *Analog VLSI: signal and information processing*, McGraw-Hill, pp.467-505, 1994.
- [Jan91a] Jantzi, S., R. Schreier and M. Snelgrove, "A bandpass Σ - Δ A/D converter for a digital AM receiver", *International Conference on Analogue to Digital and Digital to Analogue Conversion*, pp. 75-80, September 1991.
- [Jan91b] Jantzi, S., R. Schreier and M. Snelgrove, "Bandpass sigma-delta analog-to-digital conversion", *IEEE Transactions on Circuits and Systems*, vol. 38, no. 11, pp. 1406-1409, November 1991.
- [Jan93] Jantzi, S.A., W.M. Snelgrove and P.F. Ferguson, "A fourth-order bandpass sigma delta modulator", *IEEE Journal of Solid-State Circuits*, vol. 28., no. 3, pp. 282-291, March 1993.
- [Jan94a] Jantzi, S., K. Martin, M. Snelgrove and A. Sedra, "A complex bandpass Δ - Σ converter for digital radio", *ISCAS*, vol. 5, pp. 453-456, London, May 1994.
- [Jan94b] Jantzi, S., C. Ouslis and A. Sedra, "Transfer function design for $\Delta\Sigma$ converters", *ISCAS*, vol. 5, pp. 433-436, London, May 1994.
- [Jan96a] Jantzi, S. A., K. W. Martin and A. S. Sedra, "The effects of mismatch in complex bandpass $\Delta\Sigma$ modulators", *ISCAS*, vol. 1, Atlanta, pp. 227-230, May 1996.
- [Jan96b] Jantzi, S., R. Schreier and M. Snelgrove, "The design of bandpass delta-sigma ADCs" in *Delta-Sigma Data Converters*, S. R. Norsworthy, R. Schreier and G. C. Temes, IEEE Press, ch. 9, 1996.
- [Jan97] Jantzi, S. A., K. W. Martin and A. S. Sedra, "Quadrature bandpass $\Delta\Sigma$ modulation for digital radio", *IEEE Journal of Solid-State Circuits*, vol. 32, no. 12, pp. 1935-1949, December 1997.
- [Jay97] Jayaraman, A., P. Asbeck, K. Nary, S. Beccue and K. Wang, "Bandpass delta-sigma modulator with 800 MHz center frequency", *Gallium Arsenide Integrated Circuit Symposium: Technical Digest*, pp. 95-98, 1997.
- [Kal96] Kale, I. and R.C.S. Morling, " Σ - Δ modulation and polyphase filtering - the key to high-fidelity data conversion and instrumentation", *International Workshop on ADC Modelling*, Smolenice Castle, Slovakia, pp. 183-192, May 1996.
- [Kar90] Karema, T., T. Ritoniemi and H. Tenhunen, "An oversampled sigma-delta A/D converter circuit using two-stage fourth-order modulator", *ISCAS*, pp. 3279-3282, May 1990.
- [Ken88] Kenney, J. G. and L.R. Carley, "CLANS: A high-level synthesis tool for high resolution data converters", *IEEE International Conference on Computer-Aided Design*, pp. 496-499, 1988.

- [Koz00] Kozak, M., Private Communication, Department of Electronic Systems, University of Westminster, 2000.
- [Kru96] Krukowski, A., I. Kale and R.C.S. Morling, "Applications of polyphase filters for bandpass sigma-delta analog-to-digital conversion", International Workshop on ADC Modelling, Smolenice Castle, pp. 85-90, Slovakia, May 1996.
- [Kuo96] Kuo, C.J., C.T. Liu and C.J. Hou, "Sigma-delta modulator for bandpass signal", *ISCAS'96*, vol. I, Atlanta, pp. 29-32, May 1996.
- [Laa96] Laakso, T. I., V. Valimaki, M. Karjalainen and U. K. Laine, "Splitting the unit delay - Tools for fractional delay filter design", *IEEE Signal Processing Magazine*, vol. 13, no. 1, pp. 30-60, January 1996.
- [Lee87] Lee, W.L., "A novel higher-order interpolative modulator topology for high resolution oversampling A/D converters", MSc Thesis, Massachusetts Institute of Technology, Cambridge, June 1987.
- [Leo97a] Leong, C. H. and G. W. Roberts, "High-order bandpass sigma-delta modulators for high speed D/A applications", *Electronics Letters*, vol. 33, no. 6, pp. 454-455, March 1997.
- [Leo97b] Leong, C. H. and G. W. Roberts, "An effective implementation of high-order bandpass sigma-delta modulators for high speed D/A applications", *ISCAS*, vol. I, pp. 49-52, Hong Kong, June 1997.
- [Leu91] Leung, B., "The oversampling technique for analog to digital conversion: a tutorial overview", *Analog Integrated Circuits and Signal Processing 1*, pp. 65-74, 1991.
- [Li99] Li, B., L. Zheng and H. Tenhunen, "Hierarchical modelling of sigma delta modulators for noise coupling analysis", *Southwest Symposium on Mixed-Signal design*, pp. 58-62, 1999.
- [Liu97] Liu, H., X. Yu, T. Sculley and R. Bamberger, "A fourth-order bandpass delta-sigma A/D converter with input modulation network and digitally programmable passband", *ISCAS*, vol. I, Hong Kong, pp. 385-388, June 1997.
- [Lon88] Longo, L. and M. Copeland, "A 13 bit ISDN-band oversampled ADC using two-stage third-order noise-shaping", *IEEE Proc. Custom IC Conf.*, pp. 21.2.1-21.2.4, January 1988.
- [Lon93] Longo, L. and B. Horng, "A 15b 30kHz bandpass sigma-delta modulator", *IEEE International Solid-State Circuits Conference*, session 14, pp. 226-227, February 1993.
- [Lou99] Louis, L. and G. W. Roberts, "An eighth-order bandpass $\Delta\Sigma$ modulator for A/D conversion in digital radio", *IEEE Journal of Solid-State Circuits*, vol. 34, no. 4, pp. 423-431, April 1999.
- [Man99] Mann, S. I. and D. P. Taylor, "Limit cycle behaviour in the double-loop bandpass $\Sigma-\Delta$ A/D converter", *IEEE Transactions on Circuits & Systems -II: Analog and Digital Signal Processing*, vol. 46, no. 8, pp. 1086-1089, August 1999.

- [Mar97] Marques, A., V. Peluso, M. Steyaert and W. Sansen, "Optimal parameters for cascade $\Delta\Sigma$ modulators", vol. 1, *ISCAS*, pp. 61-65, Hong Kong, June 1997.
- [Mar98b] Marques, A. M., V. Peluso, M. S. J. Steyaert and W. Sansen, "Optimal parameters for $\Delta\Sigma$ modulator topologies", *IEEE Transactions on Circuits & Systems -II: Analog and Digital Signal Processing*, vol. 45, no. 9, pp. 1232-1241, September 1998.
- [Mat87] Matsuya, Y., K. Uchimura, A. Iwata, T. Kobayashi, M. Ishikawa and T. Yoshitome, "A 16-bit oversampling a-to-D conversion technology using triple-integration noise shaping", *IEEE Journal of Solid-State Circuits*, vol. 22, sc-22, no. 6, pp. 921-929, December 1987.
- [Mat89b] Mathew, M.I. and C.P. Lewis, "A review of sigma-delta modulation structures", *IEE Colloquium on Advanced A/D and D/A Conversion Techniques and Applications*, pp. 4/1-4/8, London, May 1989.
- [Mat90] Mathew, M.I. and C.P. Lewis, "Noise performance comparison for third and fourth order cascaded sigma-delta modulators having parameter tolerance errors", *Electronics Letters*, vol. 26, no. 3, pp. 158-159, February 1990.
- [Mat92] Matsuya, Y. and Y. Akazawa, "Multi-stage noise shaping technology and its application to precision measurement", pp. 540-542, 1992.
- [Med98a] Medeiro, F., B. Perez-Verdu, J.M. de la Rosa and A. Rodriguez-Vazquez, "Multi-bit cascade Σ - Δ modulator for high-speed A/D conversion with reduced sensitivity to DAC errors", *Electronics Letters*, vol. 34, no. 5, pp. 422-423, March 1998.
- [Med98b] Medeiro, F., B. Perez-Verdu, J. M. de la Rosa and A. Rodriguez-Vazquez, "Fourth-order cascade SC Σ - Δ modulators: a comparative study ", *IEEE Transactions on Circuits and Systems- I: Fundamental Theory and Applications*, vol. 45, no. 10, pp. 1041-1051, October 1998.
- [Mia98] Miao, G., H. C. Yang and P. Tang, "An oversampled A/D converter using cascaded fourth-order sigma-delta modulation and current steering logic", *ISCAS'98*, vol. 1, pp. 412-415, 1998.
- [Mit93] Mitra, S. K. and J. F. Kaiser, *Handbook for digital signal processing*, John Wiley & Sons, ch. 10, pp. 677-720, 1993.
- [Mor94] Morling, R. C. S., I. Kale and C. W. Tsang, "The design of a sigma-delta codec for mobile telephone applications", *IEE Conference on A/D and D/A Conversion Techniques and Applications*, Cambridge, July 1994.
- [Mor96b] Morche, D., A. Aubert, E. Andre, F. Balestro and P. Senn, "A new multistage bandpass sigma-delta modulator", *ISCAS*, vol. 1, pp. 13-16, May 1996.
- [Mor96c] Morling, R. C. S., I. Kale and M. Al-Janabi, "Digital Signal Processing - Σ - Δ Modulators", On-site Course for Dialog Semi-conductors, University of Westminster, session 27, pp. 1-82, Swindon, May 1996.

- [Mou94] Moussavi, S.M. and B.H. Leung, "High-order single-stage single-bit oversampling A/D converter stabilized with local feedback loops", *IEEE Transactions on Circuits and Systems II: Analog and Digital Signal Processing*, vol. 41, no. 1, pp. 19-25, January 1994.
- [Nor92] Norsworthy, S. R., "Effective dithering of sigma-delta modulators", *ISCAS*, pp. 1304-1307, May 1992.
- [Nor93b] Norsworthy, S. R., "Optimal nonrecursive noise shaping filters for oversampling data converters, Part 2: Applications", *ISCAS*, vol. 2, pp. 1357-1360, Chicago, May 1993.
- [Nor96b] Norman, O., "A bandpass delta-sigma modulator for ultrasound imaging at 160 MHz clock rate", *IEEE Journal of Solid-State Circuits*, vol. 31, no. 12, pp. 2036-2041, December 1996.
- [Nor97] Norsworthy, S.R., R. Schreier and G.C. Temes, *Delta-Sigma Data Converters: Theory, Design and Simulation*, *IEEE Press*, 1997.
- [Oka93] Okamoto, T., Y. Maruyama, and A. Yukawa, "A stable high-order delta-sigma modulator with an FIR spectrum distributor", *IEEE Journal of Solid-State Circuits*, vol. 28, no. 7, pp. 730-735, July 1993.
- [Ong97] Ong, A. K. and B. A. Wooley, "A two-path bandpass Σ - Δ modulator for digital IF extraction at 20 MHz", *IEEE Journal of Solid-State Circuits*, vol. 32, no. 12, pp. 1920-1933, December 1997.
- [Opp99] Oppenheim, A. V., R. W. Schaffer and J. R. Buck, *Discrete-Time Signal Processing*, Prentice Hall Signal Processing Series, pp. 185-213, 1999.
- [Orf96] Orfanidis, S. J., *Introduction to signal processing*, Prentice Hall International Editions, pp. 1-97, 1996.
- [Par93] Park, S., "Principles of sigma-delta modulation for analog-to-digital converters", *Motorola Digital Signal Processors*, pp. 1/1-9/1, 1993.
- [Pat94] Pattamatta, S.V., P. Manapragada, V. Dalal and R. Schreier, "A switched-current bandpass delta-sigma modulator", *ISCAS*, vol. 5, pp. 477-480, London, May 1994.
- [Pea87] Pearce, T.H. and A.C. Baker, "Analogue to digital conversion requirements for HF radio receivers", *IEE Colloquium on System Aspects and Applications of ADCs for Radar, Sonar and Communications*, London, November 1987.
- [Pea94] Pearce, T.H., "Cascading bandpass sigma-delta A/D converters", *Advanced A/D and D/A Conversion Techniques and their Applications*, no. 393, pp. 1-6, July 1994.
- [Pei98] Pei, S. C. and C. C. Tseng, "A comb filter design using fractional-sample delay", *IEEE Transactions on Circuits and Systems II: Analog and Digital Signal Processing*, vol. 45, no. 6, pp. 649-653, June 1998.

- [Pel98] Pellon, L., "RF-to-digital receivers employing bandpass multi-bit Σ - Δ ADC architectures", *Gallium Arsenide Integrated Circuit Symposium: Technical digest*, pp. 11-14, 1998.
- [Phi96] Phillips, C. L. and R. D. Harbor, "feedback control systems", Prentice Hall International, 1996.
- [Pin91] Ping, L., "Oversampling analog/digital converters with finite zeros in noise shaping functions, *ISCAS'91*, pp. 1645-1648, 1991.
- [Pro92] Proakis, J.G. and D.G. Manolakis, *Digital signal processing: principles, algorithms and applications*, Macmillan Publishing Company, pp. 395-467, 1992.
- [Qin99] Qin, W., B. Hu and X. Ling, "Sigma-delta ADC with reduced sample rate multibit quantiser", *IEEE Transactions on Circuits & Systems -II: Analog and Digital Signal Processing*, vol. 46, no. 6, pp. 824-828, June, 1999.
- [Qiu93] Qiuting, H. and P. Maguire, "On the inherent harmonic distortion of first-order Σ - Δ modulators", *ISCAS'93*, vol. 2, pp. 1349-1352, May 1993.
- [Rab97] Rabbii, S. and B. A. Wooley, "A 1.8-V digital-audio sigma-delta modulator in 0.8- μ m CMOS", *IEEE Journal of Solid-State Circuits*, vol. 32, no. 6, pp. 783-796, June 1997.
- [Ram99] Ramesh, M. C. and K. S. Chao, "Pipelined sigma-delta modulators with interstage scaling", *MWCAS'99*, New Mexico, USA, 1999.
- [Reb89a] Rebeschini, M., N. Van Bavel, P. Rakers, R. Greene, J. Caldwell and J. Haug, "A 16-bit 160 kHz CMOS A/D converter using sigma-delta modulation", *IEEE Custom Integrated Circuits Conference*, pp. 6.1.1-6.1.5, 1989.
- [Reb89b] Rebeschini, M., N. Van Bavel, P. Rakers, R. Greene, J. Caldwell and J. Haug, "A high-resolution CMOS sigma-delta A/D converter with 320 kHz output rate", *ISCAS*, pp. 246-249, May 1989.
- [Reb90] Rebeschini, M., N. R. Van Bavel, P. Rakers, R. Greene, J. Caldwell and J. R. Haug, "A 16-bit 160 kHz A/D converter using sigma-delta modulation", *IEEE Journal of Solid-State Circuits*, vol. 25, no. 2, pp. 431-440, April 1990.
- [Rib94] Ribner, D.B., "Multistage bandpass delta sigma modulators", *IEEE Transactions on Circuits and Systems II: Analog and Digital Signal Processing*, vol. 41, no. 6, pp. 402-405, June 1994.
- [Ris94] Risbo, L., "Stability predictions for high-order Σ - Δ modulators based on quasilinear modeling", *ISCAS*, London, vol. 5, pp. 361-364, May 1994.
- [Rit77] Ritchie, G.R., "Higher order interpolation analog to digital converters", Ph.D. Dissertation, University of Pennsylvania, 1977.
- [Rit90] Ritoniemi, T., T. Karema, and H. Tenhunen, "Design of stable high order 1-bit sigma-delta modulators", *ISCAS*, pp. 3267-3270, May 1990.

- [Ros95] La Rosa, J.M., F. Medeiro, B. Perez-Verdu and A. Rodriguez-Vazquez, "A CMOS fully-differential bandpass Σ - Δ modulator using switched-current circuits", *38th Midwest Symposium on Circuits and Systems*, vol. 2, pp. 744-747, Rio de Janeiro, August 1995.
- [Ros99] Rosa, J. M., B. Perez-Verdu, F. Medeiro, R. Rio and A. Rodriguez-Vazquez, "Non-ideal quantisation noise shaping in switched-current bandpass Σ - Δ modulators", *ISCAS'99*, vol. II, pp. 476-479, Florida, 1999.
- [Sch89] Schreier, R. and M. Snelgrove, "Bandpass sigma-delta modulation", *Electronic Letters*, vol. 25, no. 23, pp. 1560-1561, November 1989.
- [Sch90] Schreier, R. and W.M. Snelgrove, "Decimation for bandpass sigma-delta analog-to-digital conversion", *IEEE*, pp. 1801-1804, 1990.
- [Sch91b] Schreier, R. and M. Snelgrove, "Stability in general Σ - Δ modulator", *ICASSP*, vol. 3, pp. 1769-1772, Toronto, May 1991.
- [Sch91c] Schreier, R., "Noise-Shaped Coding", Ph.D. Thesis, Department of Electrical Engineering, University of Toronto, 1991.
- [Sch92a] Schreier, R., G.C. Temes, A.G. Yesilyurt, Z.X. Zhang, Z. Czarnul and A. Hairapetian, "Multibit bandpass delta-sigma modulators using N-path structures", *IEEE ISCAS*, pp. 593-596, 1992.
- [Sch93b] Schreier, R., "An empirical study of high-order single-bit delta-sigma modulators", *IEEE Transactions on Circuits and Systems II: Analog and Digital Signal Processing*, vol. 40, no. 8, pp. 461-466, August 1993.
- [Sch94] Schreier, R., "On the use of chaos to reduce idle-channel tones in delta-sigma modulators", *IEEE Transactions on Circuits and Systems I: Fundamental Theory and Applications*, vol. 41, no. 8, pp. 539-547, August 1994.
- [Sch96] Schreier, R., "Bandpass delta-sigma data converters", *29th Asilomar Conference on Signals, Systems & Computers*, pp. 94-97, 1996.
- [Sho94] Shoaie, O. and W.M. Snelgrove, "Optimal bandpass continuous-time Σ - Δ modulator", *ISCAS*, vol. 5, pp. 489-492, London, May 1994.
- [Sho95] Shoaie, O. and W.M. Snelgrove, "A multi-feedback design for LC bandpass delta-sigma modulators", *ISCAS*, vol. 1, pp. 171-174, Seattle, April 1995.
- [Sho97] Shoaie, O. and W.M. Snelgrove, "Design and implementation of a tunable 40 MHz-70 MHz Gm-C Bandpass Δ - Σ modulator", *IEEE Transactions on Circuits and Systems II: Analog and Digital Signal Processing*, vol. 44, no. 7, pp. 521-530, July 1997.
- [Sim89] Simpson, D.F. and R.A. Belcher, "Feedback coding techniques - review and implementation", *IEE Colloquium on Advanced A/D and D/A Conversion Techniques and Applications*, pp. 3/1-3/8, London, May 1989.

- [Sin95] Singor, F. W. and W. M. Snelgrove, "Switched-capacitor bandpass delta-sigma A/D modulation at 10.7 MHz", *IEEE Journal of Solid-State Circuits*, vol. 30, no. 3, pp. 184-192, 1995.
- [Son95] Song, B.S., "A fourth-order bandpass delta-sigma modulator with reduced number of op-amps", *IEEE Journal of Solid-State Circuits*, vol. 30, No. 12, pp. 1309-1314, December 1995.
- [Spa62] Spang III, H.A. and P.M. Schultheiss, "Reduction of quantising noise by use of feedback", *IRE Transactions on Communication Systems*, pp. 373-380, December 1962.
- [Ste94] Steiner, P. and W. Yang, "Stability analysis of the second-order Σ - Δ modulator", *ISCAS'94*, London, vol. 5, pp. 365-368, May 1994.
- [Ste98] Stewart, R.W. and E. Pfann, "Oversampling and sigma-delta strategies for data conversion", *Electronics & Communication Engineering Journal*, vol. 10, no. 1, pp. 37-47, February 1998.
- [Ste99] Steensgaard, J. and U. Moon and G. C. Temes, "Mismatch-shaping serial digital-to-analog converter", *ISCAS*, vol. II, pp. 5-9, Florida 1999.
- [Sti88] Stikvoort, E.F., "Some remarks on the stability and performance of the noise shaper or sigma delta modulator", *IEEE Transactions on Communications*, vol. 36, no.10, pp. 1157-1162, October 1988.
- [Sun99] Sun, L., T. Lepley, F. Nozahic, A. Bellissant, T. Kwasniewski and B. Heim, "Reduced complexity, high performance digital delta-sigma modulator for fractional-N frequency synthesis", *ISCAS*, vol. II, pp. 152-155, Florida 1999.
- [Swa97] Swaminathan, A., MSc Project Report, "A single-IF receiver architecture using a complex sigma-delta modulator", Department of Electronics, Carleton University, Ottawa, 1997.
- [Tan93] Tan, N. and S. Eriksson, "Fourth-order two-stage delta-sigma modulator using both 1 bit and multibit quantisers", *Electronics Letters*, vol. 29, no. 11, pp. 937-938, May 1993.
- [Tao97a] Tao, H. and J.M. Khoury, "Direct conversion bandpass sigma-delta modulator", *Electronics Letters*, vol. 33, no. 15, pp. 1282-1283, July 1997.
- [Tao99] Tao, H. and J.M. Khoury, "A 100MHz, 400 Msample/s CMOS Direct-Conversion Bandpass $\Sigma\Delta$ modulator", *IEEE International Solid-State Circuits Conference*, session 3, pp. 60-61, 1999.
- [Tem90] Temes, G.C. and J.C. Candy, "A tutorial discussion of the oversampling method for A/D and D/A conversion", *IEEE*, pp. 910-913, 1990.
- [Tha62] Thaler, G. and M. Pastel, "Analysis and design of non-linear feedback control systems", New York: McGraw-Hill, 1962.

- [Thu91] Thurston, A.M., T.H. Pearce and M.J. Hawksford, "Bandpass implementation of the sigma-delta A-D conversion technique", *Proceedings of the IEE International Conference on Analogue-to-Digital and Digital-to-Analogue Conversion*, pp. 81-86, Swansea, September 1991.
- [Thu92] Thurston, A.M. and M.O. J. Hawksford, "Bandpass delta-sigma conversion", *IEE*, pp. 2/1-2/6, May 1992.
- [Thu94a] Thurston, A.M. and M.J. Hawksford, "Phase correction techniques for bandpass sigma-delta A/D converters", *IEE*, pp. 7/1-7/9, 1994.
- [Thu94b] Thurston, A. M. and M. J. Hawksford, "Dynamic overload recover mechanism for sigma delta modulators", *IEE Advanced A-D and D-A Conversion Techniques and their Applications*, pp. 124-129, 1994.
- [Thu95] Thurston, A.M., "Sigma-delta IF A/D converters for digital radios", *GEC Journal of Research*, vol. 12, no. 2, pp.76-85, 1995.
- [Tla96] Tlaskal, O., M. J. Underhill and D. W. R., "Digital detection of instability of higher-order bandpass sigma-delta converters", *Electronics Letters*, vol. 21, no. 32, pp. 1955-1956, October 1996.
- [Tom94] Tommazou, C., N. Battersby and S. Porta, "Circuits and Systems Tutorials", pp. 195-260, *ISCAS*, London, May 1994.
- [Tro93] Troster, G. et al., "An interpolative bandpass converter on a 1.2 μm BICMOS analog/digital array", *IEEE Journal of Solid-State Circuits*, vol. 28, no. 4, pp. 471-477, April 1993.
- [Uch88] Uchimura, K., T. Hayashi, T. Kimura and A. Iwata, "Oversampling A-to-D and D-to-A converters with multistage noise shaping modulators", *IEEE Transactions on Acoustics, Speech and Signal Processing*, vol. 36, no. 12, pp. 1899-1905, December 1988.
- [Vei96] Veillette, B.R. and G.W. Roberts "FM signal generation using delta-sigma oscillators", *ISCAS*, vol. 1, pp. 1-4, Atlanta, May 1996.
- [Wan92] Wannamaker, R. A., "Psychoacoustically optimal noise-shaping", *Journal Audio Engineering Society*, vol. 40, no. 7/8, pp. 611-620, July/August 1992.
- [Wep95] Wepman, J. A., "Analog-to-digital converters and their applications in radio receivers", *IEEE Communications Magazine*, pp. 39-45, May 1995.
- [Wil91] Williams, L.A. and B.A. Wooley, "Third-order cascaded sigma-delta modulators", *IEEE Transactions on Circuits and Systems*, vol. 38, no. 5., pp. 489-498, May 1991.
- [Wil94] Williams, L. A. and B. A. Wooley, "A third-order sigma-delta modulator with extended dynamic range", *IEEE Journal of Solid-State Circuits*, vol. 29, no. 3, pp. 193-202, March 1994.
- [Wol89] Wolff, C. M. and L. R. Carley, "Calculating the stability range, SNR, and distortion of delta sigma modulators", *ISCAS*, vol. 2, pp. 1423-1426, 1989.

[Yan94] Yang, S., M. Faulkner and R. Malyniak, "A tunable bandpass sigma-delta A/D conversion for mobile communication receiver", *IEEE*, pp. 1346-1350, 1994.

[Yin94] Yin, G. and W. Sansen, "A high-frequency and high-resolution fourth-order $\Sigma\Delta$ A/D converter in BiCMOS technology", *IEEE Journal of Solid-State Circuits*, vol. 29, no. 8, pp. 857-865, August 1994.

Appendix A

Derivation of the Hanning window correction factor to calculate the in-band SNR

The impulse response of a Hanning window is given by:

$$w(k) = \frac{1}{2} \left(1 + \cos\left(\frac{2\pi k}{N_P}\right) \right)$$

To find power, the signal needs to be squared first,

$$w^2(k) = \frac{1}{4} \left[1 + 2 \cos\left(\frac{2\pi k}{N_P}\right) + \cos^2\left(\frac{2\pi k}{N_P}\right) \right]$$

$$w^2(k) = \frac{1}{4} \left[1 + 2 \cos\left(\frac{2\pi k}{N_P}\right) + \frac{1}{2} \left(1 + \frac{\cos(4\pi k)}{N_P} \right) \right]$$

$$w^2(k) = \frac{1}{4} \left[\frac{3}{2} + 2 \cos\left(\frac{2\pi k}{N_P}\right) + \frac{1}{2} \left(\frac{\cos(4\pi k)}{N_P} \right) \right]$$

The power for a discrete-time signals can be evaluated using

$$P_X = \frac{1}{N_P} \sum_{k=0}^{N_P-1} |w(k)|^2$$

Considering each term separately

First term $\frac{1}{4N_P} \sum_{k=0}^{N_P-1} \frac{3}{2} = \frac{3}{8N_P} [N_P - 1 + 1] = \frac{3}{8}$

Second term $\frac{2}{4N_P} \sum_{k=0}^{N_P-1} \cos\left(\frac{2\pi k}{N_P}\right) = \frac{1}{2N_P} \left[(k+1) \cos\left(\frac{2\pi k}{N_P}\right) \text{slink}\left((k+1), \frac{1}{N_P}\right) \right]$

$$\frac{1}{2N_P} \left[(k+1) \cos\left(\frac{2\pi k}{N_P}\right) \frac{\sin(k+1) \frac{2\pi}{N_P}}{(k+1) \sin\left(\frac{2\pi}{N_P}\right)} \right]$$

The sin term degenerates to zero since k is an integer resulting in zero for the second term.

Third term $\frac{1}{8N_P} \sum_{k=0}^{N_P-1} \cos\left(\frac{4\pi k}{N_P}\right) = \frac{1}{8N_P} \left[(k+1) \cos\left(\frac{4\pi k}{N_P}\right) \text{slink}\left((k+1), \frac{1}{N_P}\right) \right]$

$$\frac{1}{8N_P} \left[(k+1) \cos\left(\frac{4\pi k}{N_P}\right) \frac{\sin(k+1) \frac{4\pi}{N_P}}{(k+1) \sin\left(\frac{4\pi}{N_P}\right)} \right]$$

The sin term degenerates to zero since k is an integer resulting in zero for the third term.

Therefore, the net power attenuation due to the Hanning window is $\frac{3}{8}$. To compensate for this reduction, the required correction factor is $\frac{8}{3}$.